Georg Kopplin

Marine Polysaccharides

Fucoidan, Alginate and Chitosan –
An Investigation of Physical, Chemical and
Bioactive Properties

Doctoral thesis

NTNU
Norwegian University of
Science and Technology

Georg Kopplin

Marine Polysaccharides

Fucoidan, Alginate and Chitosan – An Investigation of Physical, Chemical and Bioactive Properties

Thesis for the Degree of Philosophiae Doctor

Trondheim, January 2024

Norwegian University of Science and Technology
Faculty of Natural Sciences
Department of Biotechnology and Food Science

Preface

This thesis is submitted in partial fulfilment of the requirements for the academic title "**Philosophiae Doctor**" at the Norwegian University of Science and Technology (NTNU). The work was performed at the Norwegian Biopolymer Laboratory (NOBIPOL), Department of Biotechnology and Food Science.

The work herein was conducted under the supervision of Professor of Finn Lillelund Aachmann and co-supervision Gudmund Skjåk-Bræk. The work in this thesis was financed by the Norwegian Research Council, through the MARPOL project (Grant 221576).

The thesis consists of a general introduction, objectives of the conducted studies, summaries of the research articles, and a general discussion centred around the main topics of the scientific articles. The research articles that have been published in conjunction with this thesis are presented in the appendix.

☐ NTNU
Faculty of Natural Sciences

Summary

Marine polysaccharides, such as fucoidan, alginate and chitosan are garnering increasingly significant research interest in the field of biomedical applications due to their broad range of bioactive properties, compatibility with living tissues and their ability to form hydrogels. This thesis presents in-depth investigations of the properties and potential applications of these marine polysaccharides.

We utilized numerous analytical techniques to characterize the chemical structure of fucoidan from *Laminaria hyperborea*. A task that to our knowledge has not been accomplished before.

Using ICP-MS and Raman spectroscopy, we determined a near theoretically complete degree of sulfation (1.7). HPAEC revealed a structure almost exclusively composed of fucose residues, while NMR and methylation analysis indicated a 1→3-linked backbone structure with extensive branching. SEC-MALS uncovered a high average molecular weight (up to 1.4 MDa) and indications of short side chains.

A highly purified and well-characterized fucoidan sample was used to investigate bioactivity *in vitro* using a lepirudin-based human whole blood model. Structural features such as the degree of sulfation and molecular weight were tailored to enable elucidation of structure–function relationships. Unmodified fucoidan with a high degree of sulfation and molecular weight was demonstrated to inhibit coagulation at intermediate to high concentrations, showing similar inhibitory effects on the complement system. The work underscores the importance of both molecular weight and the degree of sulfation as key parameters for bioactive properties.

We also explored potential therapeutic effects of fucoidan on ocular diseases, specifically, age-related macular degeneration (AMD). VEGF secretion and protection from oxidative stress were investigated. The findings unveiled a positive relationship between molecular weight, bioactivity, and potential therapeutic effects for highly sulfated fucoidan. Importantly, viability was maintained for both primary porcine epithelial cells and a human epithelial cell line.

Alginate hydrogels which are attractive biomaterials for applications such as cell encapsulation, tissue engineering, coatings, and drug delivery, were examined on a fundamental scientific level. Through CD spectroscopy and molecular dynamic simulations, we obtained strong evidence supporting a previously hypothesised zipper-like junction zone formation between alginate M-blocks and chitosan.

Furthermore, we developed and investigated a novel alginate-chitosan gelling system. This system relies upon crosslinks between poly-MG-blocks and chitosan oligomers and can enable gel strengths orders of magnitude higher than those observed in poly-M-chitosan hydrogels. Rheological measurements and molecular dynamic simulations suggested a fundamentally different chain–chain interaction mechanism involving localized phase-separation.

Gels made from alginates with different block structures were crosslinked with combinations of calcium and chito-oligosaccharides. We found that up to 50% of Ca^{2+} can be replaced by chitosan oligomers (under specific conditions) without compromising gel strength or the occurrence of syneresis, while simultaneously increasing the rate of gelation. The inclusion of chitosan oligomers in the gelation mechanism allows for customizing gelling kinetics and may enhance hydrogel stability against electrolytes, a factor of great importance in biomedical applications.

Acknowledgements

I wish to express my sincere gratitude to Professor Kjell Morten Vårum, who initiated the scientific work presented herein but tragically passed away during the course of this project. Kjell Morten was an eminent scientist with international recognition in the field of marine
polysaccharides, particularly with respect to chitin and chitosan. His extensive knowledge and experience in conceptualizing experiments were pivotal to this work. The world of chitosan has lost one of its greatest pioneers.

Equal gratitude shall be given to my supervisor Finn Lillelund Aachmann, who was essential to complete this work. This is not only because of his outstanding expertise in analytical chemistry, particularly in NMR spectroscopy, but also his guidance throughout the thesis and his creative mindset when considering analytical methods and designing experiments. Furthermore, his determination not to settle for ambiguous results and his persistence in fine-tuning experiments until a clear conclusion could be obtained were truly inspiring and constructive. I also greatly appreciated his dry and slightly dark sense of humour. The right balance that makes you laugh but also provides you incentive to improve yourself and your work.

I would also like to thank my co-supervisor Professor Gudmund Skjåk-Bræk. With over 50 years of accumulated knowledge on alginates, it seems as though alginate-expertise seeps out from every pore. If you sit down and grab a cup of coffee with Gudmund, he will answer you any question about alginate you could possibly think of.

I also express my gratitude to Professor Kurt Ingar Draget. His substantial knowledge and experience in working with hydrogels played an essential role in the experimental design. His directions were instrumental in navigating the enigmatic field of composite hydrogels, ensuring that we did not get lost among the many variables.

To all my colleagues at the Biotechnology Department and the NOBIPOL laboratories, I would like to express my deepest thanks for all the great scientific and social engagements. Wenche and Ann-Sissel, the lab would not run without you. Thank you very much for providing training on all the relevant lab equipment and for assisting me with data interpretation due to your years of experience. I hope you can forgive me for any HMS-related headaches I may have caused you. Olav Aarstad is one of the most committed and reflecting scientists I have ever met. Whatever the scientific problem might be, if you explain it to Olav, he will have a good suggestion on how to solve it or what to try. A special thanks go to Joachim Kjesbu and Morten Dille for their vital input and for proofreading this thesis, as well as for our great social activities outside NTNU, like lifting heavy objects and brewing beer, respectively. Gaston, thank you for all the enthralling discussions at the coffee corner and beyond, debating anything from scientific data, to music, to politics and more. Abba, thanks for the wonderful friendship, food excursions, mountain hikes and other trips outside of our daily office life. Writing about all the great colleagues I had at NTNU would exceed the scope of this section. However, I would like to give an extra shout out to Line, Annalucia, Yiming, Ingrid, Edith, Eva and Eivind. Thank you for the many great memories and our fruitful discussions together.

Arriving in a new country naturally comes with its own challenges. Fortunately, I still remembered a Norwegian named Ailo Ravna, whom I met at WACKEN in 2006. He offered me a place to stay and a

List of publications

Paper 1:   Feng, Y.[†], **Kopplin, G.**[†], Sato, K., Draget, K.I. & Vårum, K.M.; • Alginate gels with a combination of calcium and chitosan oligomer mixtures as crosslinkers. *Carbohydrate Polymers* **2016**, 490–497 (156).

Paper 2:   **Kopplin, G.**, Rokstad, A.M., Mélida, H., Bulone, V. & Aachmann, F.L.; • Structural Characterization of Fucoidan from Laminaria hyperborea: Assessment of Coagulation and Inflammatory Properties and Their Structure-Function Relationship. *ACS Applied Bio Materials* **2018**, 1880-1892 (6).

Paper 3:   Dörschmann, P., **Kopplin, G.**, Roider, J., Klettner, A.; • Effects of Sulfated Fucans from Laminaria hyperborea Regarding VEGF Secretion, Cell Viability, and Oxidative Stress and Correlation with Molecular Weight. *Marine Drugs* **2019**, 548 (10).

Paper 4:   **Kopplin, G.**, Lervik, A., Draget, K.I. & Aachmann, F.L.; • Alginate gels crosslinked with chitosan oligomers – a systematic investigation into alginate block structure and chitosan oligomer interaction. *RCS Advances* **2021**, 13780-13798 (11)

[†]Equal contribution

Contribution to scientific publications not included in this thesis

Paper: **Kopplin, G.**, Bernsdorf, A. & Köckerling, M.; • Conductivity, Structures, Spectra, and Thermal Properties of Lithium and Sodium Tetracyanidoborates with Crown Ether Encapsulated Cations: Isolated Ions in $[A^I(12\text{-crown-4})_2][B(CN)_4]$ and 1D Chains in $[AI(15\text{-crown-5})][B(CN)_4]$ (A^I= Li, Na). *Eur. J. Inorg. Chem.* **2014**, 319–325 (2).

Paper: Dörschmann, P., Apitz, S., Hellige, I., Neupane, S., Alban, S., **Kopplin, G.**, Ptak, S., Fretté, X., Roider, J., Zille, M., Klettner, A.; • Evaluation of the effects of fucoidans from Fucus species and Laminaria hyperborea against oxidative stress and iron-dependent cell death. *Marine Drugs* **2021**, 557 (19).

Paper: Dörschmann, P., **Kopplin, G.**, Roider, J., Klettner, A.; • Interaction of high-molecular weight fucoidan from Laminaria hyperborea with natural functions of retinal pigment epithelium. *Molecular Sciences* **2023**, 24 (3).

Paper: Wekre, M., Holmelid, B., Underhaug, J., Pedersen, B., **Kopplin, G.**, Jordheim, M.; • Characterization of high-value products in the side stream of Laminaria hyperborea alginate production – targeting the phenolic content. *Algal Research* **2023**, (72).

Paper: Dörschmann, P., Akkurt, H., **Kopplin, G.**, Mikkelsen, M., Meyer, A., Roider, J., Klettner, A.; • Establishment of specific age-related macular degeneration relevant gene expression panels using porcine retinal pigment epithelium for assessing fucoidan bioactivity. *Experimental Eye Research* **2023**, 109469 (231)

Contents

1 Introduction

1.1 Alchemy, mythology and history

Algae are eukaryotic aquatic organisms that perform photosynthesis. It is a polyphyletic grouping, not based on a common shared ancestor but on phenotypical characteristics, which can be expressed by species of multiple biological clades [1,2]. Algae can be divided, according to their size, in microalgae and macroalgae, with an estimate of approximately 300 000 species, and a genetic diversity much greater than found in terrestrial plants [2]. Macroalgae, also known as seaweeds, are divided into three taxonomic classes: red (*Rhodophyta*), green (*Chlorophyta*), and brown macroalgae (*Phaeophyta*) [1].

Seaweeds have populated the earth well before the dawn of mankind and influenced our societies and culture throughout history to varying degrees [3]. Archaeologists found evidences in Britain that humans have eaten seaweed alongside fish and crustaceans in the Mesolithic era (ca. 10 000 BC) [4]. Various seaweeds have been used in medicine, as a staple food and fertilizer on the fields Since ancient times [5].

Although not reaching the same elevated status as in Asia, seaweeds still found their entry into European culture in various forms. In Ireland kelp (brown seaweed of the order *Laminariales*), was considered a gift from the gods, carried by the winter storms, to nourish the agricultural fields and soil for the forthcoming season [3]. The Norse jötunn Ægir, the giant of sea and beer brewing, is commonly portrayed wearing crown made of seaweed. In the city hall of Denmark's capitol Copenhagen, a large tile mural decorates the presidential stairs, depicting Ægir and his nine daughters, the personified waves, with seaweed covering their bodies (see Figure 1-1). The artwork and its prominent location are hinting towards the essential role seaweed in Scandinavian culture [6].

Further annotations and endorsements are sowed throughout Greek mythology. Glaucus (Γλαῦκος), a prophetic sea deity, was born a normal fishermen but, after eating a magical herb along the shore, he gained immortality [7]. Potentially a reference to seaweed washed ashore and an early discovery of fucoidan (see chapter **1.6.2 Bioactive properties of fucoidan**)?

Figure 1-1 Tile mural "Ægir og hans døtre" (1883) by Lorenz Frølich, depicting the aquatic deity Ægir and his nine daughters partially covered with seaweeds. Located at the presidential stairs in the city hall of Copenhagen [6]. Photograph, Kopplin (2016).

Figure 1-2 Mosaic of Thalassa (centre) the Greek primordial spirit of the sea, wearing clothes made of seaweed and a crown of crab-claws. Created during the C5[th] AD in Antioch, currently at the Hatay Archaeology Museum (Turkey) [8].

The Greek deity and spirit of the sea Thalassa (Θάλαττα) is commonly illustrated wearing a toga made of seaweed and a crown made of crab-claws (see Figure 1-2). She is attributed to be the origin of all living fish [9]. Her husband Pontus (Πόντος), the primordial god of the high seas and water itself, was born by Gaia and reigned before the arrival of the Olympian gods. He is depicted with seaweed for his hair and a crown made of crab-claws (Figure 1-3). In the light of current findings, could this entanglement of crustacean shells and algae along Pontus' crown, be an early forecast of chitosan and alginate (see chapter **1.4 Alginate**), forming molecular networks, able to retain large amounts of water (see chapter **1.3 Hydrogels**)?

While mythology is concealing gained knowledge through figurative speech and might have hidden early discoveries about marine polysaccharides in blurred allegories, this thesis is aiming to investigate marine biopolymers and characterize their physical, chemical, and bioactive properties, through the clear lens of modern-day scientific methods.

Figure 1-3 Mosaic of Pontus, the Greek primordial god and personification of the sea. His beard consists of waves, his hair is seaweed and his crown is made of crab-claws [7]. Created during the C1[st] – C3[rd] AD in Utica (Tunisia), currently at the Bardo National Museum in Tunis.

1.2 Marine polysaccharides

Polysaccharides are polymers of monosaccharide units linked through glycosidic bonds [10]. They constitute the main source of marine biomass and are present within flora, notably in macro- and microalgae, and in fauna such as crustaceans and molluscs [11,12]. Marine polysaccharides function primarily as structural supports in cell walls or as intracellular energy storage compounds [13].

Brown seaweed and diatoms synthesize the polysaccharide laminarin, which consists of β-(1→3)-linked glucose that is partially (1→6) branched. Laminarin primarily serves as a compound for energy storage, not unlike the terrestrial polysaccharides amylose and amylopectin colloquially known as starch [12,14].

Marine polysaccharides serving primarily structural purposes are numerous. Red seaweed cell walls are constituted mainly of galactans like carrageenan, a sulfated polymer consisting of galactose and 3,6-anhydrogalactose. Agar, a less sulfated galactan, is also found predominantly in red seaweed, although not exclusively. In green algae, sulfated polysaccharides comprised of xylose, rhamnose, iduronic acid and glucuronic acid known as ulvans are found [12,15]. In both red and green seaweeds another structural polysaccharide are the xylose-based xylans.

With a wide variety of compositions and physico-chemical properties, marine polysaccharides are increasingly attractive in research and for applications such as pharmaceuticals, nutraceuticals, cosmeceuticals, and tissue engineering [16,17]. Particularly sulfated polysaccharides like fucoidans from brown seaweed have emerged as promising macromolecules, due to their bioactive properties. Alginate and chitosan are also enticing due to their ability to form tailored highly biocompatible hydrogels [18,19]. This thesis will focus the marine polysaccharides fucoidan, alginate and chitosan (see Figure 1-4).
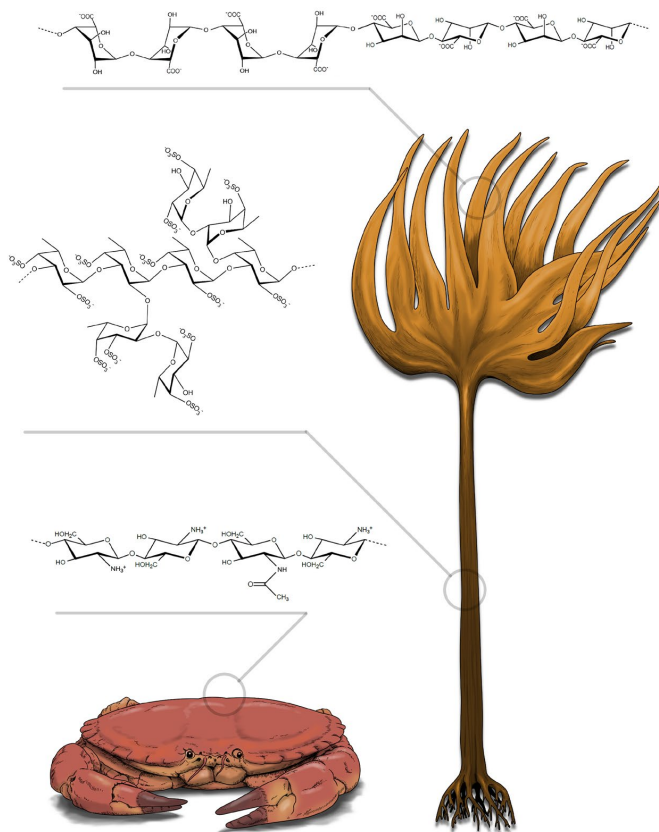
Figure 1-4 Sources of marine polysaccharides illustrated; *Laminaria hyperborea* (right) containing alginate (top structure) and fucoidan (centre structure) distributed throughout the whole plant; chitosan (bottom structure) extracted from shell of crustaceans (bottom).

1.3 Hydrogels

Hydrogels are scaffolds of crosslinked hydrophilic polymer chains able to retain large amounts of water. They are defined by specific physical properties regarding their dynamic moduli, describing elastic and inelastic responses to mechanical force [20]. The crosslinks in hydrogels can be established through covalent linkages [21,22], ionic linkages or junction zones formed through van der Waals interactions [23]. Hydrogels can mimic the natural environment of soft biological tissue, making them an attractive tool for various biomedical applications [24,25]. The broad range of different polymers, polymer mixtures, crosslinkers and crosslinking methods allows for an optimization of these three dimensional networks, widely utilized for cell encapsulation, as 3D cell growth matrix, as wound dressing and as tuneable drug delivery system [26–29].
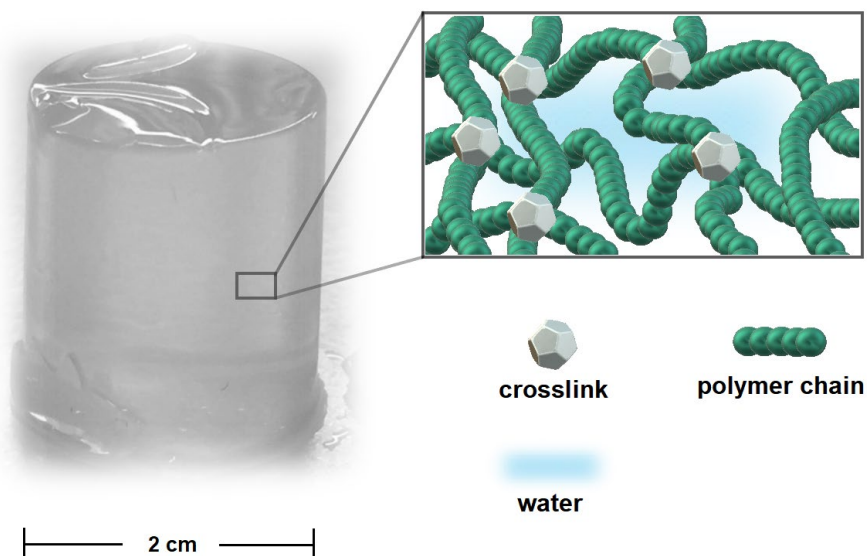
Figure 1-5 Schematic depiction of a hydrogel comprised of linear hydrophilic polymer chains, partially crosslinked to a large network retaining water (right). Alginate cylinder ionically crosslinked with calcium and chitosan oligomers (left).

Ionically crosslinked hydrogels generally feature a higher swelling sensitivity towards pH changes than their covalently crosslinked counterparts, which is particularly utilized in orally applied drug delivery systems, passing the different pH regimes of the gastrointestinal tract [29,30]. The highly swollen state of these biomaterials further facilitates the transport of nutrients into and metabolic waste products out of the hydrogel when cells are incorporated [24].

The advantage of covalently crosslinked hydrogels lies in their long-term stability. However, this advantage often comes with a reduced biocompatibility from including crosslinking molecules, which are not fully biological inert or stem from chemical methods that are harsh towards incorporated cells [21,31]. Inducing covalent bonds through radical crosslinking is an important method, applied for example at dextran hydrogels, using glycidyl acrylates crosslinker (containing an epoxy-group) and N,N,N'N'-tetramethylene-diamine together with ammonium peroxydisulfate, as initiator for the radical reaction [32,33]. In other common methods polyaldehydes, such as glutaraldehyde

(1,5-Pentanedial), are used to establish covalent bonds between the polymer chains. Polyaldehydes are particularly effective in presence of macromolecules that contain free amino groups, for instance chitosans or proteins, linking the individual chains through Schiff-base formation [34,35]. Nevertheless, the high toxicity of polyaldehydes imposes difficulties applying this method on systems aiming for cell viability and biocompatibility. A non-toxic alternative to polyaldehydes, for crosslinking chitosan and proteins, is genipin, a compound extracted from gardenia fruits [36,37].
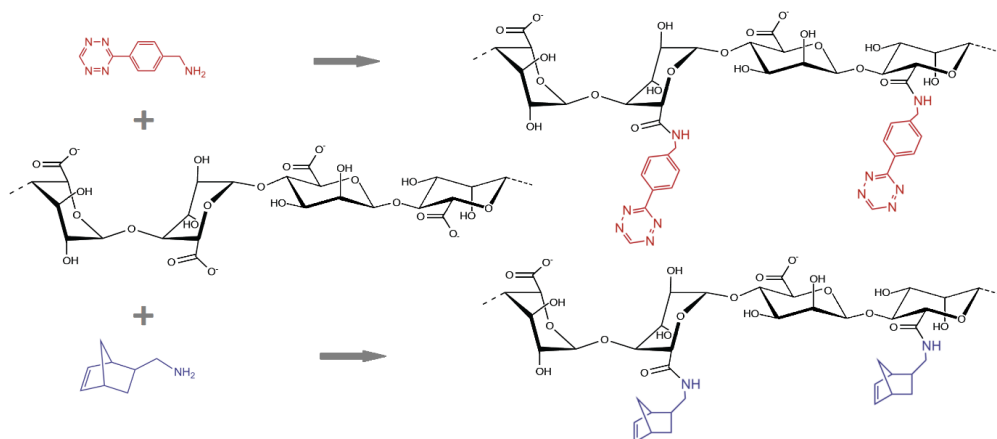
Figure 1-6 Modification of alginates (black). Aqueous carbodiimide chemistry is used to separately attach either benzylamino tetrazine (red) or norbornene methanamine (blue) to the carboxylic acid group through an amid linkage [21].

Modern methods of copper-free click chemistry have emerged as alternative approach for synthesizing covalent crosslinks, providing fast reaction rates with high chemoselectivity. Desai et al. modified alginate polymers, using tetrazine (3-(p-benzylamino)-1,2,4,5 tetrazine) and norbornene methanamine as functional groups (see Figure 1-6), allowing for intermolecular bond formation without the need of external crosslinkers, or catalysts, using a bioorthogonal 'inverse electron demand Diels–Alder' click reaction (see Figure 1-7) [21].
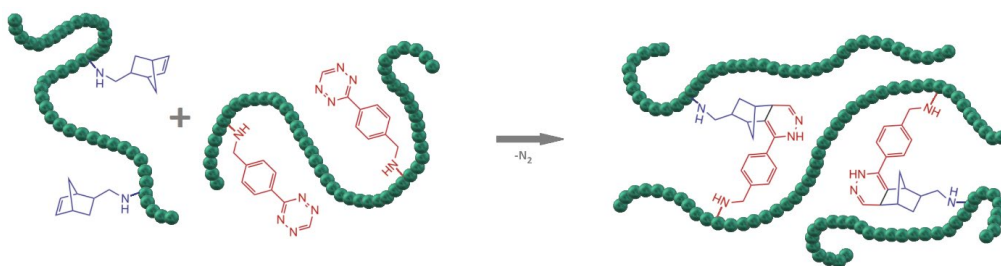
Figure 1-7 Formation of hydrogels using click chemistry [21]. Polymers (turquoise) modified with either benzylamino tetrazine (red) or norbornene methanamine (blue) are mixed and form a covalent crosslink due to a highly chemoselective Diels–Alder reaction under the loss of N_2.

Those modified polymers can also be stimulated by UV-Vis-light, allowing for a minimal invasive interference in the aqueous polymer solutions containing cells. Short light exposure time and low

intensity reduces the risk of deleterious effects on the cells [21,38]. However, these photo initiators still generate free radicals for initiating the polymerization process and the prior chemical modification of the polymers impedes on the utilization for these hydrogels in medical applications.

A non-toxic method to covalently link biopolymers such as alginate, chitosan, cellulose and proteins relies on the natural occurring phenolic compound ferulic acid [39–42]. The antioxidant ferulic acid is capable of forming crosslinks with polysaccharides and proteins via resonance stabilized free radical intermediates [43]. Combinations of covalently and ionically linked hydrogels will further expand the tool set and possible properties of highly tailored functional hydrogel.

An in-depth presentation of ionically crosslinked hydrogels is included in chapter **1.4 Alginate**. All polysaccharides discussed in this thesis, alginate, chitosan and fucoidan, are suitable candidates for highly biocompatible hydrogels.

1.3.1 Characterization of hydrogels

Hydrogels can be described as substantially diluted polymer solutions, which retain water through weak or strong intermolecular crosslinks. These diluted polymer networks are viscoelastic materials, simultaneously displaying viscous properties of the solution and elastic properties stemming from the solid scaffold [44]. The viscous part is characterized by mechanical energy applied for deformation being transformed into heat energy (loss through heat dissipation). Energy transformation through heat dissipation results in a permanent deformation. Elastic properties are characterized by the storage of mechanical energy induced by deformation and the subsequent restitution of mechanical energy. In fully elastic material, physical deformation only occurs temporarily and the original shape will be restored [45]. In more colloquial terms, they deform and "bounce back".

Beside concentration and molecular weight (M_w) of a polymer, elastic properties of a hydrogel are also strongly related to the number and stability of crosslinks within the polymer network, as well as the length of the elastic (entropic) polymer segments between adjacent crosslinks and length of junction zones [46]. The ratio of viscous versus elastic response defines the material as a viscous fluid, elastic solid or viscoelastic gel. Rheology is a widely applied method to analyse and characterize these materials. It determines the loss of energy through heat dissipation and elastic stress response with high precision. In addition, the kinetics of gelling systems can be observed, which is widely used to study particularly the formation of gels [47,48]. Young's modulus characterizes the stiffness/elasticity of a hydrogel. The instrument used to determine the Young's modulus can further give valuable data about the rupture point (point of failure), highly relevant for the application of hydrogels under strong mechanical tension e.g. in implants and biomedical purposes [49–51].

Alongside mechanical properties, spectrophotometric methods such as small-angle X-ray scattering (SAXS), small-angle neutron scattering (SANS) and Raman provides structural insides into the hydrogel structure and 3D composition [52,53].

1.3.1.1 Rheology

Rheology characterizes physical properties of materials using two dynamic moduli: the shear storage modulus (elastic modulus) (G') and the shear loss modulus (G''). The ratio between the two moduli is called phase angle (δ) and is calculated as seen in equation 1. The applied deformation is referred to as strain (γ) and the force response from the material as stress (σ). In an ideal elastic material (Hookean material) stress and strain are in phase (δ = 0°). In an ideal viscous solution (Newtonian liquid) stress and strain are 90° out of phase, implying a complete dissipation into heat energy [54].

Figure 1-8 Schematic depiction of the relation of storage modulus (G') to loss modulus (G'') expressed by the phase angle (δ).

$$\tan \delta = \frac{G''}{G'} \qquad (1)$$

To qualify as a "true gel" G' needs to exceed G'' by at least a magnitude of two and a phase angle that is frequency (f) independent over a large plateau zone [20]. The mechanical deformation in a rotational rheometer is performed by sinusoidal oscillating movements of two plates towards each other with a known angular velocity (ω = 2π · f). The analysed fluid or gel is placed in between. The deformation is kept small to avoid inducing any permanent disruption of the gel [20].

Table 1-1 Classification of viscoelastic materials by their phase angle (δ)

G' > G''	δ < 45°	viscoelastic solid
G' = G''	δ = 45°	transition
G' < G''	δ > 45°	viscoelastic liquid

To further examine the formed hydrogel, a frequency sweep can be performed, plotting G' and G'' over a large range of frequencies (e.g. 0.01–10 Hz). A true gel will display constant values for the two moduli, while an entangled polymer network (not crosslinked) will display a higher loss modulus at low frequencies and exhibit viscous behaviour. Those systems are also called "false gel" [54].

Figure 1-9 Schematic diagram of the kinetics of a gel formation. Storage modulus (G') to loss modulus (G'') increase over time (t). At the transition point (blue dotted line) the material changes from viscoelastic liquid to viscoelastic gel.

1.3.1.2 Axial compression

The Young's modulus is a mechanical property of a material that reflects its stiffness/elasticity. The material is investigated by compression or elongation measurements, observing and analysing elastic and plastic deformation. Like rheology, the relation between strain, the applied deformation, and stress the responding force (F) per area (A) is observed. The Young's modulus (E), reflects the stiffness/elasticity of a gel and can be obtained by plotting the linear viscoelastic area at the initial section of deformation, following equation 2, where l represents the height of the sample, Δl the length of deformation. By performing compression with high strain, causing plastic deformation and

breakage of the hydrogel (rupture point), additional data how the gel will behave under strong mechanical tension can be gained.

$$\frac{F}{A} = E \cdot \frac{\Delta l}{l}$$

(2)

Hydrogel networks are similar to elastic rubber systems in many regards (such as M_w dependence of the moduli, low phase angle, low frequency dependence), but differ in the mechanism how mechanical energy is stored. In rubber mechanical energy is stored through a reduction in entropy of the polymer chains [46,55], while in hydrogels mechanical energy storage is enthalpy driven, displayed a negative temperature dependence, as seen in ionically crosslinked alginate [56]. This enthalpy driven process can be largely explained due the thermodynamic energy minimum formed where highly specific binding pairs interact [57].

1.3.1.3   Syneresis

Syneresis is spontaneous contraction of the crosslinked polymer network of a gel, accompanied by expulsion of liquid to the surface of the shrinking network [58]. The degree of syneresis (S) is simply measured by the weight loss of a hydrogel, when exuding water is removed while evaporation is prohibited.

$$S = \frac{m_0 - m}{m_0} \cdot 100\%$$

(3)

Where m_0 represents the initial weight of the formed hydrogel and m is the final weight when no or no further exudation of water is observed. Syneresis in alginate hydrogels has been investigated and linked to a reorganization in ionic crosslinkers along the polymer chains, leading to a growth in the length of junction zones as well as growth in length of flexible polymer segments in between, resulting in the collapse of the 3D scaffold. SAXS experiments suggested the growing junction zones as primary driving force for syneresis in alginate hydrogels [59]. A further cause for syneresis in alginate hydrogels can be an overabundance of crosslinkers, resulting in a secondary growth of junction zones in a "zipper" like fashion [60,61].

1.4 Alginate

Alginate is a linear polysaccharide naturally occurring predominantly in the class of brown seaweed (*Phaeophyta*) [62], although various bacteria such as *Pseudomonas aeruginosa* and *Azotobacter vinelandii* incorporate alginate as exocellular polymeric material [63,64]. Alginates form a polysaccharide family comprised of the uronic acids (1→4)-linked β-D-mannuronic acid (M-unit) in $^4C_1$ conformation and its C5-epimer, α-L-guluronic acid (G-unit) in the $^1C_4$ conformation (see Figure 1-10, Figure 1-11) determined through X-ray crystallography [65].
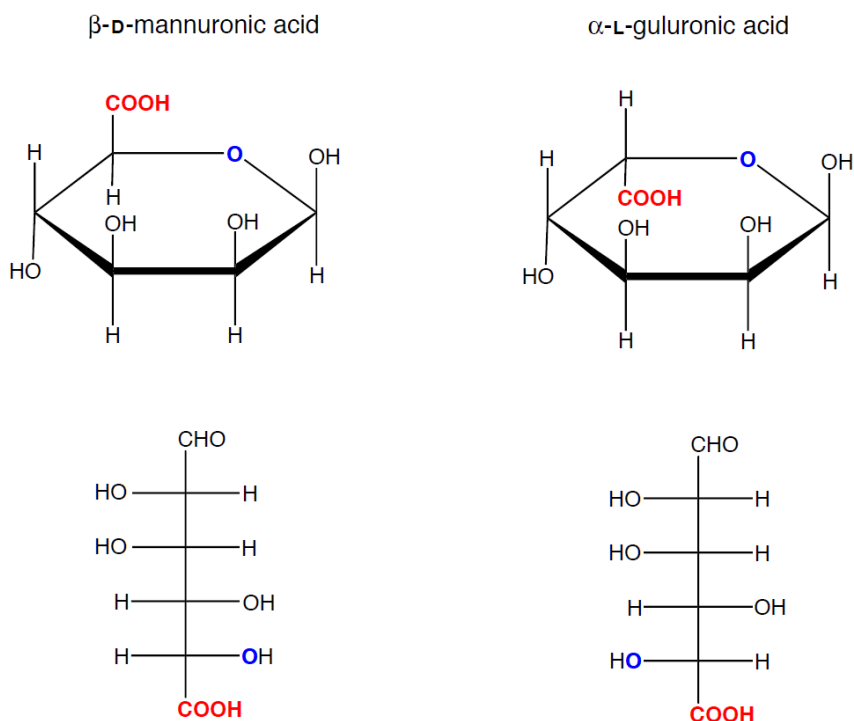
Figure 1-10 Haworth (top) and Fischer (bottom) projection of the two C5-epimers β-D-mannuronic acid (left) and α-L-guluronic acid (right), the two monomer units compiling alginate.

The acid dissociation constant (pKa) for M-units is 3.38, while it is 3.65 for the G-units, cumulating to 3.5 as an approximate pKa-value for alginates [66–68]. Beside the monosaccharide composition (M/G-ratio), the chemical and physical properties of alginates are also heavily influenced by their molecular weight and the order of sugar units within the polymer chain, their uronic acid and block sequences.

Alginate blocks are homopolymeric regions of M-units (M-blocks), G-units (G-blocks), or alternating epimers (MG-blocks) of different length [67]. The composition and distribution of uronic acids and blocks varies strongly between different seaweed species and even between their plant parts (see Table 1-2). While the frond (also referred as blade or leaf) has a G-content of about 40% (fraction of G; F_G = 0.40) the stipe (also referred as stem) contains 60–70% G, depending on a further separation of different stipe parts [61,67]. The most extreme examples found in nature are expressed in bacteria.

Azotobacter vinelandii produces alginate with about 50% G, the most pronounced difference compared to algal alginate of similar monosaccharide composition are the very long M and G blocks. *Pseudomonas aeruginosa* produces an almost pure M-alginate (called mannuronan) with an F_M from 0.90 to 0.96, which can be enhanced by genetic mutation up to $F_M = 1.0$ [63,64]. A structural feature invariably distinguishing bacterial alginates from their algal polyuronate counterparts, is the presence of O-acetyl groups, found at C-2 and C-3 position of M-units [69,70].

Alginates almost exclusively composed of regularly alternating MG-units (poly-MG) can be produced by a selected enzymatical treatment using C-5-epimerase AlgE4 purified from *A. vinelandii*. Almost pure G-alginate (poly-G) can be achieved by purified C-5-epimerase AlgE6 from the same organism [71].
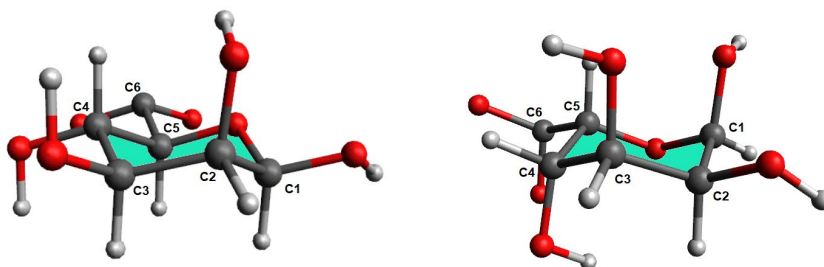
Figure 1-11 Structure model shows lowest energy (most stable conformation) for β-D-mannuronic acid in $^4C_1$ chair conformation (left) and α-L-guluronic acid in $^1C_4$ chair conformation (right). Sugar units were modelled in Avogadro using UFF energy optimization.

Table 1-2. Composition and sequence parameters of alginate from algal and bacterial alginates [64,67,71–75].

algal source	F_G	F_M	F_{GG}	F_{MM}	F_{MG}	$N_{G>1}$
Laminaria hyperborea (stipe)	0.68	0.32	0.57	0.28	0.10	14
Laminaria hyperborea (leaf)	0.46	0.54	0.36	0.43	0.18	8
Laminaria digitata	0.41	0.59	0.25	0.43	0.16	6
Ascophyllum nodosum	0.39	0.61	0.23	0.46	0.16	5
Durvillea antarctica	0.32	0.68	0.16	0.51	0.17	4
Laminaria japonica	0.65	0.35	0.18	0.48	0.17	–
Macrocystis pyrifera	0.39	0.61	0.16	0.38	0.23	6
Saccharina latissima	0.55	0.45	0.43	0.33	0.12	–
bacterial source						
Azotobacter vinelandii (AlgE4)	0.46	0.53	0.00	0.03	0.46	–
Azotobacter vinelandii (AlgE64)	0.82	0.18	0.73	0.10	0.09	–
Pseudomonas aeruginosa (epimerase-negative strain)	0	1	0	1	0	–

The main commercial applications for alginates are utilizing this unbranched polyanionic block copolymer for its potential as viscosifier, for instance in the paper or textile industry, and as emulsifier, stabilizer and gelling agent in the food industry [67]. The ability of alginate to form strong and stable, as well as thermally stable and biocompatible hydrogels through ionic crosslinking

expanded its utilization for a broad range of medical and pharmaceutical applications, from wound-dressing to drug delivery systems, cell encapsulation and 3D printing [24,29,76,77].

The most common ionically crosslinked alginate gels are established by the addition or release of multivalent cations (e.g. Ca^{2+}, Sr^{2+} and Ba^{2+}). The properties of the resulting hydrogel are influenced by the alginate itself as well as by the introduced cation. The affinity of alginate towards divalent cations increases in the following order: **Mg^{2+} < Mn^{2+} < Zn^{2+} < Ni^{2+} < Co^{2+} < Ca^{2+} < Sr^{2+} < Ba^{2+} < Cd^{2+} < Cu^{2+} < Pb^{2+}** [78]. This affinity of alginate towards divalent cations is rooted in a characteristic chelate-type ion-binding between the cation and G-blocks (see Figure 1-12), which is enable by the diaxial glycosidic linkage between two G-units, forming an intermolecular cavity between two G-blocks able to coordinate to a multivalent metal ion. This cation-G-block chelate complex is generally referred to as "egg-box-model" (see Figure 1-12 and Figure 1-13) [52,79]. The diequatorial glycosidic linkage between two M-units stereochemically prohibits the chelate-like coordination between a multivalent cation and two M-blocks, preventing the formation of a junction zone among them. An investigation into MG-block coordination to divalent cations revealed that MG-blocks can contribute to the gel formation and coordinate to metal ions that are already complexed by a G-block and form junction zones among each other. Even though, these junction zones and resulting gels are weaker than their G-block equivalent [77].
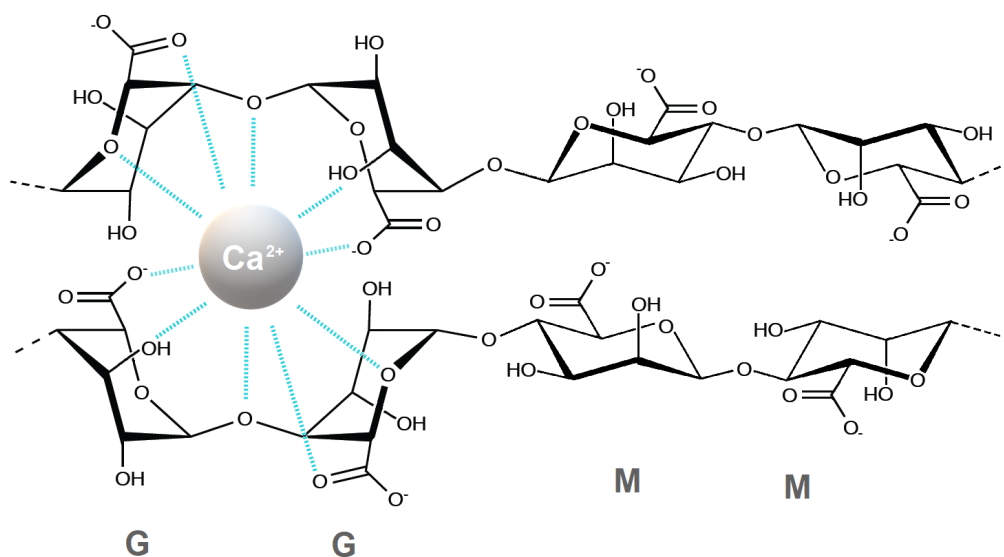
Figure 1-12 Chelate-like complexation of a calcium ion in between adjacent GG-sequences (left) of two alginate chains, MM-sequences (right); coordination indicated by blue dotted lines.

Among these alginates crosslinked by divalent cations, calcium-alginates are the most utilized and investigated type. Calcium-alginate hydrogels are intensively studied and exhibit broad utilization for cell immobilization and the protection of cells from the host's immune system [26,76,77,80]. These ionically crosslinked gels can be prepared through external gelation (diffusion method), by surrounding the dissolved alginate with a Ca^{2+} rich solution, resulting in a calcium-alginate gel formation predominately along the periphery of alginate solution. External gelation is characterized by rapid gelling kinetics and is often utilized for the immobilization of cells or bioactive agents by the encapsulation in microbeads [81]. During this method a droplets of alginate solution fall into a reservoir containing Ca^{2+} and form single gel beads entrapping its content.
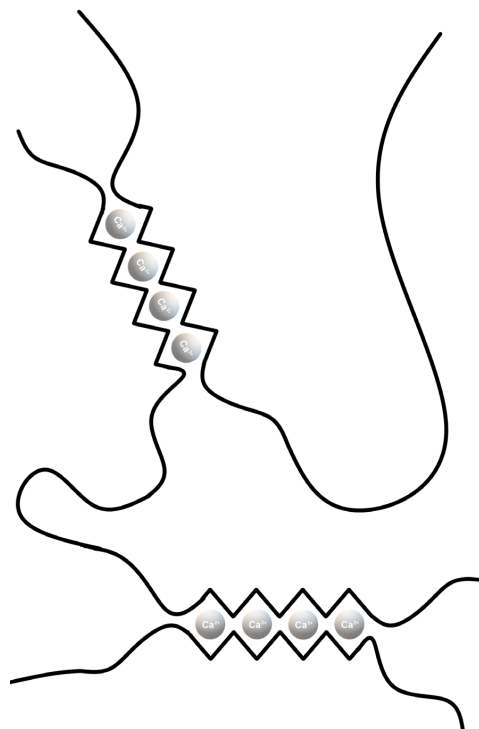
Figure 1-13 Egg-box model; G-blocks with 8 G-units each are forming a junction zone established by calcium ions (grey) between alginate a multitude of polymer chains.

A different method to external gelation is internal gelation [67]. This method is carried out by mixing insoluble calcium carbonate into the alginate solution, followed by a controlled decrease of the pH through a slow proton-donator such as the D-glucono-δ-lactone (GDL) [82], resulting in the homogeneous release of calcium ions (see Figure 1-14). The internal gelation is characterized by a slow gel formation homogeneous distribution of polymer chains and junction zones though out the gel.

As an alternative approach to the crosslinking of alginates by the formation of junction zones between divalent cations and G-blocks, Khong et al. [19] has investigated the crosslinking consecutive M-units of polymannuronic acid with fully deacetylated chitosan oligomers (D-units). These junction zones are stabilized by a match in charge distance within M-blocks and within chitosan. Both sugars, mannuronic acid from alginate and glucosamine from chitosan, are in $^4C_1$ conformation with diequatorial glycosidic linkages and exhibit a charge distance of 10.4 Å [83,84], whereas the G-blocks ($^1C_4$ conformation, diaxial glycosidic linkage) exhibit a shorter charge distance of only 8.7 Å [85] and do not form gels with polymannuronic acid (see Figure 1-15).
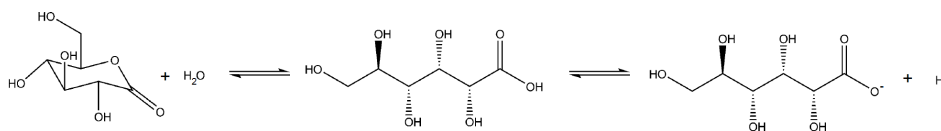
Figure 1-14 Slow release of protons by GDL – chemical equilibrium reaction of D-glucono-δ-lactone (left), D-gluconic acid and D-gluconate (right).

The junction zones are established through electrostatic interactions of the opposite charged M-blocks from alginate and D-blocks from chitosan. Hydrogen bonds between the polymer chains, as they are known from chitin, cellulose and many other polysaccharides [83,86,87], might contribute in stabilizing the junction zone. To create this kind of alginate gels, one component (either alginate or chitosan) needs to be in polymeric form, while the other one in oligomeric form. The components must be mixed in a pH regime, where the oligomer is uncharged. The pH can then be slowly adjusted to reach a pH regime where both components are charged. Again, the internal gelation method using GDL is well suitable to perform this step, creating a homogenous alginate hydrogel, crosslinked along the M-blocks (see Figure 1-16). Khong et al. demonstrated that this method is an

Figure 1-15 Simplified schematic depiction of intramolecular charge distances. deacetylated chitosan (top), M-block (centre), G-block (bottom).

alternative way to ionically crosslink alginates. This crosslinking mechanism is expanding the versatility of alginate hydrogels, is adding a layer of tunability (stronger pH dependence/response) and is utilizing the M-blocks for gel formation while keeping a high biocompatibility [88].
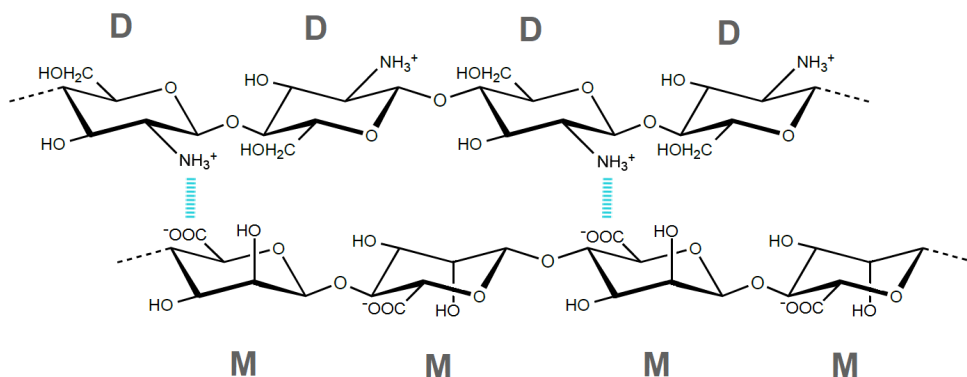
Figure 1-16 Electrostatic interaction (blue dotted line) between de-N-acetylated glucosamine units (D) of chitosan and mannuronic acid units (M) of alginate

1.4.1 Physicochemical properties and characterization of alginate

The chemical characterization of a polysaccharide, includes information about the sugar composition (for alginate the ratio of mannuronic and guluronic acid), the position and configuration of glycosidic linkages, the distribution or pattern of monomers within the polymer chain, potential branching points and the degree and pattern of functional groups (such as sulfate groups introduced through chemical modification or O-2 and O-3 acetylation occurring in bacterial alginates) [89,90]. For a full characterization, no single technique can be applied. However, a combination of different methods can reveal a conclusive picture of the composition and structure of any polysaccharide. Spectrophotometric methods such as circular dichroism (CD), have been useful tools in determining the monosaccharide composition of alginates (see chapter **1.4.1.3**). Nuclear magnetic resonance spectroscopy (NMR) can even reveal the various average block lengths of an alginate (see chapter **1.4.1.2**). Infrared (IR) and Raman spectroscopy can reveal the content of functional groups such as sulfate and acetyl and to some extent even linkage position at the monosaccharide ring structure (see chapter **1.6.1.1**). These spectrometric methods are none destructive and require low sample amounts. However, the obtained data through these methods are always averages over the whole molecule or even molecule mixture. To analyse fine structures of alginates and other polysaccharides mass spectrometry (MS) is a useful tool, elucidating the existence of unique linkage patterns and even full sequences [91–93]. Further inside on monosaccharide distributions and patterns in alginates has been gained by the combination of specific alginate lyases (cleaving the glycosidic linkage through an elimination reaction) with "high performance anion exchange chromatography with pulsed amperometric detection" (HPAEC-PAD), revealing extremely long G-blocks even in algal derived alginates [94,95].
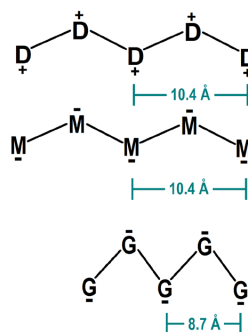
HPAEC-PAD uses a highly alkaline mobile phase (0.01–0.10 mol/L NaOH) is used instead of traditional mobile phases using Na_2SO_4, which are used rather for ionic strength than for pH regulation. At high pH above 12, small differences in the acidity of the hydroxyl groups in carbohydrates (common pK_a values are between 12 and 13) are utilized to achieve a high separation that cannot be obtained at lower pH. For the stationary phase a polymeric resin is used for non-porous microbeads, carrying anion-exchanging functional groups, electrostatically attached to larger cation-exchange resin particles. Although the total loading capacity is much lower than for porous packing materials, the band broadening is minimized, and achieved resolution is higher [96].

Beside the monosaccharide composition and sequences, biopolymers, such as the marine polysaccharides alginate, chitosan and fucoidan, naturally occur on a broad range of molecular weights. The extent of this molecular weight distribution is characterized by the term polydispersity or polydispersity index (PDI). In a copolymer like alginate, where the sugar units are epimers and therefor have the same molecular weight (M_0), the molecular weight of the polymer (M) is absolutely related to the degree of polymerization (DP), the number of sugar units in the polymer chain.

$$M = DP \cdot M_0 \tag{4}$$

The molecular weight of a polymer influences its solubility, viscosity in solution and its ability to form a hydrogel. Due to its polydispersity, the molar mass of an alginate is therefore determined as a molecular weight average. Most commonly used are the number average (M_n), weight average (M_w)

and the z-average (M_z), which is most sensitive towards the presence of the largest molecules in the sample [45].

$$M_n = \frac{\sum_i n_i \cdot M_i}{\sum_i n_i} \tag{5}$$

$$M_w = \frac{\sum_i n_i \cdot M_i^2}{\sum_i n_i \cdot M_i} \tag{6}$$

$$M_z = \frac{\sum_i n_i \cdot M_i^3}{\sum_i n_i \cdot M_i^2} \tag{7}$$

$$PDI = \frac{M_w}{M_n} \tag{8}$$

Further parameters that give insight into the properties of a biopolymer include the intrinsic viscosity ($[\eta]$) and the radius of gyration (R_G), also known as the root mean square (rms) radius [45]. The radius of gyration signifies the mass distribution around the centre of mass of the macromolecule (see Figure 1-17). It is an indirect expression of the polymers' degree of expansion, and defined as:

$$R_G^2 = \frac{\sum_i m_i \cdot r_i^2}{\sum_i m_i} \tag{9}$$

The viscosity of a solution is of both biological and technological importance. Viscosity can be defined as the measure of resistance of a fluid to deformation (flow) of a given rate (see chapter **1.3.1 Characterization of hydrogels**). The viscosity of a polymer solutions is not only influence by the molecular weight of a polymer, but also by the polymer's chain extension and shape, which ultimately constitutes the effective hydrodynamic volume occupied within the solution. The shape of the hydrodynamic volume can be seen as approach or conversion towards three idealized conformations: compact sphere, random coil and rigid rod (see Figure 1-18) [45]. All of these parameters: molecular weight average, polydispersity and polymer shape can be analysed for alginate as well as chitosan and fucoidan using SEC-MALS (see chapter **1.4.1.1 SEC-MALS**).
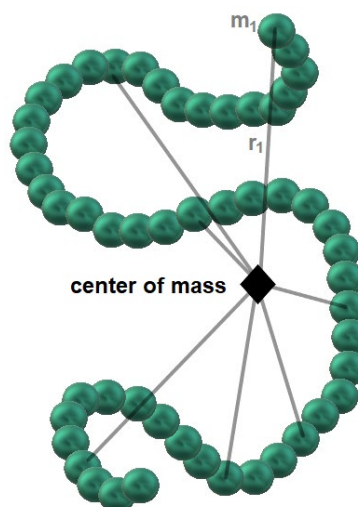
Figure 1-17 Illustration of the radius of gyration as the square mean of each mass (m) and their individual distance (r) towards a virtual centre of mass.
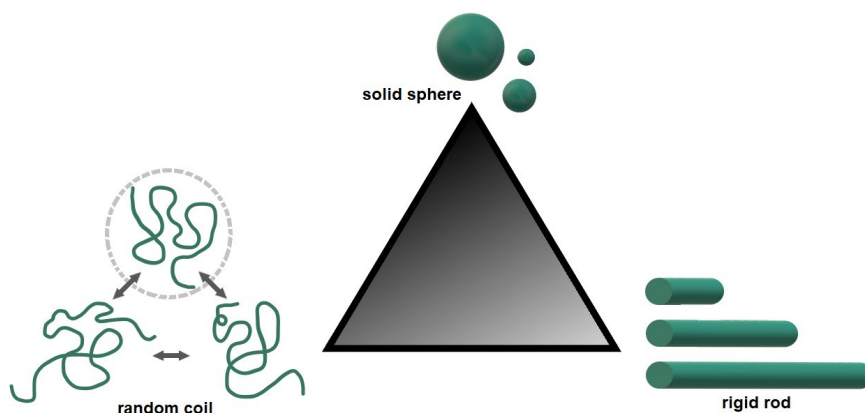
Figure 1-18 Haug's Triangle; illustration of the basic shapes of polymers in solution.

In aqueous solution, alginate has an extended random coil conformation due to electrostatic repulsion and inherent chain stiffness [97,98]. Because of the extended shape (towards rigid rod), alginate forms highly viscous solutions. The viscosity of an aqueous alginate solution is dependent on the alginate's molecular weight, the pH (charge density along the polymer chain and therefore repulsion and chain stiffness), the salt concentration (high ionic strength shields from electrostatic repulsion along the chain), as well as the temperature [99]. The intrinsic viscosity ([η]) is a polymers property, describing the inherent viscosity of a polymer in a given solution, independent of its concentration. It is an extrapolation of the specific viscosity (η_{sp}) towards zero concentration (c).

$$[\eta] = \lim_{c \to 0} \frac{\eta_{sp}}{c} \tag{10}$$

1.4.1.1 SEC-MALS

Size Exclusion Chromatography (SEC) coupled with Multi Angle Light Scattering (MALS) is combining a chromatographic method, separating molecules according to their molecular weight, in particular their hydrodynamic volume (see chapter **1.5.1.1**), with the ability of molecules in solution to scatter light based on their size.

Light scattering has become a common technique to determine the molecular weight of polymers and macromolecules. Light can interact with matter in various ways; absorption, reflection, transmission, refraction, diffraction, and scattering (see Figure 1-19).

Light scattering is caused by interactions between photons and their character as propagating wave in an electromagnetic field (light) and the electrons of a molecule or particle [100]. The molecule can be polarized due to interactions of the electron cloud through the electric field component of the light wave (see Figure 1-20). An oscillating dipole moment (μ) is induced, given as:

$$\mu = \alpha \cdot E \qquad (11)$$

Where α is a factor for the polarizability of the molecule and E represents the amplitude of the incident light, given as:

$$E = E_0 \cdot \cos 2\pi\nu t \qquad (12)$$

With ν as the frequency of the light wave (ν = c · λ) and t as time. The frequency is proportional to the wavelength (λ) and speed of light in vacuum (c). The polarizability α is related to the refractive index (n) by the equation:

$$n^2 - n_0^2 = 4\pi N\alpha \qquad (13)$$
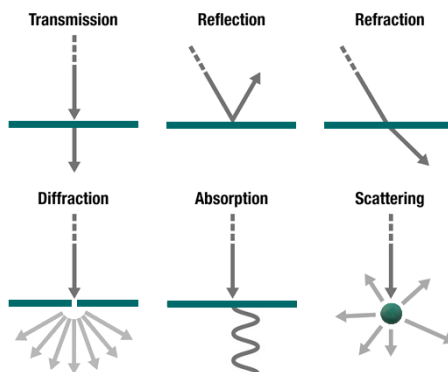
Figure 1-19 Illustration of the different possible interactions of light (grey) with matter (turquoise); absorption as heat energy or re-emission with modified frequency (waved line).

Where n_0 is the refractive index of the solvent and N the number of particles or molecules in solution, which is directly related to the concentration (c). Therefore, the refractive index and polarizability can be determined experimentally by the refractive index increment (dn/dc), through simply measuring the refractive index of different known concentration and plotting the slope.
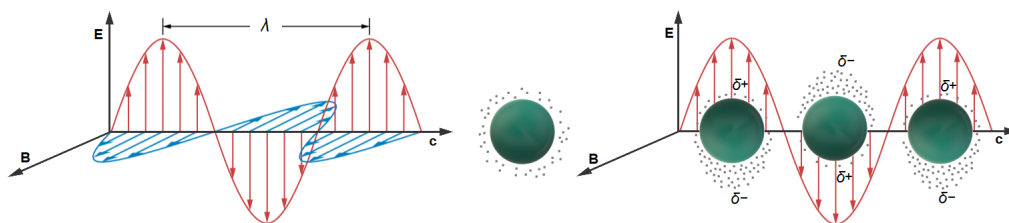
Figure 1-20 Light wave propagating in direction c; Oscillation in the electric field E (red); Oscillation in the magnetic field (blue); Wavelength λ; Molecule (turquoise) surrounded by electrons (grey dots); polarization of the molecule due to interaction of the electron cloud with the electric field of the light wave (right); Oscillating dipole illustrated by partial charges δ.

The oscillating dipole of a polarized molecule is a source for electromagnetic radiation. The emission occurs in the same wavelength as the incident light (elastic scattering) and in all direction [101]. However, the ratio of the intensity of incident light (I_0) versus scattered light (I_S) is extreme low and usually in an order of about 10^{-9}, given by the formula:

$$\frac{I_S}{I_0} = \frac{1}{\lambda^4} \qquad (14)$$

The scattering of light is dependent on the wavelength, but also on the size of the molecule or particle.

Figure 1-21 Illustration of a light wave scattered from a molecule (turquoise) at angle θ to the incident light (dashed arrow).

If the molecules in solution are smaller than 1/20 of the wavelength (R_G < λ/20) the scattering becomes practically independent from the scattering angle (isotropic scattering; scattering intensity follows the distribution of a regular Rayleigh scattering [102]). For an Nd:YAG laser with λ = 532 nm, this ratio transfers to an R_G of about 25 nm, which includes polysaccharides such as alginate and chitosan up to a molecular weight of approximately 100 kDa. With increasing molecular weight, the scattering decreases strongly towards higher scattering angles (anisotropic scattering). From the graphical shape of this decrease, information about the molecules size and shape (Figure 1-18) can be deduced [100]. The main scattering equation can be formulated as:

$$\frac{K \cdot c}{R_\theta} = \frac{1}{M_w} + 2A_2 \cdot c + \cdots \qquad (15)$$

Where R_θ is a Rayleigh factor accounting for the angular dependence of light scattering, K is an optical constant relating to the refractive index increment and wavelength and A_2 (simply called second virial coefficient) represents the interaction of molecules with the solvent and each other. A_2 accounts for the non-ideal character of the solvent and attractive (negative A_2) and repulsive (positive A_2) interactions between the molecules [103]. The general angular dependence of scattered light can be expressed as:

$$I_s = I_0 \frac{8\pi^4 \alpha^2}{\lambda^4 d^2} \cdot (1 + \cos^2 \theta) \qquad \longrightarrow \qquad R_\theta = \frac{I_s}{I_0} \cdot \left(\frac{d^2}{1 + \cos^2 \theta} \right) \qquad (16)$$

With d as the distance between the light source and the detector (instrument dependent). Large particles or molecules contain a multitude of scattering centres. These scattering centres are not moving independently from each other, as for small molecules, but interrelated. This results in very angular dependent interference patterns. To account for the angular dependent interference and anisotropic scattering of large molecules the factor P(θ) is introduced, leading to the full light scattering equation.

$$\frac{K \cdot c}{R_\theta} = P(\theta)^{-1} \cdot \left(\frac{1}{M_w} + 2A_2 \cdot c + \cdots \right) = \left(1 + \frac{16\pi^2 R_G^2}{3\lambda^2} \sin^2 \left(\frac{\theta}{2} \right) + \cdots \right) \cdot \left(\frac{1}{M_w} + 2A_2 \cdot c + \cdots \right) \qquad (17)$$

Polysaccharides naturally occur polydisperse, which makes them more similar to synthetic polymers than to other biopolymers such as proteins or DNA, regarding their molecular weight distribution [104]. Adding SEC to a MALS setup, fractionates the polydisperse sample into a large array of artificial slices (usually 1000–5000 depending on the experimental setup) [105]. The concentration of the sample within each slice is directly proportional to the refractive index determined by an RI-detector (alternatively a UV detector can be used, depending on the type of sample), while the scattering intensity is proportional to both, concentration and molecular weight (see equation 15).

Through a set of linear regressions and extrapolations; first to zero-angle (determining the M_w at the intercept ($\theta = 0$) and A_2 by the slope) followed by a plot to zero-concentration (Zimm-plot), the radius of gyration R_G can be determined [97].

Since SEC-MALS provides M_w and R_G data along the molecular weight distribution, the change in R_G can be plotted against M_w providing information about the shape of the examined molecule. The slope of a double-logarithmic plot provides us with the shape factor (a):

$$R_{G,i} = BM_i^a \qquad \longrightarrow \qquad \log R_{G,i} = a \log M_i + B \qquad (18)$$

Since B is a constant, the relation of M_w to R_G can be simplified to $R_G \propto M^a$. For the idealised shapes (see Figure 1-18) the radius of gyration will grow by a factor of a = 1 for a rigid rod, a = 0.333 for a sphere and a = 0.5–0.6 for a random coil shape (in a good solvent), which can be explained by a simple geometrical examination. Alginate fits similar to chitosan and pullulan best with the model of a random coil (see Table 1-3), while xanthan, due to its stiff double helical structure fits best with the model of a rigid rod [106].

Table 1-3. Examples for different polysaccharides in a good solvent, with their average molecular weight (M_w), second virial coefficient (A_2), refractive index increment (dn/dc) and shape factor (a).

polysaccharide	M_w	A_2	(dn/dc)	a
alginate [105]	297 kDa	$5 \cdot 10^{-3}$	0.151	0.60
chitosan [107]	270 kDa	$2–6 \cdot 10^{-3}$	0.142	0.59
pullulan P-1390 [105,108]	806 kDa	$2 \cdot 10^{-4}$	0.148	0.58
xanthan [106,109]	510 kDa	$1 \cdot 10^{-4}$	0.138	0.90–0.95

By analysing different alginates through classical light scattering, Smidsrød et al. established in 1973 that the relative chain extension of the three types of building blocks increased in the order **MG < MM < GG**, leading to the conclusion of highest flexibility in alginates rich in MG-blocks and highest stiffness for those rich in G-blocks [110]. A second and independent experimental approach to the study of chain stiffness in polyelectrolytes was established based on the dependence on the intrinsic viscosity and the ionic strength, the empirical B-parameter or Smidsrød-Parameter confirmed these results [111], as well as computer models (Monte Carlo model, Markov model) performed by Stokke et al. [112]. However, later studies by Christensen et al. (2006) saw no difference in chain extension, chain stiffness and persistence length for the three different blocks, at least within their given solvent conditions (ionic strength: 0.17 M and 1.0 M) [105].

1.4.1.2 NMR spectroscopy

Nuclear magnetic resonance spectroscopy is focussing on the magnetic properties of certain nuclei. Beside mass and charge, the nucleus of an atom also has the property of spin. The total nuclear spin (I) is an accumulation of spins of its nucleons (protons and neutrons). Both protons and neutrons possess a spin of ½. In an isotope with an even number of protons and neutrons (e.g. ^{12}C, ^{16}O, ^{32}S) the spins will cancel each other out, resulting in an overall spin of $I=0$ and therefore, have no magnetic dipole moment. Those atoms cannot be observed by NMR. If the proton or neutron number is odd, as characteristic spin of $I=½$ is found (e.g. ^{1}H, ^{13}C, ^{15}N; isotopes is most relevant for NMR).

From quantum mechanical considerations, it can be deduced that a nuclear spin I will have $2 I + 1$ possible orientations (i.e. two orientations for $I=½$ nuclei; α low energy, ß high energy). Without an external magnetic field (B_0), these orientations are of equal energy. If a magnetic field is applied, two things will occur: first, the orientations will split into spin states of different energy levels (ΔE) and second, spins will start to precess at the Larmor frequency (ω). The population at the different energy levels will follow a Boltzmann distribution, where lower energy levels are slightly more populated than higher energy ones. An NMR signal can be observed by exciting nuclei with a radiofrequency (ν) that matches the Larmor frequency [113,114].
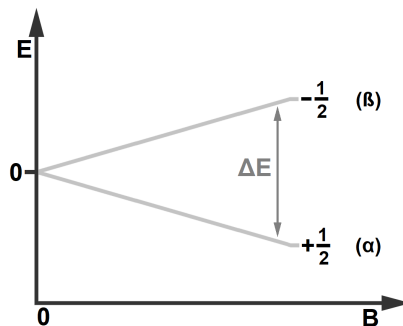
Figure 1-22 Schematic depiction of the energy difference (ΔE) between two spin states (½) increases with increasing magnetic field (B).

$$\Delta E = \frac{\gamma \mathrm{h} B_{eff}}{2\pi} \qquad \Delta E = \mathrm{h}\nu \qquad \omega = -\gamma B_{eff} \qquad (19)$$

The energy difference (ΔE) is the product of the effective magnetic field at the nucleus (B), the gyromagnetic ratio (γ) a constant for each nucleus, and the Planck constant (h). The external magnetic field (B_0) induces a counter magnetic field (B_i) in opposite direction in the electron shell, which partially shields the nucleus from B_0 (shielding). The nuclear spins therefore experience an effective magnetic field ($B_{eff} = B_0 - B_i$) that determines their spin precession frequency (equation 19). This electron-induced frequency variation is called the chemical shift (δ), which is the main component of NMR spectra and contains information about the electronic/chemical environment around the nucleus (i.e. molecular structure), and is influenced by the electron density in its surrounding. The NMR instrument detects the energy emission when the nucleus relaxes back from the excited state. From these data valuable information about the molecular structure and interaction can be obtained. Most notably, the chemical shift (δ), providing information about the composition of the atomic group. Other parameters that can be derived from NMR spectra are: the coupling constants, providing information about adjacent atom groups; the signal intensity, giving quantitative information on the detected nuclei; and relaxation time, giving information on the molecular dynamics. From these data valuable information about the molecular structure and interaction can be obtained.
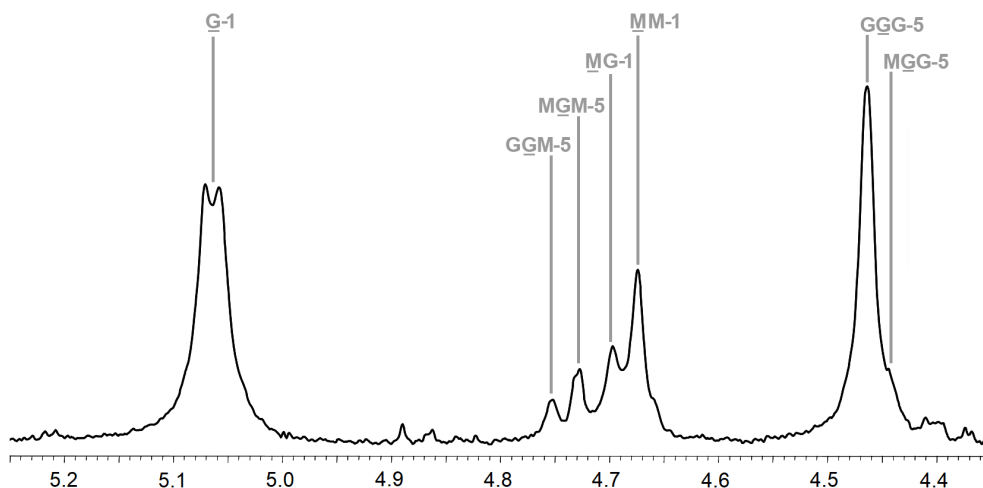
Figure 1-23 ^{1}H-NMR spectrum of the anomeric region for alginate from *Laminaria hyperborea* (300 MHz) recorded at 90 °C. Numbers (bottom, black) represent the chemical shift δ in ppm. Underlining refers to the observed saccharide in specific saccharide sequences (grey, numbers refer to specific protons of the underlined sugar unit).

NMR is a versatile technique for studying biopolymers such as proteins but also polysaccharides [115]. Many in depth studies have been performed, using NMR to elucidate the sugar composition, sequences and the average block lengths [69,116–120]. The introduction of high-resolution ^{1}H and ^{13}C NMR-spectroscopy makes it possible to determine not only the monad fractions F_M and F_G, but also the fraction of the four diads (neighbours within the polymer chain) F_{GG}, F_{GM}, F_{MG} and F_{MM}, and up to eight triads F_{GGM}, F_{MGG}, F_{GMG}, F_{MGM}, F_{GMM}, F_{MMG} and F_{MMM} as demonstrated in Figure 1-23.

The intensity (I) of each signal in the NMR spectrum is directly proportional to the protons (or carbons, depending on the NMR method) quantity within the molecule. The intensity can be determined by the area below each signal. The molar fractions within alginate can be calculated with a set of equations and obligatory relations to each other. Some are exemplified as follows:

$$F_G = \frac{I_G}{I_{total}}$$

$$F_M = 1 - F_G$$

$$F_G = F_{GM} + F_{GG}$$

$$1 = F_{GG} + F_{GM} + F_{MG} + F_{MM} \tag{20}$$

$$F_{GG} = F_{GGM} + F_{GGG}$$

$$F_{MGG} = F_{GGM}$$

21

A more detailed relation and elaboration can be found in Grasdalen et al. 1981 & 1983. In addition to obtaining the quantity of each fraction, even the average block length ($N_{G>1}$) can be calculated follows, elucidating a highly detailed picture of the sugar composition of this linear marine polysaccharide.

$$N_{G>1} = \frac{F_G - F_{MGM}}{F_{GGM}}$$

(21)

High field NMR spectroscopy represents a powerful tool to monitor reactions directly and to deduct reaction mechanisms. By quantifying reducing end resonances during an acid hydrolysis, Holtan et al. (2006) demonstrated that G–M glycosidic linkages were hydrolysed faster than M–G linkages (up to 12.8 times at pH 2.8 and 100 °C)[91]. Providing evidence of an intramolecular catalysis of the glycosidic cleavage through protons directly donated by the undissociated carboxyl groups.

1.4.1.3 Circular dichroism

Circular dichroism (CD) spectroscopy is an absorption spectroscopic technique, where the difference in absorption (A) of left-handed circular polarised light (LCP) and right-handed circular polarised light (RCP) by a medium is measured. CD occurs if a molecule contains one or more chiral chromophores (light-absorbing groups). Molecules that absorb LCP and RCP differently are optically active[121,122]. The CD of a chiral molecule is wavelength (λ) dependent and can be expressed as follows:

$$\Delta A = A_{LCP} - A_{RCP}$$

(22)

Electromagnetic radiation consists of oscillating electric and magnetic fields (waves) perpendicular to each other and to the direction of propagation (see Figure 1-20). Most light sources emit those waves oscillating at random angles perpendicular to the propagation direction.

Linear polarized light occurs when the electric field vector oscillates in a single plane. All polarised light states can be exemplified as the sum of two linearly polarised states at right angles to each other (usually referenced to as vertically and horizontally polarised light) displayed in Figure 1-24. If the vertically and horizontally polarised state are in phase with each other, the resultant wave ceases to be linear polarized. If the vertically and horizontally polarised states are out of phase, the resultant light wave will oscillate elliptically. If the two linear polarized states are out of phase by exactly ¼ of the wavelength, the resultant light will be circular polarized (see Figure 1-24). Here, the electric field vector maintains a constant magnitude while rotating around the propagation axis (one full rotation occurs in a distance equal to the wavelength). In linear polarized light the
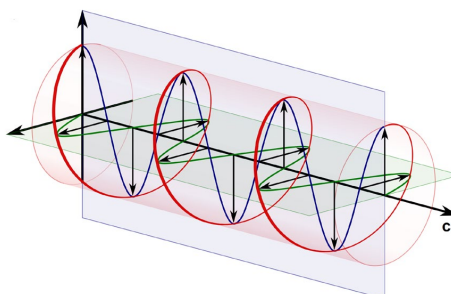
Figure 1-24 Circular polarized light (red) illustrated as the sum of two linearly polarized light states perpendicular to each other. The vertically (blue) and horizontally (green) state are out of phase by ¼ wavelength, resulting in circular oscillation, propagating in direction c.

direction of the vector direction stays constant while the magnitude oscillates. In circularly polarized light the vector magnitude stays constant while the direction oscillates. Although CD and optical rotation, which is measured using a polarimeter, are closely related, the CD of a chiral molecule can only be obtained at wavelengths that are being absorbed by the molecule [123].

CD is used to analyse all types and sizes of chiral molecules but finds its most important applications in the study of large biomolecules, since the CD spectrum of a macromolecule is not only the sum of chiral units but can reveal structures of higher order and detect conformational changes. The secondary structure of proteins can be distinguished between α-helix, β-sheet, and random coil structure of proteins as well as of mixtures thereof. Changes in conformation can be observed and plotted against changes in the chemical environment. Important factors that are often analysed are temperature, pH, solubility and interaction with other molecules [121,124,125].

Beside the absorption ΔA, other common units to express the CD are the molar absorptivity Δε, which is related to the absorption by the Lambert-Beer law, accounting for the concentration (c) of the sample and the length (l) of the sample cuvette, as well as the degree of ellipticity θ, which is a legacy unit, derived from a geometric examination of the difference in absorption of LCP and RCP [122].

$$A = \varepsilon \cdot c \cdot l \qquad \Delta\varepsilon = \varepsilon_{LCP} - \varepsilon_{RCP} \qquad \theta = \Delta A \cdot 32.982 \qquad (23)$$

The polysaccharide xanthan, which naturally occurs in a double helical structure, has been studied by Matsuda et al. (2009) monitoring the denaturation and renaturation of its double helix, along gradients of temperature, ionic strength, and sample concentration, using a CD spectrometer and SEC-MALS. The critical denaturation temperature was determined to be 80 °C while renaturation and aggregation patterns strongly depend on sample and salt concentration [106].

Alginate has been studied through circular dichroism in various ways. The three types of blocks M-blocks, G-blocks and MG-blocks differ essentially in their circular dichroism spectra (see Figure 1-25). While the poly-G lies completely in the area of negative ellipticity, poly-M shows an intense positive band between 190–210 nm, predominantly caused by n→π* transitions [126]. Morris et al. (1975) found that the M/G ratio can be calculated by the ratio of peak height to trough depth. However, it has been found that the CD spectrum of alternating MG-sequences, is not identical to an equimolar mixture of poly-M and poly-G. This made it possible, through a linear equation, to
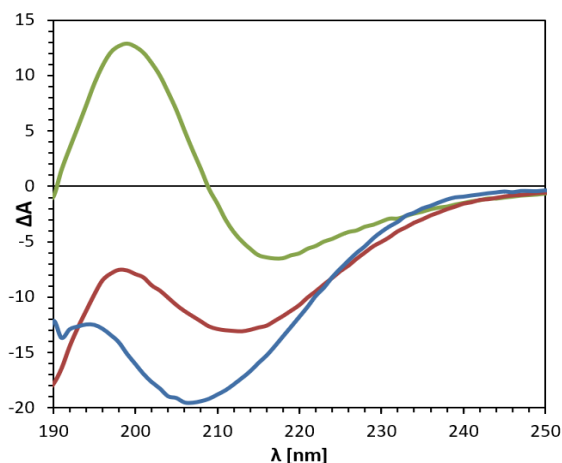
Figure 1-25 Circular Dichroism (CD) spectrum of three different alginates; poly-M (green), poly-G (blue) and poly-MG (red); sample concentration 0.4 g/L, recorded at pH = 4.5, T = 25°C, l = 1 cm.

determine the block composition of an alginate in a fast, non-destructive way, requiring low sample volumes [127]. Due to the availability of pure poly-MG, Donati et al. (2003) improved this equation by determining coefficients for all three diads (F_{MM}, F_{GG}, F_{MG+GM}) from pure M-, G- and MG-polymers, increasing the accuracy of determining the block composition of an alginate [125].

Further has CD spectroscopy been used to investigate the coordination of alginate to calcium ions, giving additional insight in the formation of hydrogels and the associated "egg-box" formation (see Figure 1-13). Donati et al. (2005) recorded CD spectra of poly-M, poly-G and poly-MG with and without the addition of calcium [128]. After the addition of Ca^{2+} a coordinating effect, leading to a change in polymer conformation (higher order), was clearly demonstrated for both poly-G and poly-MG (albeit to a lesser degree in the latter polymer), whereas poly-M showed no conformational changes in presence of calcium (see Figure 1-26). The findings provided further evidence to the egg-box-model (for G-blocks) and indicate the ability of poly-MG to form cavities along the polysaccharide chain, suitable to accommodate divalent cations in a chelate type of binding, although weaker than for poly-G. In combination with Young's modulus, rheology and syneresis analysis the presence of MG/MG junction zones as well as GG/MG junctions in calcium alginate hydrogels was suggested.

Figure 1-26 CD spectra of three of three different alginates (solid line), upon addition of calcium ions (dotted line); poly-M (top), poly-MG (centre) and poly-G (bottom); illustration taken from Donati et al (2005).

CD spectra of alginate coordinated with the positively charged aromatic compound pinacyanol, have been shown to form different kinds of aggregates both at different concentration levels as well as for either guluronate-rich or mannuronate-rich alginate [129].

1.5 Chitosan

Chitosans are derived from one of nature's most abundant biopolymers, chitin. They form a family of linear polysaccharides consisting of (1→4)-β-linked 2-acetamido-2-deoxy-D-glucopyranose (GlcNAc or A-unit) and its de-N-acetylated analogue 2-amino-2-deoxy-D-glucopyranose or shorter glucosamine (GlcN or D-unit) shown in see Figure 1-27. These polycationic polysaccharides can be prepared with varying degree of acetylation (F_A) and polymerization (DP) [130]. The amine-group of the D-unit has a pKa-value of ca. 6.5 [131–133]. Therefore, the pH value effects the overall charge of the polymer and many of its properties such as its water-solubility [134].
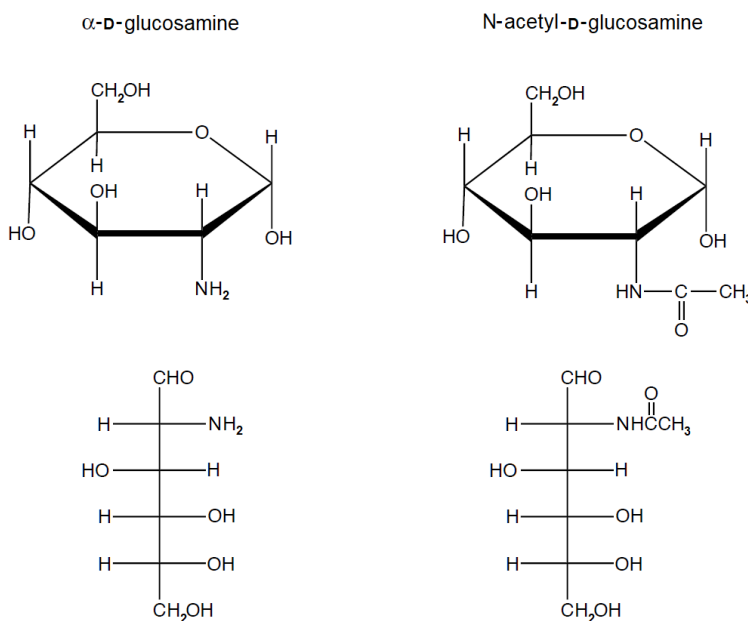
Figure 1-27 Haworth (top) and Fischer (bottom) projection of the two monosaccharides α-D-Glucosamine (left) and N-acetyl-α-D-glucosamine (right), the two monomer units compiling chitosan.

Chitosan is usually generated by de-N-acetylation of chitin, through a chemical treatment of chitin in strong alkaline conditions [135–138]. In nature, chitin exists in three different crystalline allomorphs: the α-, β- and γ-form [139]. These differ in the alignment of the polymer chains or orientation of the microfibrils. The most common form is α-chitin, where the adjacent polymer chains run in opposite directions (antiparallel). This structure is stabilized by inter- and intramolecular hydrogen bonds (see Figure 1-28). The polymer chains eventually crystallize and form microfibrils by self-assembly [140].

While in α-chitin, the layers of polymer chains are arranged in an anti-parallel fashion, β-chitin has a parallel chain arrangement [140,141]. In this parallel alignment, in β-chitin the poly-N-acetylglucosamine chains only form intramolecular hydrogen bonds, and no H-bonds between the chains. The result of this parallel arrangement is higher flexibility than in the antiparallel arrangement of α-chitin [142]. Nevertheless, β-chitin still provides an enormous structural strength [142–144].
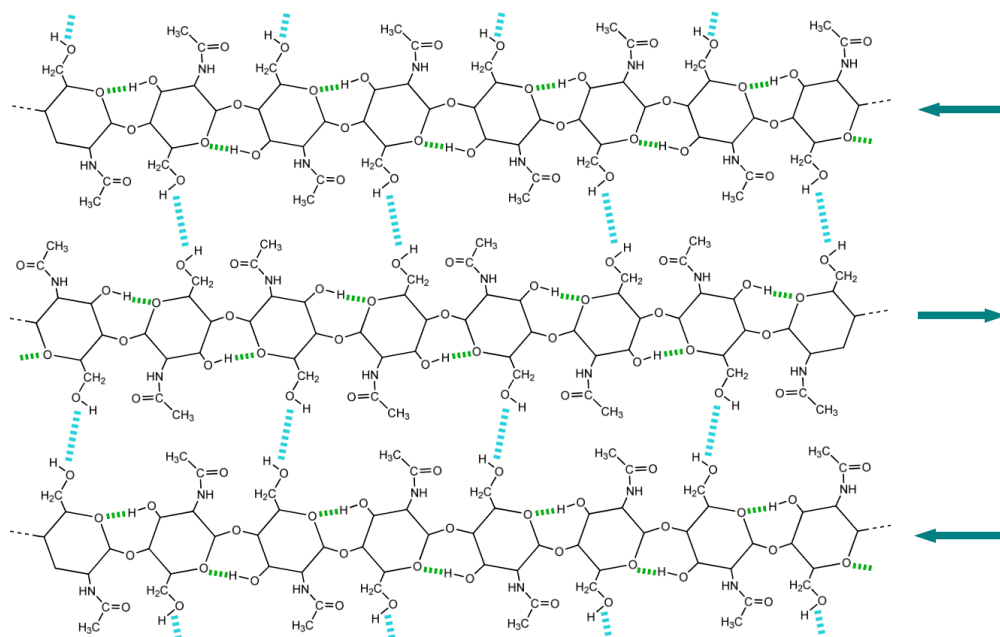
Figure 1-28 Structure of α-chitin with chitin polymer chains running in antiparallel direction (arrow direction towards the non-reducing end). The crystal structure is stabilized by intramolecular hydrogen bonds (green) and intermolecular hydrogen bonds (blue). [illustration adapted and modified from Khong (2013) [145]].

In γ-chitin, the third allomorph, every third polysaccharide chain is arranged antiparallel to the two preceding ones (see Figure 1-29). γ-Chitin has been isolated from mushrooms [146], while β-chitin has been found in the exoskeleton of insects, the cell wall of microalga, squid-bones and fungi [88,146–148].

However, the most common form of chitin in nature remains α-chitin, which is the major structural polysaccharide for building the hard exoskeletons of crustaceans and insects [139].

In every organism, chitin is found covalently crosslinked to other structural components, except for the β-chitin found in diatoms. Covalent linkages have been determined towards glucans in fungal cell walls, either

Figure 1-29 Illustration of the poly-N-acetylglucoseamine chain arrangement within the three different crystalline forms of chitin, α-, β- and γ-chitin

directly, as glycosidic linkage or via peptide bridges [149]. In crustaceans, the peculiar hardness of their exoskeleton is achieved through mineralization, especially calcification through $CaCO_3$, of their chitin shell. In terrestrial insects sclerotization, the crosslinking through phenolic compounds plays a bigger role in hardening the shell [150,151].

Chitosan from crustacean shells, the main industrial source for chitin, is generated by first demineralizing the shells in acid, using acid concentrations from 0.25 to 2 mol/L (most often HCl) and for 1 to 48 h at temperatures from 0 to 100 °C [152].

$$2\ HCl + CaCO_3 \longrightarrow CaCl_2 + H2O + CO_2\uparrow$$

Beside dissolving the calcium carbonate and related salts within the shell, the present acid is also catalysing the hydrolysis of the glycosidic linkages in the chitin molecules, leading to a depolymerization. Partial de-N-acetylation occurs in addition. However, it has been shown that the rate of acid-catalysed de-N-acetylation at the given conditions is much lower than the rate of depolymerization [153]. In order to reduce the partial depolymerization of the polysaccharide chains, organic acids, such as formic-, acetic-, and citric acid, have been tried for demineralization too, leading to longer polymer chains (higher M_w) but reduced yield [154].

After demineralization, a deproteination is performed, using alkaline conditions at elevated temperatures. Usually NaOH or KOH are used at concentrations from 0.125 to 5.0 mol/L, and temperatures ranging from 30 to 100 °C but also up to 160 °C [139,154]. Similar to the demineralisation the harsh alkaline environment also leads to a partial deacetylation and depolymerization, although the alkaline hydrolysation rate of glycosidic linkages is relatively slow in most sugars, including GlcNAc and GlcN in chitosan. Still, in order to chemically break the relatively stable peptide bonds within the proteins, and between proteins and chitin, the right deproteination conditions have to be chosen according to the targeted chitin or chitosan [155].

The de-N-acetylation is performed at even harsher conditions in 50% NaOH solution (about 19 mol/L) and at high temperatures up to 121 °C [139]. Chitosan with a low degree of acetylation (F_A) and high molecular weight can be obtained through a multi-step de-N-acetylation process [156]. The reported activation energies, for the de-N-acetylation of GlcNAc, range from 16.2 to 56 kJ/mol [157,158], while the activation energy for the alkaline hydrolysis of glycosidic linkages (starch and cellulose) has been reported ranging from 105 to 249 kJ/mol [158,159].

Analog to alginates and their M- and G-units, the content of A- and D-units in chitosan is given as a fraction of acetylated and deacetylated sugar units (GlcNAc and GlcN), the F_A or more commonly referred to as the degree of acetylation (DA) and deacetylation (DD), with the definition:

$$DA = \frac{n_{GlcNAc}}{n_{GlcNAc} + n_{GlcN}} = 1 - DD \tag{24}$$

The A and D distribution in chitosan always appears in random order, which is the necessary consequence of the chemical deacetylation method. Most commercial chitosans have an F_A between 0.001 and 0.70 and are in an M_w range from 300–500 kDa [138].
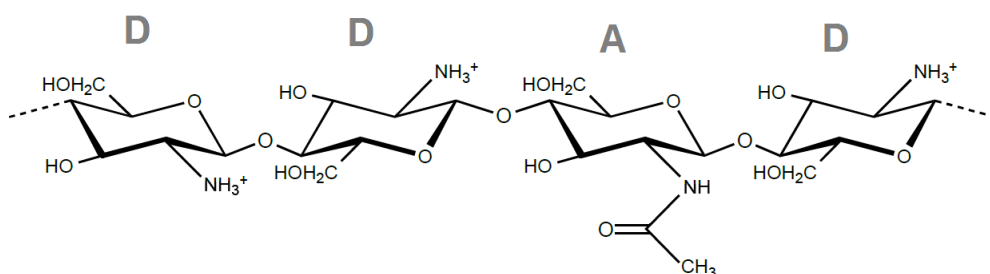
Figure 1-30 Section from a chitosan chain with an F_A = 0.25; Monosaccharide units: de-N-acetylated glucosamine (D) units, N-acetyl-glucosamine (A).

Chitosan, just as alginate, can form stable, fully biocompatible hydrogels, through ionic crosslinking. Research studies have shown that beside using alginate oligomers as a crosslinker, applying the internal gelation method (setup: chitosan polymers and alginate oligomer, see chapter **1.4**), chitosan can also form hydrogels with multiple negatively charged oligomers such as tripolyphosphate, applying a diffusion method using a semipermeable membrane [19,160]. The external gelation via dropping a chitosan solution into a reservoir containing polymeric polyanions is also applicable.

Long chitosan chains, able to form viscous hydrogels or strong fibres with unique properties, due to their polycationic nature, can further be used to prepare oligomer fragments, referred to as Chito-oligosaccharides (CHOS). Both chemical and enzymatical methods can be utilized, resulting in CHOS with different DP, F_A and sequence patterns CHOS [84]. An extensive study on chitinase B (Chi-B), revealed that this enzyme cleaves chitosan only if an acetyl unit is present in -1 chain position, therefore always leaving an acetylated monosaccharide unit at the reducing end of the sugar chain, a further tool to generate and modify tailored CHOS [84,161].

For the chemical preparation of CHOS, acid hydrolysis is commonly used. The acid catalysed hydrolysation cleaves the glycosidic linkage with 2 to 3 orders of magnitude faster for A–A and A–D linkages than for D–A and D–D linkages, where a positively charged amino group is in close proximity to the glycosidic linkage. It further has been found that the rate of acid catalysed de-N-acetylation is 54 times lower than the hydrolysis of a glycosidic linkage prior to a D-unit [162]. An additional chemical method for generating CHOS is the degradation with nitrous acid (HNO_2), which leads to the formation of 2,5-anhydro-D-mannose at the reducing end [161]. Here the chain scission occurs as a result of the de-amination of GlcN followed by the formation of the furanose ring, while A-units (GlcNAc) remain unaffected.

CHOS have attracted much attention in recent years as they have been suggested to exhibit numerous biological effects, which are utilizes for instance for tumour growth inhibition, as inhibitors for fungal growth on crops or as vectors in gene therapy [18,160,161,163]. Chitosan is known for its high biocompatibility, biodegradability [164,165] and low toxicity [166,167], and even antiviral and antibacterial effects have been shown [88,168–170].

Those properties while simultaneously being the only naturally occurring polycationic biopolymer makes chitosan suitable for a magnitude of applications pharmaceutical and medical field such as drug delivery systems, implants and wound healing devices [171–173]. Tailoring of chitosans with respect to DP, polydispersity, F_A and acetyl distribution is providing tools for controlling their function and properties in relation to their biological effects and makes them a highly suitable material for developing new biomaterials and biomedical applications.

1.5.1 Chemical characterization of chitosan

The parameters with the highest impact on chitins and chitosans properties are the molecular weight (M_w), the degree of acetylation (F_A), and for chitin the degree of crystallinity (x_c). Crystallinity refers to the degree of structural order within a solid. In a perfect crystal, all atoms and molecules are arranged in a repetitive pattern of identical unit cell towards all directions in space, expressing long-range order. Chitin polymer chains stabilize by inter- and intramolecular hydrogen bonds (see Figure 1-28), increasing the hardness of the material and reducing its solubility [174]. The degree of crystallinity of a polymer refers to the mass fraction in crystalline state versus in amorphous state. The degree of crystallinity is usually determined through X-ray diffraction, especially powder X-ray diffraction (XRD), by comparing the intensity of the diffracted X-rays from crystalline regions (I_c) against the halo intensity diffracted from the amorphous region (I_a) [175]. Beside XRD, which is the most common technique, the crystallinity can be determined by calorimetric methods such as differential scanning calorimetry (DSC) or calorimetric combustion, comparing the combustion enthalpy (or melting enthalpy for DSC respectively) of the analysed sample (H_s) with values obtained from ideal crystals (H_c) and fully amorphous material (H_a) of the same polymer [176].

$$x_c = \frac{I_c}{I_c + I_a} = \frac{H_a - H_s}{H_a - H_c} \tag{25}$$

In addition to chitin, a biopolymer where crystallinity has a large impact on its characteristics and applications is cellulose, which is found in the cell wall of all three types of macroalgae; red, green and brown seaweed [87,177–179].

The molecular weight of polymeric chitin and chitosan can be analysed using SEC-MALS, similar to other polysaccharides like alginate and fucoidan (chapter **1.4.1.1**). However, the low solubility of highly acetylated chitin limits the applicability. Further does the pK_a-value of ca. 6.5 (for deacetylated glucosamine units) need consideration for adjusting the pH of the eluent in the chromatographic system. The degree of polymerisation (DP) and DP-distribution of chitosan and chito-oligosaccharides (CHOS) can be determined precisely by coupling size exclusion chromatography with an RI-detector

(see chapter **1.5.1.1**). The degree of acetylation can be easily determined by UV-spectroscopy. The absorbance maximum for N-acetyl glucosamine is found at λ_{max} = 201 nm, where the absorbance is approximately 130 times stronger than for glucosamine, which can be neglected [180,181]. Further common methods to determine the F_A are IR-spectroscopy, focussing on the carbonyl stretching vibration at wavenumber $v_{C=O}$ = 1663 cm^{-1} and 1626 cm^{-1} of the acetyl group [182,183], and destructive methods such as elemental analysis, measuring the nitrogen content in relation to carbon, where a C/N-ratio of 5.145 represents fully de-N-acetylated chitosan an 6.861 fully acetylated chitin [184,185]; and pyrolysis coupled with gas chromatography (GC), where chitin or chitosan is pyrolyzed at about 450 °C, forming acetaldehyde beside various other volatile nitrogen and carbon containing compounds, enabling the calculation of the F_A [186]. However, both pyrolysis and elemental analysis are very sensitive towards impurities of proteins (N).

Furthermore, circular dichroism (see chapter **1.4.1.3**) can be used to determine the degree of acetylation, detecting an n→π* transition, located around 211 nm. This transition is independent of the α-β-anomeric equilibrium, degree of polymerization, pH and ionic strength [187,188].

NMR spectroscopy (**1.4.1.2**) has been proven to be a powerful tool for analysing various aspects of chitosans and especially CHOS. Chitin's poor solubility in most solvents reduces the applicability of this technique. However, Einbu & Vårum (2008) obtained ^{1}H-NMR spectra of chitin, dissolved and hydrolysed in concentrated DCl (37% wt.) [162]. In this experiment, the solubility was increased by heating the chitin, suspended in DCl up to 40 °C for (30 min.). The F_A was calculated based on the intensity of the H-1 and H-2 proton signals coming from GlcNAc versus GlcN. Albeit, in those strongly acidic conditions, potential deacetylation has to be considered. An additional approach is to estimate the F_A based on the intensities of the methyl group protons, located at the acetyl group versus the combined intensity of the H-2 to H-6 protons along the pyranose ring [189].

1.5.1.1 Size Exclusion Chromatography (SEC)

Chromatography is a collective term for several separation methods that separate molecules or particles based on their size (M_w and shape), total charge, polarity or volatility [190]. Size exclusion chromatography (SEC) utilizes porous materials, such as silica, alumina, kieselguhr (diatoms), polyamide, polycarbonate and polyacrylonitrile as well as organic materials such as agarose-dextran-composites (Superdex®) or large covalently crosslinked cellulose particles (Spherilose®) as stationary phase, while the mobile phase can be any eluent that dissolves the analysed sample properly and in case of charged molecules, provides sufficient ionic strength and pH buffer capacity [190].
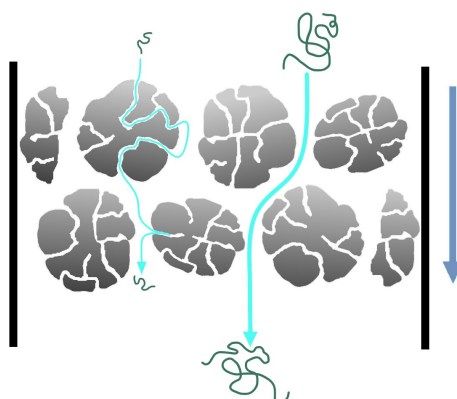
Figure 1-31 Schematic depiction of the SEC principle. An eluent (flow direction, blue arrow) is passing through a column filled with porous material (grey). Polymers (turquoise) are passing the porous material in different paths (cyan arrows) according to their size, leading to different elution times.

SEC separates molecule mixtures along their hydrodynamic volume (influenced by their molecular weight, shape, and charge). The stationary phase consists of spherical porous particles with roughly defined pore sizes. The eluent within these pores can be assigned to the stationary phase too. The mobile phase is the solvent (eluent) that flows between the spherical porous particles. Eluent exchange from the mobile phase to the porous stationary phase is rather caused by diffusion than by directional flow [191].

If the polydisperse sample is dissolved in a small volume of the mobile phase (eluent) and injected into the SEC-system, the molecules of various size and shape travel through the column filled with porous packing material (stationary phase). Molecules with a hydrodynamic volume significantly larger than the pore size of the packing material are excluded from diffusion into the pores and elute faster. They are only present in the interstitial liquid with little to no retention. Smaller particles can enter the different pores, leading to longer retention times due to diffusion. The smaller the molecules, the deeper and more frequent the pores can be entered, and the longer the retention time (see Figure 1-31). The degree of retention in the column depends on the hydrodynamic volume of the molecules relative to the pore size. The separation capacity (dependant on column material, column, length, eluent and sample) can be expressed by the plate number, which sets the total retention time (peak maximum) in relation to the peak width [192]. The plate number is a pure theoretical value, helping to evaluate the performance of an SEC system.

In addition to the DP, DP distribution and even determining acetylation [161], SEC is mainly used for preparative separation (fractionation) of molecules as well es for purification. All three aspects can be seen in Figure 1-32. The DP distribution can be determined by calculating and comparing the area of each oligomer peak (blue dotted lines). After separation through the SEC columns, fractions of individual oligomers or oligomer mixtures can be isolated (red line). Additional purification occurs due to removal of salt, which naturally exposes the longest retention time (salt peak) [192].
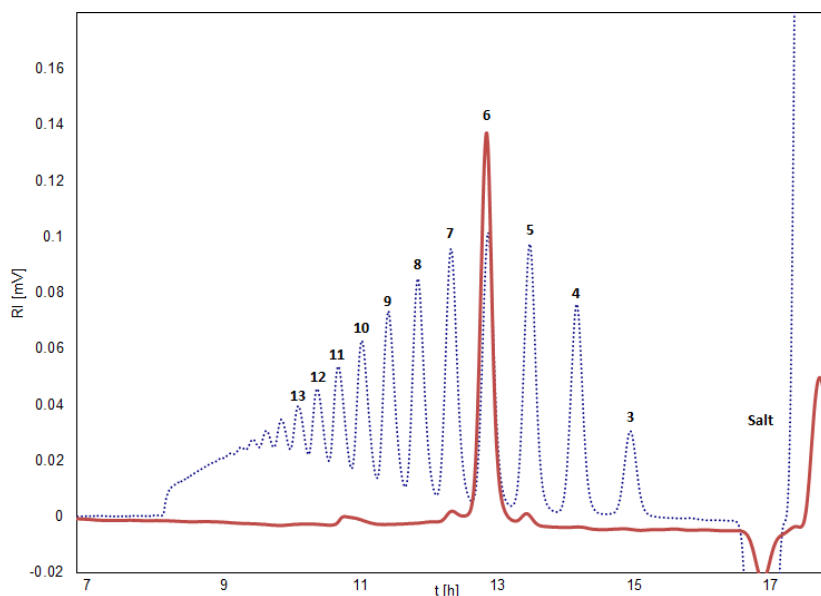
Figure 1-32 Chromatogram of a chitosan oligomer mixture (blue dotted line); DP of each oligomer (bold black numbers); isolated hexamer fraction (red line) re-run on the SEC-system.

1.6 Fucoidan

Fucoidans are sulfated polysaccharides, predominantly consisting of the sugar unit L-fucose (see Figure 1-33). They are mostly found in brown seaweeds (*Phaeophyta*) [193], but also occur in *echinoderms*, marine invertebrates like sea urchins, sea cucumbers, and sea stars [194–197]. Fucoidans are a diverse group of bio-molecules with highly heterogeneous structures. Their chemical structures differ in terms of sugar composition, glycosidic linkages, branching points, molecular weight, degree of sulfation as well as degree of acetylation [198–200].
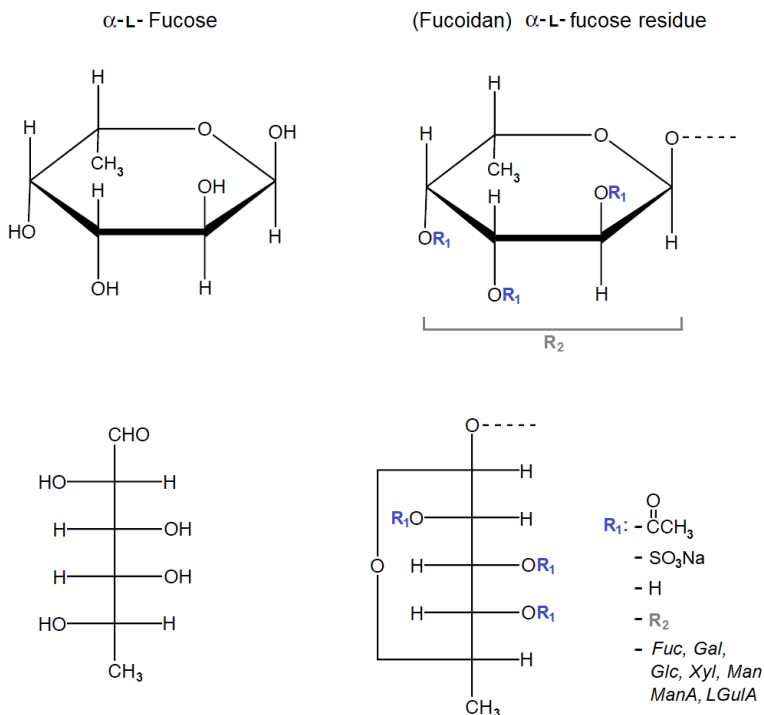
Figure 1-33 Haworth (top) and Fischer (bottom) projection of α-L-fucose (left) and an α-L-fucose residue within fucoidan (right), displaying the multiplicity of residues, functional groups and branching points.

The first isolation and partial characterization of "fucoidin" (former term) was conducted by Harald Kylin in 1913 [201]. The name fucoidan was introduced in 1959 by McNeely in order to conform with IUPAC nomenclature, recommending the suffix '-ose' for monosaccharides and '-an' for polysaccharides based on this particular sugar residue [202,203]. The term fucoidan has changed over time, covering a large array of fucose containing sulfated polysaccharides (FCSP).

In order to systematize the nomenclature of this highly diverse group bio-macromolecules, Deniaud-Bouët et al. (2017), have extensively discussed structural features of FCSPs and attributed IUPAC recommendations accordingly [204]. Deniaud-Bouët recommends the term fucan for FCSPs if the backbone structure is based on fucosyl residues while the term fucoidan should be used for FCSP with a diverse backbone structure containing various neutral sugars and/or uronic acids. Under this

definition, fucoidans include a great diversity of polysaccharides of heterogeneous composition (i.e. fucogalactans, fucoglucuromannans, xylofucoglucuromannans) and origin [199,205]. Consequently, a correct denomination of FCSPs requires not only knowledge about the monosaccharide composition, but also a structural elucidation, in particular of the backbone structure, which to this day is a challenging task. Instead of a full structural characterization, in most studies only aspects of the molecular structure or composition are investigated. Due to the high prevalence in literature and commercial products, the well-established term fucoidan will be used in this thesis synonymously with FCSP, comprising the entirety of this diverse group of fucose containing sulfated polysaccharides.

Different structural characteristics will lead to different chemical, physical and in particular bioactive properties [206–209]. Highly relevant for the emerging market of medical and pharmacological fucoidan applications (see in chapter **1.6.2.**).

To provide an overview of the differences in monosaccharide composition, molecular weight, degree of sulfation (DS), degree of acetylation (F_A), and branching, Table 1-4 shows the chemical composition of various fucoidans that have been intensely studied over the last decades. Furthermore, suggested backbone structures, repeating units and determined structural fragments are provided, to the extent that these highly complex marine polysaccharides are elucidated so far.

Homogeneous chemical structures with strict glycosidic linkage patterns can be found in fucoidans isolated from the phylum of *echinoderms*, marine animals with approximately 7000 described living species, with no freshwater or terrestrial representative [210]. Most echinodermal fucoidans are sulfated homopolymers composed of fucose-oligosaccharide repeating units, which only slightly differ in patterns of sulfation or fucosylation [211,212]. Some of these fucans are even reported to be fully linear (e.g. *Thelenota ananas*, *Lytechinus variegates*, *Arbacia lixula*), showing much less complexity than their algal counterparts [195,213]. Even with a regular fucose backbone structure, fucans found in brown seaweed remain highly heterogenous, often containing significant portions of galactose, xylose, glucose, mannose, uronic acids, rhamnose and other sugars, and are highly and randomly branched [211]. According to their sugar composition fucans can be further classified into xylofucans, containing predominantly fucose and xylose (e.g. *Punctaria plantaginea*) or galactofucans, containing mostly fucose and galactose (e.g. *Saccharina longicruris*, *Undaria pinnatifida*, *Sargassum polycystum*, *Laminaria japonica*) [199,205,214–217].

The backbone structure of most fucoidans consists of (1→3) and (1→4) glycosidic linkages (e.g. *Ascophyllum nodosum*, *Fucus serratus*, *Fucus vesiculosus*) [198,218–220]. Side chains are most often linked through (1→2) or (1→4) glycosidic linkages. The sulfate content also varies considerably from 14.5% as in *Cladosiphon novae* up to 53.8% in *Laminaria hyperborea* [209,221].

Table 1-4. Overview of chemical composition and structure suggestions of fucoidans from different algal and echinodermal sources. The sugar composition is given relative to 100%, different uronic acids as summarized as UrA. The sulfate content is based on the total dry weight (w/w), (* sulfate content is calculated based on provided DS). The average molecular weight M_w is based on the highest reported values so far (only including purified but not deliberately degraded fucoidans).

Algal source	Sugar composition [%]		NaSO$_3$ [%, w/w]	M_w [kDa]	Structure (suggestion)	Ref.
Ascophyllum nodosum	Fuc: Gal: Glc: Man: Xyl: UrA:	54.5 9.6 2.3 5.3 9.0 19.3	24.4	1486	Backbone: [→3)-α-L-Fuc(2SO$_3$⁻)-(1→4)- α-L-Fuc(2,3-diSO$_3$⁻)-(1→] Substituents: Other sugar residues mostly located at C-4	[198,200,219,222]
Chorda filum	Fuc: Gal: Glc: Man: Xyl: UrA:	76.9 2.3 3.1 1.5 traces 15.4	17	–	Backbone: [→3)-α-L-Fuc-(1→3)-α-L-Fuc-(1→3)-α-L-Fuc-(1→3)-α-L-Fuc-(1→3[α-L-Fuc-(1→2)])-α-L-Fuc-(1→] Substituents: Sulfate groups mainly located at C-4, partially at C-2, partial acetylation at C-2	[223]
Cladosiphon okamuranus	Fuc: Gal: Glc: Man: Xyl: UrA:	54.0 – 3.8 – 1.2 40.9	15.1	200	Backbone: [→3)-α-L-Fuc(4SO$_3$⁻)-(1→3[α-D-UrA-(1→2)])-α-L-Fuc(4SO$_3$⁻)-(1→3)- α-L-Fuc-(1→3)- α-L-Fuc-(1→]	[198,224,225]
Cystoseira sedoides	Fuc: Gal: Glc: Man: Xyl: UrA:	89 – – – – 11	16.3	642	Substituents: Most sulfate groups located at the C-2 and C-3 position	[226]
Fucus distichus	Fuc: Gal: Glc: Man: Xyl: UrA:	96.2 1.9 – – 1.9 traces	34.8	85	Backbone: [→3)-α-L-Fuc(2,4-diSO$_3$⁻)-(1→4)-α-L-Fuc(2SO$_3$⁻)-(1→] Comment: O-acetylation detected in traces in IR and NMR	[198,227–229]
Fucus evanescens	Fuc: Gal: Glc: Man: Xyl: UrA:	94.8 2.6 – – 2.6 traces	36.3	181	Backbone: [→3)-α-L-Fuc(2SO$_3$⁻)-(1→4)-α-L-Fuc(2SO$_3$⁻)-(1→] Comment: Alternating 1→3 and 1→4 linkages with sulfate at C-2 position, partly acetylated at C-4	[198,227,230,231]
Fucus serratus	Fuc: Gal: Glc: Man: Xyl: UrA:	56.0 10.8 4.5 4.7 5.4 18.5	29.2	602	Backbone: [→3)-α-L-Fuc(2SO$_3$⁻)-(1→4)-α-L-Fuc(2SO$_3$⁻)-(1→] Fragments: [→3)-α-L-Fuc-(1→4[α-L-Fuc-(1→4)-α-L-Fuc(1→3)])-α-L-Fuc-(1→4)-α-L-Fuc-(1→] Substituents: Sulfate groups mainly located at C-2, partially at C-4, acetyl groups were detected at C-4 of 1→3 linked fucose residues	[198,218,231]
Fucus vesiculosus	Fuc: Gal: Glc: Man: Xyl: UrA:	53.2 10.2 4.5 6.3 4.9 21.0	23.6	1328	Backbone: [→3)-α-L-Fuc(2SO$_3$⁻)-(1→]	[198,231,232]

Algal source	Sugar composition [%]		NaSO₃ [%, w/w]	M_W [kDa]	Structure (suggestion)	Ref.
Laminaria digitata	Fuc: Gal: Glc: Man: Xyl: UrA:	62.2 13.3 2.9 3.5 3.9 14.5	27.5	454	–	198,231
Laminaria japonica	Fuc: Gal: Glc: Man: Xyl: UrA: Rha:	46.4 20.5 6.5 8.7 3.6 10.3 3.2	30.6*	144	Backbone: [→3)-α-L-Fuc(2,4diSO₃⁻)-(1→4)-α-L-Fuc(4SO₃⁻)-(1→3)- α-L-Fuc(2SO₃⁻)-(1→3[α-L-Fuc-(1→2)])-α-L-Fuc-(1→] Fragments: [→6)-ß-D-Gal(3,4diSO₃⁻)-(1→6)-ß-D-Gal(4SO₃⁻)-(1→] Substituents: Galactose fragment mostly connected to C-4, most sulfate groups at C-2 and C-3	233–235
Laminaria hyperborea	Fuc: Gal: Glc: Man: Xyl: UrA:	97.8 2.2 traces – – –	53.8	1548	Backbone: [→3)-α-L-Fuc(2,4diSO₃⁻)-(1→3)-α-L-Fuc(4SO₃⁻)-(1→3[α-L-Fuc(2,4diSO₃⁻)-(1→3)-α-L-Fuc(4SO₃⁻)-(1→2)])-α-L-Fuc(2,4diSO₃⁻)-(1→] Fragments: [→3)-α-L-Fuc(2SO₃⁻)-(1→3[α-L-Fuc(2,4diSO₃⁻)-(1→4)])-α-L-Fuc(2,4diSO₃⁻)-(1→] Comment: Almost fully sulfated structure with a 1→3 backbone and a high amount of short side chains connected at C-2 or C-4 position	209,236
Saccharina latissima	Fuc: Gal: Glc: Man: Xyl: UrA:	72.7 9.1 4.4 2.0 2.4 9.5	29.6	1401	Backbone: [→3)-α-L-Fuc(4SO₃⁻)-(1→3[α-L-Fuc-(1→2)])-α-L-Fuc(2,3-diSO₃⁻)-(1→3)- α-L-Fuc-(1→] Fragments: [→6)-ß-D-Gal-(1→6[ß-D-Gal-(1→4)- α-L-Fuc-(1→3)])-ß-D-Gal-(1→] [→2)-α-D-Man-(1→4)-ß-D-UrA-(1→2)-α-D-Man-(1→4[α-L-Fuc-(1→3)])-ß-D-UrA-(1→] [→4)-ß-D-Xyl-(1→4)-ß-D-Xyl-(1→] Substituents: Fucose branching mainly at C-2, other sugars mostly connected at C-4, sulfate groups at both C-2 and C-4 auf fucose residues	198,199,207,231
Undaria pinnatifida	Fuc: Gal: Glc: Man: Xyl: UrA:	50.9 44.6 – 0.3 4.2 –	30.2	1246	Backbone: [→3)-ß-D-Gal(4Ac)-(1→3)-ß-D-Gal(2,4diSO₃⁻)-(1→3)-α-L-Fuc(2Ac,4SO₃⁻)-(1→4)-α-L-Fuc-(2SO₃⁻)-(1→3)-α-L-Fuc(2SO₃⁻,4Ac)-(1→] Comments: High degree of acetylation F_A = 0.24, often referred in literature as galactofucan (although the backbone structure is not exclusively composed of fucose)	237–239

Echinodermal source	Sugar composition [%]		NaSO$_3$ [%, w/w]	M$_W$ [kDa]	Structure (suggestion)	Ref.
Arbacia lixula	Fuc:	100	13.1*	–	[→4)-α-L-Fuc(2SO$_3^-$)-(1→4)-α-L-Fuc(2SO$_3^-$)-(1→4)-α-L-Fuc-(1→4)-α-L-Fuc-(1→4)-(1→] Comment: Fully linear and highly regular fucan	[195,211]
	Gal:	–				
	Glc:	–				
	Man:	–				
	Xyl:	–				
	UrA:	–				
Holothuria edulis	Fuc:	100	24.9*	616	[→2[α-L-Fuc-(1→4)]-α-L-Fuc-(1→3)-α-L-Fuc(2SO$_3^-$)-(1→3)-α-L-Fuc(2SO$_3^-$)-(1→3)- α-L-Fuc-(2,4-diSO$_3^-$)-(1→] Comment: Highly regular tetrasaccharide repeating backbone unit with a single unsulfated fucose residue as side chain	[240]
	Gal:	–				
	Glc:	–				
	Man:	–				
	Xyl:	–				
	UrA:	–				
Lytechinus variegates	Fuc:	100	45.5*	290	[→3)-α-L-Fuc(2SO$_3^-$)-(1→3)-α-L-Fuc(4SO$_3^-$)-(1→3)-α-L-Fuc(2SO$_3^-$)-(1→3)-α-L-Fuc(2SO$_3^-$)-(1→3)-(1→] Comment: Fully linear and highly regular fucan	[194,211]
	Gal:	–				
	Glc:	–				
	Man:	–				
	Xyl:	–				
	UrA:	–				
Ludwigothurea grisea	Fuc:	100	27.7*	554	[→2[α-L-Fuc-(1→4)]-α-L-Fuc-(1→3)-α-L-Fuc(2SO$_3^-$)-(1→3)-α-L-Fuc(2SO$_3^-$)-(1→3)- α-L-Fuc-(2,4-diSO$_3^-$)-(1→] Comment: Regular tetrasaccharide repeating unit with a single unsulfated fucose residue as side chain in about every second tetramer	[241]
	Gal:	–				
	Glc:	–				
	Man:	–				
	Xyl:	–				
	UrA:	–				

The dry matter content of fucoidan ranges from 5–10% for most seaweeds, but higher numbers such as 11.6% for *Ascophyllum nodosum* or even 18.2% for *Fucus vesiculosus* have been reported [200,232,242]. Despite the large dry matter content allocated to fucoidans, the exact function this biopolymer fulfils within the seaweed is still not fully understood.

Due to its high molecular weight and similar distribution throughout the seaweed, fucoidan often has been suggested as a structural polymer, providing flexibility and toughness to the seaweed cell wall structure [243,244]. Deniaud-Bouët et al. (2014) suggested an association of fucoidan with cellulose microfibrils, based on a series of sequential extraction experiments, by utilizing enzymatic (alginate lyase and cellulase) as well as chemical degradation methods, followed by an analysis of the obtained extracts [244]. The results of these experiments suggest that fucoidans act as major crosslinking glycans in brown algal cell walls, interlocking the cellulosic scaffold (see Figure 1-34). However, no direct or intermediated link between cellulose and fucoidan has yet been proven. A different suggestion is related to the high number of charges along these polyanionic macromolecules. The high degree of sulfation might play a major role in ion retention, which contributes to the regulation of the osmotic pressure in an saline environment [245]. This functional suggestion is further supported by the widespread occurrence of fucoidans in marine invertebrates, which, belonging to the animal kingdom, do not contain cell walls. The occurrence of fucoidans in various marine organisms appears not correlated with phylogenetic distances but with a convergent adaptation to a high salt environment [246].

In addition fucoidan facilitate water and ion retention in extracellular matrices, to cope with osmotic stress and effects of desiccation during low tide and exposure [247,248].

However, structural, and functional purposes of polysaccharide are not mutually exclusive. Fucoidans might primarily serve for regulating the osmotic pressure, while simultaneously providing a significant cell wall-reinforcement. Differences in the cation selectivity of polyanions alginate and fucoidan, combined with their distinct in situ localization, are likely to result in gradients of cation distribution throughout the wall, further influencing physical and metabolic processes, displaying structural and functional properties equally [245].

Fucoidan's bioactive properties have been investigated to great extend (see chapter **1.6.2**). These bioactive properties appear not to be related to salinity or osmotic pressure regulation, but to the ability of these sulfated marine polysaccharides to mimic the structure of mammalian glycosaminoglycans [249]. Glycosaminoglycans (GAGs), also known as mucopolysaccharides, are present in every mammalian tissue. GAGs do not only act as lubricant within the mucus and joints, newer studies also suggest a key role in cell signalling functions, which serve to modulate a vast amount of biochemical processes [250]. Among these processes are the regulation of cell growth and proliferation, promotion of cell adhesion, wound repair and anticoagulation [251]. The similarity between the carbohydrate moieties of GAGs and fucoidans might be the key factor in the signal transmission or inhibition [249].
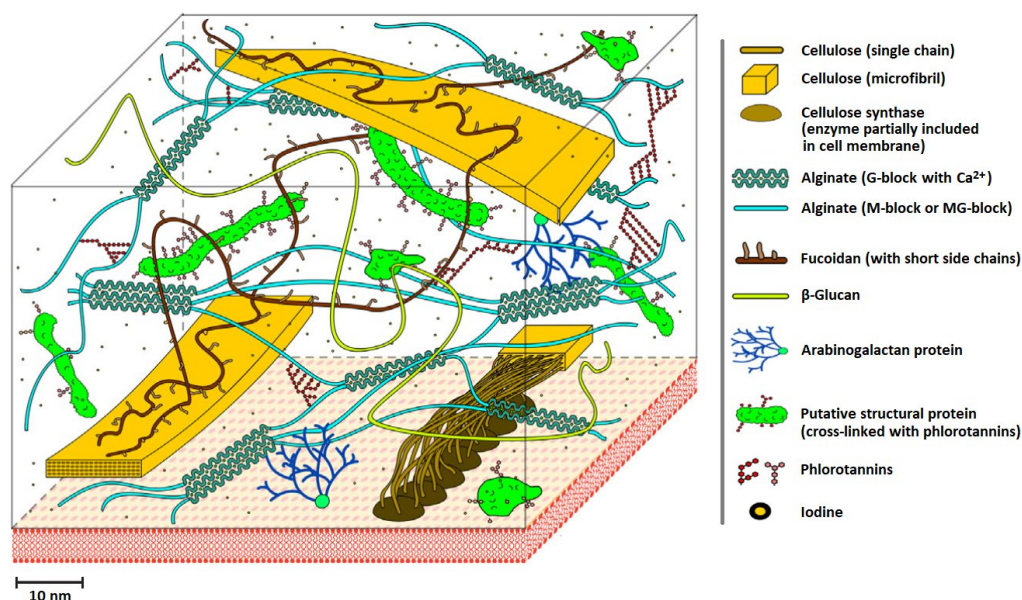
Figure 1-34 Cell wall model for brown algae. Cellulose microfibrils are sparse and with a ribbon shape and together with alginates and fucoidan form the major part of cell wall polymers. Fucoidan is potentially acting as cross-linker between cellulose microfibrils and proteins. Phlorotannins and other polyphenols might also act as a cross-linker between proteins and polysaccharides, both via covalent bonds as well as hydrophobic interactions. Large amounts of iodide are also found in the wall, but its association with other polymers remains elusive [illustration adapted and modified from Charrier et al. (2019) [13]].

1.6.1 Chemical properties and characterization of fucoidan

The complete structural characterization requires of fucoidan the combination of multiple of analytical methods, as well as a deliberate reduction in molecular complexity through chemical and enzymatic methods such as desulfation, hydrolysis and fractionation.

Total sugar analysis is essential to determine the sugar composition of a fucoidan. To achieve a complete hydrolysis with reduced risk of oxidation reactions, the polysaccharides are hydrolysed in the presence of 2 M trifluoroacetic acid (TFA) at 121 °C for 1.5 h [252,253]. The resulting neutral monosaccharides are then dissolved in dimethyl sulfoxide (DMSO) and converted to sugar alcohols by reducing the C1 aldehyde group with sodium borohydride $NaBH_4$ [254]. Subsequently acetic anhydride is used to convert the sugar alcohols into alditol acetates, which can be separated through gas chromatography (GC) in high resolution [255,256]. For the determination of uronic acids, the TFA hydrolysates should be analysed using high-performance anion-exchange chromatography (HPAEC) as described in chapter **1.4.1**.

The degree of sulfation (DS), the average number of sulfate groups per monosaccharide residue, is determined by quantifying the total sulfur (S) content relative to the total fucose content (see equation 26, wherein w refers to the weight fraction and M to the molar mass in g·mol^{-1}), or depending on the polysaccharide, in relation to the total sugar content and composition [257].

$$w(\text{SO}_4) = \frac{w(\text{S}) \cdot M(\text{SO}_3 + \text{Na} - \text{H})}{M(\text{S})} = 1 - w(\text{fucose}) \tag{26}$$

$$DS = \frac{w(\text{SO}_4) \cdot M(\text{fucose} - \text{H}_2\text{O})}{M(\text{SO}_3 + \text{Na} - \text{H}) \cdot w(\text{fucose})} \tag{27}$$

Inductively coupled plasma mass spectrometry (ICP-MS) is the most reliable method to determine the S content in polysaccharide samples. The injected sample passes through the heating zones of the plasma torch. Therein it is dried, vaporized, atomized, and ionized. At temperatures between 6000–7000 °C elements are reliably and ionized, representing the elemental composition of the sample [258]. An alternative method is the sulfur quantification through combustion in a CNS elemental analyser, wherein sulfur is measured in form of SO_2. However, this thermal decomposition is a highly endothermic process, which requires temperatures significantly above 1000 °C [257,259,260].

$$\text{R}_2\text{SO}_4 \longrightarrow 2\text{RO} + \text{SO}_2\uparrow$$

Most elemental analysers are utilized to detect organic sulfur, which is covalently linked sulfur found in thiol groups or disulfide bridges. The detection of sulfates requires specialized equipment operating at higher temperatures.

Furthermore, the sulfate content can be estimated through FTIR and Raman spectroscopy. Even though this method is less quantitative and requires a wide range of reference samples (fingerprint scans), it also provides information on the position of the SO_4-group at the monosaccharide residue (see chapter **1.6.1.1**).

Solvolytic desulfation is a widely used method for liberating SO_4-groups from polysaccharides, without severe hydrolysation of glycosidic linkages [261]. Chemical modification through solvolytic desulfation has been demonstrated for heparins, heparan sulfate, chondroitin sulfates, carrageenans, fucogalactans and fucoidans [262–264]. The technique usually involves heating the pyridinium salt of the sulfated polysaccharide in an aprotic solvent like DMSO, dimethyl formamide or dioxane in the presence of extra pyridine and small amounts of water or methanol. The reaction mechanism (see Figure 1-35) partially suggested by Ryo Takano (2002) involves the formation of a sulfur trioxide pyridine complex [265].
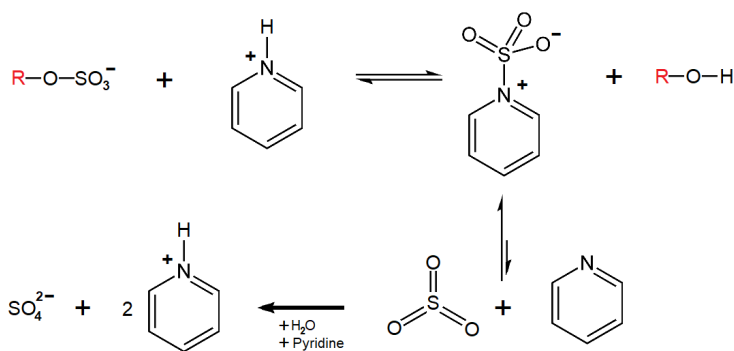
Figure 1-35 Suggested reaction mechanism for the solvolytic desulfation of carbohydrates through the formation of a sulfur trioxide pyridine complex.

Monosaccharide linkage analysis or glycosidic linkage analysis is a useful tool to identify branching points within the polysaccharide, identify terminal sugar moieties as well as providing clues on the backbone structure [252]. A complete desulfation of the fucoidan molecule is a prerequisite for a successful glycosidic linkage analysis. The analysis is performed by methylating the polysaccharide, using CH_3I in an alkaline aprotic environment (e.g. NaOH dissolved in DMSO) [266]. Subsequently the glycosidic linkages are hydrolysed, converted into alditol acetates. Thereafter, analysis is conducted in a similar manner to the total sugar analysis described above.

NMR spectroscopy (**1.4.1.2**), particularly 2D NMR is a powerful method for elucidating the structure of fucoidans. COSY (Correlation Spectroscopy); helps to establish neighbouring connectivities in the sugar rings via ^1H, ^1H –scalar couplings. From the appearance of cross peaks, the magnitude of the scalar coupling and thereby the relative stereochemistry along the sugar ring can be deduced. TOCSY (Total Correlation Spectroscopy); is useful for oligo- and polysaccharides because monosaccharide spin systems can be determined, and protons can usually be assigned to different monosaccharide units. The signal dispersion is typically best in the anomeric region. HSQC (Heteronuclear Single Quantum Correlation) is a powerful technique to identify anomeric protons/carbons and helps to distinguish CH from CH_2 moieties. To track the connection between neighbouring C/H groups H2BC (Heteronuclear 2-Bond Quantum Correlation) are used. HMBC (Heteronuclear Multiple Bond Correlation); provides information on connections across a glycosidic bond [267].

Chizhov et al. (1999) confirmed the presence of a homofucan in the brown seaweed *Chorda filum*, when he combined COSY and TOCSY spectra and demonstrated that all anomeric signals belonged to α-fucopyranoside residues. Through HMQC he provided evidence that previously found acetate was not an impurity but a constituent of the polysaccharide [223]. Chevolot et al. (2001) used a ROESY spectrum to prove that the previously confirmed sugar residues 2,3-disulphated fucose and 2-

sulphated fucose form an alternating repeating disaccharide unit [219]. When analysing fucoidan from *Fucus serratus*, using COSY, TOCSY and HSQC, Bilan et al. (2006) identified α-fucose, β-xylose and β-galactose, as well as the two main of glycosidic linkages constituted by (1→3)- and (1→4)-linked α-L-fucose residues [218].

Enzymatic modification through fucosidases or sulfoesterases is another tool to simplify or alter the fucoidan structure and gain further information on the structural characteristics. Sakurama et al. (2012) isolated a GH29 enzyme (BbAfcB) from *Bifidobacterium bifidum* and found that it acted exclusively on terminal α-(1→3/4)-fucose linkages [268]. Daniel et al. (2001) studied sulfoesterase from the marine mollusk *Pecten maximus* on fucoidan from *Ascophyllum nodosum*. Through assigning the carbon chemical shifts for each of the three isomers, 2-O-, 3-O-, and 4-O-sulfated-L-fucose, used as reference values in the NMR spectra, a high regioselectivity for the O-2 position of the fucopyranoside on algal fucoidan was evident [220].

1.6.1.1 Infrared and Raman spectroscopy

Through infrared and Raman spectroscopy the energy difference between the ground state and different vibrational states of molecules or molecule groups is studied. Vibrational spectroscopy is widely used to provide information on chemical structures, to identify substances from the characteristic spectral patterns (fingerprinting scans), and to determine either quantitatively or semi-quantitatively the amount of a substance in a sample or matrix [269].

The energy difference between the ground state and vibration states can be described using the model of an harmonic oscillator, where the reduced mass (m_r) is based on the atoms involved in the oscillation movement and the force constant (f) corresponding the strength of the with the covalent (sometimes ionic) bond [269].

$$\Delta E = \frac{h}{2\pi} \cdot \sqrt{\frac{f}{m_r}} \qquad (28)$$

Only discrete energy levels in the electron cloud of a molecule are allowed (quantization), which implies that only distinct vibration modes are allowed. The number of possible vibration modes, also called the degrees of freedom or vibrational freedom (F_V) is defined by the number of atoms (N) in a molecule, minus the translational freedom (F_T, usually 3 for the movement in space) and rotational freedom (F_R, usually 3, but 2 for linear molecules):

$$F_V = 3N - F_T - F_R \qquad (29)$$

The energy changes detected in vibrational spectroscopy are those required to cause nuclear motion. Light with a wavelength corresponding to the energy gap between the ground state and the vibration state ($\Delta E = h \cdot v$), can either be

symmetric stretch
Raman active

asymmetric stretch
IR active

symmetric deformation
Raman active
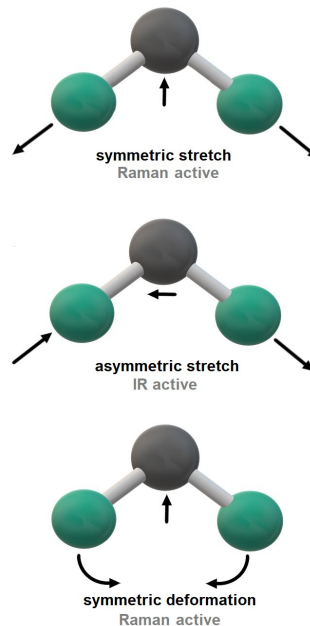
Figure 1-36 Schematic depiction of the three possible vibration modes for a three-atomic nonlinear molecule.

absorbed during promotion to a higher state, or emitted during relaxation. Infrared spectroscopy detects the photon absorption, Raman spectroscopy the emission of photons during these vibrational energy state transitions. For a vibrational mode to absorb infrared light, it must result in a periodic change in the dipole moment of the molecule. These vibrations are labelled IR active. On the other hand, for a vibrational mode to be Raman active, the dipole moment has to stay constant, while the molecular polarizability must change during the vibration. Asymmetric vibrations are most often IR-active and symmetric vibrations are usually Raman-active (see Figure 1-36). Thus IR and Raman spectroscopy are complementary methods to examine the vibrational modes of molecules [269].

Raman spectroscopy is based on Raman scattering. In Raman scattering, the light interacts with the molecule and distorts (polarizes) the electron cloud around the nuclei, forming a short-lived state (virtual state). In most cases the electrons will immediately return from the unstable virtual state to the ground state, emitting photons of identical wavelength (elastic scattering). This is the dominant process and called Rayleigh scattering (see also chapter **1.4.1.1**). However, if nuclear motion is induced during the electron cloud distortion, the molecule may return to a vibrational state instead of the ground state, emitting a photon with less energy than the incident light (see Figure 1-37). The frequency difference between the incident light and the emitted light is called the Raman shift and proportional to the energy gap between the ground state and vibrational mode. Raman scattering is inelastic. If a molecule returns from the virtual state to an excited vibrational state, the emitted photon lost energy (stokes scattering). In the less likely event that the molecule already has been in an excited vibrational state and then gets distorted by incident light, the emitted photon gains the corresponding energy (anti-Stokes scattering) [269].

Figure 1-37 Jablonski diagram showing the origin of Rayleigh and Raman scattering, and the energy transitions relevant for vibrational spectroscopy. The virtual state is a short-lived distortion of the electric field by the incident light; Energy (E), electronic states (S), vibrational states (v), wavelength (λ), frequency (v).

Vibrational spectroscopy is widely leveraged in industry for rapidly and cost-efficient identification of polysaccharides from various seaweeds. Both infrared and Raman spectroscopy can be applied directly on the milled raw material and identify the raw ma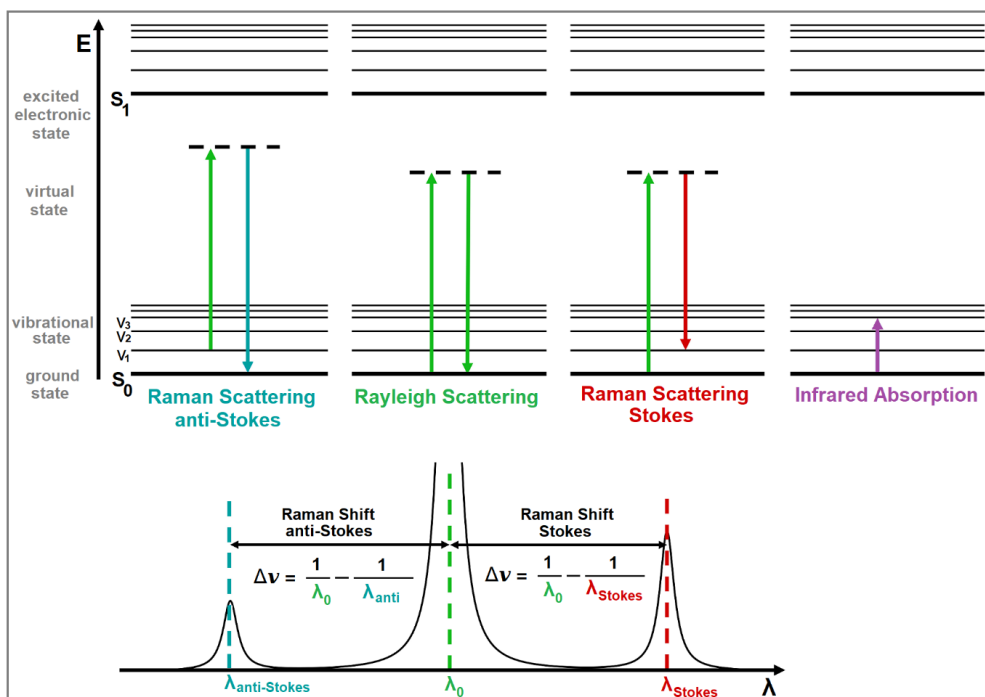terial quality and distinguishing between species through identification of the polysaccharide contained such as agar, carrageenans and polygalactans. The polysaccharides are identified predominantly through characteristic symmetric and antisymmetric vibrations of sulfate groups. The vibration bands depend on the sulfate position along the monosaccharide as well as on the sugar species [270,271]. Different glycosidic linkages can be qualitatively distinguished both through Raman and IR spectra [272].

According to Mackie (1971) the M/G ratio of an alginate can be estimated semi-quantitatively using IR and characteristic bands at 808 and 787 cm^{-1}, assigned to mannuronic and guluronic acid, respectively [273]. In combination with formic acid hydrolysis, Chandía et al. (2001) demonstrated that infrared spectroscopy can be used to accurately determine the M/G ratio of alginate extracted from *Lessonia trabeculata.* The mannuronate rich fraction presents two bands at 893 and 822 cm^{-1} while the guluronate rich fraction showed four characteristic bands at 947, 903, 813 and 780 cm^{-1}. The estimates of M/G ratio were shown to correspond with quantifications using NMR [274].

Through surface-enhanced Raman scattering (SERS) of sodium alginates, Campos-Vallette et al. (2010) distinguished between the three alginate block structures, homopolymeric M-blocks and G-blocks, as well as alternating MG-block (see chapter **1.4**). A distinct asymmetric stretching vibration for the carboxyl group was detected with a band at 1545 cm^{-1} for MG-blocks, 1598–1616 cm^{-1} for MM-blocks, and 1642–1644 cm^{-1} for GG-blocks, as well as characteristic ring breathing vibrations for the different block structures [275].

In 1993 Patankar et al. used infrared spectroscopy to revise the suggested structure of fucoidan from *Fucus vesiculosus*. Due to an absorption at 844 cm^{-1} with a small shoulder at 833 cm^{-1}, he suggested the presence sulfate groups in axial C-4 position. Shoulder bands at 820 cm^{-1} indicated sulfate in equatorial C-2 and C-4 position [276].

Raman spectroscopic analyses on N- and O- sulfated heparin standards have revealed strong bands from symmetric S-O stretching vibrations at 1039 and 1055 cm^{-1}, respectively. Through direct comparison with infrared spectra, it has been demonstrated that Raman is the superior spectrophotometric method for a qualitative and quantitative characterization of sulfation in polysaccharides [277].

Recently (2021) Ptak et al. investigated different fucoidan extraction methods and the complementary use of infrared and Raman spectroscopy to analyse crude fucoidan extracts from *Fucus vesiculosus*. Major advantages highlighted by the authors are the minimal sample preparation requirements, short measurement times, and the detection and potential classification of impurities. Furthermore, through the complementary use, structural insight is gained that would be otherwise unattained from each technique used in isolation (see Table 1-5) [278].

Table 1-5. Vibrational bands relevant for the characterization of fucoidan; δ and ν refers to bending and stretching vibrations, τ refers to torsion vibrations, s to symmetrical and as to anti symmetrical modes.

Wavenumber [cm⁻¹]	Vibrational mode	Assignment	Activity	Ref.
428	δ(pyranoid ring C-O-C) δ(pyranoid ring C-C-C)	Carbohydrate	Raman	[279]
571	δ(pyranoid ring C-C-O) τ(C-O)	Carbohydrate	Raman	[279]
608	δ_s(pyranoid ring C-C-O)	Carbohydrate	Raman	[279]
726	δ(pyranoid ring C-C-O)	Carbohydrate	Raman	[279]
826	δ(2C-O-S)	Sulfate ester at C-2 at (1→3)-linked α-L-fucose	Raman	[278]
838	ν(2C-O-S), ν(α-pyranoid ring C-C)	Sulfate ester at C-2 α-L-fucose	Infrared	[237,271,278]
839	δ(4C-O-S)	Sulfate ester at C-4	Raman	[277,280]
965	ν(C-O in C-O-C) δ(C-O-H)	Glycosidic linkage ß(C-O-H)	Infrared	[281]
970–1200	ν(pyranoid ring C-C) ν(C-O)	Carbohydrate	Raman	[270,281–283]
993	ν(glycosidic C-O) ν_{as}(C-O-C) ν(C-C) ν(C-O), ß(C-C-H) ν(pyranoid ring C-O) ν(pyranoid ring C-C) ß(C-C-H)	Carbohydrate	Infrared Raman	[281]
1014–1030	δ(C-O-H) ν(C-C) ν(C-O-S)	Carbohydrates Fucoidan	Infrared	[278,281]
1066	ν_s(O=S=O) ν(2C-O-S)	Sulfate group Sulfate ester	Raman	[237,271,284]
1078	ν(C-O) ν(C-C) δ(C-O-H)	Carbohydrate	Infrared Raman	[279,281,285]
1160	ν(C-O)	Carbohydrate	Infrared	[281]
1217	ν(S=O)	Sulfate group	Infrared	[280]
1257	ν(S=O)	Sulfate group	Infrared	[280]
1273	ν_{as}(O=S=O)	Sulfate group	Raman	[280]
1277–1279	τ(CH₂)	Methyl group	Infrared Raman	[281]
1336	ν(C-O) δ(C-O-H)	Carbohydrate	Raman	[281]
1387	δ_s(CH₃)	Methyl group	Infrared	[286]
1446	ν_s(COO)	Alginate	Raman	[275]
1454	δ_s(CH₃)	Methyl group	Raman	[237]
1611–1616	ν_{as}(COO)	Alginate	Raman	[275]
1636	ν(C=O) ν(C=C) ν(C=N)	Double bond stretching	Infrared	[278]
1650–1800	ν(C=O)	Carbohydrate	Raman	[278]
2947	ν(C-H)	Carbohydrate	Raman	[286,287]
3409	ν(O-H)	Carbohydrate	Infrared	[281]

1.6.2 Bioactive properties of fucoidan

Fucoidans isolated from brown seaweeds have gained considerable attention due to a large array of promising bioactive properties such as antiangiogenic, immunomodulatory, anti-inflammatory, antidiabetic, antiviral and anticancer properties [288]. A major research field is the structure function relation of fucoidan. Numerous original research papers as well as review papers have attempted to correlate biological activities with distinct structural features such as molecular weight, degree of sulfation and branching [198,206,278,289,290]. Although a detailed structure–function relation remains elusive in many cases, a correlation of structural features with selected observed bioactive responses and their underlying mechanism will be approached in this chapter.

1.6.2.1 Anti-inflammatory properties of fucoidan

Inflammation is broadly characterized as an innate physiological defence response, a response to cues such as damaged or malfunctional tissue, pathogens, or noxious compounds [291,292]. Acute inflammation refers to responses that last for a few days, typically observable by signs such as swelling, redness, heat, pain, and loss of function. These overt signs of inflammation are mediated by several signalling molecules resulting in vasodilation, increased blood flow and permeability at the site of inflammation [291,292]. In short, these responses permit greater access and recruitment of host immune cells to respond to inflammatory cues. Controlled inflammatory responses are beneficial. However, inflammation may extend to months or years leading to chronic inflammation, for instance by failing to eliminate the causative inflammatory agent or persistent cues caused by endogenous mechanisms such as autoimmunity. Chronic inflammatory responses are associated with the pathogenesis of several diseases such as arthritis, cardiovascular diseases, diabetes, obesity, neurodegenerative diseases and tumour development [288].

Cytokines are small proteins secreted by the cells and function as signalling molecules in inflammatory and immune responses. Cytokines are divided into pro- and anti-inflammatory cytokines. Pro-inflammatory cytokines include (IL-1β, IL6, and TNF-α) act to intensify the existing disease, whereas anti-inflammatory cytokines (IL-4, IL-10, IL-11, and IL-13) reduce inflammation and promote healing [288,293–295]. The effects of fucoidan on NF-κB-mediated inflammatory response in rats with acute myocardial infarction was demonstrated by Lu et al. (2019). It was reported that fucoidan downregulated NF-κB-signalling as well as IL-6 and TNF-α secretion, effectively improving the inflammatory condition and reducing myocardial injuries in the rats [296]. Fucoidan has been shown in numerous studies to effectively downregulate pro-inflammatory cytokines and has been suggested as a potential therapeutic agent against inflammatory conditions [297].

Chemokines, a type of cytokines, are a family of low molecular weight proteins that to guide the migration of leukocytes [294]. Based on their chemical structure, particularly their cysteine residues, chemokines are assigned to four groups: C chemokines (lymphotactin), C-C chemokines (MCP-1, monocyte inflammatory protein), C-X-C chemokines, and CXXXC chemokines [294]. Numerous studies have shown an anti-inflammatory effects of fucoidan, based on inhibited chemokine secretion [288,298]. Wang et al. (2016) for instance demonstrated that the chemokine CCL3 (also known as MIP-1α) was inhibited by fucoidans in the male C57BL/6J mice model, that were fed a high-fat, high-sucrose diet.

The authors claim that the CCL3 downregulation resulted in a reduced inflammatory response in high glucose stressed-activated pancreatic islet cells and protected those cells against apoptosis [288,299].

Toll-like receptors (TLRs) are a group of pattern recognition receptors located on the outer cell membranes and endosome membranes [300]. TLRs recognize molecular motifs, pathogen-associated molecular patterns (PAMPs) associated with exogenous microorganisms, such as bacteria, viruses, and pathogens. TLRs also recognize damage-associated molecular patterns (DAMPs), released from necrotic cells or extracellular matrix molecules that upregulate following injury. TLRs are a part of the innate immune system [301]. Microbial metabolites that activate TRLs trigger an intracellular signalling cascades, including NF-κB, which induces the production of pro-inflammatory cytokines and chemokines [296]. Dutot et al. (2019) investigated the anti-inflammatory effect of fucoidan in the respiratory tract against poly (I:C) inflammatory responses. It was observed that fucoidan treatments led to a reduction of poly (I:C)-stimulated inflammatory responses in human primary bronchial epithelial cells, attributes to a downregulation of TLR3 gene expression [302].

1.6.2.2   Antiangiogenic properties of fucoidan

Angiogenesis, the formation of new blood vessels, occurs during tissue growth and repair and healing processes, but it is also regarded as a hallmark for pathological tissue development such as tumour progression and various diabetic and inflammatory diseases [289,303,304].

Unfortunately, in most cases, the chemical structures of the fucoidans used in the biological experiments were not fully characterized and a detailed structure–function relation requires further investigation. However, a review study by Ustyuzhanina et al. (2014) found that angiogenetic properties highly depend on the molecular weight. While antiangiogenic activity is connected to high-molecular weight fucoidans, proangiogenic activity can be induced by low-molecular weight fucoidans [289]. When tested with otherwise similar fucoidans, an increasing degree of sulfation was found to positively correlate with antiangiogenic and anti-tumour activities [305,306]. Clément et al. (2010) studied the influence of branching on the bioactivity of fucoidans. It was found that branched fucoidan oligosaccharides displayed higher anti-complementary activity than linear counterparts, when tested with a similar degree of sulfation. It is speculated that receptor recognition might be tight to chain stiffness and chain conformation just as much as molecular weight and degree of sulfation [278,290,307].

Although a direct correlation of structural properties and bioactive properties remains difficult, this group of sulfated polysaccharides has demonstrated high potential as agents for regulating both inflammatory response systems as well as angiogenesis.

The bioactive properties of fucoidan likely stems from its structural similarities to the carbohydrate moieties in glycosaminoglycans like heparin, heparan sulfate and Chondroitin sulfate. Those GAGs play a key role in cell signalling processes and the modulation of vast amounts of biochemical processes [249,250]. Heparan sulfate proteoglycans are components of the cell surface and extracellular matrix and were shown to play an important role in angiogenesis [308–310]. Interactions of heparan sulfate proteoglycan fragments with growth factors, cytokines and chemokines have been

demonstrated. The formation of ternary complexes of heparan sulfate fragments with receptors has been shown, resulting in competitive inhibition [311–313]. Robinson et al. (2006) revealed that for an interaction between the vascular endothelial growth factor (VEGF) and heparan sulfates chains, the polysaccharide should contain two highly sulfated oligosaccharide domains, flanked by a partially sulfated fragment, showing that both sulfation degree and sulfation pattern play an important role for the bioactivity [314]. Due to their heterogenous structural patterns in terms of sulfation, sugar composition and branching, fucoidans have were observed to induce similar angiogenic effects [205].

The influence of fucoidans on signal molecules, known to be involved in the regulation of angiogenesis, has been investigated in numerous studies. Growth factors, particularly VEGF and fibroblast growth factors (FGF), which activate cell migration and tube formation play a key role in angiogenesis [315,316]. The inhibition or reduced secretion of vascular endothelial growth factors is of key importance to reduce angiogenesis. Dithmar et. al. (2014) studied the influence of commercial fucoidans on the VEGF secretion and antiangiogenic effects on porcine and human retinal pigment epithelium (RPE). Fucoidan displayed no toxicity and did not diminish proliferation or phagocytosis, but reduced wound healing in RPE cells and RPE/choroid explants [317]. Retinal pigment epithelium was chosen due to the connection of choroidal neovascularisation (an abnormal formation of new vessels from the choroidea into the retina of the eye) and **age-related macular degeneration (AMD)**, a leading cause for blindness in the industrialized countries. The authors suggest fucoidan as an effective agent to reduce VEGF expression and as a potential therapy against exudative AMD [317].

1.6.2.3 Anticancer properties of fucoidan

The anticancer properties of fucoidan are multifaceted and can interact with the formation of tumours on multiple levels [318]. After cardiac disorders, cancer is the second biggest cause of death in industrialized countries, accounting for every fourth death. Cancer is a complex disease caused primarily by acquired genetic changes that provide tumour cells an upside in terms of proliferation [319]. The predominant methods of cancer treatment worldwide are surgery, radiation-, and chemotherapy, but their extensive side effects limit their benefit and curative effect. The quest for low-toxicity marine drugs that can prevent or treat cancer, or support established methods and mitigate their side effects is a research area with high focus [318].

The anticancer and antimetastatic activities of fucoidans were demonstrated for cells of diverse histogenesis, including human lung, breast, colon, prostate, liver and bladder cancer cells [320,321].

Cancer development is a dynamic and long-term biological process, involving a plethora of components and interactions and a stepwise progression that eventually leads to metastasis. Fucoidan can inhibit the tumorigenesis by four different mechanisms: (I) cell cycle arrest, (II) induction of apoptosis, (III) antiangiogenic- and (IV) anti-inflammatory activities [318].

(I) Alekseyenko et al. (2007), transplanted Lewis lung cancer cells in C57BL/6 mice and observed that tumour mass and metastasis were significantly reduced in mice administered with 25 mg/kg (injected intraperitoneally) fucoidan [322]. Fukahori at al. (2008) demonstrated that fucoidan therapy (22.5

mg/mL) induced a cell cycle arrest in the G_2/M phase and inhibited cell growth *in vitro* in human cancer cell lines [323].

(II) Apoptosis, the programmed and desired cell death, is an essential homeostatic function of normal cells in multicellular organisms. Inhibition of apoptosis is however a common feature of cancer cells. Fucoidan can promote apoptosis in cancer cells by activating apoptotic signalling. In human lymphoma HS-Sultan cell lines, fucoidan (100 μg/mL) suppresses tumour growth and promotes apoptosis [324,325].

(III) The antiangiogenic properties of fucoidan, as described above, are an important tool in limiting access of neoplastic cells to nutrients and oxygen. Cancer cells rely on an adequate supply of both to proliferate. Antiangiogenic therapy has proven to be an effective way to slow tumour growth and can support conventional cancer treatment [326]. The combination of fucoidan extracted from *Cladosiphon novae-caledoniae* with conventional anticancer drugs such as tamoxifen, cisplatin, and paclitaxel was shown to inhibit cell growth and cell cycle in MCF-7 breast cancer cells as well as promoting apoptosis [327]. For fucoidan extracted from *Laminaria japonica*, a tumour growth inhibition of 33–47% for nasopharyngeal carcinoma cells was determined in vivo and *in vitro* studies [328].

(IV) Another major factor the development of cancer is inflammation. According to recent studies, up to 20% of human cancers are related to chronic and unresolved inflammations, caused by viral and bacterial infections, exposure to irritants, or autoimmune diseases [288,329]. Thus, inhibition of excessive inflammatory responses is a critical factor to mitigate the risk of cancer development. Aspects of immune modulation through fucoidan involve cytokine inhibition, chemokine inhibition, and inhibition of toll-like receptors (see **1.6.2.1**).

1.6.2.4 Anticoagulant properties of fucoidan

Blood coagulation is initiated by coagulation factors to stop the flow of blood though injured vessels when abnormal vascular conditions occur, or when exposure to non-endothelial surfaces at sites of vascular injuries is detected [330]. Through the interference of endogenous or exogenous anti-coagulants with coagulation factors, the blood coagulation can be stopped [331]. Heparin (a sulfated glycosaminoglycan usually extracted from porcine tissues) is the most commonly used antithrombotic/anticoagulant drug. However, side effects from heparin such as thrombocytopenia, haemorrhagic effect, and ineffectiveness in congenital or acquired antithrombin deficiencies, and incapacity to inhibit thrombin bound to fibrin are well documented [330,332]. Wang et al. (2010) demonstrated that fucoidan from *Laminaria japonica* displayed several anti-coagulant activities similar to heparin [233]. The anticoagulant activity of sulfated polysaccharides has been shown to depend on their molecular weight, their sulfation degree, and also the distribution of sulfate groups in the repeating units as well as on the structure of the polymeric backbone [211]. Although the anti-coagulant effect of heparin remains higher than for various analysed fucoidans, the absence of documented side effects so far suggests the potential use of fucoidan as substitute or support for heparin as anticoagulative treatment [233].

2 Objectives of the thesis

Marine polysaccharides are the subject of increasing research interest in the field of biomedical applications due to a wide range of bioactive properties, compatibility with living tissues and their ability to form hydrogels. Chemical, physical, and bioactive properties of three marine polysaccharides fucoidan, alginate and chitosan were investigated in this thesis.

Objective 1: Fully characterize the chemical structure of fucoidan from *Laminaria hyperborea* (Paper 2)

Objective 2: Elucidate structure–function relationships of fucoidan from *Laminaria hyperborea* and assess bioactive properties (Paper 2 and 3)

Objective 3: Investigate alginate-chitosan polyelectrolyte hydrogels, including their gelling properties and interaction mechanism (Paper 1 and 4)

In Paper 2, numerous analytical techniques were utilized to thoroughly characterize the chemical structure of fucoidan from *Laminaria hyperborea*. A task that to our knowledge has not been solved before. Among the techniques were NMR spectroscopy, ICP-MS, SEC-MALS, Raman spectroscopy, and monosaccharide analysis as the primary tools employed to achieve the first objective.

Several bioactive properties of this complex group of fucose containing polysaccharide have been reported. However, most studies lack a detailed structural characterization or even purified fucoidan samples. Thus, there is a need to investigate the bioactive properties of fucoidans using well-characterized macromolecules to establish a comprehensive structure–function relationship. In Paper 2, our aim was to investigate the influence of molecular weight and degree of sulfation on bioactive properties of fucoidan applied in a lepirudin-based human whole blood model. To obtain samples of fucoidan tailored to specific degrees of sulfation and molecular weights, we employed chemical modification through solvolytic desulfation and mild acid hydrolysis, respectively. In Paper 3, we evaluated the bioactivity of fucoidan from *L. hyperborea* in ocular cells. We assessed cell viability, protection from oxidative stress, and the secretion of vascular endothelial growth factor (VEGF). Furthermore, we examined the relationship between these parameters and the molecular weight of fucoidan.

Alginate gels crosslinked with chitosan oligomers were investigated in Paper 1 and 4. The interaction between these polyelectrolytes were studied on a macroscopic and microscopic level. The gelling mechanism and the potential formation of junction zones between chitosan and alginates with different block structures were systematically investigated in Paper 4. To achieve this, we employed circular dichroism spectroscopy, rheology, as well as molecular dynamic simulations. In Paper 1, we examined the mechanical properties, gelling kinetics, and syneresis using chitosan oligomers to partially replace calcium ions for crosslinking. With Papers 1 and 4, our goal was to expand the theoretical framework for understanding the interaction mechanisms underlying the formation of alginate-chitosan oligomer hydrogels. Furthermore, we aimed to uncover additional tools for tailoring alginate hydrogels relevant in various biomedical applications including tissue engineering, coatings or as delivery systems for pharmaceuticals, nutraceuticals, and other bioactive compounds.

3 Summary of the papers

Paper 1: **Alginate gels with a combination of calcium and chitosan oligomer mixtures as crosslinkers**

In this paper we investigated a concept of ionic gelation of alginates using chitosan oligomers as crosslinkers. Because chitosan oligomers crosslink alginate's M-blocks, while calcium ions (Ca^{2+}) form junction zones with G-blocks, it was hypothesised that a combination of chitosan oligomers and calcium ions might positively impact gelling parameters such as gel strength, gelling kinetics, or syneresis.

Alginate from *Laminaria hyperborea* with an intermediate G content ($F_G = 0.46$), and high G content ($F_G = 0.68$), derived from leaves and stipes, respectively, were used in this study. The alginates were characterized using NMR and SEC-MALS. The chitosan oligomers mixture (MCO) was characterized through NMR and SEC. An internal method of gelation was applied using GDL and two different crosslinkers, Ca^{2+} and MCO ($DP_n = 3.96$, FA = 0.045), as well as combinations of Ca^{2+} and MCO.

Firstly, the maximum concentration of crosslinker before the onset of syneresis was determined for each alginate crosslinked with MCO or Ca^{2+} individually. For pure calcium-alginate gels, the maximum concentrations of calcium without significant syneresis were 15 and 16.5 mM for leaf alginate, and stipe alginate respectively. Using MCO for crosslinking alginate gels, the maximum MCO concentration was 25 mM (calculated as the molar concentration of the D-unit monomer) for both alginates.

Alginate gel cylinders (10 g/L) and various combinations of crosslinker concentrations were evaluated through uniaxial compression and rheology. By uniaxial compression, the Young's modulus of hydrogels was determined, using the linear slope region obtained from the force-deformation curves at low deformation ($\leq$ 5% strain). Syneresis was determined by weighing the cylinder after careful removal of expulsed water after 24 h of gel formation. Gelling kinetics were analysed through rheology with a low oscillation frequency (1 Hz) and strain (0.001) to ensure that measurements did not disrupt the gelation process.

This study showed chitosan oligomers and calcium ions can be used simultaneously to crosslink alginate applying internal gelation. It was demonstrated that up to 50% of the calcium can be substituted with chitosan oligomers without a reduction in final gel strength or increase in syneresis for intermediate-G leaf alginate, and up to 25% for high-G stipe alginate respectively. The rheological experiments revealed a faster gel formation for MCO crosslinked alginate gels, and a higher final gel strength for Ca^{2+} crosslinked alginate. However, the gels with mixed crosslinkers reached a final gel strength similar to calcium crosslinked alginate while displaying fast gelling kinetics similar to MCO crosslinked alginate, providing additional tools to modulate the gel formation and tailor the properties of an alginate gel.

Paper 2: **Structural Characterization of Fucoidan from *Laminaria hyperborea*: Assessment of Coagulation and Inflammatory Properties and Their Structure-Function Relationship**

The aim of this study was to characterize fucoidan isolated from *Laminaria hyperborea* to obtain structure–function relationships. Furthermore, fucoidan was tailored to elucidate how molecular weight and degree of sulfation affect bioactivity in human whole blood.

To elucidate the complex and heterogeneous structure of the purified fucoidan (pFuc) molecule, a combination of several analytical techniques was applied. Through total sugar analysis a sugar composition of almost exclusively fucose (97.8%) and a smaller percentage of galactose (2.2%). Glycosidic linkage analysis showed (1→3)-α-L-fuco-pyranose (31.9%) to be the dominant residue, followed by 1→2 linked (13.2%) and 1→4 linked (7.7%) fuco-pyranose as well as high degree of branching (22.4%). Through SEC-MALS a molecular weight of M_w = 469 kDa was determined. The slope a = 0.78 of a Mark–Houwink–Sakurada plot, and the slope b = 0.65 of an RMS conformation plot indicated a flexible random coil shape of the molecule, suggesting a highly flexible backbone with short side chains. ICP-MS revealed a sulfate content of 53.8%, corresponding to a calculated degree of sulfation (DS) of 1.7, or near complete O2 and O4 sulfation of the macromolecule. Raman spectroscopy determined SO_4 located axial at 4C and equatorial at 2C as well as an absence of acetylation. By NMR, chemical shifts (proton and carbon) were assigned and revealed a highly heterogeneous structure in terms of glycosidic linkages. Combining the results from NMR, glycosidic linkage analysis and SEC-MALS, a 1→3-linked backbone structure was suggested, together with an additional five possible structural fragments (equal ratio).

A fully desulfated fucoidan (dsFuc) derivative was produced via solvolytic desulfation. Briefly, the sodium counterions of fucoidan were exchanged with pyridinium ions, using cation exchange columns. The pyridinium-fucoidan was solved in DMSO at 80°C for 30 minutes. The lower molecular weight fucoidan sample was obtained via mild acid hydrolysis at pH = 3.0, 70°C, 30 minutes (hFuc).

The bioactivity of all samples (pFuc, hFuc, dsFuc, using sulfated alginate and heparin as references) was assessed using a lepirudin-based whole blood model. The immediate responses by coagulation and complement cascades were measured by prothrombin factor 1 and 2 (PTF1.2) and the terminal complement complex (TCC), respectively. Cytokines involved in inflammation were detected in a 27-plex cytokine assay. Fucoidan with a high M_w and high DS inhibited coagulation, complement and the cytokines PDGF-BB, RANTES, and IP-10, while activating MCP-1. These effects were obtained at a concentration of 1000 µg/mL and partly at 100 µg/mL. However, at low concentration (10 µg/mL), a coagulation stimulating effect of highly sulfated fucoidans (DS = 1.7, M_w = 469 kDa or 20.3) was obtained. This indicates a level of complexity in the effects linked to the sulfation degree requiring further studies to provide mechanistic insights.

Through comparison of the well-defined samples pFuc, hFuc, dsFuc, sulfated alginate and heparin it was demonstrated that the anticoagulant effects of these polysaccharides depend predominantly on the degree of sulfation, to lesser extend on the molecular weight, whereas branching and sugar composition showed no significant influence on coagulation.

The finding that fucose is the principal sugar unit combined with near complete theoretical sulfation is observed provides a high overall simplicity of the analysed biopolymer isolated from *L. hyperborea*. Nevertheless, the large variety of glycosidic linkages, branching points and their random distribution, still results in a heterogeneous structure. Due to the lack of repeating units a fully defined primary structure cannot be determined but through combination of several analytical techniques, a reasonable approximation of a hypothetical structure of the fucoidan molecule was achieved.
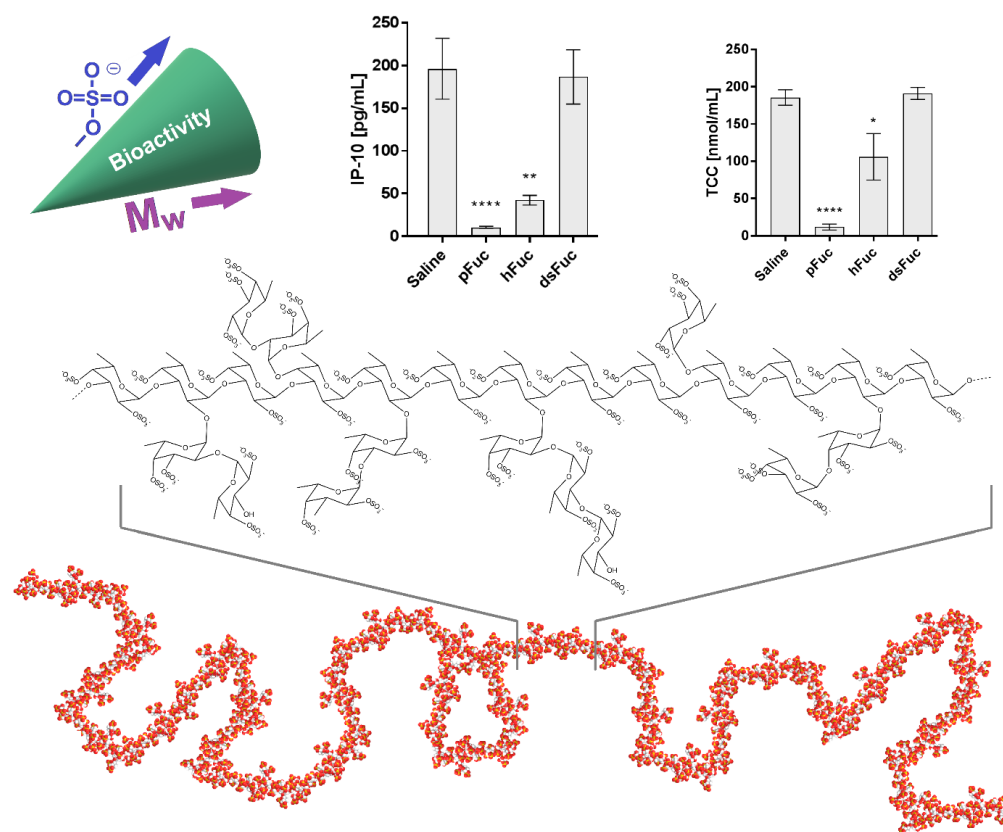
Figure 3-1 Graphical abstract – (Middle) possible structural fragment of 25 fucose residues elucidated in this study; (Bottom) structural fragment applied as building blocks for a full-scale structural model (DP = 750, Rw = 37 nm) of fucoidan from *L. hyperborea*. Atom colour: H = white, C = grey, O = red, S = yellow; (Top) Depicting the structure–function relation for the analysed fucoidans, showing an increase of various bioactive properties with increase in molecular weight and degree of sulfation.

Paper 3: **Effects of Sulfated Fucans from *Laminaria hyperborea* Regarding VEGF Secretion, Cell Viability, and Oxidative Stress and Correlation with Molecular Weight**

In this study we further investigated the bioactive properties of fucoidan (herein referred to as sulfated fucan), with respect to secretion of vascular endothelial growth factor (VEGF), protection from oxidative stress and cell viability in ocular cells.

Three fucans from *Laminaria hyperborea* with different molecular weight were prepared, chemically characterized, and evaluated. High molecular weight sulfated fucan (M_w = 1548.6 kDa, Fuc1) was extracted with warm water and purified through ultrafiltration. Lower-molecular-weight samples (M_w = 499 kDa, Fuc2; 26.9 kDa, Fuc3) were obtained by mild acid hydrolysis of ultrapurified sulfated fucan, followed by dialysis. The sulfated fucan samples were analysed through SEC-MALS, ICP-MS, and GC. All samples showed a high degree of sulfation (DS) of about 1.7 sulfate groups per sugar unit, confirming the molecular weight as the key difference between the samples, ensuring high comparability for bioactivity assessments.

Bioactivity (cell viability, oxidative stress protection and VEGF secretion) was measured in *in vitro* cell cultures using human-derived cell lines uveal melanoma (OMM-1), retinal pigment epithelium (ARPE-19) and porcine-derived primary cells from retinal pigment epithelium (RPE).

It was found that Fuc2 and Fuc3 were antiproliferative for OMM-1, but not for ARPE. Fuc1 protected OMM-1. VEGF secretion was lowered with all fucans except Fuc3 in ARPE-19 and RPE. Furthermore, it was found that the cell viability of ARPE-19 and RPE was not influenced by any *L. hyperborea* fucan for up to three days of treatment; this excludes toxic effects important for further studies.

The sulfated fucan origin and extraction method for the three sulfated fucan samples was the same isolating molecular weight average (Fuc1 > Fuc2 > Fuc3) as the experimental variable.
The results suggest a positive correlation between molecular weight of sulfated fucans and biological activity. As a potential therapeutic agent for ocular disease, a higher molecular weight sulfated fucan may elicit greater effects.

Paper 4: **Alginate gels crosslinked with chitosan oligomers – a systematic investigation into alginate block structure and chitosan oligomer interaction**

The concept of alginate gels crosslinked with chitosan oligomers was further researched in this publication. The interaction of these polyelectrolytes, the gelling mechanism and the potential formation of junction zones was systematically investigated.

Three alginates with fundamentally different block structures, poly-M, poly-G, and poly-MG, were selected for ionic crosslinking with chitosan oligosaccharides (CHOS). Interactions were investigated using circular dichroism (CD), rheology, and computer simulations.
Strong evidence was obtained, supporting the previously proposed gelling principle of poly-M alginate crosslinked with chitosan oligomers due to matching in charge distance between the two polyelectrolytes [19]. Furthermore, a unique high gel strength poly-MG chitosan gelling system was revealed.

CD spectroscopy showed an increased chiroptical activity for the poly-M chitosan gelling system, indictive of induced conformational changes and higher ordered structures. The increased chiroptical activity change was also greater for CHOS with higher DP. For poly-G and poly-MG no change in chiroptical activity was detected upon addition of CHOS.

Rheological measurement revealed a storage modulus (G') of < 900 Pa for poly-MG (1%) CHOS (0.3%) hydrogels, orders of magnitude greater than for CHOS crosslinked poly-M. Upon addition of salt (50–500 mM NaCl) to poly-M CHOS gelling systems, the gel formation slowed down and the final gel strength decreased with increasing amounts of salt. This effect was likely caused by competition at the junction zones between the charged polyelectrolytes and the NaCl ions. This is in line with the suggested model of zipper-like junction zones between CHOS and poly-M. However, for the ionically crosslinked poly-MG chitosan hydrogels the gel strength increased upon the addition of salt (G' < 1600 Pa at 50 mM NaCl), suggesting a stabilization of the junction zones through hydrophobic interactions and/or a phase separation, which to our knowledge has not been reported before.

Molecular dynamics (MD) simulations were applied to further investigate these findings, comparing interaction energies, charge distances and chain alignments. MD simulations showed an increase in interaction energies between chitosan and alginate upon the addition of NaCl for poly-MG, while for poly-M and poly-G the addition of NaCl decreased the interaction energies with chitosan. Furthermore, for poly-MG CHOS gelling systems upon addition of salt, a higher number of interactions (contact points) was calculated than for any other simulated gelling system.

The high gel strengths especially upon the addition of salt, the data obtained from MD simulations, as well as the observed turbidity of the poly-MG chitosan gelling system, simultaneously with CD measurements having shown no systematic alignment or induced conformational change, implies a fundamentally different effect supporting the chitosan poly-MG junction zones.

The described CHOS poly-MG gelling systems displaying high gel strengths, are known to be highly biocompatible and have revealed a high tolerance to a broad range of salt concentrations present in various biological systems. Accordingly, the findings herein may support the biomedical use of poly-MG chitosan gels and provide additional tools for tailoring alginate hydrogels.
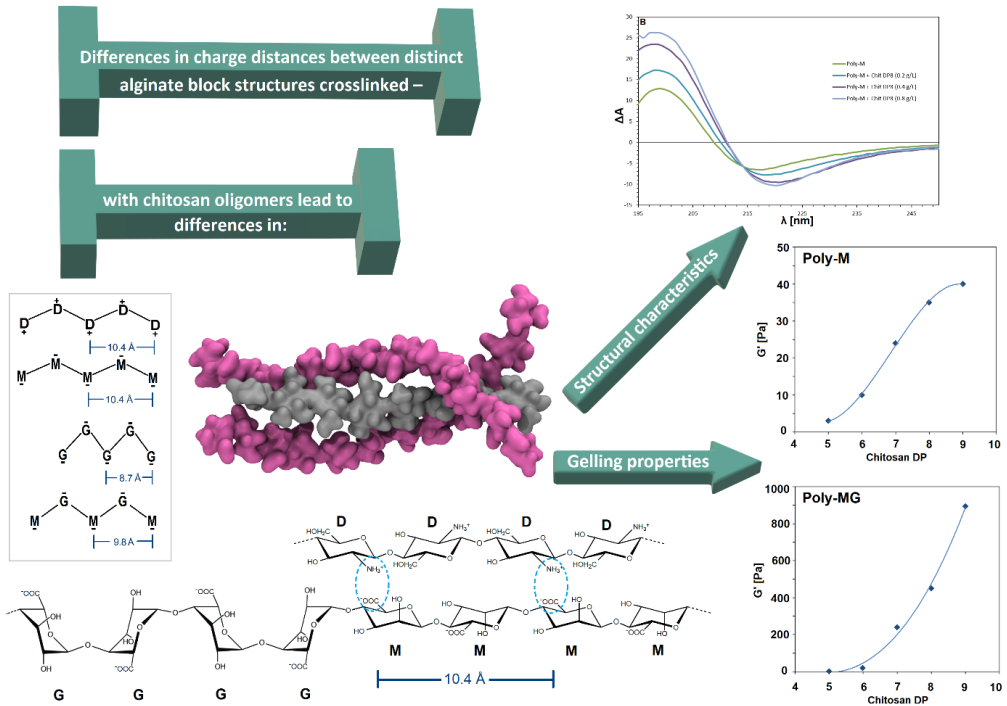
Figure 3-2 Graphical abstract – Text: " Differences in charge distances between distinct alginate block structures crosslinked with chitosan oligomers lead to differences in structural characteristics & gelling properties"; (Bottom and left) schematic depiction of the intramolecular charge distances along each side of the used poly- and oligosaccharide chains. Ionic interactions of potentially aligned charged de-N-acetylated chitosan and a charged alginate M-block indicated (light blue circles). Monosaccharide units: glucosamine (D), mannuronate (M), guluronate (G); (Middle) snapshot of structure alignment from molecular dynamics simulations of a 2:1 alginate:chitosan systems to exemplify how the alginate oligomers (colour pink) can wrap around the chitosan oligomer (colour grey); (Top right) circular dichroism spectra of poly-M with chitosan DP = 8 at different concentrations, showing a clear shift in the CD absorption bands, indicating changes in the secondary structure of the alginate; (Right) diagram of the final gel strength of alginate (poly-M and poly-MG) gel crosslinked with chitosan oligomers. The diagram depicts the final gel strength determined after 5 h versus the degree of polymerization of chitosan crosslinker.

4 General discussion

Polysaccharides have been integral to the evolution of human history and technological development. Beginning with the simple cultivation of plants for consumption, our comprehension of polysaccharides has evolved into an expansive scientific field covering polysaccharide structure and chemistry. We have come to recognize the vital roles polysaccharides play in our biology and physiology. As our understanding expands, it paves the way for new challenges, inquiries, and opportunities that are yet to be addressed.

Within the field of polysaccharide science, there are still uncharted waters within the fundamental elucidation of polysaccharide structures. There are also insights to be discovered in how these structures interact with biological systems to trigger responses. Of particular interest to the applied branches of polysaccharide science is the prospective utility of these versatile macromolecules in biomedical applications.

Certain polysaccharides, such as alginates, possess the ability to form hydrogels. Generally non-toxic and well-tolerated in biological systems, these are ideal for use with cells and tissues. Accordingly, these polysaccharides are sought-after in tissue engineering applications to produce tissue culture models, biological scaffolds, or in cell encapsulation for therapy, as well as drug delivery systems.

The potential uses of polysaccharides are not confined to hydrogels. In solution, polysaccharides may also prove beneficial, given their properties such as immunostimulatory, antiviral, and anti-inflammatory effects. The subsequent section will discuss both the application of polysaccharides in hydrogels and the biological activities of polysaccharides in solution.

The chapter will outline the most important aspects and innovative findings from the research conducted. The discussion will also revolve around how the work both contrasts with and contributes to the existing body of knowledge in the field of polysaccharide science.

4.1 Structural characterization of fucoidan from *Laminaria hyperborea* (Paper 2)

Detailed structural elucidation of fucoidans is challenging due to their extensive heterogeneity and lack of repetitive motifs within the macromolecule. In this study we combined the analytical results from various spectroscopic, spectrometric and chromatographic methods and performed a comprehensive structural characterization of a purified fucoidan from *L. hyperborea*.

For a full structural characterization of fucoidan, a series of complementary analytical approaches is required. Most fucoidan studies are subject to at least one of the following three limitations: (I) Only a limited set of structural features are analysed, (II) the fucoidan is insufficiently purified or fractionated, or (III), chemical alteration such as depolymerization and subsequent purification may conceal structural features.

Chevolot et al. (2001) relied only on methylation analysis and NMR spectroscopy for analysing fucoidan from *Ascophyllum nodosum*, revealing a fucose disaccharide repeating backbone-structure [219]. However, to obtain those results, the fucoidan was depolymerized to fucooligosaccharides with a DP of 8 to 14. This depolymerization may obfuscate characterization of larger branching patterns as well as the overall shape of the molecule. A subsequent study by Foley et al. (2011) analysed higher molecular weight fucoidan from *A. nodosum*, revealing the presence of galactose, xylose and glucose. One limitation in the latter study was that the fucoidan fraction was likely somewhat too crude to provide definite and precise characterization [333]. Anastyuk et al. (2010) utilized tandem MALDI and ESI mass spectrometry to characterize fucoidan from *Laminaria cichorioides*. Their study demonstrated MALDI-TOFMS as an effective tool for elucidating various structural fragments, sulfation patterns and glycosidic linkages [334]. However, due to absent complementary analysis by NMR or NMR in conjunction with methylation analysis, structural characterization is limited to a qualitative nature.

An extensive structural characterization of fucoidan from the sea cucumber species *Holothuria tubulosa* was carried out by Chang et al. (2016) [335]. Methylation analysis and NMR spectroscopy was used to determine glycosidic linkages and branching. Enzymatic degradation, using a fucoidanase, was applied to cleave glycosidic linkages in the polymer chain without desulfation. These low molecular weight fractions revealed glycosidic linkage patterns. Furthermore, the locations of sulfate groups were determined using NMR spectroscopy. While highly informative for fucoidans derived from echinoderms, these fucoidans exhibit greater structural homogeneity compared to those sourced from algae, as presented in this study (Paper 2). Therefore, employing a similar approach would unlikely yield NMR spectra of comparable quality. In Paper 2 (supplementary material) a depolymerization approach yielding similar results was conducted. Mild acid hydrolysis as well as a subsequent fractionation through size exclusion chromatography was performed. Neither the hydrolysis nor the fractionation led to simpler and more uniform spectra. Instead, complexity increased, suggesting that glycosidic linkages and branching points are randomly distributed in fucoidan from *L. hyperborea*. In recent years a plethora of fucoidan degrading enzymes from various microbial organisms have been discovered, selectively cleaving glycosidic linkages and sulfate groups [336]. Applying these fucoidanases and sulfatases could circumvent increasing complexity through degradation and potentially elucidate fine structures occurring within these heterogenous algal molecules [337].

To elucidate the structure of the polymer, a series of complementary analytical approaches, i.e., NMR, ICP-MS, Raman spectroscopy, and monosaccharide linkage analysis were performed on a highly purified high molecular weight (469 kDa, DP = 750) fucoidan from *L. hyperborea* (pFuc). Additionally, a desulfated derivative of the same batch of fucoidan was produced (dsFuc). An almost complete desulfation was achieved by a modified version of the solvolytic desulfation procedure from Inoue et al. (1976) [261]. However, SEC-MALS data showed that also a significant depolymerization (7.3 kDa, DP = 40) occurred, which must be considered in further structural assessment.

Glycosidic linkage analysis revealed (1→3)-linked fucose as the most abundant (31.9%) unit in the polymer (see Table 4-1), followed by (1→2)-linked fucose (13.2%) and (1→4)-linked fucose (7.7%). The combined number of branched fucose residues (adding up to 22.4%) matches with the number of terminal fucose residues, proving the length of desulfated fucoidan samples as sufficient and

internally verifying the data. Similar to the past work by Cumashi et al. (2007) on fucoidan from *L. digitata* [198], the results obtained in Paper 2 suggest 1→3 as the dominant glycosidic linkage in the backbone. On the other hand, the backbone structure was revealed to contain a high number 1→2,3 branching points resembling those revealed in *S. latissima*. In short, these similarities may be explained phylogenetically as all the aforementioned sources of seaweed are of the *Laminariales* species.

Table 4-1. Linkage analysis of the desulfated fucoidan, performed in three technical replicates. Molecular percentage and the corresponding standard deviations are indicated.

	t-Fuc	1,2-Fuc	1,3-Fuc	1,4-Fuc	1,2,3-Fuc	1,2,4-Fuc	1,3,4-Fuc	1,6-Gal	1,4,6-Gal	1,3,6-Gal
Mol%	23.2	13.2	31.9	7.7	13.1	4.5	4.8	0.8	0.5	0.4
SD	2.2	0.5	1.0	0.2	1.1	0.5	0.2	0.1	0.1	0.0

A total sugar analysis was performed on the unmodified pFuc. Gas chromatography revealed a monosaccharide content of mostly fucose (97.8 ± 0.2 %) and a minor galactose constituent (2.2 ± 0.2 %). These results were also supported by proton NMR data. Two strong signals in the anomeric region with an approximate ratio of 1:2 likely reflect the ratio of (1→2) to (1→3)-fucose obtained from the glycosidic linkage analysis. Furthermore, strong signals in the methyl region, correspond to the C-6 methyl protons of fucopyranose. The ratio between the integral for the anomeric proton {H-1} (5.1-5.8 ppm; Integral: 1.000), internal pyranose ring protons {H-2,3,4,5} (3.6-5.1 ppm; Integral: 4.186) and methyl group protons {H3-6} (1.0-1.8 ppm; Integral: 3.122) supports the results from the monosaccharide analysis consisting largely of fucose units. Giving another indication that the molecular structure in dsFuc is representative of the structure occurring pFuc. Due to the high molecular weight of pFuc NMR signals were too broad to extract more structural data from the spectra but comparison between the modified and unmodified fucoidan gave additional confirmation in the validity of the obtained data from both NMR as well as total sugar analysis.

The complexity of the spectra increased following mild acid hydrolysis. This increase was likely caused by the formation of new reducing and non-reducing ends, which diversifies the formerly near completely sulfated α-L-fucopyranose units with similar glycosidic linkage patterns. Solvolytic desulfation was a key step to achieve a more homogenous fucoidan without severe depolymerization allowing for 2D NMR spectroscopic measurements and assignment of chemical shifts for structural elucidation. The uniformity of the spectra obtained from unmodified pFuc, compared to the complex spectra following mild acid hydrolysis, reinforces the hypothesis of a (1→3)-linked main chain.

ICP-MS emerged as an important tool to accurately determine the degree of sulfation. While Raman spectroscopy can assign the location of the sulfate group along the sugar ring, it is not as quantitatively accurate as ICP-MS. Although vibrational spectroscopy is often referred to as a semi-quantitative method. On the hand with a larger array of fucoidan samples with known sulfate concentration (calibration curve) Raman spectroscopy could likely be used to quantify the degree of sulfation, while retaining the advantage of revealing the position of the sulfate groups [273,338].

Raman spectroscopy revealed no vibration between 1650–1800 cm^{-1}. These bands are related to C=O vibrations and their absence verifies the absence of acetyl groups and uronic acids in pFuc [339]. This is in good agreement with the results from proton and carbon NMR. Furthermore, a comparison between the pFuc and dsFuc showed that the sulfate groups in axial 4C position (839.8 cm^{-1}) were entirely removed by the desulfation treatment whereas the sulfate group in 2C remained to a minor extent, as indicated by the less affected band at 1065.3 cm^{-1}.

SEC-MALS was used to determine the molecular weight of the molecule in addition to the overall shape, chain conformation and branching pattern. Two different plot types have been used to verify the shape of polymer. An RMS conformation plot, where radius of gyration (R_n) was plotted against M and a slope (b) of 0.65 was obtained, resembling a random coil vector model (sphere b = 0.3; random coil b = 0.5; rigid rod b = 1) and a Mark-Houwink-Sakurada plot ([η] versus M), which resulted in a slope (a) of 0.78, also aligning with the theoretical value of a random coil shape (sphere a = 0; random coil a = 0.8; rigid rod a = 1.8), both plots indicating a large polymer with a highly flexible chain [45]. Combined with the results from the monosaccharide linkage analysis of a dominant glycosidic linkage and a high interception of branching points, the overall structure of a large, highly flexible molecule with short side chains can be deduced.

Fucoidan from *L. hyperborea* displays a complex and diverse structure. Thus, numerous combinations of glycosidic linkages and sulfate group positions are likely present in the molecule. Nevertheless, by combining the results from all mentioned analytical methods, a set of five possible structural fragments (equal ratio) was suggested. In short, the scientific value of the work herein (Paper 2) lies within broadening the understanding of fucoidan by more accurate representations of its structure.

4.2 Structure–function relationship and bioactive properties of fucoidan (Paper 2 and 3)

In Paper 2 and 3 we addressed the structure–function relationship of fucoidan and its bioactive properties. To investigate bioactivities, we sought to mitigate the presence of impurities and therefore we used highly purified fucoidan. Furthermore, to acquire a conclusive set of data we also conducted a meticulous characterization of fucoidan samples. To isolate which structural features were interlinked with activities we modified distinct structural features, while keeping others as similar as possible, thus retaining comparability between the samples.

Tsou at al. (2022) investigated antitumor and antioxidant effects of fucoidan extracted from *Sargassum ilicifolium*. The kelp was sampled from five different regions along the Taiwanese coastline and the fucoidan was extracted at two different temperatures [340]. The cytotoxicity and potential anticancer activity of these fucoidan extracts was assessed *in vitro* using three cell lines: Murine fibroblasts from adipose tissue (L929), human epithelial carcinoma cells from lung tissue (A549) and human epithelial carcinoma cells from colonic tissue (HCT116). Notably, none of the extracts showed toxicity to the non-cancerous cell line (L929). However, one extract obtained at lower temperature decreased the viability of the cancerous cell line derived from human lung tissue (A549).

The work of Tsou et al. offers an interesting look into some bioactive properties of fucoidans, while simultaneously illustrating the complex nature of fucoidan's bioactivity as revealed by the variable responses in different cell types. The samples were rigorously characterized for their degree of sulfation, monosaccharide composition and polyphenol content. Nevertheless, the considerable differences between the samples arguably obfuscate a clear path to revealing which structural properties lead to biological functions. In a recent review by Weelden et al. (2019), the structure–function relationship of fucoidan in relation to its anticancer properties was investigated. The bioavailability of fucoidan was examined in addition to some biological pathways in which fucoidan might interact [341]. In a similar vein as what could be inferred from Tsou and co-authors' study, Weelden et al., highlight the lack of conclusive structure–function relationships. They point out that one of the complicating factors is the compositional diversity of fucoidans, which can vary widely due to differences in extraction methods and species origins.

Lastly, a review by Ale et al. (2011) provided an in-depth discussion on bioactive properties, collating data on anticoagulant, antitumour and immune-response activity and linking these with structural features [342]. Ale et al., argued that the presence or potential presence of impurities such as polyphenols, mannitol, alginate and laminarin, are likely to confound interpretations of structure–function relationships in fucoidan.

In short, the current body of literature underscores the need for the methodology we employed for the fucoidan samples in our research (Paper 2 and 3). In the present work, structural features such as degree of sulfation and molecular weight were tailored for between-sample comparability to isolate structure–function relationships. In our studies (Paper 2 and 3) impurity was mitigated by extensive ultrafiltration of the fucoidan samples, graphene filtering and subsequent analyses of endotoxin concentration. This approach may provide a framework for future work on fucoidan by minimizing confounding variables to reveal accurate structure–function relationships (see Table 4-2).

Table 4-2. Data overview of fucoidan samples used in Paper 2 and 3. Degree of sulfation (DS), weight average molar mass (M_w), number average molar mass (M_n), degree of polymerization (DP), number average radius of gyration (R_n), Z-average radius of gyration (R_z), intrinsic viscosity determined by SMV1 ($[\eta]$), slope of a Mark-Houwink-Sakurada plot (a: $[\eta]$ versus M), slope of an RMS conformation plot (b: R_n versus M).

PAPER 2	DS	M_w [kDa]	M_n [kDa]	DP	R_n [nm]	$[\eta]$ [mL/g]	a	b
pFuc	1.70	469	218	750	27.4	98	0.78	0.65
dsFuc	0.12	7.3	5.8	40	–	6	–	–
hFuc	1.70	20.3	10.6	37	–	5	–	–

PAPER 3	DS	M_w [kDa]	M_n [kDa]	DP	R_z [nm]			b
Fuc1	1.70	1548	1021	3512	83.0			0.66
Fuc2	1.70	499	241	829	47.1			0.66
Fuc3	1.70	26.9	13.9	48	–			–

Sulfated polysaccharides are recognized as integral components of the extracellular matrix (ECM). The ECM is, briefly described, a three-dimensional structure composed of biomolecules within tissues [343]. Sulfated polysaccharides, through their anionic charge, mediate interactions with various signal molecules such as growth factors and cytokines. These interactions regulate cellular behaviour

such as migration, proliferation, and differentiation. Further, sulfated polysaccharides have been found to display a range of both pro and anti-inflammatory responses [344]. Accordingly, these biomacromolecules pose great interest for various biomedical and tissue engineering applications.

Clinically, the most used sulfated polysaccharide is heparin, with an estimated annual production of 100 tonnes [345]. Despite the diverse bioactivity of sulfated polysaccharides, heparin is used mainly for its anticoagulatory properties. A limitation of sulfated polysaccharides naturally present in the ECM is rapid turnover which may constrain their use as biomaterials intended for long-term implantation [346]. A key disadvantage with for instance heparin is the complex and extensive extraction process typically from animal tissues (e.g. pork intestines) which has a history of contamination with fatal consequences [345].

In Paper 2, bioactive properties of fucoidan were investigated *in vitro* using a lepirudin-based human whole blood model [81,347]. The effects on coagulation and complement were measured by prothrombin factor 1 and 2 (PTF1.2) and the terminal complement complex (TCC), respectively. A coagulation inhibitory effect was seen by all fucoidan samples at the highest concentration (1000 µg/mL), but at an intermediate concentration (100 µg/mL) this effect was maintained only for the native purified fucoidan (pFuc), and not for the hydrolysed (hFuc) nor the desulfated fucoidan (dsFuc). With respect to the complement system, inhibition was observed for native fucoidan (pFuc) at intermediate and high concentration. This suggests that both the molecular weight and degree of sulfation of fucoidan influence the inhibition of coagulation and the complement system. Similarly for cytokines, significant increases were seen observed for native fucoidan in the case MCP-1, whereas IP-10, PDGF-BB and RANTES were significantly reduced. These differences are likely attributable to the positive charge of these cytokines and thus electrostatic interactions with the sulfate groups of fucoidan. Furthermore, higher molecular weight appeared to be associated with more extensive effects.

Given the clear relationship between sulfation and bioactivity for fucoidan from *L. hyperborea*, exclusively the molecular weight was varied in Paper 3. In this research study, the potential therapeutic effects on ocular diseases, specifically, age-related macular degeneration (AMD) were examined. The effect of fucoidan was studied *in vitro* using primary porcine retinal pigment epithelial cells (RPE), and human-derived cell lines uveal melanoma (OMM-1), and immortalized retinal pigmented epithelium (ARPE-19). Naturally, it is important to ensure the safety of fucoidan for therapy of diseases such as AMD. Both primary RPE and ARPE-19 showed no decrease in viability which holds promise for future in vivo studies to further investigate the safety. Interestingly, only the uveal melanoma (OMM-1) showed decreased viability when exposed to intermediate (Fuc2, 499 kDa) and low molecular weight (Fuc3, 26.9 kDa) fucoidan. While not the objective of the present study, this may point to other promising bioactivities of fucoidan, such as anti-cancer activity. In wet AMD an overproduction of vascular endothelial growth factor (VEGF), leads to formation of abnormal blood vessels causing blindness. Thus, treatments that mitigate excess VEGF expression may also prevent blindness [348]. Another contributing to the loss of vision in AMD is oxidative stress, which if substantial may lead to cell death [349]. In Paper 3, both VEGF secretion and protection from oxidative stress was investigated and moreover seem to suggest a positive relationship between molecular weight and bioactivity. While anti-oxidative properties of fucoidans have been suggested previously, as highlighted by Weelden et al., the literature may in part be confounded by the presence of

contaminants [341,350]. Antioxidative properties may be readily explained by the presence of polyphenols. However, the use of an ultra-pure fucoidan such as herein, makes this reason unlikely. Furthermore, a direct radical scavenging mechanism based on the structure of fucoidan seems unlikely. The present work may suggest that fucoidan does in fact elicit protection from oxidative stress, but indirectly, by interaction with innate cellular mechanisms of antioxidant systems [351–353].

A relevant aspect not investigated in our studies, is the absorption and bioavailability of the different fucoidans. While a high molecular weight fucoidan might higher bioactivity, a potential downside could be a lower absorption through the intestinal track if it is administered orally. In China fucoidan from *Saccharina japonica* is applied as active pharmaceutical ingredient against renal diseases such as chronic renal failure, acute kidney injury and diabetic nephropathy [354]. For this medical application low molecular weight fucoidan was shown to be more effective, likely due to higher bioavailability and uptake into the bloodstream.

In brief, there is much left to be uncovered for the use of fucoidan as a therapeutic macromolecule. The work performed for this thesis highlights some of the fundamental bioactivities of fucoidan *in vitro* in human blood as well as a potential biomedical use in the treatment of ocular diseases. Importantly, a structure–function relationship was demonstrated revealing the degree of sulfation and molecular weight to be key parameters in bioactivity. These effects were demonstrated in a thoroughly characterized and pure fucoidan.

4.3 Alginate–chitosan hydrogels: gelling properties and interaction mechanism (Paper 1 and 4)

Alginate and alginate hydrogels are widely used in medical products, cosmetics and in the food industry. The properties of these hydrogels depend on the type of alginate (mainly molecular weight and block structure) as well as on the type of crosslinker and crosslinking mechanism. Alginates have the innate to form physically crosslinked gels in the presence multivalent cations such as Ca^{2+}, Sr^{2+} or Ba^{2+}. This mechanism has traditionally been explained by the egg-box model, in which G-blocks on alginate chains coordinate around and cooperatively bind calcium cations [79].

Alginate–chitosan junction zones established between the M-blocks of an alginate chain and chitosan oligomers were investigated as an alternative ionic crosslinking mechanism for alginates by Khong et al. (2013). They demonstrated in their study that fully de-acetylated chitosan D-blocks successfully crosslink poly-mannuronate (poly-M), forming stable hydrogels, but do not crosslink poly-guluronate (poly-G). The suggested explanation for the formation of stable junction zones between alginate M-blocks and chitosan D-blocks was a match in charge distance along the polysaccharide block structures [19]. This proof of concept sparked the need for a further investigation.

In Paper 4, three alginates with fundamentally different block structures, poly-M, poly-G, and poly-MG, have been investigated upon ionic crosslinking with chitosan oligosaccharides (CHOS) with a defined degree of polymerization.

In brief, the results obtained, strongly support the previously proposed gelling principle of poly-M alginate crosslinked with chitosan oligomers. The gel strength increased with the DP of the CHOS, due to the formation of more stable junction zones.

To study the formation of junction zones in ionically crosslinked hydrogels and to investigate the interaction mechanism is a challenging task. Few analytical techniques are suited to examine the interactions in aqueous conditions. Our attempts to characterize the interactions through NMR were hampered by precipitation of the poly- or oligosaccharides, when these were added in equal amounts. Furthermore, the obtained spectra displayed a strong peak broadening without noticeable signal shifts (data not published).

In a study by Donati et al. (2005), the ionic crosslinking of three different alginates (poly-M, poly-MG and poly-G) using calcium ions was analysed via circular dichroism spectroscopy (CD) [128]. A clear change in circular polarized light absorption occurred when poly-G was crosslinked with calcium ions. This indicates a chain–chain association when G-sequences bind calcium by a chelate-type interaction. This potential formation of a higher ordered structure is often described as the "egg-box" model [52,126]. Donati and co-authors also demonstrated the interaction of calcium ions with polyalternating MG-blocks, albeit with a less pronounced change in chiroptical activity compared to poly-G. Furthermore, no change in CD absorption occurred for poly-M, demonstrating CD spectroscopy as a suitable technique to examine ionic crosslinks in alginate gels.

In Paper 4, a series of experiments similar to the work of Donati et al., was drafted. The chiroptical properties were investigated for three different alginate block types upon the addition of stoichiometric amounts of chitosan oligomers. The CD spectra revealed an increased chiroptical activity for poly-M chitosan gelling systems. This is indicative of induced conformational changes and the formation of higher ordered structures [106,128], in agreement with the previously proposed "zipper-like" junction zones between chitosan and mannuronan (see Figure 4-1). No similar change in chiroptical activity was observed for poly-MG nor for poly-G chitosan oligomer gelling system.
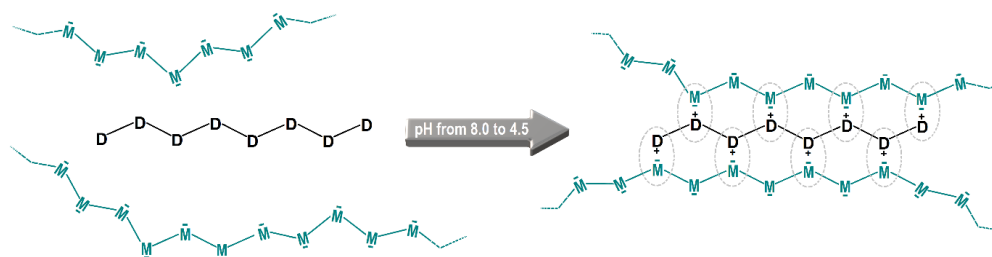

Figure 4-1 Schematic illustration of the interaction between a chitosan oligomer (black) and poly-M alginate (green) at different pH levels. Monosaccharide units: glucosamine (D), mannuronate (M). At pH ≤ 8 the amino groups of chitosan are mostly uncharged, while the carboxyl groups of alginate are mostly charged. At pH 4.0–5.0 both chitosan and alginate are predominantly charged, leading to ionic crosslinking of the two components and a zipper-like chain alignment due to the similar charge distance in both compounds.

Even though no induced structural effects were observed in the CD spectra for MG-blocks, the poly-MG-CHOS gels displayed high gel strengths during rheological experiments, orders of magnitude above their poly-M counterparts. This observation was unexpected and may allude to a fundamentally different mechanism of gelation. Thus, additional experiments to further describe the gelling system were needed.

A known and well-described phenomenon is the deceleration of gelling kinetics and reduction in gel strength upon the addition of salt to ionically crosslinked hydrogels [355–357]. The salt ions shield attractive electrostatic forces of the ionic crosslinker and polyelectrolyte and reduce the entropic driving force for electrostatic interaction. Greater concentrations of salt might therefore result in a weaker gel, a collapse of the gel network or precipitation of the polymer [358].

To evaluate the influence of salt on the gelling properties of this mixed polyelectrolyte gelling system, both poly-M and poly-MG chitosan gels were prepared with varied NaCl concentrations present and measured using rheology. The addition of salt (NaCl) that led to a decelerated gel formation and lower final gel strength for the poly-M gelling system. However, the opposite effect was displayed for poly-MG with an increase in gel strength by a factor of four. This may also be indicative of a fundamentally different crosslinking mechanism.

An additional observation, indicating a different formation of junction zones came from the visual appearance of the gels. While poly-M-CHOS gels appeared mostly transparent, their poly-MG analogue was highly turbid. Possibly pointing towards a stabilisation of the junction zones through hydrophobic interaction or local phase separation [359].

To gain further insight into the formation of junction zones, binding energies, chain alignments were investigated, and computer simulations performed. Alginate block oligomers (DP = 12 and 24) and chitosan oligomers (DP = 4 and 8) were used for these experiments. Within the scope of the simulations, no major differences in binding energy between CHOS and the three different alginate block types were observed. Nevertheless, the calculations confirmed that the chitosan-MG-complex was the only simulated chain association where the binding energy increased upon the addition of salt. This suggests an additional stabilization of the junction zone by hydrophobic interactions, not present in poly-M-chitosan-hydrogels. On the other hand, calculations of the coulomb potential (charge-based interactions) and Lennard-Jones potential (hydrophobic interactions) revealed only small contributions of hydrophobic interactions. Therefore, hydrophobic interactions alone are unlikely to account for the large difference in gel strength between the two gelling systems.

Additionally, the CHOS poly-MG hydrogel might be stabilized through a local phase separation effect along the junction zone. Although this remains speculative, the increasing turbidity during the poly-MG chitosan hydrogel formation as well as the gel strength compared to the poly-M gel supports this hypothesis. Unfortunately, results regarding a potential phase separation were not obtained due to the low molecular weight alginate block-units and the confined virtual space in which the simulations were performed. Another possibility is that phase separation requires the aggregation of multiple junction zones, which are known to exist for calcium crosslinked alginates [360]. Future simulations could address this limitation and incorporate a higher number of polyelectrolyte pairs.

The examined chitosan poly-MG gelling systems in this study, did not only display high gel strengths, but they are also known to be highly biocompatible and are stable in a broad range of salt concentrations. This stability may be relevant in application for hydrogels applied in various biological systems, for coating, drug delivery or cell encapsulation [361].

Boisseson et al. (2004), modified alginates by covalently linking long hydrophobic alkanes (octadecyl and dodecyl chains) to the polysaccharide backbone, improving the hydrogel stability against salt (NaCl) [362]. Crosslinking the MG-Blocks of an alginate with chitosan oligomers might be a more elegant solution to improve the stability against salt without the need for a harsh chemical modification of the biopolymer chain.

Combinations of crosslinkers were investigated in Paper 1. After Khong et al. (2013) demonstrated that chitosan oligomers form junction with alginate M-blocks. We hypothesised that adding CHOS to commercial alginates, such as leaf and stipe alginate from *Laminaria hyperborea*, might increase the overall gel strength due to the formation of additional junction zones. However, all initial tests adding CHOS to known formulations for calcium alginate hydrogels led to syneresis (expulsion of water and shrinkage). Since syneresis is an undesired effect in most commercial and biomedical applications, a different design for the study was opted for.

First, the highest concentration of crosslinker applicable without the occurrence of syneresis was determined for each alginate and crosslinker separately. These maximum concentration of Ca^{2+} or CHOS before syneresis were defined as 100%. Combinations of crosslinkers were performed based on a percentage wise substitution (e.g., 75% of max. Ca^{2+} were combined with 25% of max. CHOS).

Both leaf and stipe alginate produced weaker hydrogels when crosslinked solely with a commercial CHOS mixture (DP_n = 3.96), than their calcium crosslinked counterparts. On the other hand, the trend in gel strength between the two crosslinker concentration maxima for each alginate was not linear. It was shown that up to 50% of calcium in the leaf alginate sample and 25% in the stipe alginate sample could be substituted with chitosan oligomers, without compromising gel strength. In addition, the samples with high gel strength and combinations of calcium and chitosan crosslinker displayed faster gelling kinetics compared to calcium alone. A possible explanation could be that CHOS are protonated faster, since protons released through GDL can arrive at the oligosaccharide almost instantly due to the tunnel-effect in water. Calcium ions, on the other hand, are restrained by the gradual dissolution of $CaCO_3$ particles. Additionally, the higher ratio of GDL to CHOS compared to the gels crosslinked exclusively by CHOS might contribute to faster gelling kinetics.

Despite calcium ions being generally considered safe, Chan & Mooney (2013) pointed out that the release of calcium ions from alginate gels can promote inflammatory responses *in vitro* and in vivo [363]. The knowledge gained in Paper 1 may provide an approach to minimize the release of calcium and related inflammatory responses, while maintaining the mechanical properties of the desired alginate hydrogel.

The choice of a chitosan oligomer mixture (DP_n = 3.96) is a clear limitation in the study performed in Paper 1. Even though the goal of the experimental setup was to target M- blocks and G-blocks, the

results obtained in Paper 4 indicate a large potential contribution from MG-blocks crosslinked with chitosan oligomers (DP ≥ 7), which should be studied in the future.

Both studies (Paper 1 and 4) expand the understanding of alginate hydrogel crosslinking and provide additional tools for tailoring hydrogels. CHOS or composite CHOS-Ca^{2+} hydrogels may be relevant for applications within physiological conditions. MG-blocks crosslinked with chitosan oligosaccharides displayed exceptionally high gel strengths, while simultaneously showing high stability towards exposure to salt. M-blocks crosslinked with CHOS showed faster gelling kinetics and a different sensitivity towards pH-changes. Furthermore, it was shown that CHOS and Ca^{2+} crosslinking mechanisms are compatible and can be leveraged for faster gelation while maintaining high gel strength.

5   Future perspective and concluding remarks

This work conducted in conjunction with this thesis was motivated by the growing interest in marine polysaccharides. These materials are both abundant in nature and they possess great potential for a multitude of biomedical applications. The focus of this thesis was on fucoidan, alginate, and chitosan.

The conducted research included a thorough characterization of the molecular structure of fucoidan from *L. hyperborea.* It was determined that fucoidan from *L. hyperborea* is near a complete theoretical degree of sulfation (1.7). It is composed almost exclusively of fucose residues, has a high molecular weight (up to 1.4 MDa), and displays extensive branching with short side chains. Although our current results point towards a heterogenous and random distribution of structural features, future studies could leverage enzymes i.e. fucoidanases and novel desulfatases, to further elucidate structural patterns [336,337].

A highly purified and well-characterized fucoidan was used to investigate bioactivity *in vitro* using a lepirudin-based human whole blood model. Structural features such as the degree of sulfation and molecular weight were tailored for between-sample comparability to isolate structure–function relationships. Unmodified fucoidan with a high degree of sulfation and molecular weight was demonstrated to inhibit coagulation at intermediate to high concentrations with similar inhibitions of the complement system. The work highlighted the importance of both the molecular weight and the degree of sulfation as parameters for bioactive properties in further studies.

Based on the relationship between sulfation and bioactivity, a series of fully sulfated fucoidans, with different molecular weight, was tested for its potential therapeutic effects on ocular diseases, specifically, age-related macular degeneration (AMD). VEGF secretion and protection from oxidative stress were investigated and moreover indicated a positive relationship between molecular weight, bioactivity and potential therapeutic effects. While assessing the cell viability of three types of cell lines against the different fucoidans, no decrease in viability was observed for any of the epithelium cell lines. However, highly sulfated low and intermediate molecular weight fucoidan decreased the cell viability of uveal melanoma (OMM-1) cells. These results may indicate a potential for anti-cancer activity, while retaining viability in non-cancerous cells. The anti-cancer activities of fucoidan may be of interest in future studies related to biomedical applications [341].

Alginate hydrogels which are attractive biomaterials in tissue engineering, coatings and drug delivery, were examined on a fundamental scientific level. Interaction mechanisms and binding energies were characterized. To bridge the gap to applied science and real-world use, commercially available alginates from *L. hyperborea* were also used. The formation of junction zones between alginate M-blocks and fully de-acetylated chitosan oligomers, proposed as a zipper-like gelling concept by Khong et al. (2013), was further investigated in this thesis [19]. Strong evidence was obtained for the formation of secondary structures due to an alignment in charge distance of the oppositely charged polyelectrolytes. Furthermore, an alginate-chitosan gelling system was investigated showing crosslinking of poly-MG-blocks with chitosan oligomers. This gelling system displayed gel strengths orders of magnitude higher compared to their poly-M counterparts as well as stronger gels in the presence of salt. This is contrary to what has been observed for traditional ionically crosslinked hydrogels, pointing towards a fundamentally different chain–chain interaction mechanism [357,362].

While alginate is commonly crosslinked by calcium ions, here we chose to replace a fraction with chitosan oligosaccharides. Up to 50% of Ca^{2+} ions could be replaced by chitosan oligomers (under given conditions) without a loss in gel strength, while simultaneously increasing the rate of gelation. In short, the addition of chitosan oligomers as part of the gelation mechanism affords customization of gelling kinetics as well as a reduction in the use of calcium which can act inflammatory in hydrogels aimed for biomedical use [17,363]. Lastly, the alginate crosslinking demonstrated herein may confer greater hydrogel stability when used in biological systems containing electrolytes, which is a commonly highlighted hurdle for long-term applications [24,29,31,77,361].

There is great potential for composite hydrogels of alginate and fucoidan [364]. Alginate hydrogels provide a good vantage point for tissue engineering and cell encapsulation. On the other hand these are still considerably dissimilar to the microenvironment provided partly by proteoglycans in the extracellular matrix [365]. Sulfated polysaccharides can promote cell fates that may be desirable in tissue engineering applications such as maintenance of phenotypes and proliferation [366]. Sulfated polysaccharides have also shown promise in reducing fibrotic responses that hinder the survival of encapsulated cells in therapy [367–369]. A promising attempt to emulate the glycosaminoglycan rich environment found in the ECM, while maintaining the gelling properties, was attained through chemical sulfation of alginate [368,370,371]. However, mixed gels with incorporating fucoidan might provide similar properties without the need of harsh chemical modifications that fundamentally alter the structure of alginate and typically involves the use of solvents [364].

Additional experiments were performed, incorporating high molecular weight fucoidan into a calcium-alginate hydrogels (see Figure 5-1). Preliminary results indicated (data not published) that even integrating substantial amounts of fucoidan, only marginally altered the gelling properties, pointing towards a wide range of biomedical applications utilizing various physical, chemical and bioactive properties of these marine polysaccharides [346,372,373].
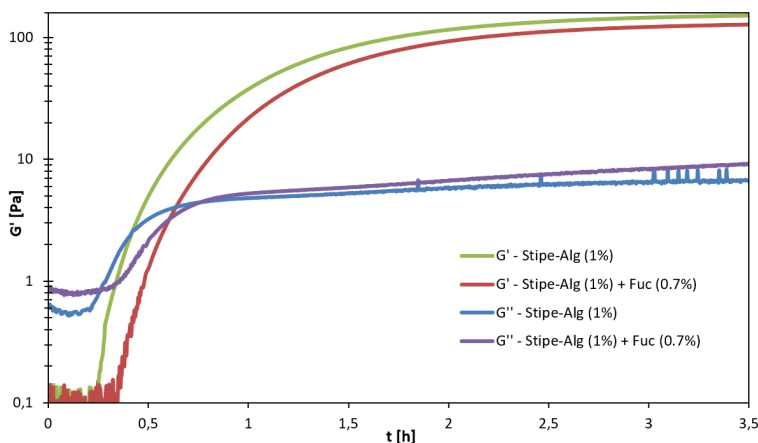

Figure 5-1 Comparison of the kinetics of gelation for calcium alginate gels, with and without added fucoidan. G' and G'' were determined as a function of time. All solutions had a composition of 10 g/L stipe alginate from *L. hyperborea*, 1.2 g/L CaCO₃ and 3.1 g/L GDL. Samples with added high molecular weight fucoidan at 7 g/L (red and purple line) displayed only minor differences in kinetics and final gel strength compared to samples without added fucoidan (green and blue line).

6   References

1.   Barsanti, L. & Gualtieri, P. *Algae: Anatomy, Biochemistry, and Biotechnology*. (CRC Press, 2014).

2.   Scott, S. A. *et al.* Biodiesel from algae: Challenges and prospects. *Curr. Opin. Biotechnol.* **21**, 277–286 (2010).

3.   Pérez-Lloréns, J. L., Mouritsen, O. G., Rhatigan, P., Cornish, M. L. & Critchley, A. T. Seaweeds in mythology, folklore, poetry, and life. *Journal of Applied Phycology* vol. 32 3157–3182 at https://doi.org/10.1007/s10811-020-02133-0 (2020).

4.   Brothwell, D. & Dimbleby, G. *Environmental aspects of coasts and islands*. vol. 1 (British Archaeological Reports, 1981).

5.   Chapman, V. *Seaweeds and their Uses*. (Methuen & Co. Ltd, 1950).

6.   Københavns Kommune. Fredningsværdier - Københavns Rådhus. *Københavns Ejendomme* **2010**–**7.82.**, (2014).

7.   Kerényi, K. *Die Mythologie der Griechen*. (DTV Deutscher Taschenbuch Verlag, 1966).

8.   Eraslan, Ş. Tethys and Thalassa in mosaic art. *Art-Sanat* **4**, 1–13 (2015).

9.   Turner, P. & Coulter, C. R. *Dictionary of Ancient Deities*. (Oxford University Press, 2001).

10. Raemdonck, K., Martens, T. F., Braeckmans, K., Demeester, J. & De Smedt, S. C. Polysaccharide-based nucleic acid nanoformulations. *Adv. Drug Deliv. Rev.* **65**, 1123–1147 (2013).

11. Kraan, S. Algal polysaccharides, novel applications and outlook. *Carbohydrates - Compr. Stud. Glycobiol. Glycotechnol.* 489–532 (2012) doi:10.5772/51572.

12. Bäumgen, M., Dutschei, T. & Bornscheuer, U. T. Marine Polysaccharides: Occurrence, Enzymatic Degradation and Utilization. *ChemBioChem* **22**, 2247–2256 (2021).

13. Charrier, B., Rabillé, H. & Billoud, B. Gazing at Cell Wall Expansion under a Golden Light. *Trends Plant Sci.* **24**, 130–141 (2019).

14. Seung, D. Amylose in starch: towards an understanding of biosynthesis, structure and function. *New Phytol.* **228**, 1490–1504 (2020).

15. Lahaye, M. & Robic, A. Structure and function properties of Ulvan, a polysaccharide from green seaweeds. *Biomacromolecules* **8**, 1765–1774 (2007).

16. Barbosa, A. I., Coutinho, A. J., Costa Lima, S. A. & Reis, S. Marine Polysaccharides in Pharmaceutical Applications: Fucoidan and Chitosan as Key Players in the Drug Delivery Match Field. *Mar. Drugs 2019, Vol. 17, Page 654* **17**, 654 (2019).

17. Shen, S., Chen, X., Shen, Z. & Chen, H. Marine Polysaccharides for Wound Dressings Application: An Overview. *Pharm. 2021, Vol. 13, Page 1666* **13**, 1666 (2021).

18. Nilsen-Nygaard, J., Strand, S., Vårum, K., Draget, K. & Nordgård, C. Chitosan: Gels and Interfacial Properties. *Polymers (Basel).* **7**, 552–579 (2015).

19. Khong, T. T., Aarstad, O. A., Skjåk-Bræk, G., Draget, K. I. & Vårum, K. M. Gelling concept combining chitosan and alginate - Proof of principle. *Biomacromolecules* **14**, 2765–2771 (2013).

20. Ross-Murphy, S. B. Rheological methods. in *Biophysical Methods in Food Research* (ed. Chan, H. W. S.) 137–199 (Blackwell Scientific Publications, 1984).

21. Desai, R. M., Koshy, S. T., Hilderbrand, S. a., Mooney, D. J. & Joshi, N. S. Versatile click alginate hydrogels crosslinked via tetrazine-norbornene chemistry. *Biomaterials* **50**, 30–37 (2015).

22. Li, H. Preparation and Characterization of Homogeneous Hydroxyapatite/Chitosan Composite Scaffolds via In-Situ Hydration. *J. Biomater. Nanobiotechnol.* **01**, 42–49 (2010).

23. Mi, F. L. *et al.* Chitosan-polyelectrolyte complexation for the preparation of gel beads and controlled release of anticancer drug. II. Effect of pH-dependent ionic crosslinking or interpolymer complex using tripolyphosphate or polyphosphate as reagent. *J. Appl. Polym. Sci.* **74**, 1093–1107 (1999).

24. Drury, J. L. & Mooney, D. J. Hydrogels for tissue engineering: Scaffold design variables and applications. *Biomaterials* **24**, 4337–4351 (2003).

25. El-Sherbiny, I. M. & Yacoub, M. H. Hydrogel scaffolds for tissue engineering: Progress and challenges. *Glob. Cardiol. Sci. Pract.* **2013**, 38 (2013).

26. Smidsrød, O. & Skjåk-Bræk, G. Alginate as immobilization matrix for cells. *Minerva Biotecnol.* **8**, 71–78 (1990).

27. González-Díaz, E. & Varghese, S. Hydrogels as Extracellular Matrix Analogs. *Gels* **2**, 20 (2016).

28. Cunha, L. & Grenha, A. Sulfated seaweed polysaccharides as multifunctional materials in drug delivery applications. *Mar. Drugs* **14**, (2016).

29. Tønnesen, H. H. & Karlsen, J. Alginate in drug delivery systems. *Drug Dev. Ind. Pharm.* **28**, 621–630 (2002).

30. Guan, Y. L., Shao, L. E. I. & De Yao, K. A Study on Correlation Between Water State and Swelling Kinetics of Chitosan-Based Hydrogels. *J. Appl. Polym. Sci.* **61**, 2325–2335 (1996).

31. Lee, K. Y. *et al.* Controlling Mechanical and Swelling Properties of Alginate Hydrogels Independently by Cross-Linker Type and Cross-Linking Density. *Macromolecules* **33**, 4291–4294 (2000).

32. Hennink, W. E. & van Nostrum, C. F. Novel crosslinking methods to design hydrogels. *Adv. Drug Deliv. Rev.* **64**, 223–236 (2012).

33. Edman, P., Ekman, B. & Sjöholm, I. Immobilization of proteins in microspheres of biodegradable polyacryldextran. *J. Pharm. Sci.* **69**, 838–842 (1980).

34. Akakuru, O. A. & Isiuku, B. O. Chitosan Hydrogels and their Glutaraldehyde-Crosslinked Counterparts as Potential Drug Release and Tissue Engineering Systems - Synthesis, Characterization, Swelling Kinetics and Mechanism. *J. Phys. Chem. Biophys.* **07**, (2017).

35. Tian, Z., Liu, W. & Li, G. The microstructure and stability of collagen hydrogel cross-linked by glutaraldehyde. *Polym. Degrad. Stab.* **130**, 264–270 (2016).

36. Yu, S. H., Wu, S. J., Wu, J. Y., Wen, D. Y. & Mi, F. L. Preparation of fucoidan-shelled and genipin-crosslinked chitosan beads for antibacterial application. *Carbohydr. Polym.* **126**, 97–107 (2015).

37. Jin, J., Song, M. & Hourston, D. J. Novel chitosan-based films cross-linked by genipin with improved physical properties. *Biomacromolecules* **5**, 162–168 (2004).

38. Karver, M. R., Weissleder, R. & Hilderbrand, S. A. Synthesis and evaluation of a series of 1,2,4,5-tetrazines for bioorthogonal conjugation. *Bioconjug. Chem.* **22**, 2263–2270 (2011).

39. Zhu, J., Wu, H. & Sun, Q. Preparation of crosslinked active bilayer film based on chitosan and alginate for regulating ascorbate-glutathione cycle of postharvest cherry tomato (Lycopersicon esculentum). *Int. J. Biol. Macromol.* **130**, 584–594 (2019).

40. Mathew, S. & Abraham, T. E. Characterisation of ferulic acid incorporated starch-chitosan blend films. *Food Hydrocoll.* **22**, 826–835 (2008).

41. Nicolau-Lapeña, I. *et al.* Combination of ferulic acid with Aloe vera gel or alginate coatings for shelf-life prolongation of fresh-cut apples. *Food Packag. Shelf Life* **27**, 100620 (2021).

42. Ou, S., Wang, Y., Tang, S., Huang, C. & Jackson, M. G. Role of ferulic acid in preparing edible films from soy protein isolate. *J. Food Eng.* **70**, 205–210 (2005).

43. Itagaki, S. *et al.* In vitro and in vivo antioxidant properties of ferulic acid: A comparative study with other natural oxidation inhibitors. *Food Chem.* **114**, 466–471 (2009).

44. Norde, W. *Colloids and Interfaces in Life Sciences and Bionanotechnology*. (CRC Press, 2011).

45. Smidsrød, O. & Moe, S. *Biopolymer Chemistry*. (Tapir Uttrykk, 2008).

46. Treloar, L. R. G. *The Physics of Rubber Elasticity*. (Oxfort University Press, 2005).

47. Draget, K. I. *et al.* Ionic and acid gel formation of epimerised alginates; the effect of AlgE4. *Int. J. Biol. Macromol.* **27**, 117–122 (2000).

48. Gwon, S. H., Yoon, J., Seok, H. K., Oh, K. H. & Sun, J. Y. Gelation dynamics of ionically crosslinked alginate gel with various cations. *Macromol. Res.* **23**, 1112–1116 (2015).

49. Lee, D., Zhang, H. & Ryu, S. Elastic Modulus Measurement of Hydrogels. in 1–21 (Springer, Cham, 2018). doi:10.1007/978-3-319-76573-0_60-1.

50. Anseth, K. S., Bowman, C. N. & Brannon-Peppas, L. Mechanical properties of hydrogels and their experimental determination. *Biomaterials* vol. 17 1647–1657 at

https://doi.org/10.1016/0142-9612(96)87644-7 (1996).

51.	Ambrosio, L., De Santis, R. & Nicolais, L. Composite hydrogels for implants. *Proc. Inst. Mech. Eng. H.* **212**, 93–9 (1998).

52.	Sikorski, P., Mo, F., Skjåk-Bræk, G. & Stokke, B. T. Evidence for egg-box-compatible interactions in calcium - Alginate gels from fiber x-ray diffraction. *Biomacromolecules* **8**, 2098–2103 (2007).

53.	Pielesz, A. Raman Spectroscopy as a Tool for Analysing Dye Distribution in Alginate Hydrogels. *FIBRES Text. East. Eur.* **15**, 136–140 (2007).

54.	Ross-Murphy, S. B. Rheological Methods. in *Physical Techniques for the Study of Food Biopolymers* 343–392 (Springer US, 1994). doi:10.1007/978-1-4615-2101-3_7.

55.	Mark, J. E. Rubber elasticity. *J. Chem. Educ.* **58**, 898 (1981).

56.	Moe, S. T., Draget, K. I., Skjåk-Bræk, G. & Simdsrød, O. Temperature dependence of the elastic modulus of alginate gels. *Carbohydr. Polym.* (1992) doi:10.1016/0144-8617(92)90081-Z.

57.	Yu, A. C. *et al.* Physical networks from entropy-driven non-covalent interactions. *Nat. Commun. 2021 121* **12**, 1–9 (2021).

58.	Scherer, G. W. Mechanics of syneresis I. Theory. *J. Non. Cryst. Solids* (1989) doi:10.1016/0022-3093(89)90328-1.

59.	Draget, K. I. *et al.* Effects of molecular weight and elastic segment flexibility on syneresis in Ca-alginate gels. *Food Hydrocoll.* **15**, 485–490 (2001).

60.	Mørch, Ý. A., Donati, I., Strand, B. L. & Skjåk-Bræk, G. Molecular Engineering as an Approach to Design New Functional Properties of Alginate. *Biomacromolecules* **8**, 2809–2814 (2007).

61.	Feng, Y., Kopplin, G., Sato, K., Draget, K. I. & Vårum, K. M. Alginate gels with a combination of calcium and chitosan oligomer mixtures as crosslinkers. *Carbohydr. Polym.* **156**, 490–497 (2017).

62.	Painter, T. J. Algal Polysaccharides. in *The Polysaccharides* (ed. Aspinall, G. O.) 195–285 (1983). doi:10.1016/B978-0-12-065602-8.50009-1.

63.	Linker, A. & Jones, R. S. A new polysaccharide resembling alginic acid isolated from pseudomonads. *J. Biol. Chem.* **241**, 3845–51 (1966).

64.	Gorin, P. A. J. & Spencer, J. F. T. Exocellular aginic acid from Azotobacter vinelandii. *Can. J. Chem.* **44**, 993–998 (1966).

65.	Atkins, E. D. T., Nieduszynski, I. A., Mackie, W., Parker, K. D. & Smolko, E. E. Structural components of alginic acid. I. The crystalline structure of poly-β-D-mannuronic acid. Results of X-ray diffraction and polarized infrared studies. *Biopolymers* **12**, 1865–1878 (1973).

66.	Haug, A. Composition and properties of alginates. (Norwegian Institute of Seaweed Research, 1964).

67.	Draget, K. I., Moe, S., Skjåk-Bræk, G. & Smidsrød, O. *Food Polysaccharides and their applications*. (CRC Press, Taylor & Francis Group, LLC, 2006).

68.	Fukushima, M., Tatsumi, K. & Wada, S. Evaluation of the Intrinsic Acid-Dissociation Constant of Alginic Acid by Considering the Electrostatic Effect. *Anal. Sci.* **15**, 1153–1155 (1999).

69.	Skjåk-Bræk, G., Grasdalen, H. & Larsen, B. Monomer sequence and acetylation pattern in some bacterial alginates. *Carbohydr. Res.* **154**, 239–250 (1986).

70.	Nivens, D. E., Ohman, D. E., Williams, J. & Franklin, M. J. Role of alginate and its O acetylation in formation of Pseudomonas aeruginosa microcolonies and biofilms. *J. Bacteriol.* **183**, 1047–1057 (2001).

71.	Høidal, H. K., Ertesvåg, H., Skjåk-Bræk, G., Stokke, B. T. & Valla, S. The recombinant Azotobacter vinelandii mannuronan C-5-epimerase AlgE4 epimerizes alginate by a nonrandom attack mechanism. *J. Biol. Chem.* **274**, 12316–12322 (1999).

72.	Masuelli, M. A. & Illanes, C. O. Review of the characterization of sodium alginate by intrinsic viscosity measurements . Comparative analysis between conventional and single point methods. *Int. J. Biomater. Sci. Eng.* **1**, 1–11 (2014).

73.	Rehm, B. H. A. & Moradali, M. F. *Alginates and Their Biomedical Applications*. vol. 11 (Springer Series in Biomaterials Science and Engineering, 2018).

74. Aarstad, O., Strand, B. L., Klepp-Andersen, L. M. & Skjåk-Bræk, G. Analysis of G-block distributions and their impact on gel properties of in vitro epimerized mannuronan. *Biomacromolecules* **14**, 3409–3416 (2013).

75. Buchinger, E. *et al.* Structural and Functional Characterization of the R-modules in Alginate C-5 Epimerases AlgE4 and AlgE6 from Azotobacter vinelandii. *J. Biol. Chem.* **289**, 31382–31396 (2014).

76. Draget, K. I. & Skjåk-Bræk, G. Chapter 7. Alginates: Existing and Potential Biotechnological and Medical Applications. in *Renewable Resources for Functional Polymers and Biomaterials: Polysaccharides, Proteins and Polyesters* 186–209 (2011). doi:10.1039/9781849733519-00186.

77. Mørch, Ý., Donati, I. & Strand, B. Effect of Ca 2+ , Ba 2+ , and Sr 2+ on Alginate Microbeads. *Biomacromolecules* **7**, 1471–1480 (2006).

78. Haug, A. The affinity of some divalent metals to different types of alginates. *Acta Chem Scand* **15**, 1794–1795 (1961).

79. Grant, G. T., Morris, E. R., Rees, D. A., Smith, P. J. C. & Thom, D. Biological interactions between polysaccharides and divalent cations: The egg-box model. *FEBS Lett.* **32**, 195–198 (1973).

80. Leong, J.-Y. *et al.* Advances in fabricating spherical alginate hydrogels with controlled particle designs by ionotropic gelation as encapsulation systems. *Particuology* **24**, 44–60 (2015).

81. Rokstad, A. M. *et al.* Alginate microbeads are complement compatible, in contrast to polycation containing microcapsules, as revealed in a human whole blood model. *Acta Biomater.* **7**, 2566–2578 (2011).

82. Pocker, Y. & Green, E. Hydrolysis of D-Glucono-δ-lactone. I. General Acid—Base Catalysis, Solvent Deuterium Isotope Effects, and Transition State Characterization. *J. Am. Chem. Soc.* **95**, 113–119 (1973).

83. Minke, R. & Blackwell, J. The structure of α-chitin. *J. Mol. Biol.* **120**, 167–181 (1978).

84. Sørbotten, A., Horn, S. J., Eijsink, V. G. H. & Vårum, K. M. Degradation of chitosans with chitinase B from Serratia marcescens. *FEBS J.* **272**, 538–549 (2005).

85. Atkins, E. D., Mackie, W. & Smolko, E. E. Crystalline structures of alginic acids. *Nature* **225**, 626–8 (1970).

86. Shen, T. & Gnanakaran, S. The stability of cellulose: A statistical perspective from a coarse-grained model of hydrogen-bond networks. *Biophys. J.* **96**, 3032–3040 (2009).

87. Kovalenko, V. I. Crystalline cellulose: structure and hydrogen bonds. *Russ. Chem. Rev.* **79**, 231–241 (2010).

88. Dutta, P. K., Tripathi, S., Mehrotra, G. K. & Dutta, J. Perspectives for chitosan based antimicrobial films in food applications. *Food Chem.* **114**, 1173–1182 (2009).

89. Usov, A. I. Alginic acids and alginates: analytical methods used for their estimation and characterisation of composition and primary structure. *Russ. Chem. Rev.* **68**, 957–966 (1999).

90. Arlov, Ø., Aachmann, F. L., Sundan, A., Espevik, T. & Skjåk-Bræk, G. Heparin-like properties of sulfated alginates with defined sequences and sulfation degrees. *Biomacromolecules* **15**, 2744–2750 (2014).

91. Holtan, S., Zhang, Q., Strand, W. I. & Skjåk-Bræk, G. Characterization of the Hydrolysis Mechanism of Polyalternating Alginate in Weak Acid and Assignment of the Resulting MG-Oligosaccharides by NMR Spectroscopy and ESI–Mass Spectrometry. *Biomacromolecules* **7**, 2108–2121 (2006).

92. Zaccheus, M. V. *et al.* Structural studies of the O-antigen polysaccharide from Escherichia coli TD2158 having O18 serogroup specificity and aspects of its interaction with the tailspike endoglycosidase of the infecting bacteriophage HK620. *Carbohydr. Res.* **357**, 118–125 (2012).

93. Bowman, K. A. *et al.* Single molecule investigation of the onset and minimum size of the calcium-mediated junction zone in alginate. *Carbohydr. Polym.* (2016) doi:10.1016/j.carbpol.2016.04.043.

94. Aarstad, O. A., Tøndervik, A., Sletta, H. & Skjåk-Bræk, G. Alginate sequencing: An analysis of

block distribution in alginates using specific alginate degrading enzymes. *Biomacromolecules* **13**, 106–116 (2012).

95. Heyraud, A., Colin-Morel, P., Girond, S., Richard, C. & Kloareg, B. HPLC analysis of saturated or unsaturated oligoguluronates and oligomannuronates. Application to the determination of the action pattern of Haliotis tuberculata alginate lyase. *Carbohydr. Res.* **291**, 115–26 (1996).

96. Dionex. Product manual for CarboPac® MA1,CarboPac® PA1, CarboPac® PA1 and CarboPac® PA100. http://www.dionex.com/enus/%0Awebdocs/4375-Man-031824-08-CarboPac-Combined-May10.pdf (2020).

97. Smidsrød, O. *et al.* A Light Scattering Study of Alginate. *Acta Chem. Scand.* **22**, 797–810 (1968).

98. Smidsrød, O. Solution properties of alginate. *Carbohydr. Res.* (1970) doi:10.1016/S0008-6215(00)80593-5.

99. Kes, M. & Christensen, B. E. A re-investigation of the Mark-Houwink-Sakurada parameters for cellulose in Cuen: A study based on size-exclusion chromatography combined with multi-angle light scattering and viscometry. *J. Chromatogr. A* **1281**, 32–37 (2013).

100. Podzimek, S. *Light Scattering, Size Exclusion Chromatography and Asymmetric Flow Field Flow Fractionation: Powerful Tools for the Characterization of Polymers, Proteins and Nanoparticles*. *Light Scattering, Size Exclusion Chromatography and Asymmetric Flow Field Flow Fractionation: Powerful Tools for the Characterization of Polymers, Proteins and Nanoparticles* (John Wiley and Sons, 2011). doi:10.1002/9780470877975.

101. Dawson, P. L. & Acton, J. C. Impact of proteins on food color. in *Proteins in Food Processing: Second Edition* 599–638 (Elsevier Inc., 2018). doi:10.1016/B978-0-08-100722-8.00023-1.

102. Andrews, D. L. Rayleigh Scattering and Raman Effect, Theory. in *Encyclopedia of Spectroscopy and Spectrometry* 924–930 (Elsevier Inc., 2017). doi:10.1016/B978-0-12-409547-2.11337-X.

103. Takahashi, A., Kato, T. & Nagasawa, M. The Second Virial Coefficient of Polyelectrolytes. *J. Phys. Chem.* **71**, 2001–2010 (1967).

104. Harding, S. E. *et al.* Extended Fujita approach to the molecular weight distribution of polysaccharides and other polymeric systems. *Methods* **54**, 136–144 (2011).

105. Vold, I. M. N., Kristiansen, K. A. & Christensen, B. E. A study of the chain stiffness and extension of alginates, in vitro epimerized alginates, and periodate-oxidized alginates using size-exclusion chromatography combined with light scattering and viscosity detectors. *Biomacromolecules* **7**, 2136–2146 (2006).

106. Matsuda, Y., Biyajima, Y. & Sato, T. Thermal denaturation, renaturation, and aggregation of a double-helical polysaccharide xanthan in aqueous solution. *Polym. J.* **41**, 526–532 (2009).

107. Christensen, B. E., Vold, I. M. N. & Vårum, K. M. Chain stiffness and extension of chitosans and periodate oxidised chitosans studied by size-exclusion chromatography combined with light scattering and viscosity detectors. *Carbohydr. Polym.* **74**, 559–565 (2008).

108. Duval, C., Le Cerf, D., Picton, L. & Muller, G. Aggregation of amphiphilic pullulan derivatives evidenced by on-line flow field flow fractionation/multi-angle laser light scattering. in *Journal of Chromatography B: Biomedical Sciences and Applications* (2001). doi:10.1016/S0378-4347(00)00517-X.

109. Capron, I., Grisel, M. & Muller, G. On-line Size Exclusion Chromatography and Multiangle Laser Light Scattering of High-Molecular-Weight Rigid Polysaccharides. *Int. J. Polym. Anal. Charact.* **2**, 9–20 (1995).

110. Smidsrød, O., Glover, R. M. & Whittington, S. G. The relative extension of alginates having different chemical composition. *Carbohydr. Res.* (1973) doi:10.1016/S0008-6215(00)82430-1.

111. Smidsrød, O. & Haug, A. Estimation of the relative stiffness of the molecular chain in polyelectrolytes from measurements of viscosity at different ionic strengths. *Biopolymers* **10**, 1213–1227 (1971).

112. Stokke, B. T., Smidsrød, O. & Brant, D. A. Predicted influence of monomer sequence distribution and acetylation on the extension of naturally occurring alginates. *Carbohydr. Polym.* (1993) doi:10.1016/0144-8617(93)90166-2.

113. Schwedt, G. *Analytische Chemie - Grundlagen, Methoden und Praxis*. (Wiley-VCH, 2008).

114. Günter, H. *NMR Spectroscopy: Basic Principles, Concepts and Applications in Chemistry, 3rd Edition*. (Wiley-VCH Verlag GmbH & Co. KGaA, 2013).

115. Cavanagh, J., Fairbrother, W. J., Palmer, A. G., Skelton, N. J. & Rance, M. *Protein NMR Spectroscopy*. *Protein NMR Spectroscopy* (Elsevier Inc., 2007). doi:10.1016/B978-0-12-164491-8.X5000-3.

116. Lattner, D., Flemming, H. C. & Mayer, C. 13C-NMR study of the interaction of bacterial alginate with bivalent cations. *Int. J. Biol. Macromol.* (2003) doi:10.1016/S0141-8130(03)00070-9.

117. Schürks, N., Wingender, J., Flemming, H. C. & Mayer, C. Monomer composition and sequence of alginates from Pseudomonas aeruginosa. *Int. J. Biol. Macromol.* (2002) doi:10.1016/S0141-8130(02)00002-8.

118. Penman, A. & Sanderson, G. R. A method for the determination of uronic acid sequence in alginates. *Carbohydr. Res.* (1972) doi:10.1016/S0008-6215(00)81637-7.

119. Grasdalen, H., Larsen, B. & Smidsrød, O. 13C NMR Studies of Monomeric Coposition and Sequence in Alginate. *Carbohydr. Res.* **89**, 179–191 (1981).

120. Grasdalen, H. High-field, 1H-NMR spectroscopy of alginate: sequential structure and linkage conformations. *Carbohydr. Res.* **118**, 255–260 (1983).

121. Woody, R. W. Theory of Circular Dichroism of Proteins. in *Circular Dichroism and the Conformational Analysis of Biomolecules* 25–67 (Springer US, 1996). doi:10.1007/978-1-4757-2508-7_2.

122. Berova, N., Nakanishi, K. & Woody, R. W. *Circular Dichroism: Principles and Applications*. (Wiley-VCH, 2000).

123. Snatzke, G. *Optical rotatory dispersion and circular dichroism in organic chemistry*. (Heyden, 1967).

124. Price, N. C. & Stevens, E. The refolding of denatured rabbit muscle pyruvate kinase. *Biochem. J.* **209**, 763–770 (1983).

125. Donati, I. *et al.* Determination of the diadic composition of alginate by means of circular dichroism: A fast and accurate improved method. *Carbohydr. Res.* **338**, 1139–1142 (2003).

126. Morris, E. R., Rees, D. A., Sanderson, G. R. & Thom, D. Conformation and circular dichroism of uronic acid residues in glycosides and polysaccharides. *J. Chem. Soc. Perkin Trans. 2* 1418–1425 (1975) doi:10.1039/P29750001418.

127. Morris, E. R., Rees, D. A. & Thom, D. Characterisation of alginate composition and block-structure by circular dichroism. *Carbohydr. Res.* **81**, 305–314 (1980).

128. Donati, I. *et al.* New hypothesis on the role of alternating sequences in calcium-alginate gels. *Biomacromolecules* **6**, 1031–1040 (2005).

129. Khouri, S. J., Knierim, R. & Buss, V. Induced circular dichroism of the interaction between pinacyanol and algal alginates. *Carbohydr. Res.* **344**, 1729–1733 (2009).

130. Vårum, K. M. & Smidsrød, O. Structure–property relationship in chitosans. in *Polysaccharides - Structural Diversity and Functional Versatility* (ed. Dumitriu, S.) 625–642 (CRC Press: Boca Raton, 2005).

131. Anthonsen, M. W. & Smidsrød, O. Hydrogen ion titration of chitosans with varying degrees of N-acetylation by monitoring induced 1H-NMR chemical shifts. *Carbohydr. Polym.* **26**, 303–305 (1995).

132. Strand, S. P., Tømmeraas, K., Vårum, K. M. & Østgaard, K. Electrophoretic Light Scattering Studies of Chitosans with Different Degrees of N -acetylation. *Biomacromolecules* **2**, 1310–1314 (2001).

133. Tsukada, S. & Inoue, Y. Conformational properties of chito-oligosaccharides: titration, optical rotation, and carbon-13 N.M.R. studies of chito-oligosaccharides. *Carbohydr. Res.* **88**, 19–38 (1981).

134. Vårum, K. M., Ottøy, M. H. & Smidsrød, O. Water-solubility of partially N-acetylated chitosans as a function of pH: effect of chemical composition and depolymerisation. *Carbohydr. Polym.* **25**, 65–70 (1994).

135. Ishiguro, K., Yoshie, N., Sakurai, M. & Inoue, Y. A 1H NMR study of a fragment of partially N-deacetylated chitin produced by lysozyme degradation. *Carbohydr. Res.* **237**, 333–338 (1992).

136. Vårum, K. M., Anthonsen, M. W., Grasdalen, H. & Smidsrod, O. Determination of the degree of N-acetylation and the distribution of N-acetyl groups in partially N-deacetylated chitins (chitosans) by high-field n.m.r. spectroscopy. *Carbohydr. Res.* **211**, 17–23 (1991).

137. Vårum, K. M., Anthonsen, M. W., Grasdalen, H. & Smidsrod, O. 13C-NMR studies of the acetylation sequences in partially N-deacetylated chitins (chitosans). *Carbohydr. Res.* **217**, 19–27 (1991).

138. Bellich, B., D'Agostino, I., Semeraro, S., Gamini, A. & Cesàro, A. "The Good, the Bad and the Ugly" of Chitosans. *Mar. Drugs* **14**, 99 (2016).

139. Younes, I. & Rinaudo, M. Chitin and Chitosan Preparation from Marine Sources. Structure, Properties and Applications. *Mar. Drugs* **13**, 1133–1174 (2015).

140. Gooday, G. W. The Ecology of Chitin Degradation. in 387–430 (1990). doi:10.1007/978-1-4684-7612-5_10.

141. Zhang, M., Haga, A., Sekiguchi, H. & Hirano, S. Structure of insect chitin isolated from beetle larva cuticle and silkworm (Bombyx mori) pupa exuvia. *Int. J. Biol. Macromol.* (2000) doi:10.1016/S0141-8130(99)00123-3.

142. Yen, M. T., Yang, J. H. & Mau, J. L. Physicochemical characterization of chitin and chitosan from crab shells. *Carbohydr. Polym.* (2009) doi:10.1016/j.carbpol.2008.06.006.

143. Moon, H. *et al.* Di-erent molecular interaction between collagen and - or -chitin in mechanically improved electrospun composite. *Mar. Drugs* **17**, (2019).

144. Kaya, M., Seyyar, O., Baran, T., Erdoğan, S. & Kar, M. A physicochemical characterization of fully acetylated chitin structure isolated from two spider species: With new surface morphology. *Int. J. Biol. Macromol.* **65**, 553–558 (2014).

145. Khong, T. T. Vietnamese chitin raw material , the chitin de - N - acetylation reaction , and a new chitosan - alginate gelling concept. (NTNU - Thesis, 2013).

146. White, S. A., Farina, P. R. & Fulton, I. Production and isolation of chitosan from Mucor rouxii. *Appl. Environ. Microbiol.* **38**, 323–328 (1979).

147. Mohadi, R., Hidayati, N. & Lesbani, A. Isolation of β-Chitosan from Squid Bone as Raw Material to Synthesize of Hybrid Photocatalysts TiO2-Chitosan. in *Journal of Physics: Conference Series* vol. 1095 (Institute of Physics Publishing, 2018).

148. Arcidiacono, S. & Kaplan, D. L. Molecular weight distribution of chitosan isolated from Mucor rouxii under different culture and processing conditions. *Biotechnol. Bioeng.* **39**, 281–286 (1992).

149. Lee, K. K. *et al.* Elevated cell wall chitin in Candida albicans confers echinocandin resistance in vivo. *Antimicrob. Agents Chemother.* **56**, 208–217 (2012).

150. Andersen, S. O. Cuticular Sclerotization and Tanning. in *Insect Molecular Biology and Biochemistry* 167–192 (Elsevier, 2012). doi:10.1016/B978-0-12-384747-8.10006-6.

151. Peter, M. G., Kegel, G. & Keller, R. Structural Studies on Sclerotized Insect Cuticle. in *Chitin in Nature and Technology* 21–28 (Springer US, 1986). doi:10.1007/978-1-4613-2167-5_4.

152. Percot, A., Viton, C. & Domard, A. Optimization of Chitin Extraction from Shrimp Shells. *Biomacromolecules* **4**, 12–18 (2003).

153. Rødde, R. H., Einbu, A. & Vårum, K. M. A seasonal study of the chemical composition and chitin quality of shrimp shells obtained from northern shrimp (Pandalus borealis). *Carbohydr. Polym.* **71**, 388–393 (2008).

154. Charoenvuttitham, P., Shi, J. & Mittal, G. S. Chitin extraction from black tiger shrimp (Penaeus monodon) waste using organic acids. *Sep. Sci. Technol.* **41**, 1135–1153 (2006).

155. Synowiecki, J. & Al-Khateeb, N. A. Production, Properties, and Some New Applications of Chitin and Its Derivatives. *Crit. Rev. Food Sci. Nutr.* **43**, 145–171 (2003).

156. Lamarque, G., Viton, C. & Domard, A. Comparative Study of the First Heterogeneous Deacetylation of α- and β-Chitins in a Multistep Process. *Biomacromolecules* **5**, 992–1001 (2004).

157. Chang, K. L. B., Tsai, G., Lee, J. & Fu, W. R. Heterogeneous N-deacetylation of chitin in alkaline solution. *Carbohydr. Res.* **303**, 327–332 (1997).

158. Yaghobi, N. & Hormozi, F. Multistage deacetylation of chitin: Kinetics study. *Carbohydr. Polym.* **81**, 892–896 (2010).

159. HOLLO, J. & LASZLO, E. Kinetical comparison of the acidic, alkaline and enzymatic hydrolysis of starch. *Period. Polytech. Chem. Eng.* **14**, 33–46 (1970).

160. Sacco, P. *et al.* Concepts for Developing Physical Gels of Chitosan and of Chitosan Derivatives. *Gels* **4**, 67 (2018).

161. Aam, B. B. *et al.* Production of chitooligosaccharides and their potential applications in medicine. *Mar. Drugs* **8**, 1482–1517 (2010).

162. Einbu, A. & Vårum, K. M. Characterization of Chitin and Its Hydrolysis to GlcNAc and GlcN. *Biomacromolecules* **9**, 1870–1875 (2008).

163. Furlani, F. *et al.* Nucleation, reorganization and disassembly of an active network from lactose-modified chitosan mimicking biological matrices. *Carbohydr. Polym.* **208**, 451–456 (2019).

164. Nordtveit, R. J., Vårum, K. M. & Smidsrød, O. Degradation of partially N-acetylated chitosans with hen egg white and human lysozyme. *Carbohydr. Polym.* **29**, 163–167 (1996).

165. Vårum, K. M., Myhr, M. M., Hjerde, R. J. N. & Smidsrød, O. In vitro degradation rates of partially N-acetylated chitosans in human serum. *Carbohydr. Res.* **299**, 99–101 (1997).

166. Köping-Höggård, M. *et al.* Chitosan as a nonviral gene delivery system. Structure-property relationships and characteristics compared with polyethylenimine in vitro and after lung administration in vivo. *Gene Ther.* **8**, 1108–1121 (2001).

167. Strand, S., Danielsen, S., Christensen, B. E. & Vårum, K. M. Influence of Chitosan Structure on the Formation and Stability of DNA- Chitosan Polyelectrolyte Complexes. *Biomacromolecules* **6**, 3357–3366 (2005).

168. Felt, O., Carrel, A., Baehni, P., Buri, P. & Gurny, R. Chitosan as tear substitute: a wetting agent endowed with antimicrobial efficacy. *J. Ocul. Pharmacol. Ther.* **16**, 261–70 (2000).

169. Liu, X. F., Guan, Y. L., Yang, D. Z., Li, Z. & Yao, K. D. Antibacterial Action of Chitosan and Carboxymethlyated Chitosan. *J. Appl. Polym. Sci.* **79**, 1324–1335 (2000).

170. Mellegård, H., Strand, S. P., Christensen, B. E., Granum, P. E. & Hardy, S. P. Antibacterial activity of chemically defined chitosans: Influence of molecular weight, degree of acetylation and test organism. *Int. J. Food Microbiol.* **148**, 48–54 (2011).

171. Xia, W., Liu, P., Zhang, J. & Chen, J. Biological activities of chitosan and chitooligosaccharides. *Food Hydrocoll.* **25**, 170–179 (2011).

172. Ong, S. Y., Wu, J., Moochhala, S. M., Tan, M. H. & Lu, J. Development of a chitosan-based wound dressing with improved hemostatic and antimicrobial properties. *Biomaterials* **29**, 4323–4332 (2008).

173. Ueno, H., Mori, T. & Fujinaga, T. Topical formulations and wound healing applications of chitosan. *Adv. Drug Deliv. Rev.* **52**, 105–115 (2001).

174. Merzendorfer, H. & Zimoch, L. Chitin metabolism in insects: Structure, function and regulation of chitin synthases and chitinases. *J. Exp. Biol.* **206**, 4393–4412 (2003).

175. Chung, F. H. & Scott, R. W. New approach to determination of crystallinity of polymers by X-ray diffraction. *urn:issn:0021-8898* **6**, 225–230 (1973).

176. Huot, J. C. *et al.* Evaluating the suitability of highly cross-linked and remelted materials for use in posterior stabilized knees. *J. Biomed. Mater. Res. Part B Appl. Biomater.* **95B**, 298–307 (2010).

177. Samiee, S., Ahmadzadeh, H., Hosseini, M. & Lyon, S. Algae as a Source of Microcrystalline Cellulose. in *Advanced Bioprocessing for Alternative Fuels, Biobased Chemicals, and Bioproducts* 331–350 (Elsevier, 2019). doi:10.1016/b978-0-12-817941-3.00017-6.

178. Thygesen, A., Oddershede, J., Lilholt, H., Thomsen, A. B. & Ståhl, K. On the determination of crystallinity and cellulose content in plant fibres. *Cellulose* **12**, 563–576 (2005).

179. Park, S., Baker, J. O., Himmel, M. E., Parilla, P. A. & Johnson, D. K. Cellulose crystallinity index:

Measurement techniques and their impact on interpreting cellulase performance. *Biotechnol. Biofuels* **3**, 1–10 (2010).

180. Muzzarelli, R. A. A. & Rocchetti, R. Determination of the degree of acetylation of chitosans by first derivative ultraviolet spectrophotometry. *Carbohydr. Polym.* (1985) doi:10.1016/0144-8617(85)90005-0.

181. Liu, D., Wei, Y., Yao, P. & Jiang, L. Determination of the degree of acetylation of chitosan by UV spectrophotometry using dual standards. *Carbohydr. Res.* **341**, 782–785 (2006).

182. Shigemasa, Y., Matsuura, H., Sashiwa, H. & Saimoto, H. Evaluation of different absorbance ratios from infrared spectroscopy for analyzing the degree of deacetylation in chitin. *Int. J. Biol. Macromol.* (1996) doi:10.1016/0141-8130(95)01079-3.

183. Duarte, M. L., Ferreira, M. C., Marvão, M. R. & Rocha, J. An optimised method to determine the degree of acetylation of chitin and chitosan by FTIR spectroscopy. *Int. J. Biol. Macromol.* (2002) doi:10.1016/S0141-8130(02)00039-9.

184. Muzzarelli, R. A. A. & Tanfani, F. The N-permethylation of chitosan and the preparation of N-trimethyl chitosan iodide. *Carbohydr. Polym.* (1985) doi:10.1016/0144-8617(85)90037-2.

185. Kasaai, M. R. Various Methods for Determination of the Degree of N-Acetylation of Chitin and Chitosan: A Review. *J. Agric. Food Chem.* **57**, 1667–1676 (2009).

186. Sato, H. *et al.* Determination of the Degree of Acetylation of Chitin/Chitosan by Pyrolysis-Gas Chromatography in the Presence of Oxalic Acid. *Anal. Chem.* **70**, 7–12 (1998).

187. Domard, A. Determination of N-acetyl content in chitosan samples by c.d. measurements. *Int. J. Biol. Macromol.* **9**, 333–336 (1987).

188. Lakkis, J. & Villota, R. Effect of acylation on substructural properties of proteins: a study using fluorescence and circular dichroism. *J. Agric. Food Chem.* **40**, 553–560 (1992).

189. Hirai, A., Odani, H. & Nakajima, A. Determination of degree of deacetylation of chitosan by 1H NMR spectroscopy. *Polym. Bull.* **26**, 87–94 (1991).

190. Barth, H. G., Boyes, B. E. & Jackson, C. Size Exclusion Chromatography and Related Separation Techniques. *Anal. Chem.* **70**, 251–278 (1998).

191. Potschka, M. Mechanism of size-exclusion chromatography. I. Role of convection and obstructed diffusion in size-exclusion chromatography. *J. Chromatogr. A* (1993) doi:10.1016/0021-9673(93)83287-3.

192. Mori, S. & Barth, H. G. Fundamental Concepts. in *Size Exclusion Chromatography* 11–29 (Springer Berlin Heidelberg, 1999). doi:10.1007/978-3-662-03910-6_2.

193. Kusaykin, M. *et al.* Structure, biological activity, and enzymatic transformation of fucoidans from the brown seaweeds. *Biotechnol. J.* **3**, 904–915 (2008).

194. Mulloy, B., Ribeiro, A. C., Alves, A. P., Vieira, R. P. & Mourão, P. A. S. S. Sulfated fucans from echinoderms have a regular tetrasaccharide repeating unit defined by specific patterns of sulfation at the 0-2 and 0-4 positions. *J. Biol. Chem.* **269**, 22113–22123 (1994).

195. Alves, A. P., Mulloy, B., Diniz, J. A. & Mourão, P. A. S. S. Sulfated polysaccharides from the egg jelly layer are species-specific inducers of acrosomal reaction in sperms of sea urchins. *J. Biol. Chem.* **272**, 6965–6971 (1997).

196. Kariya, Y. *et al.* Isolation and partial characterization of fucan sulfates from the body wall of sea cucumber Stichopus japonicus and their ability to inhibit osteoclastogenesis. *Carbohydr. Res.* **339**, 1339–1346 (2004).

197. Yu, L. *et al.* Structural study of fucoidan from sea cucumber acaudina molpadioides: A fucoidan containing novel tetrafucose repeating unit. *Food Chem.* **142**, 197–200 (2014).

198. Cumashi, A. *et al.* A comparative study of the anti-inflammatory, anticoagulant, antiangiogenic, and antiadhesive activities of nine different fucoidans from brown seaweeds. *Glycobiology* **17**, 541–552 (2007).

199. Bilan, M. I. *et al.* Further studies on the composition and structure of a fucoidan preparation from the brown alga Saccharina latissima. *Carbohydr. Res.* **345**, 2038–2047 (2010).

200. Fletcher, H. R., Biller, P., Ross, A. B. & Adams, J. M. M. The seasonal variation of fucoidan within three species of brown macroalgae. *Algal Res.* **22**, 79–86 (2017).

201. Kylin, H. Zur Biochemie der Meeresalgen. *Hoppe. Seylers. Z. Physiol. Chem.* **83**, 171–197 (1913).
202. McNeely, W. H. *Industrial Gums: Polysaccharides and Their Derivatives*. (Academic Press, 1959).
203. Mcnaught, A. D. *et al.* Nomenclature of Carbohydrates. *Pure Appl. Chem* **68**, 1919–2008 (1996).
204. Deniaud-Bouët, E., Hardouin, K., Potin, P., Kloareg, B. & Hervé, C. A review about brown algal cell walls and fucose-containing sulfated polysaccharides: Cell wall context, biomedical properties and key research challenges. *Carbohydr. Polym.* **175**, 395–408 (2017).
205. Ustyuzhanina, N. E. *et al.* Anticoagulant and antithrombotic activities of modified xylofucan sulfate from the brown alga Punctaria plantaginea. *Carbohydr. Polym.* **136**, 826–833 (2016).
206. Berteau, O. & Mulloy, B. Sulfated fucans, fresh perspectives: Structures, functions, and biological properties of sulfated fucans and an overview of enzymes active toward this class of polysaccharide. *Glycobiology* **13**, 29–40 (2003).
207. Gómez-Ordóñez, E., Jiménez-Escrig, A. & Rupérez, P. Molecular weight distribution of polysaccharides from edible seaweeds by high-performance size-exclusion chromatography (HPSEC). *Talanta* **93**, 153–159 (2012).
208. Sichert, A. *et al.* Ion-exchange purification and structural characterization of five sulfated fucoidans from brown algae. *Glycobiology* **31**, 352–357 (2021).
209. Kopplin, G. *et al.* Structural Characterization of Fucoidan from Laminaria hyperborea : Assessment of Coagulation and Inflammatory Properties and Their Structure–Function Relationship. *ACS Appl. Bio Mater.* **1**, 1880–1892 (2018).
210. Brusca, R. & Brusca, G. *Invertebrates*. vol. 4 (Oxford Academic, 2004).
211. Pereira, M. S., Mulloy, B. & Mourão, P. A. S. Structure and anticoagulant activity of sulfated fucans. Comparison between the regular, repetitive, and linear fucans from echinoderms with the more heterogeneous and branched polymers from brown algae. *J. Biol. Chem.* **274**, 7656–7667 (1999).
212. Pomin, V. H. An overview about the structure-function relationship of marine sulfated homopolysaccharides with regular chemical structures. *Biopolymers* **91**, 601–609 (2009).
213. Yu, L. *et al.* Structure and rheological characteristics of fucoidan from sea cucumber Apostichopus japonicus. *Food Chem.* **180**, 71–76 (2015).
214. Rioux, L. E., Turgeon, S. L. & Beaulieu, M. Structural characterization of laminaran and galactofucan extracted from the brown seaweed Saccharina longicruris. *Phytochemistry* **71**, 1586–1595 (2010).
215. Bilan, M. I. *et al.* Preliminary investigation of a highly sulfated galactofucan fraction isolated from the brown alga Sargassum polycystum. *Carbohydr. Res.* **377**, 48–57 (2013).
216. Zvyagintseva, T. N. *et al.* Water-soluble polysaccharides of some far-eastern brown seaweeds. Distribution, structure, and their dependence on the developmental conditions. *J. Exp. Mar. Bio. Ecol.* **294**, 1–13 (2003).
217. Liu, F. *et al.* Fucoidan extract derived from Undaria pinnatifida inhibits angiogenesis by human umbilical vein endothelial cells. *Phytomedicine* **19**, 797–803 (2012).
218. Bilan, M. I., Grachev, A. a., Shashkov, A. S., Nifantiev, N. E. & Usov, A. I. Structure of a fucoidan from the brown seaweed Fucus serratus L. *Carbohydr. Res.* **341**, 238–245 (2006).
219. Chevolot, L., Mulloy, B., Ratiskol, J., Foucault, A. & Colliec-Jouault, S. A disaccharide repeat unit is the major structure in fucoidans from two species of brown algae. *Carbohydr. Res.* **330**, 529–535 (2001).
220. Daniel, R. *et al.* Regioselective desulfation of sulfated L-fucopyranoside by a new sulfoesterase from the marine mollusk Pecten maximus: Application to the structural study of algal fucoidan (Ascophyllum nodosum). *Eur. J. Biochem.* **268**, 5617–5626 (2001).
221. Ye, J. *et al.* Enzyme-digested fucoidan extracts derived from seaweed Mozuku of Cladosiphon novae-caledoniae kylin inhibit invasion and angiogenesis of tumor cells. *Cytotechnology* **47**, 117–126 (2005).

222. Daniel, R. *et al.* Electrospray ionization mass spectrometry of oligosaccharides derived from fucoidan of Ascophyllum nodosum. *Carbohydr. Res.* **342**, 826–834 (2007).

223. Chizhov, A. O. *et al.* A study of fucoidan from the brown seaweed Chorda filum. *Carbohydr. Res.* **320**, 108–119 (1999).

224. Sakai, T., Ishizuka, K., Shimanaka, K., Ikai, K. & Kato, I. Structures of Oligosaccharides Derived from Cladosiphon okamuranus Fucoidan by Digestion with Marine Bacterial Enzymes. *Mar. Biotechnol.* **5**, 536–544 (2003).

225. Shimizu, J. *et al.* Proportion of Murine Cytotoxic T Cells is Increased by High Molecular-Weight Fucoidan Extracted from Okinawa mozuku (Cladosiphon okamuranus). *J. Heal. Sci.* **51**, 394–397 (2005).

226. Hadj Ammar, H. *et al.* Physico-chemical characterization and pharmacological evaluation of sulfated polysaccharides from three species of Mediterranean brown algae of the genus Cystoseira. (2012) doi:10.1186/s40199-015-0089-6.

227. Ale, M. T. A. & Meyer, A. S. Fucoidans from brown seaweeds: an update on structures, extraction techniques and use of enzymes as tools for structural elucidation. *RSC Adv.* **3**, 8131–8141 (2013).

228. Bilan, M. I. *et al.* A highly regular fraction of a fucoidan from the brown seaweed Fucus distichus L. *Carbohydr. Res.* **339**, 511–517 (2004).

229. Bilan, M. I. *et al.* Effect of Enzyme Preparation from the Marine Mollusk Littorina kurila on Fucoidan from the Brown Alga Fucus distichus. *Biochem. 2005 7012* **70**, 1321–1326 (2005).

230. Menshova, R. V. *et al.* Fucoidans from brown alga Fucus evanescens: Structure and biological activity. *Front. Mar. Sci.* **3**, 129 (2016).

231. Neupane, S., Bittkau, K. S. & Alban, S. Size distribution and chain conformation of six different fucoidans using size-exclusion chromatography with multiple detection. *J. Chromatogr. A* **1612**, 460658 (2020).

232. Rodriguez-Jasso, R. M., Mussatto, S. I., Pastrana, L., Aguilar, C. N. & Teixeira, J. A. Chemical composition and antioxidant activity of sulphated polysaccharides extracted from Fucus vesiculosus using different hydrothermal processes. *Chem. Pap. 2013 682* **68**, 203–209 (2013).

233. Wang, J., Zhang, Q., Zhang, Z., Song, H. & Li, P. Potential antioxidant and anticoagulant capacity of low molecular weight fucoidan fractions extracted from Laminaria japonica. *Int. J. Biol. Macromol.* **46**, 6–12 (2010).

234. Hou, Y., Wang, J., Jin, W., Zhang, H. & Zhang, Q. Degradation of Laminaria japonica fucoidan by hydrogen peroxide and antioxidant activities of the degradation products of different molecular weights. *Carbohydr. Polym.* **87**, 153–159 (2012).

235. Li, H. Y. *et al.* Isolation, structural characterization and bioactivities of polysaccharides from Laminaria japonica: A review. *Food Chem.* **370**, 131010 (2022).

236. Dörschmann, P., Kopplin, G., Roider, J. & Klettner, A. Effects of Sulfated Fucans from Laminaria hyperborea Regarding VEGF Secretion, Cell Viability, and Oxidative Stress and Correlation with Molecular Weight. *Mar. Drugs* **17**, 548 (2019).

237. Synytsya, A. *et al.* Structure and antitumour activity of fucoidan isolated from sporophyll of Korean brown seaweed Undaria pinnatifida. *Carbohydr. Polym.* **81**, 41–48 (2010).

238. Vishchuk, O. S., Tarbeeva, D. V., Ermakova, S. P. & Zvyagintseva, T. N. Structural characteristics and biological activity of fucoidans from the brown algae Alaria sp. and Saccharina japonica of different reproductive status. *Chem. Biodivers.* **9**, 817–828 (2012).

239. Vishchuk, O. S., Ermakova, S. P. & Zvyagintseva, T. N. The fucoidans from brown algae of Far-Eastern seas: Anti-tumor activity and structure-function relationship. *Food Chem.* **141**, 1211–1217 (2013).

240. Luo, L. *et al.* Comparison of Physicochemical Characteristics and Anticoagulant Activities of Polysaccharides from Three Sea Cucumbers. *Mar. Drugs 2013, Vol. 11, Pages 399-417* **11**, 399–417 (2013).

241. Wu, M. *et al.* Structural Analysis and Anticoagulant Activities of the Novel Sulfated Fucan Possessing a Regular Well-Defined Repeating Unit from Sea Cucumber. *Mar. Drugs 2015, Vol.*

13, Pages 2063-2084 **13**, 2063–2084 (2015).

242. Holdt, S. L. & Kraan, S. Bioactive compounds in seaweed: Functional food applications and legislation. *J. Appl. Phycol.* **23**, 543–597 (2011).

243. García-Ríos, V., Ríos-Leal, E., Robledo, D. & Freile-Pelegrín, Y. Polysaccharides composition from tropical brown seaweeds. *Phycol. Res.* **60**, 305–315 (2012).

244. Deniaud-Bouët, E. *et al.* Chemical and enzymatic fractionation of cell walls from Fucales: insights into the structure of the extracellular matrix of brown algae. *Ann. Bot.* **114**, 1203–1216 (2014).

245. Kloareg, B., Demarty, M. & Mabeau, S. Polyanionic characteristics of purified sulphated homofucans from brown algae. *Int. J. Biol. Macromol.* **8**, 380–386 (1986).

246. Aquino, R. S., Grativol, C. & Mourão, P. A. S. S. Rising from the Sea: Correlations between Sulfated Polysaccharides and Salinity in Plants. **6**, e18862 (2011).

247. Senthilkumar, K., Manivasagan, P., Venkatesan, J. & Kim, S. K. Brown seaweed fucoidan: Biological activity and apoptosis, growth signaling mechanism in cancer. *Int. J. Biol. Macromol.* **60**, 366–374 (2013).

248. Torode, T. A. *et al.* Monoclonal Antibodies Directed to Fucoidan Preparations from Brown Algae. *PLoS One* **10**, e0118366 (2015).

249. Pomin, V. H. Sulfated glycans in inflammation. *European Journal of Medicinal Chemistry* vol. 92 353–369 at https://doi.org/10.1016/j.ejmech.2015.01.002 (2015).

250. Afratis, N. *et al.* Glycosaminoglycans: key players in cancer cell biology and treatment. *FEBS J.* **279**, 1177–1197 (2012).

251. Raman, R., Sasisekharan, V. & Sasisekharan, R. Structural Insights into Biological Roles of Protein-Glycosaminoglycan Interactions. *Chem. Biol.* **12**, 267–277 (2005).

252. Mélida, H., Sandoval-Sierra, J. V., Diéguez-Uribeondo, J. & Bulone, V. Analyses of extracellular carbohydrates in oomycetes unveil the existence of three different cell wall types. *Eukaryot. Cell* **12**, 194–203 (2013).

253. Fengel, D. & Wegener, G. Hydrolysis of Polysaccharides with Trifluoroacetic Acid and its Application to Rapid Wood and Pulp Analysis. *Adv. Chem.* **181**, 145–158 (1979).

254. Blakeney, A. B., Harris, P. J., Henry, R. J. & Stone, B. A. A simple and rapid preparation of alditol acetates for monosaccharide analysis. *Carbohydr. Res.* **113**, 291–299 (1983).

255. Voiges, K., Adden, R., Rinken, M. & Mischnick, P. Critical re-investigation of the alditol acetate method for analysis of substituent distribution in methyl cellulose. *Cellulose* **19**, 993–1004 (2012).

256. Albersheim, P., Nevins, D. J., English, P. D. & Karr, A. A method for the analysis of sugars in plant cell-wall polysaccharides by gas-liquid chromatography. *Carbohydr. Res.* **5**, 340–345 (1967).

257. Birgersson, P. S. *et al.* Sequential extraction and fractionation of four polysaccharides from cultivated brown algae Saccharina latissima and Alaria esculenta. *Algal Res.* **69**, 102928 (2023).

258. Thomas, R. *Practical Guide to ICP-MS : A Tutorial for Beginners*. (CRC Press, 2008). doi:10.1201/9781420067873.

259. Hammerschmidt, J. & Wrobel, M. Decomposition of Metal Sulfates – A SO2-Source for Sulfuric Acid Production. in *Sulphur and Sulphuric Acid Conference* 87–100 (The Southern African Institute of Mining and Metallurgy, 2009).

260. Corgnale, C., Gorensek, M. B. & Summers, W. A. Review of Sulfuric Acid Decomposition Processes for Sulfur-Based Thermochemical Hydrogen Production Cycles. *Process. 2020, Vol. 8, Page 1383* **8**, 1383 (2020).

261. Inoue, Y. & Nagasawa, K. Selective N-desulfation of heparin with dimethyl sulfoxide containing water or methanol. *Carbohydr. Res.* **46**, 87–95 (1976).

262. Miller, I. J. & Blunt, J. W. Desulfation of algal galactans. *Carbohydr. Res.* **309**, 39–43 (1998).

263. Navarro, D. a., Flores, M. L. & Stortz, C. a. Microwave-assisted desulfation of sulfated polysaccharides. *Carbohydr. Polym.* **69**, 742–747 (2007).

264. Takano, R., Matsuo, M., Kamei-Hayashi, K., Hara, S. & Hlrase, S. A Novel Regioselective Desulfation Method Specific to Carbohydrate 6-Sulfate Using Silylating Reagents. *Biosci. Biotechnol. Biochem.* **56**, 1577–1580 (1992).

265. Takano, R. Desulfation of sulfated carbohydrates. *Trends Glycosci. Glycotechnol.* **14**, 343–351 (2002).

266. Ciucanu, I. & Kerek, F. A simple and rapid method for the permethylation of carbohydrates. *Carbohydr. Res.* **131**, 209–217 (1984).

267. Łowicki, D., Czarny, A. & Mlynarski, J. NMR of carbohydrates. *Nucl. Magn. Reson.* **42**, 383–419 (2013).

268. Sakurama, H. *et al.* Differences in the Substrate Specificities and Active-Site Structures of Two - L -Fucosidases (Glycoside Hydrolase Family 29) from Bacteroides thetaiotaomicron. *Biosc. Biotech. Biochem.* **76**, 1022–1024 (2012).

269. Smith, E. & Dent, G. *Modern Raman Spectroscopy - A Practical Approach*. (John Wiley & Sons, Ltd, 2004). doi:10.1002/0470011831.

270. Sekkal, M., Legrand, P., Huvenne, J. P. & Verdus, M. C. The use of FTIR microspectrometry as a new tool for the identification in situ of polygalactanes in red seaweeds. *J. Mol. Struct.* **294**, 227–230 (1993).

271. Pereira, L., Amado, A. M., Critchley, A. T., van de Velde, F. & Ribeiro-Claro, P. J. A. A. Identification of selected seaweed polysaccharides (phycocolloids) by vibrational spectroscopy (FTIR-ATR and FT-Raman). *Food Hydrocoll.* **23**, 1903–1909 (2009).

272. Kačuráková, M. & Mathlouthi, M. FTIR and laser-Raman spectra of oligosaccharides in water: Characterization of the glycosidic bond. *Carbohydr. Res.* **284**, 145–157 (1996).

273. Mackie, W. Semi-quantitative estimation of the composition of alginates by infra-red spectroscopy. *Carbohydr. Res.* **20**, 413–415 (1971).

274. Chandia, N. P., Matsuhiro, B. & Vasquez, A. E. Alginic acids in Lessonia trabeculata: characterization by formic acid hydrolysis and FT-IR spectroscopy. *Carbohydr. Polym.* **46**, 81–87 (2001).

275. Campos-Vallette, M. M. *et al.* Characterization of sodium alginate and its block fractions by surface-enhanced Raman spectroscopy. *J. Raman Spectrosc.* **41**, 758–763 (2010).

276. Patankar, M. S., Oehninger, S., Barnett, T., Williams, R. L. & Clark, G. F. A revised structure for fucoidan may explain some of its biological activities. *J. Biol. Chem.* **268**, 21770–21776 (1993).

277. Atha, D. H., Gaigalas, A. K. & Reipa, V. Structural analysis of heparin by Raman spectroscopy. *J. Pharm. Sci.* **85**, 52–56 (1996).

278. Ptak, S. H., Sanchez, L., Fretté, X. & Kurouski, D. Complementarity of Raman and Infrared spectroscopy for rapid characterization of fucoidan extracts. *Plant Methods* **17**, 1–10 (2021).

279. Almeida, M. R. *et al.* Determination of amylose content in starch using Raman spectroscopy and multivariate calibration analysis. *Anal. Bioanal. Chem.* **397**, 2693–2701 (2010).

280. Mathlouthi, M. & Koenig, J. L. Vibrational Spectra of Carbohydrates. *Adv. Carbohydr. Chem. Biochem.* **44**, 7–89 (1987).

281. Wiercigroch, E. *et al.* Raman and infrared spectroscopy of carbohydrates: A review. *Spectrochim. Acta Part A Mol. Biomol. Spectrosc.* **185**, 317–335 (2017).

282. Pielesz, A. & Biniaś, W. Cellulose acetate membrane electrophoresis and FTIR spectroscopy as methods of identifying a fucoidan in Fucus vesiculosus Linnaeus. *Carbohydr. Res.* **345**, 2676–2682 (2010).

283. Kiefer, W., Mazzolini, A. P. & Stoddart, P. R. Recent Advances in linear and nonlinear Raman spectroscopy I. *J. Raman Spectrosc.* **38**, 1538–1553 (2007).

284. Pielesz, A., Biniaś, W. & Paluch, J. Mild acid hydrolysis of fucoidan: Characterization by electrophoresis and FT-Raman spectroscopy. *Carbohydr. Res.* **346**, 1937–1944 (2011).

285. Pereira, L., Sousa, A., Coelho, H., Amado, A. M. & Ribeiro-Claro, P. J. A. Use of FTIR, FT-Raman and 13C-NMR spectroscopy for identification of some seaweed phycocolloids. *Biomol. Eng.* **20**, 223–228 (2003).

286. Tipson, R. S. *Infrared Spectroscopy of Carbohydrates: A Review of the Literature*.

https://digital.library.unt.edu/ark:/67531/metadc70397/m1/3/ (1968).

287. Abbate, S., Conti, G. & Naggi, A. Characterisation of the glycosidic linkage by infrared and Raman spectroscopy in the C-H stretching region: α,α-trehalose and α,α-trehalose-2,3,4,6,6-d10. *Carbohydr. Res.* **210**, 1–12 (1991).

288. Asanka Sanjeewa, K. K., Herath, K. H. I. N. M., Yang, H. W., Choi, C. S. & Jeon, Y. J. Anti-Inflammatory Mechanisms of Fucoidans to Treat Inflammatory Diseases: A Review. *Mar. Drugs 2021, Vol. 19, Page 678* **19**, 678 (2021).

289. Ustyuzhanina, N. E. *et al.* Fucoidans: Pro- or antiangiogenic agents? *Glycobiology* **24**, 1265–1274 (2014).

290. Clément, M. J. *et al.* NMR characterization and molecular modeling of fucoidan showing the importance of oligosaccharide branching in its anticomplementary activity. *Glycobiology* **20**, 883–894 (2010).

291. Pahwa, R., Goyal, A. & Jialal, I. Chronic Inflammation. *Pathobiol. Hum. Dis. A Dyn. Encycl. Dis. Mech.* 300–314 (2022) doi:10.1016/B978-0-12-386456-7.01808-6.

292. Hannoodee, S. & Nasuruddin, D. N. Acute Inflammatory Response. *Nature* **206**, 20 (2022).

293. Dinarello, C. A. Proinflammatory Cytokines. *Chest* **118**, 503–508 (2000).

294. Zhang, J. M. & An, J. Cytokines, inflammation, and pain. *Int. Anesthesiol. Clin.* **45**, 27–37 (2007).

295. Rokstad, A. M. *et al.* The induction of cytokines by polycation containing microspheres by a complement dependent mechanism. *Biomaterials* **34**, 621–630 (2013).

296. Lu, X. *et al.* Effect of Fucoidan on NF-κB-Mediated Inflammatory Response in Rats with Acute Myocardial Infarction. *J. Biomater. Tissue Eng.* **9**, 1376–1380 (2019).

297. Ahmad, T. *et al.* Fucoidan as an inhibitor of pro-inflammatory cytokines: Potential candidate for treating inflammatory-related conditions. *FASEB J.* **36**, (2022).

298. Chen, L. M. *et al.* Oligo-Fucoidan prevents IL-6 and CCL2 production and cooperates with p53 to suppress ATM signaling and tumor progression. *Sci. Reports 2017 71* **7**, 1–12 (2017).

299. Wang, J., Hu, S., Wang, J., Li, S. & Jiang, W. Fucoidan from Acaudina molpadioides protects pancreatic islet against cell apoptosis via inhibition of inflammation in type 2 diabetic mice. *Food Sci. Biotechnol.* **25**, 293–300 (2016).

300. Duan, T., Du, Y., Xing, C., Wang, H. Y. & Wang, R. F. Toll-Like Receptor Signaling and Its Role in Cell-Mediated Immunity. *Front. Immunol.* **13**, (2022).

301. Kawasaki, T. & Kawai, T. Toll-like receptor signaling pathways. *Front. Immunol.* **5**, 461 (2014).

302. Dutot, M. *et al.* A marine-sourced fucoidan solution inhibits Toll-like-receptor-3-induced cytokine release by human bronchial epithelial cells. *Int. J. Biol. Macromol.* **130**, 429–436 (2019).

303. Potente, M., Gerhardt, H. & Carmeliet, P. Basic and Therapeutic Aspects of Angiogenesis. *Cell* **146**, 873–887 (2011).

304. Carmeliet, P. & Jain, R. K. Angiogenesis in cancer and other diseases. *Nat. 2000 4076801* **407**, 249–257 (2000).

305. Koyanagi, S., Tanigawa, N., Nakagawa, H., Soeda, S. & Shimeno, H. Oversulfation of fucoidan enhances its anti-angiogenic and antitumor activities. *Biochem. Pharmacol.* **65**, 173–9 (2003).

306. Qiu, X., Amarasekara, A. & Doctor, V. Effect of oversulfation on the chemical and biological properties of fucoidan. *Carbohydr. Polym.* **63**, 224–228 (2006).

307. Wei, X. *et al.* Chain conformation and biological activities of hyperbranched fucoidan derived from brown algae and its desulfated derivative. *Carbohydr. Polym.* **208**, 86–96 (2019).

308. Knelson, E. H., Nee, J. C. & Blobe, G. C. Heparan sulfate signaling in cancer. *Trends Biochem. Sci.* **39**, 277–288 (2014).

309. Casu, B., Naggi, A. & Torri, G. Heparin-derived heparan sulfate mimics to modulate heparan sulfate-protein interaction in inflammation and cancer. *Matrix Biol.* **29**, 442–452 (2010).

310. Van Wijk, X. M. *et al.* Interfering with UDP-GlcNAc metabolism and heparan sulfate expression using a sugar analogue reduces angiogenesis. *ACS Chem. Biol.* **8**, 2331–2338 (2013).

311. Mulloy, B. & Rider, C. C. Cytokines and proteoglycans: an introductory overview. *Biochem.*

Soc. Trans. **34**, 409–413 (2006).

312. Brown, A., Robinson, C. J., Gallagher, J. T. & Blundell, T. L. Cooperative Heparin-Mediated Oligomerization of Fibroblast Growth Factor-1 (FGF1) Precedes Recruitment of FGFR2 to Ternary Complexes. *Biophys. J.* **104**, 1720–1730 (2013).

313. Borsig, L. Heparin as an Inhibitor of Cancer Progression. *Prog. Mol. Biol. Transl. Sci.* **93**, 335–349 (2010).

314. Robinson, C. J., Mulloy, B., Gallagher, J. T. & Stringer, S. E. VEGF165-binding Sites within Heparan Sulfate Encompass Two Highly Sulfated Domains and Can Be Liberated by K5 Lyase. *J. Biol. Chem.* **281**, 1731–1740 (2006).

315. Ribatti, D. The crucial role of vascular permeability factor/vascular endothelial growth factor in angiogenesis: a historical review. *Br. J. Haematol.* **128**, 303–309 (2005).

316. Stringer, S. E. The role of heparan sulphate proteoglycans in angiogenesis. *Biochem. Soc. Trans.* **34**, 451–453 (2006).

317. Dithmer, M. *et al.* Fucoidan Reduces Secretion and Expression of Vascular Endothelial Growth Factor in the Retinal Pigment Epithelium and Reduces Angiogenesis In Vitro. *PLoS One* **9**, e89150 (2014).

318. Jin, J. O. *et al.* Seaweeds in the Oncology Arena: Anti-Cancer Potential of Fucoidan as a Drug—A Review. *Mol. 2022, Vol. 27, Page 6032* **27**, 6032 (2022).

319. Friedman, A. Cancer as Multifaceted Disease. *Math. Model. Nat. Phenom.* **7**, 3–28 (2012).

320. Hsu, H. Y. *et al.* Fucoidan induces changes in the epithelial to mesenchymal transition and decreases metastasis by enhancing ubiquitin-dependent TGFβ receptor degradation in breast cancer. *Carcinogenesis* **34**, 874–884 (2013).

321. Anisimova, N. Y. *et al.* Anti-angiogenic properties of sulfated polysaccharides fucoidans and their analogs. *Russ. Chem. Bull.* **71**, 2505–2514 (2022).

322. Alekseyenko, T. V. *et al.* Antitumor and antimetastatic activity of fucoidan, a sulfated polysaccharide isolated from the Okhotsk sea Fucus evanescens brown alga. *Bull. Exp. Biol. Med.* **143**, 730–732 (2007).

323. Fukahori, S. *et al.* Fucoidan, a major component of brown seaweed, prohibits the growth of human cancer cell lines in vitro. *Mol. Med. Rep.* **1**, 537–542 (2008).

324. Kim, E. J., Park, S. Y., Lee, J. Y. & Park, J. H. Y. Fucoidan present in brown algae induces apoptosis of human colon cancer cells. *BMC Gastroenterol.* **10**, 1–11 (2010).

325. Aisa, Y. *et al.* Fucoidan induces apoptosis of human HS-Sultan cells accompanied by activation of caspase-3 and down-regulation of ERK Pathways. *Am. J. Hematol.* **78**, 7–14 (2005).

326. Nishida, N., Yano, H., Nishida, T., Kamura, T. & Kojiro, M. Angiogenesis in Cancer. *Vasc. Health Risk Manag.* **2**, 213 (2006).

327. Zhang, Z., Teruya, K., Yoshida, T., Eto, H. & Shirahata, S. Fucoidan Extract Enhances the Anti-Cancer Activity of Chemotherapeutic Agents in MDA-MB-231 and MCF-7 Breast Cancer Cells. *Mar. Drugs 2013, Vol. 11, Pages 81-98* **11**, 81–98 (2013).

328. Zeng, M. *et al.* Laminaria Japonica Polysaccharides effectively inhibited the growth of nasopharyngeal carcinoma cells in vivo and in vitro study. *Exp. Toxicol. Pathol.* **69**, 527–532 (2017).

329. Lai, J. lun *et al.* Indirubin Inhibits LPS-Induced Inflammation via TLR4 Abrogation Mediated by the NF-kB and MAPK Signaling Pathways. *Inflammation* **40**, 1–12 (2017).

330. Ngo, D. H. & Kim, S. K. Sulfated polysaccharides as bioactive agents from marine algae. *Int. J. Biol. Macromol.* **62**, 70–75 (2013).

331. Kim, S. K. & Wijesekara, I. Development and biological activities of marine-derived bioactive peptides: A review. *J. Funct. Foods* **2**, 1–9 (2010).

332. Costa, L. S. *et al.* Biological activities of sulfated polysaccharides from tropical seaweeds. *Biomed. Pharmacother.* **64**, 21–28 (2010).

333. Foley, S. A., Mulloy, B. & Tuohy, M. G. An unfractionated fucoidan from Ascophyllum nodosum: Extraction, characterization, and apoptotic effects in vitro. *J. Nat. Prod.* **74**, 1851–1861 (2011).

334. Anastyuk, S. D. *et al.* Structural analysis of a highly sulfated fucan from the brown alga Laminaria cichorioides by tandem MALDI and ESI mass spectrometry. *Carbohydr. Res.* **345**, 2206–2212 (2010).

335. Chang, Y. *et al.* Primary structure and chain conformation of fucoidan extracted from sea cucumber Holothuria tubulosa. *Carbohydr. Polym.* **136**, 1091–1097 (2016).

336. Sichert, A. *et al.* Verrucomicrobia use hundreds of enzymes to digest the algal polysaccharide fucoidan. *Nat. Microbiol.* 1–14 (2020) doi:10.1038/s41564-020-0720-2.

337. Silchenko, A. S. *et al.* Discovery of a fucoidan endo-4O-sulfatase: Regioselective 4O-desulfation of fucoidans and its effect on anticancer activity in vitro. *Carbohydr. Polym.* **271**, 118449 (2021).

338. Smith, M. *et al.* A Semi-quantitative method for the detection of fentanyl using surface-enhanced Raman scattering (SERS) with a handheld Raman instrument. *J. Forensic Sci.* **66**, 505–519 (2021).

339. Adebajo, M. O., Frost, R. L., Kloprogge, J. T. & Kokot, S. Raman spectroscopic investigation of acetylation of raw cotton. *Spectrochim. Acta - Part A Mol. Biomol. Spectrosc.* **64**, 448–453 (2006).

340. Tsou, M. H., Lee, C. C., Wu, Z. Y., Lee, Z. H. & Lin, H. M. Bioactivity of crude fucoidan extracted from Sargassum ilicifolium (Turner) C. Agardh. *Sci. Reports 2022 121* **12**, 1–10 (2022).

341. van Weelden, G. *et al.* Fucoidan structure and activity in relation to anti-cancer mechanisms. *Mar. Drugs* **17**, (2019).

342. Ale, M. T., Mikkelsen, J. D. & Meyer, A. S. Important determinants for fucoidan bioactivity: A critical review of structure-function relations and extraction methods for fucose-containing sulfated polysaccharides from brown seaweeds. *Mar. Drugs* **9**, 2106–2130 (2011).

343. Silva, J. C. *et al.* Compositional and structural analysis of glycosaminoglycans in cell-derived extracellular matrices. *Glycoconj. J.* **36**, 141–154 (2019).

344. Weiler, J. M., Yurt, R. W., Fearon, D. T. & Frank Austen, K. Modulation of the formation of the amplification convertase of complement, C3b, Bb, by native and commercial heparin. *J. Exp. Med.* **147**, 409–421 (1978).

345. Liu, H., Zhang, Z. & Linhardt, R. J. Lessons learned from the contamination of heparin. *Nat. Prod. Rep.* **26**, 313–321 (2009).

346. Arlov, Ø. & Skjåk-Bræk, G. Sulfated Alginates as Heparin Analogues: A Review of Chemical and Functional Properties. *Mol. 2017, Vol. 22, Page 778* **22**, 778 (2017).

347. Mollnes, T. E. *et al.* Essential role of the C5a receptor in E coli – induced oxidative burst and phagocytosis revealed by a novel lepirudin-based human whole blood model of inflammation Essential role of the C5a receptor in E coli – induced oxidative burst and phagocytosis rev. *Blood* **100**, 1869–1877 (2002).

348. Finger, R. P. *et al.* Anti-vascular endothelial growth factor in neovascular age-related macular degeneration-A systematic review of the impact of anti-VEGF on patient outcomes and healthcare systems. *BMC Ophthalmol.* **20**, 1–14 (2020).

349. Klettner, A. Oxidative stress induced cellular signaling in RPE cells. *Front. Biosci. (Schol. Ed).* **4**, 392–411 (2012).

350. Losada-Barreiro, S. & Bravo-Díaz, C. Free radicals and polyphenols: The redox chemistry of neurodegenerative diseases. *Eur. J. Med. Chem.* **133**, 379–402 (2017).

351. Foresti, R. *et al.* Nrf2 activators modulate oxidative stress responses and bioenergetic profiles of human retinal epithelial cells cultured in normal or high glucose conditions. *Pharmacol. Res.* **99**, 296–307 (2015).

352. Wang, Y. Q., Wei, J. G., Tu, M. J., Gu, J. G. & Zhang, W. Fucoidan Alleviates Acetaminophen-Induced Hepatotoxicity via Oxidative Stress Inhibition and Nrf2 Translocation. *Int. J. Mol. Sci. 2018, Vol. 19, Page 4050* **19**, 4050 (2018).

353. Ryu, M. J. & Chung, H. S. Fucoidan reduces oxidative stress by regulating the gene expression of HO-1 and SOD-1 through the Nrf2/ERK signaling pathway in HaCaT cells. *Mol. Med. Rep.* **14**, 3255–3260 (2016).

354. Wang, J., Geng, L., Yue, Y. & Zhang, Q. Use of fucoidan to treat renal diseases: A review of 15 years of clinic studies. in *Progress in Molecular Biology and Translational Science* vol. 163 95–111 (Elsevier B.V., 2019).

355. Smidsrod, O. & Haug, A. Dependence upon the gel-sol state of the ion-exchange properties of alginates. *Acta Chem. Scand.* **26**, 2063–2074 (1972).

356. Wang, X. & Spencer, H. G. Calcium alginate gels: Formation and stability in the presence of an inert electrolyte. *Polymer (Guildf).* **39**, 2759–2764 (1998).

357. Tanaka, T. Gels. *Sci. Am.* **244**, 124–138 (1981).

358. Tang, Y. *et al.* Production and characterisation of novel injectable chitosan/ methylcellulose/salt blend hydrogels with potential application as tissue engineering scaffolds. *Carbohydr. Polym.* **82**, 833–841 (2010).

359. Nowak, A. P., Breedveld, V., Pine, D. J. & Deming, T. J. Unusual Salt Stability in Highly Charged Diblock Co-polypeptide Hydrogels. *J. Am. Chem. Soc.* **125**, 15666–15670 (2003).

360. Hecht, H. & Srebnik, S. Structural Characterization of Sodium Alginate and Calcium Alginate. *Biomacromolecules* **17**, 2160–2167 (2016).

361. Strand, B. L., Coron, A. E. & Skjak-Braek, G. Current and Future Perspectives on Alginate Encapsulated Pancreatic Islet. *Stem Cells Transl. Med.* **6**, 1053–1058 (2017).

362. De Boisseson, M. R. *et al.* Physical alginate hydrogels based on hydrophobic or dual hydrophobic/ionic interactions: Bead formation, structure, and stability. *J. Colloid Interface Sci.* **273**, 131–139 (2004).

363. Chan, G. & Mooney, D. J. Ca2+ released from calcium alginate gels can promote inflammatory responses in vitro and in vivo. *Acta Biomater.* **9**, 9281–9291 (2013).

364. Karunanithi, P. *et al.* Three dimensional alginate-fucoidan composite hydrogel augments the chondrogenic differentiation of mesenchymal stromal cells. *Carbohydr. Polym.* **147**, 294–303 (2016).

365. Xu, J. *et al.* Chondrogenic Differentiation of Human Mesenchymal Stem Cells in Three-Dimensional Alginate Gels. *https://home.liebertpub.com/tea* **14**, 667–680 (2008).

366. Öztürk, E. *et al.* Sulfated Hydrogel Matrices Direct Mitogenicity and Maintenance of Chondrocyte Phenotype through Activation of FGF Signaling. *Adv. Funct. Mater.* **26**, 3649–3662 (2016).

367. Vaithilingam, V. *et al.* Beneficial Effects of Coating Alginate Microcapsules with Macromolecular Heparin Conjugates–In Vitro and In Vivo Study. *https://home.liebertpub.com/tea* **20**, 324–334 (2013).

368. Syanda, A. M. *et al.* Sulfated Alginate Reduces Pericapsular Fibrotic Overgrowth on Encapsulated cGMP-Compliant hPSC-Hepatocytes in Mice. *Front. Bioeng. Biotechnol.* **9**, 816542 (2022).

369. Coron, A. E. *et al.* Pericapsular fibrotic overgrowth mitigated in immunocompetent mice through microbead formulations based on sulfated or intermediate G alginates. *Acta Biomater.* **137**, 172–185 (2022).

370. Arlov, Ø., Aachmann, F. L., Feyzi, E., Sundan, A. & Skjåk-Bræk, G. The Impact of Chain Length and Flexibility in the Interaction between Sulfated Alginates and HGF and FGF-2. *Biomacromolecules* **16**, 3417–3424 (2015).

371. Arlov, Ø., Skjæk-Bræk, G. & Rokstad, A. M. Sulfated alginate microspheres associate with factor H and dampen the inflammatory cytokine response. *Acta Biomater.* **42**, 180–188 (2016).

372. Zheng, K. H. *et al.* 99Mtc-Fucoidan As Diagnostic Agent For P-Selectin Imaging: First-In-Human Evaluation (Phase I). *Atherosclerosis* **287**, e143 (2019).

373. Fitton, J. H., Stringer, D. N., Park, A. Y. & Karpiniec, S. S. Therapies from Fucoidan: New Developments. *Mar. Drugs 2019, Vol. 17, Page 571* **17**, 571 (2019).

Paper 1

Alginate gels with a combination of calcium and chitosan oligomer mixtures as crosslinkers

Yiming Feng [a,1], Georg Kopplin [a,1], Kimihiko Sato [b], Kurt I. Draget [a], Kjell M. Vårum [a,*]

[a] Norwegian Biopolymer Laboratory (NOBIPOL), Department of Biotechnology, Norwegian University of Science and Technology, 7491 Trondheim, Norway
[b] Koyo Chemical Co. Ltd, Osaka, Japan

ARTICLE INFO

ABSTRACT

Alginates are polysaccharides that are widely used in relation to their ability to form gels. Recently we reported that alginates may also form gels with chitosan oligomers as crosslinkers (Khong, Aarstad, Skjåk-Bræk, Draget, & Vårum, 2013). The purpose of the present study was to characterize alginate gels crosslinked with calcium and chitosan oligomers. Using two different alginates of similar molecular weights but different chemical composition, i.e. guluronic acid content of 46 and 68%, we found that both alginates could form homogeneous gels with calcium and chitosan oligomers separately and without syneresis. Systematic combinations of calcium and chitosan oligomers as crosslinkers were tested, showing that up to 50% of the calcium could be substituted with chitosan oligomers without reduction in gel strength or increased syneresis for the alginate with the lowest guluronic acid content. Furthermore, the kinetics of the combined gels were different from pure calcium alginate gels.

© 2016 Elsevier Ltd. All rights reserved.

1. Introduction

Chitosans form a family of linear polysaccharides consisting of $(1 \rightarrow 4)$-β-linked 2-acetamido-2-deoxy-D-glucopyranose (GlcNAc or A-unit) and its de-*N*-acetylated analogue (GlcN or D-unit). These polycationic derivatives of one of Nature's most abundant biopolymers (chitin) can be prepared with varying degree of polymerization (DP) and degree of acetylation (F_A) (Vårum & Smidsrød, 2005). The amine-group of the D-unit has a pK_a-value of ca. 6.5 (Anthonsen & Smidsrød, 1995; Strand, Tømmeraas, Vårum, & Østgaard, 2001; Tsukada & Inoue, 1981) and therefore the amount of charges also influences properties as their water-solubility as a function of pH (Vårum, Ottøy, & Smidsrød, 1994).

Chito-oligosaccharides (CHOS), i.e. shorter fragments of chitosans composed of the same building units and glycosidic linkages, can be prepared using both chemical and enzymatic methods. CHOS have attracted much attention in recent years as they have been suggested to exhibit numerous biological effects (Aam et al., 2010; Nilsen-Nygaard, Strand, Vårum, Draget, & Nordgård, 2015).

Alginates form a polysaccharide family (occurring in brown algae and bacteria) comprised of $(1 \rightarrow 4)$-linked β-D-mannuronic acid (M-unit) in the $^4C_1$ conformation and its C5-epimer, α-L-

guluronic acid (G-unit) in the $^1C_4$ conformation with a pK_a-value of ca. 3.5. These linear polyanionic block copolymers are composed of homopolymeric regions of M-units (M-blocks) or G-units (G-blocks), interspaced by regions of alternating epimers (MG-blocks) of different length (Draget, Moe, Skjåk-Bræk, & Smidsrød, 2006).

Hydrogels are cross-linked hydrophilic polymer chains able to capture large amounts water, defined by specific properties regarding their dynamic (Ross-Murphy, 1984). The cross-links in hydrogels can be established through covalent linkages (Desai, Koshy, Hilderbrand, Mooney, & Joshi, 2015; Li, 2010) or through ionic linkages (Mi et al., 1999). Ionically crosslinked hydrogels generally feature a higher swelling sensitivity to pH changes than their covalently crosslinked counterparts, which extends their potential applications since a further tuning of the hydrogel to their specific environment becomes possible (Cuan et al., 1996). Chitosan is known for its high biocompatibility, biodegradability (Nordtveit, Vårum, & Smidsrød, 1996; Vårum, Myhr, Hjerde, & Smidsrød, 1997) and low toxicity (Köping-Höggård et al., 2001; Strand, Danielsen, Christensen, & Vårum, 2005). Moreover, antimicrobial effects (Dutta, Tripathi, Mehrotra, & Dutta, 2009; Felt, Carrel, Baehni, Buri, & Gurny, 2000; Liu, Guan, Yang, Li, & Yao, 2000; Mellegård, Strand, Christensen, Granum, & Hardy, 2011) have been shown, which are beneficial for applications such as drug delivery, implants (Xia, Liu, Zhang, & Chen, 2011) and wound healing (Ong, Wu, Moochhala, Tan, & Lu, 2008; Ueno, Mori, & Fujinaga, 2001). Tailoring of chitosans with respect to DP, polydispersity, F_A and

---

* Corresponding author.
  E-mail address: kjell.m.varum@ntnu.no (K.M. Vårum).
[1] These authors contributed equally to the paper.

acetyl distribution is providing tools for controlling their function and properties in relation to their biological effects.

Alginates are able to form ionically crosslinked hydrogels in the presence of multivalent cations (e.g. Ca^{2+}, Sr^{2+} and Ba^{2+}). Calcium-alginate gels are intensively studied and widely used for cell immobilization and protection of the cells from the host's immune system (Draget & SkjåK-Braek, 2011; Leong et al., 2015; Strand, Mørch, & Skjåk-Bræk, 2000). These gels can be prepared through internal gelation or a diffusion method (Draget et al., 2006). The internal gelation provides a mechanism where insoluble calcium carbonate is mixed with an alginate solution, followed by a controlled lowering of the pH through a proton-donor such as the slowly hydrolyzing D-glucono-δ-lactone (GDL), causing a homogeneous release of the calcium ions and subsequent gel formation. The calcium ions show specific interactions with the G-units and form junctions zones specifically between G-blocks (Sikorski, Mo, Skjåk-Bræk, & Stokke, 2007). Khong, Aarstad, Skjåk-Bræk, Draget, and Vårum (2013) has shown the possibility of forming junction zones between consecutive M-units (using polymannuronic acid) crosslinked with fully deacetylated chitosan oligomers, and it was found that at the same conditions only very weak gels were formed using polyguluronic acid (poly-G). This new gelling system, also induced by the homogeneous lowering of the pH thereby charging the chitosan oligomers using the slowly hydrolyzing proton-donor GDL, provides a new possibility of crosslinking alginates. The suggested reason for this difference in the gelling properties between alginate composed of poly-M and poly-G is the match in charge distance between the chitosan and poly-M ($^4C_1$ conformation, diequatorial glycosidic linkage) of about 10.4 Å (Minke & Blackwell, 1978; Sørbotten, Horn, Eijsink, & Vårum, 2005) whereas the G-blocks ($^1C_4$ conformation, diaxial glycosidic linkage) exhibits a shorter charge distance of only 8.7 Å (Atkins, Mackie, & Smolko, 1970).

It seems then that Ca^{2+} and chitosan oligomers can provide crosslinkers for alginates where calcium ions are crosslinking through the G-blocks and the chitosan oligomers most effectively through the M-blocks. For certain cell lines immobilized in calcium alginate gels it has been found that the calcium ions can have negative effects (Chan & Mooney, 2013). Here we have undertaken a study of gelling properties of two different alginates of different composition using combinations of the two crosslinkers, where we have applied the internal gelation method (see Scheme 1) with the two different crosslinkers and measured the gel strength (Young's modulus) and syneresis as well as the gelling kinetics of the new gels.

2. Experimental

2.1. Materials

The mixture of chitosan oligomer mixture (MCO) was provided by Koyo Chem Co Ltd (lot number 121017WG). MCO was characterized by Size Exclusion Chromatography (see Fig. 1 in Supplementary material). The number-average degree of polymerization (DP_n) and the degree of acetylation (F_A) of the MCO as well as degree of and the individual oligomers (see Table 1 in Supplementary material) were determined by ^1H NMR (see Fig. 2 in Supplementary material) as described previously (Sørbotten et al., 2005). Two alginate samples (provided by FMC Biopolymer AS, Drammen, Norway) were isolated from stipe and from leaf of *Laminaria hyperborea*. Data for chemical composition and sequences and the molecular weight average are given in Table 1. Chemical composition and sequences in terms of diads, triads and average block length were determined by ^1H NMR and ^{13}C NMR as described previously (Grasdalen, Larsen, & Smidsrød, 1977).

Weight and number average molecular weight were determined by SEC-MALLS. D–Glucono δ-lactone (GDL) was purchased from Sigma-Aldrich. $CaCO_3$ was (Reag. Ph Eur) was purchased from Merck. Other chemicals were of analytical grade and used without any further purification.

2.2. Gel preparation

Alginate samples were dissolved in distilled water at a concentration of 3% (30 mg/mL). MCO was dissolved in distilled water at a concentration of 10% and the pH was adjusted to 8.0 by 1 M NaOH. 1.0 g of the alginate solution was weighted into a glass vial and a maximum of 182 μL of the MCO (amount determined by syneresis experiments) was added together with distilled water to obtain a total volume of 2 mL. The mixture was stirred for 10 min and 26.6 mg of GDL were dissolved in 1 mL distilled water right before adding to mixture followed by intensive stirring. Ca^{2+} cross linked alginate gels were prepared by adding a suspension of a maximum of 3.6 mg $CaCO_3$ (amount determined by syneresis experiments) and 1 mL of distilled water to 1 mL alginate solution. The mixture was stirred for 10 min and 12.9 mg of GDL were dissolved in 1 mL distilled water right before adding to the mixture followed by intensive stirring. Determined amounts for MCO and $CaCO_3$ were set as 100%. Used amounts in the mixed gels (0–100%) are based these values (see details of calculations in Supplementary material).

Gel cylinders were made by placing aqueous solution of sodium alginate and solution of chitosan oligomers mixture, containing dispersed $CaCO_3$ and freshly dissolved GDL, in the cylinder wells (diameter = 16 mm, length = 18 mm) of the 24-well plate and covering the cylinders with a lid. After 24 h the gels were taken out and ready for the measurement.

2.3. Syneresis and gel strength

Syneresis was measured as final gel weight after gentle wiping off excess water relative to the initial gel weight determined by the total volume of the gelling solution in each well. Gel strength was determined by compression measurements of the gel cylinder until rupture by using a texture analyzer (TA.XT.-Plus Texture Analyzer from Stable Micro Systems, Surrey, UK) equipped with a cylindrical probe (P/35, diameter = 35 mm) operated at a speed of 0.10 mm/s. A minimum of three parallels were determined. Young's modulus was calculated from the slope of the initial zone of the resulting stress-strain curve, defined as the ratio of tensile stress to tensile strain. Rupture strength was determined as the force when the gel ruptured. The height and diameter of each gel were manually measured by a digital caliper. A load cell with a capacity of 5 kg was used and the instrument was calibrated prior to the measurement.

2.4. Rheological measurement

The rheological characterization of the mixed alginate gels was performed using a Stresstech Rheometer (RheoLogica Instruments, Sweden) fitted with a cone-and-plate geometry (cone angle of 4° and diameter of 40 mm). To prevent drying of the samples during measurement, the sample was covered with a layer of low-viscosity silicon oil. A minimum of two parallels were performed for each kinetic gelling experiment.

The test methods employed were oscillatory time and stress sweep at a constant temperature of 20 °C. For time sweep, the experiments were performed at a low oscillation frequency (1 Hz) and a small strain (0.001) to ensure that the measuring conditions did not disrupt the gelation process. The strain sweep, at a constant frequency of 1 Hz, was used to determine the linear viscoelastic region (LVR) of the hydrogels. Frequency sweep experiments were performed in the linear viscoelastic region (0.01–10 Hz) with a con-
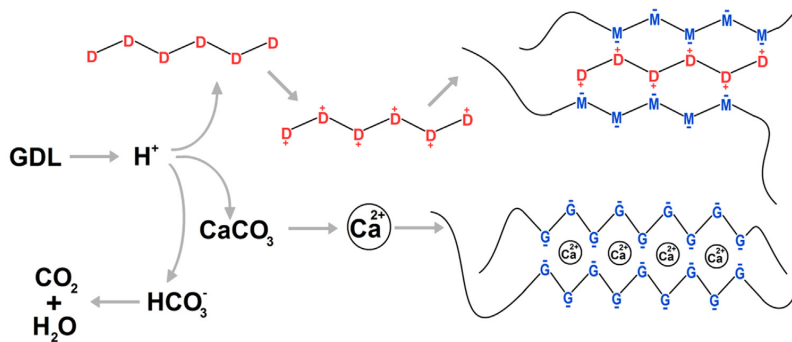
Scheme 1. Schematic illustration of the combined internal gelation of alginate crosslinked with calcium and MCO. D: glucosamine, M: mannuronate unit, G: guluronate unit, GDL: D-Glucono δ-lactone.

stant strain of 0.001 and a delay time of 0.033 min between the measurements to characterize the viscoelastic properties as a function of frequency.

3. Results and discussion

3.1. Characterization of chitosan oligomers

The size distribution of the mixed chitosan oligomers (MCO) was characterized (See Fig. 1 in Supplementary material), showing a dominance of oligomers with DP from 2 to 6. The higher DP oligomers (DP ≥ 7) are in lower amounts, although oligomers with DP up to 20 can be identified. Isolated fractions were collected and characterized by ^{1}H NMR spectroscopy to determine their degree of acetylation (F_A), see Table 1 in Supplementary material. The oligomers with DP 5 or less were all fully de-N-acetylated, while the hexamer had a F_A of 0.05 and then gradually increasing with increasing DP up to 0.28 (DP ≥ 19), as seen in the anomer region of the ^{1}H NMR spectra of isolated chitosan oligomer fractions (Fig. 2 in Supplementary material). Anomeric reducing end protons of a D-unit are found at 5.43 ppm (α-form) and at 4.92 ppm (β-form). The absence of α- and β-anomer of reducing end A-units (at 5.19 and 4.61 ppm) for oligomers with DP ≤ 5 shows that these chitosan oligomers fractions are fully de-N-acetylated (Ishiguro, Yoshie, Sakurai, & Inoue, 1992). The internal D-units resonate between 4.8 and 4.9 ppm while the internal A-units resonate at 4.6 ppm which can be seen in the spectra of oligomer fractions with DP ≥ 6 (Vårum, Anthonsen, Grasdalen, & Smidsrod, 1991). Also, the A-units seem are not found at the reducing end of any of the acetylated oligomers (see Fig. 2 in Supplementary material), as no resonances of reducing end A-units could be identified.

3.2. Characterization of alginates

Two alginate samples isolated from stipe and leaf of L. hyperborea with similar molecular weight were used for the gel experiments. The content of guluronate and mannuronate (F_G and F_M), diad sequences and selected triad sequences together with average block lengths of these alginates (Grasdalen, Larsen, & Smisrod, 1981; Grasdalen, 1983) were determined (see Table 1).

3.3. Gel strength and kinetics of gelation as function of added GDL

The two commercially available alginates with quite different composition (high and low G-content) but similar molecular weights (Table 1) were used for the gelling experiments. The pKa-value of the carboxyl groups is about 3.5 (Haug, 1964), and therefore
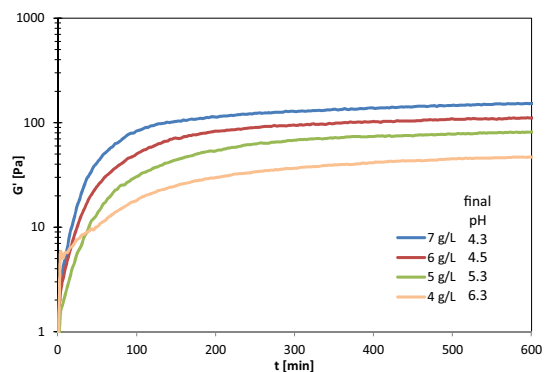
Fig. 1. Kinetics of gelation as a function of GDL concentration. To a leaf alginate solution (10 g/L) a fixed amount of MCO (7 g/L) was added, and then increasing an amount of GDL (4–7 g/L) was added and the G' was determined as a function of time. G'' and delta are not shown in the Figure for reasons of clarity.

will be fully charged at neutral pH. The intrinsic pKa-values of the amino-groups has been determined for fully de-N-acetylated MCO with increasing chain length (monomer to heptamer) and found to be ca. 6.7 for the higher DP oligomers whereas the dimer had a pKa-value of 7.6 (Tsukada & Inoue, 1981), which means that the total MCO will be mainly uncharged at the pH 7.5 which is the pH where MCO and alginate is mixed (see Experimental for details). Even though the neutral solubility decreases with increasing chain length and decreasing F_A (Vårum et al., 1994), no precipitation was observed at pH 7.5. This can be explained by the increase in F_A with increasing chain length (Vårum et al., 1994). The gelation was performed as previously described (Khong et al., 2013). The kinetics of gelation were followed by measuring the storage modulus (G') and the loss modulus (G'') as a function of the time. The pH at the apparent equilibrium was measured in addition. For all experiments a fixed MCO conc. of 7 g/L and alginate conc. of 10 g/L was used.

A frequency sweep control experiment without adding the proton donating substance D-glucono-δ-lactone (GDL) was performed (data not given) that showed liquid like properties of the alginate MCO solution at pH 7.5 (G'' higher than G', phase angle close to 90°) at a broad frequency range (0.01–10 Hz).

Fig. 1 shows the time dependence of the storage modulus of a leaf alginate crosslinked with MCO with increasing amounts of GDL. For all different mixtures a phase transition from predominant viscous to predominant elastic properties, where G' exceeds G'' and

Table 1

Chemical composition, block length (determined by ^{1}H NMR and ^{13}C NMR (*) spectroscopy), Number and Weight average Molecular Weights and Polydispersity Index (PI) (determined by SEC MALLS) of the two Alginates.

alginate source	F_G	F_M	F_{GG}	F_{MM}	F_{MG}	F_{GGG}	F_{MMM}	$N_{G>1}$	$N_{M>1}$	M_W (10^3 g mol^{-1})	M_n (10^3 g mol^{-1})	PI
L. hyperborea stipe	0.68	0.32	0.57	0.28*	0.10*	0.53	0.17*	14	3.2*	270	97.4	2.78
L. hyperborea leaf	0.46	0.54	0.36	0.43*	0.18*	0.20	0.19*	4.8	3.6*	220	105.4	2.09

the phase angle drops below 45°, occurring within the first minute, which indicates a fast gelling system (G" and δ are not depicted here). For the 7 g/L GDL mixture G' increases rapidly during the first 2 h of the measurement, starts to level off and prolongs into an apparent equilibrium after approx. 130 min. However, the ongoing small inclination indicates that some reorganization within the hydrogel network continues. For the remaining samples the apparent equilibrium approaches after approx. 180 min (6 g/L GDL), 210 min (5 g/L GDL) and 250 min (4 g/L GDL). These results show that the amount of GDL added to a solution with a fied concentration of alginate and MCO has direct influence on the gelling kinetics, the final pH and the final gel strength, as previously shown in alginates composed only of M-units (poly-M) (Khong et al., 2013).

3.4. Kinetics of gelation as function of the MCO concentration

Furthermore, the gelling kinetics of the two alginates were followed by measuring the storage modulus (G') and the loss modulus (G") as a function of the time, for a series of experiments with a fixed conc. of alginate (10 g/L), an increasing conc. of MCO (4–8 g/L) and a stoichiometrically adjusted amount of GDL corresponding to the number of introduced amino groups through MCO and a final pH of 4.4 (detailed calculations given in Supplementary information). Fig. 2 shows the time dependence of the storage modulus (G') with increasing amounts of MCO. It emerges that a higher concentration of MCO crosslinkers is leading to more rigid gels. A similar increase in G' with increasing chitosan oligomer mixture concentration was also observed for poly-M (Khong et al., 2013). The gelling kinetics are similar for all MCO and GDL concentration with a rapid increase of G' in the start, followed by an approaching equilibrium after 170 min for the leaf alginate (Fig. 2A) and 130 min for the stipe alginate (Fig. 2B). This is different from the kinetics of gelling with poly-M and MCO, where the rates of gelling was found to increase with increasing MCO concentrations, which could be attributed to a higher number of junctions in the gel network with increasing crosslinker concentration (Khong, 2013). However, care should be taken to directly compare the gelling kinetics described by Khong (Khong, 2013) with the current gelling system as the gelling systems are different both with respect to the MCO crosslinker that were used (different DP-distribution), and as the crosslinker in the gelling system described herein is a mixture of calcium and MCO.

The kinetics of gelling is influenced both by the concentration of the proton donator GDL (Fig. 1) and by the concentration of the proton acceptor and crosslinker MCO. This can be explained by the fact that the protons donated by GDL become equally distributed among the MCO. To form a stable junction zone it is estimated that the chitosan oligomer should have at least four positively charged D-units (with a strong increase of gel strength for every further charged D-unit) (Khong, 2013). If MCO concentration is increased and the GDL concentration is increased equally then the kinetics will be the same, which was also reflected by pH measurements during the experiment (data not given).

Fig. 2 shows that stipe alginate forms weaker gels than leaf alginate at the same MCO concentration, but reaches the equilibrium earlier. This difference in gel strength can be explained by the alginate composition (see Table 1). Stipe alginate has a similar mannuronic acid block length ($N_{M>1}$) and contains a small fraction of very long M-blocks (Aarstad, Tøndervik, Sletta, & Skjåk-Bræk,
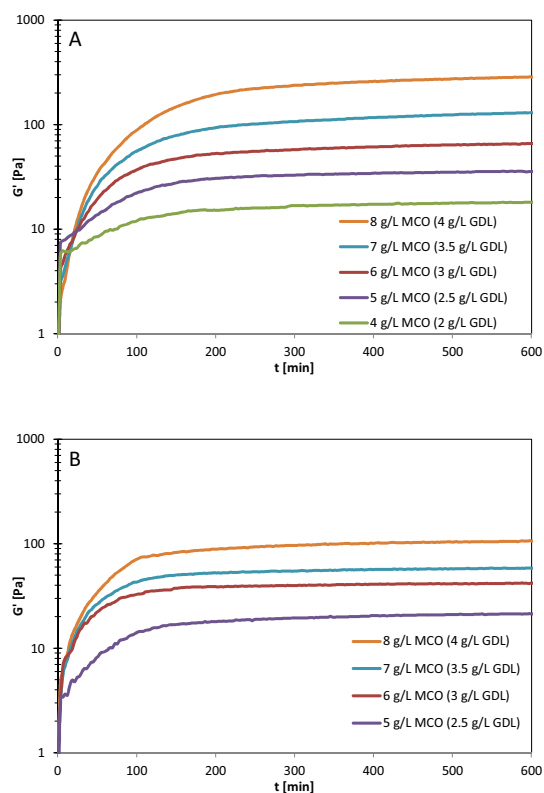

Fig. 2. Kinetics of gelation as a function of MCO added. (A) Leaf alginate. (B) Stipe alginate.

2012) but a lower fraction of mannuronic acid (F_M) compared to leaf alginate. However, the M-block length distribution of the leaf alginate has not been determined. It could be that the gelling kinetics could be important for the final gel strength, and that the difference between the two alginates of different chemical composition could be explained by differences in the possibility of reorganization of the crosslinkers in the gel, as has been suggested for alginate acid gels (Draget et al., 2000).

3.5. Gel strength and syneresis of mixed gels

The dependence of Young's modulus (E) and syneresis as a function of the concentration of MCO and Ca^{2+} was determined for the two alginates (see Figs. 3 and 4). A set of experiments were designed where the concentrations of MCO and calcium were systematically varied. For pure calcium-alginate gels, the maximum concentrations of calcium (100%) without significant syneresis were 15 and 16.5 mM for leaf and stipe alginate, respectively, while for chitosan oligomer alginate gels the maximum MCO (100%) concentration without significant syneresis was 25 mM (calculated as the molar
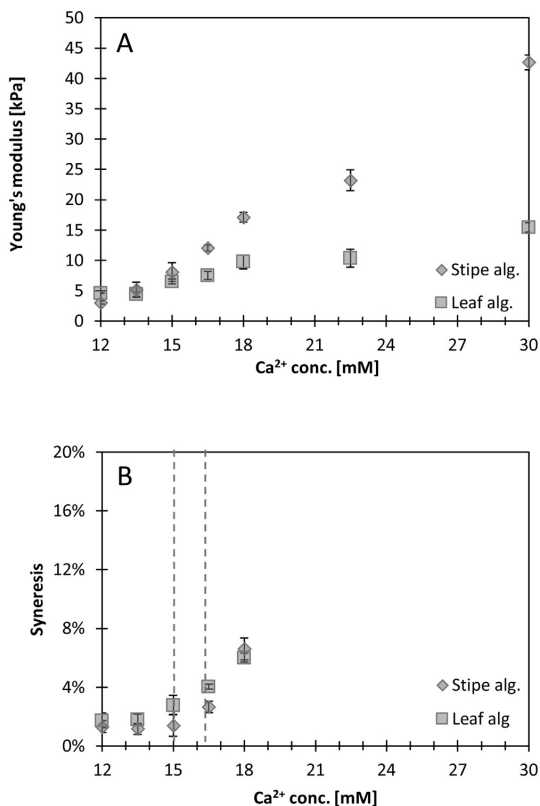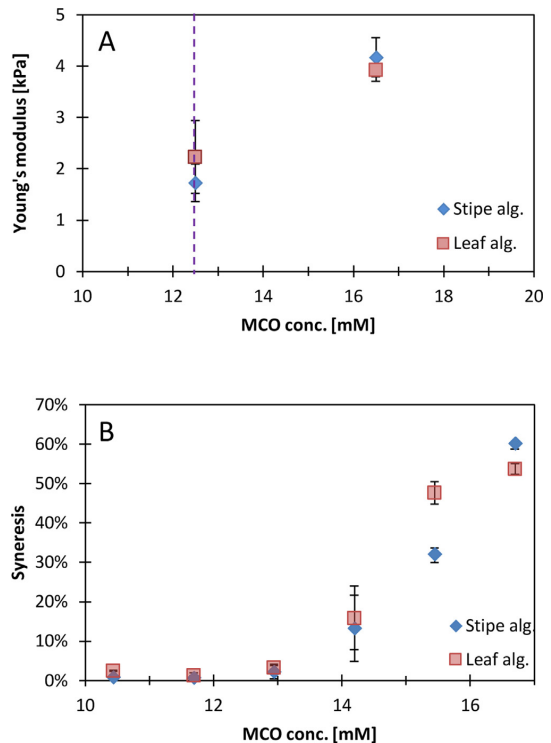
Fig. 3. Gel strength (Young's modulus) and syneresis of 1% alginate gels as a function of calcium concentration. (A) Gel strength as determined by the Young's modulus. (B) Syneresis, left dashed line: max. Ca²⁺ conc. before syneresis occurs in leaf alginate, right dashed line: max. Ca²⁺ conc. before syneresis occurs in stipe alginate.

Fig. 4. Gel strength (Young's modulus) and syneresis of 1% alginate gels as a function of MCO concentration. (A) Gel strength as function of MCO concentration (conc. related to $(GlcN)_2$). (B) Syneresis, dashed line: max. chitosan conc. before syneresis occurs in (both) alginates.

concentration of the D-unit monomer) for both alginates. Accordingly, when preparing a leaf alginate with a mixture of 50% calcium and 50% MCO, the calcium concentration is reduced to 7.5 mM and the MCO concentration to 12.5 mM. Detailed values for the concentration of calcium, MCO and GDL are given in the Supplementary information.

In Fig. 5 is shown the results (Young's modulus and syneresis) with the leaf alginate when gels were prepared with only calcium as crosslinker, only MCO as crosslinker as well as mixtures of the two crosslinkers. It can be seen that the calcium-alginate gels are clearly stronger than the MCO-alginate gels with E of 6 and 3 kPa, respectively. However, mixed gels with half the calcium concentration can also be prepared without significant reduction in gel strength (E). Pure calcium-alginate gels with a 50% reduction in calcium concentration would result in a drastic reduction in E to less than 2 kPa, while a 25% reduction in the calcium concentration would result in a gel with a E of 2.8 kPa (yellow triangles in Fig. 5A). Clearly, mixed calcium-MCO alginate gels can be made with a drastic reduction in calcium-concentrations without reduction in the gel strength. These gels could be applied in systems where a reduced calcium concentration is preferred, e.g. for immobilization of calcium-sensitive cells. Such gels can also be made without significant syneresis (Fig. 5B).

In Fig. 6 is shown the results of similar gel experiments with the stipe alginate. For this alginate, the expected results of a stronger

calcium-alginate gels was found, and a more drastic reduction in the gel strength was seen when using only MCO as cross-linker (E of 12 and 1.8 kPa, respectively; see Fig. 6A). However, for the mixed gels with stipe alginate, the calcium concentration could not be reduced as much as for the mixed gels with leaf alginate without a reduction in the gel strength (Fig. 6A). Pure calcium-alginate gels with a 25% reduction in calcium concentration would result in a drastic reduction in E to 3 kPa. With the mixed gels the gel strength can be maintained with a 25% reduction in calcium concentration. Pure calcium-alginate gels with a 25% reduction in calcium concentration would have a E of 3 kPa, i.e. a more than 70% reduction (yellow triangles in Fig. 6A). For a mixed stipe alginate gel with a 50% reduction of calcium-concentration, this gel would still maintain more than 70% of the gel strength (yellow triangles in Fig. 6A). Such stipe alginate gels can also be made without significant syneresis (Fig. 6B).

3.6. Kinetics of gelation of the mixed gels

We also measured the gelling kinetics of the mixed gels for the two alginates were followed by measuring the storage modulus (G') and the loss modulus (G") as a function of the time Fig. 7. The concentrations of all components are identical to the set of experiments previously described. In Fig. 7A is shown the kinetics of gelling of leaf alginate crosslinked with calcium (100%), MCO (100%) and the mixed gels (50% calcium and 50% MCO). Clearly, the fastest gel formation is in the gelling system with the MCO. The slowest gel formation is with the calcium that is released from the
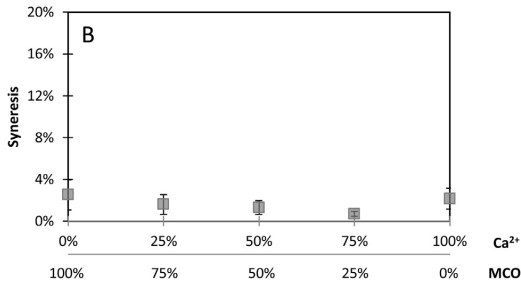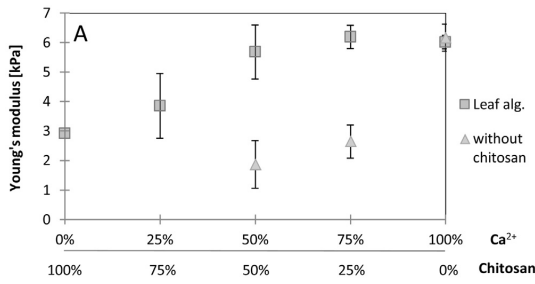
Fig. 5. Gel strength and syneresis of leaf alginate crosslinked with varying amounts of MCO and calcium (100% Ca²⁺: 1.2 g/L, 100% MCO: 6 g/L). (A) Gel strength as Young's modulus, squares: mixture of Ca²⁺ and MCO. For comparison the gel strength of alginate when only calcium is added has been included (triangles). (B) Syneresis, squares: mixture of Ca²⁺ and MCO.)
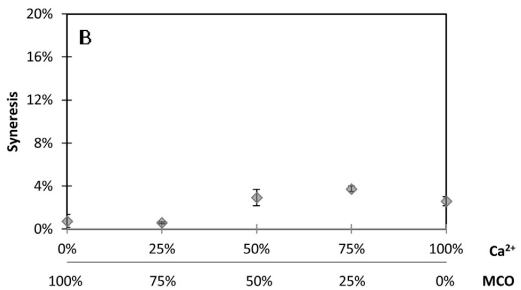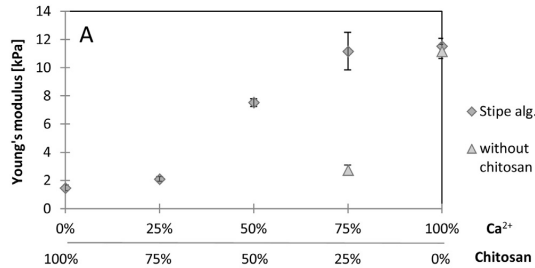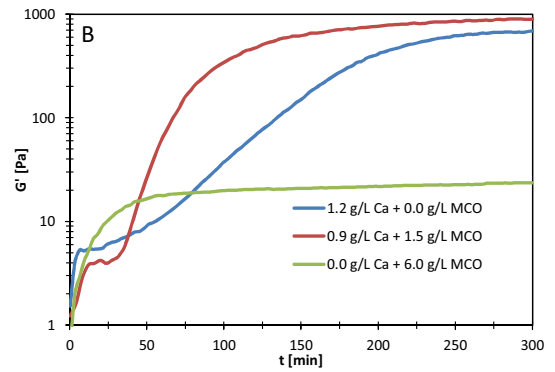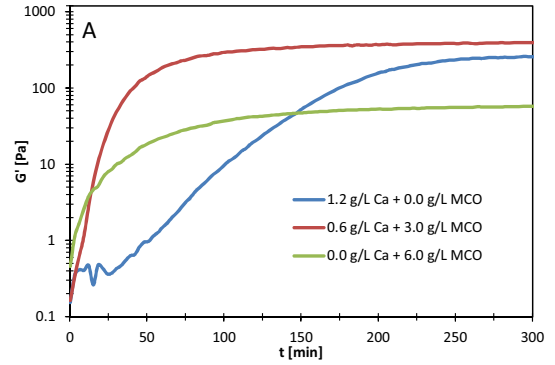

Fig. 6. Gel strength and syneresis of stipe alginate crosslinked with varying amounts of MCO and calcium (100% Ca²⁺: 1.3 g/L, 100% Chit: 6 g/L). (A) Gel strength as Young's modulus, squares: mixture of Ca²⁺ and chitosan. For comparison the gel strength of alginate when only calcium is added has been included (triangles). (B) Syneresis, squares: mixture of Ca²⁺ and chitosan.

Fig. 7. Comparison of the kinetics of gelation when internal gelling was performed with only calcium (orange line), only MCO (green lines) and with a mixture of calcium and MCO (purple line). (A) Leaf alginate. (B) Stipe alginate.

solid calcium-carbonate. This is most probably because the rate-limiting step in the gel formation with calcium is the dissolution and release of calcium from the solid calcium-carbonate (Draget, Østgaard, & Smidsrød, 1990), while in the alginate-MCO gelling system the rate-limiting step is the release of protons from GDL (which in turn protonates the chitosan oligomers). The gelling kinetics of the mixed gels is in between the calcium and the MCO gelling systems. The mixed gel reveals an incorporation of both properties, the gelling kinetics of the MCO crosslinked gel and the gel strength of the calcium-alginate gel. A possible explanation could be that the MCO gets protonated faster because of the higher ratio of GDL to MCO (see Fig. 1) compared to the pure MCO crosslinked gel. For stipe alginate (Fig. 7B) the difference in gelling kinetics and in gel strength between the pure calcium-alginate gel and the pure MCO crosslinked gel is even more pronounced. Both can be explained by the alginate composition (see Table 1) as previously described for pure MCO crosslinked gels.

The mixed gel shows similar behavior for stipe and leaf alginates, with a gel strength similar to pure calcium-alginate gel but with faster gelling kinetics. The onset of gelation of the mixed gel is not as fast as for the pure MCO crosslinked gel. This can be explained by the lower concentration of MCO (1.5 g/L for 25%) which is not enough to form a gel on its own but the gelation proceeds faster for mixed gel (approached equilibrium after 250 min) as for the pure calcium-alginate gel (approached equilibrium after 400 min) as soon as enough Ca²⁺ is released to form a gel.

4. Conclusions

Homogeneous alginate gels crosslinked with both calcium and chitosan oligomers can be prepared by internal gelling using a proton donor to simultaneously release calcium ions and protonate chitosan oligomers. Up to 50% of the calcium in alginate gels could be substituted with chitosan oligomers without loss in gel strength or change in syneresis, which means that the new gels have potential new applications for e.g. immobilization of calcium-sensitive cells.

Acknowledgments

Appendix A. Supplementary data

Supplementary data associated with this article can be found, in the online version, at http://dx.doi.org/10.1016/j.carbpol.2016.09.006.

References

Aam, B. B., Heggset, E. B., Norberg, A. L., Sørlie, M., Vårum, K. M., & Eijsink, V. G. H. (2010). Production of chitooligosaccharides and their potential applications in medicine. *Marine Drugs*, 8(5), 1482–1517. http://dx.doi.org/10.3390/md8051482

Aarstad, O. A., Tøndervik, A., Sletta, H., & Skjåk-Bræk, G. (2012). Alginate sequencing: An analysis of block distribution in alginates using specific alginate degrading enzymes. *Biomacromolecules*, 13(1), 106–116. http://dx.doi.org/10.1021/bm2013026

Anthonsen, M. W., & Smidsrød, O. (1995). Hydrogen ion titration of chitosans with varying degrees of N-acetylation by monitoring induced 1H-NMR chemical shifts. *Carbohydrate Polymers*, 26(4), 303–305. http://dx.doi.org/10.1016/0144-8617(95)00010-5

Atkins, E. D., Mackie, W., & Smolko, E. E. (1970). Crystalline structures of alginic acids. *Nature*, 225(5233), 626–628. http://dx.doi.org/10.1038/225626a0

Chan, G., & Mooney, D. J. (2013). Ca2+ released from calcium alginate gels can promote inflammatory responses in vitro and in vivo. *Acta Biomaterialia*, 9(12), 9281–9291. http://dx.doi.org/10.1016/j.actbio.2013.08.002

Cuan, Y. U. N. L. I. N., Shao, L. E. I., Yaoz, K. D. E., Guan, Y. L., Shao, L. E. I., & De Yao, K. (1996). A study on correlation between water state and swelling kinetics of chitosan-Based hydrogels. *Journal of Applied Polymer Science*, 61(13), 2325–2335. http://dx.doi.org/10.1002/(SICI)1097-4628(19960926)61:13<2325:AID-APP11>3.0. CO;2-3

Desai, R. M., Koshy, S. T., Hilderbrand, S. A., Mooney, D. J., & Joshi, N. S. (2015). Versatile click alginate hydrogels crosslinked via tetrazine-norbornene chemistry. *Biomaterials*, 50(1), 30–37. http://dx.doi.org/10.1016/j.biomaterials.2015.01.048

Draget, K. I., & SkjåK-Braek, G. (2011). Alginates: Existing and potential biotechnological and medical applications, 186–209. In Peter A. Williams (Ed.), *RSC Polymer Chemistry Series No. I. Renewable Resources for Functional Polymers and Biomaterials*.

Draget, K. I., Østgaard, K., & Smidsrød, O. (1990). Homogeneous alginate gels: A technical approach. *Carbohydrate Polymers*, 14(2), 159–178. http://dx.doi.org/10.1016/0144-8617(90)90028-q

Draget, K. I., Strand, B., Hartmann, M., Valla, S., Smidsrød, O., & Skjåk-Bræk, G. (2000). Ionic and acid gel formation of epimerised alginates; the effect of AlgE4. *International Journal of Biological Macromolecules*, 27(2), 117–122. http://dx.doi.org/10.1016/s0141-8130(00)00115-x

Draget, K. I., Moe, S., Skjåk-Bræk, G., & Smidsrød, O. (2006). Alginates. In *Food polysaccharides and their applications* (2nd ed., pp. 289–334). Boca Raton: CRC Press.

Dutta, P. K., Tripathi, S., Mehrotra, G. K., & Dutta, J. (2009). Perspectives for chitosan based antimicrobial films in food applications. *Food Chemistry*, 114(4), 1173–1182. http://dx.doi.org/10.1016/j.foodchem.2008.11.047

Felt, O., Carrel, A., Baehni, P., Buri, P., & Gurny, R. (2000). Chitosan as tear substitute: A wetting agent endowed with antimicrobial efficacy. *Journal of Ocular Pharmacology and Therapeutics*, 16(3), 261–270. http://dx.doi.org/10.1089/jop.2000.16.261

Grasdalen, H., Larsen, B., & Smidsrød, O. (1977). 13C NMR studies of alginate. *Carbohydrate Research, 56*, C11–C15.

Grasdalen, H., Larsen, B., & Smisrod, O. (1981). 13C-NMR studies of monomeric composition and sequence in alginate. *Carbohydrate Research*, 89(2), 179–191. http://dx.doi.org/10.1016/S0008-6215(00)85243-X

Grasdalen, H. (1983). High-field, 1H-NMR spectroscopy of alginate: Sequential structure and linkage conformations. *Carbohydrate Research, 118*, 255–260.

Haug, A. (1964). *Report No. 30—Composition and properties of alginates*. Norwegian Institute of Seaweed Research.

Ishiguro, K., Yoshie, N., Sakurai, M., & Inoue, Y. (1992). A 1H NMR study of a fragment of partially N-deacetylated chitin produced by lysozyme degradation. *Carbohydrate Research*, 237(C), 333–338. http://dx.doi.org/10.1016/S0008-6215(92)84257-S

Köping-Höggård, M., Tubulekas, I., Guan, H., Edwards, K., Nilsson, M., Vårum, K. M., & Artursson, P. (2001). Chitosan as a nonviral gene delivery system. Structure-property relationships and characteristics compared with polyethylenimine in vitro and after lung administration in vivo. *Gene Therapy*, 8(14), 1108–1121. http://dx.doi.org/10.1038/sj.gt.3301492

Khong, T. T., Aarstad, O. A., Skjåk-Bræk, G., Draget, K. I., & Vårum, K. M. (2013). Gelling concept combining chitosan and alginate—Proof of principle. *Biomacromolecules*, 14, 2765–2771. http://dx.doi.org/10.1021/bm400610b

Khong, T. T. (2013). Vietnamese chitin raw material, the chitin de-N-acetylation reaction, and a new chitosan-alginate gelling concept. NTNU–Thesis.

Leong, J.-Y., Lam, W.-H., Ho, K.-W., Voo, W.-P., Lee, M. F.-X., Lim, H.-P., . . . & Chan, E.-S. (2015). Advances in fabricating spherical alginate hydrogels with controlled particle designs by ionotropic gelation as encapsulation systems. *Particuology*, 24, 44–60. http://dx.doi.org/10.1016/j.partic.2015.09.004

Li, H. (2010). Preparation and characterization of homogeneous hydroxyapatite/chitosan composite scaffolds via in-situ hydration. *Journal of Biomaterials and Nanobiotechnology*, 01(01), 42–49. http://dx.doi.org/10.4236/jbnb.2010.11006

Liu, X. F., Guan, Y. L., Yang, D. Z., Li, Z., & Yao, K. D. (2000). Antibacterial action of chitosan and carboxymethylated chitosan. *Journal of Applied Polymer Science*, 79(March), 1324–1335. http://dx.doi.org/10.1002/1097-4628(20010214)79:7<1324:AID-APP210>3.0.CO;2-L

Mellegård, H., Strand, S. P., Christensen, B. E., Granum, P. E., & Hardy, S. P. (2011). Antibacterial activity of chemically defined chitosans: Influence of molecular weight, degree of acetylation and test organism. *International Journal of Food Microbiology*, 148(1), 48–54. http://dx.doi.org/10.1016/j.ijfoodmicro.2011.04.023

Mi, F. L., Shyu, S. S., Wong, T. B., Jang, S. F., Lee, S. T., & Lu, K. T. (1999). Chitosan-polyelectrolyte complexation for the preparation of gel beads and controlled release of anticancer drug. II. Effect of pH-dependent ionic crosslinking or interpolymer complex using tripolyphosphate or polyphosphate as reagent. *Journal of Applied Polymer Science*, 74(5), 1093–1107. http://dx.doi.org/10.1002/(SICI)1097-4628(19991031)74:5<1093:AID-APP6>3.0.CO;2-C

Minke, R., & Blackwell, J. (1978). The structure of α-chitin. *Journal of Molecular Biology*, 120(2), 167–181. http://dx.doi.org/10.1016/0022-2836(78)90063-3

Nilsen-Nygaard, J., Strand, S., Vårum, K., Draget, K., & Nordgård, C. (2015). Chitosan: Gels and interfacial properties. *Polymers*, 7(3), 552–579. http://dx.doi.org/10.3390/polym7030552

Nordtveit, R. J., Vårum, K. M., & Smidsrød, O. (1996). Degradation of partially N-acetylated chitosans with hen egg white and human lysozyme. *Carbohydrate Polymers*, 29(2), 163–167. http://dx.doi.org/10.1016/0144-8617(96)00003-3

Ong, S. Y., Wu, J., Moochhala, S. M., Tan, M. H., & Lu, J. (2008). Development of a chitosan-based wound dressing with improved hemostatic and antimicrobial properties. *Biomaterials*, 29(32), 4323–4332. http://dx.doi.org/10.1016/j.biomaterials.2008.07.034

Ross-Murphy, S. B. (1984). Rheological methods. In H. W. S. Chan (Ed.), *Biophysical methods in food research* (pp. 137–199). Blackwell Scientific Publications.

Sørbotten, A., Horn, S. J., Eijsink, V. G. H., & Vårum, K. M. (2005). Degradation of chitosans with chitinase B from Serratia marcescens. *FEBS Journal*, 272(2), 538–549. http://dx.doi.org/10.1111/j.1742-4658.2004.04495.x

Sikorski, P., Mo, F., Skjåk-Bræk, G., & Stokke, B. T. (2007). Evidence for egg-box-compatible interactions in calcium—Alginate gels from fiber x-ray diffraction. *Biomacromolecules*, 8(7), 2098–2103. http://dx.doi.org/10.1021/bm0701503

Strand, B. L., Mørch, Y., & Skjåk-Bræk, G. (2000). Alginate as immobilization matrix for cells. *Minerva Biotecnologica*, 12(4), 223–233. http://dx.doi.org/10.1016/0167-7799(90)90139-O

Strand, S. P., Tømmeraas, K., Vårum, K. M., & Østgaard, K. (2001). Electrophoretic light scattering studies of chitosans with different degrees of N-acetylation. *Biomacromolecules*, 2(4), 1310–1314. http://dx.doi.org/10.1021/bm015598x

Strand, S. P., Danielsen, S., Christensen, B. E., & Vårum, K. M. (2005). Influence of chitosan structure on the formation and stability of DNA–chitosan polyelectrolyte complexes. *Biomacromolecules*, 6(6), 3357–3366. Retrieved from. http://pubs.acs.org/doi/abs/10.1021/bm0503726

Tsukada, S., & Inoue, Y. (1981). Conformational properties of chito-oligosaccharides: Titration, optical rotation, and carbon-13 N.M.R. Studies of chito-oligosaccharides. *Carbohydrate Research*, 88(1), 19–38. http://dx.doi.org/10.1016/S0008-6215(00)84598-X

Ueno, H., Mori, T., & Fujinaga, T. (2001). Topical formulations and wound healing applications of chitosan. *Advanced Drug Delivery Reviews*, 52(2), 105–115. http://dx.doi.org/10.1016/s0169-409x(01)00189-2

Vårum, K. M., & Smidsrød, O. (2005). Structure-property relationship in chitosans. In S. Dumitriu (Ed.), *Polysaccharides—Structural diversity and functional versatility* (2nd ed., pp. 625–642). Boca Raton: CRC Press.

Vårum, K. M., Anthonsen, M. W., Grasdalen, H., & Smidsrod, O. (1991). Determination of the degree of N-acetylation and the distribution of N-acetyl groups in partially N-deacetylated chitins (chitosans) by high-field NMR spectroscopy. *Carbohydrate Research*, 211(1), 17–23. http://dx.doi.org/10.1016/0008-6215(91)84142-2

Vårum, K. M., Ottøy, M. H., & Smidsrød, O. (1994). Water-solubility of partially N-acetylated chitosans as a function of pH: Effect of chemical composition and depolymerisation. *Carbohydrate Polymers*, *25*(2), 65–70. http://dx.doi.org/10.1016/0144-8617(94)90140-6

Vårum, K. M., Myhr, M. M., Hjerde, R. J. N., & Smidsrød, O. (1997). In vitro degradation rates of partially N-acetylated chitosans in human serum. *Carbohydrate Research*, *299*(1–2), 99–101. http://dx.doi.org/10.1016/S0008-6215(96)00332-1

Xia, W., Liu, P., Zhang, J., & Chen, J. (2011). Biological activities of chitosan and chitooligosaccharides. *Food Hydrocolloids*, *25*(2), 170–179. http://dx.doi.org/10.1016/j.foodhyd.2010.03.003

SUPPLEMENTARY MATERIAL

A. **Characterization of chitosan oligomers and alginates**
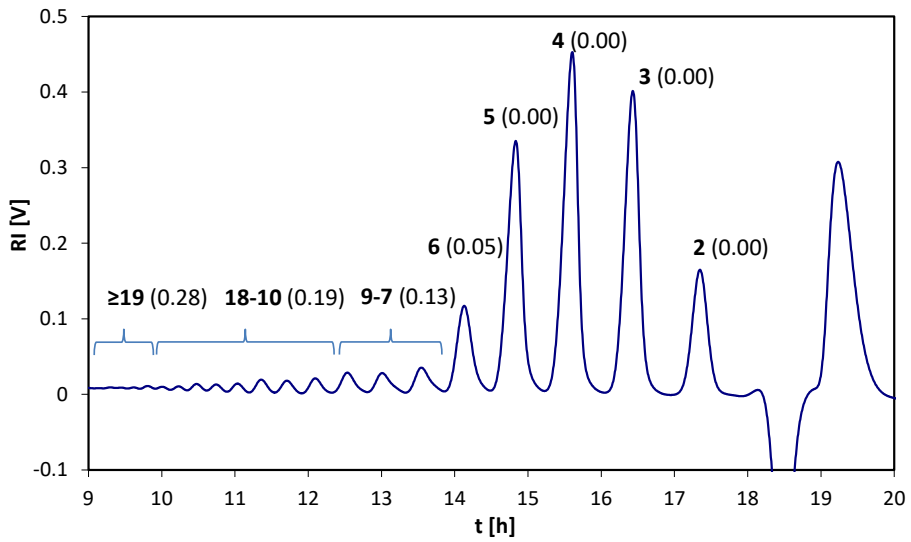
Figure 1. Size exclusion chromatogram of MCO. The number of units in the oligomer peak is given in bold numbers, the degree of acetylation (F_A) in parenthesis, e.g. 6 (0.05) means the oligomer with 6 units and F_A of 0.05.
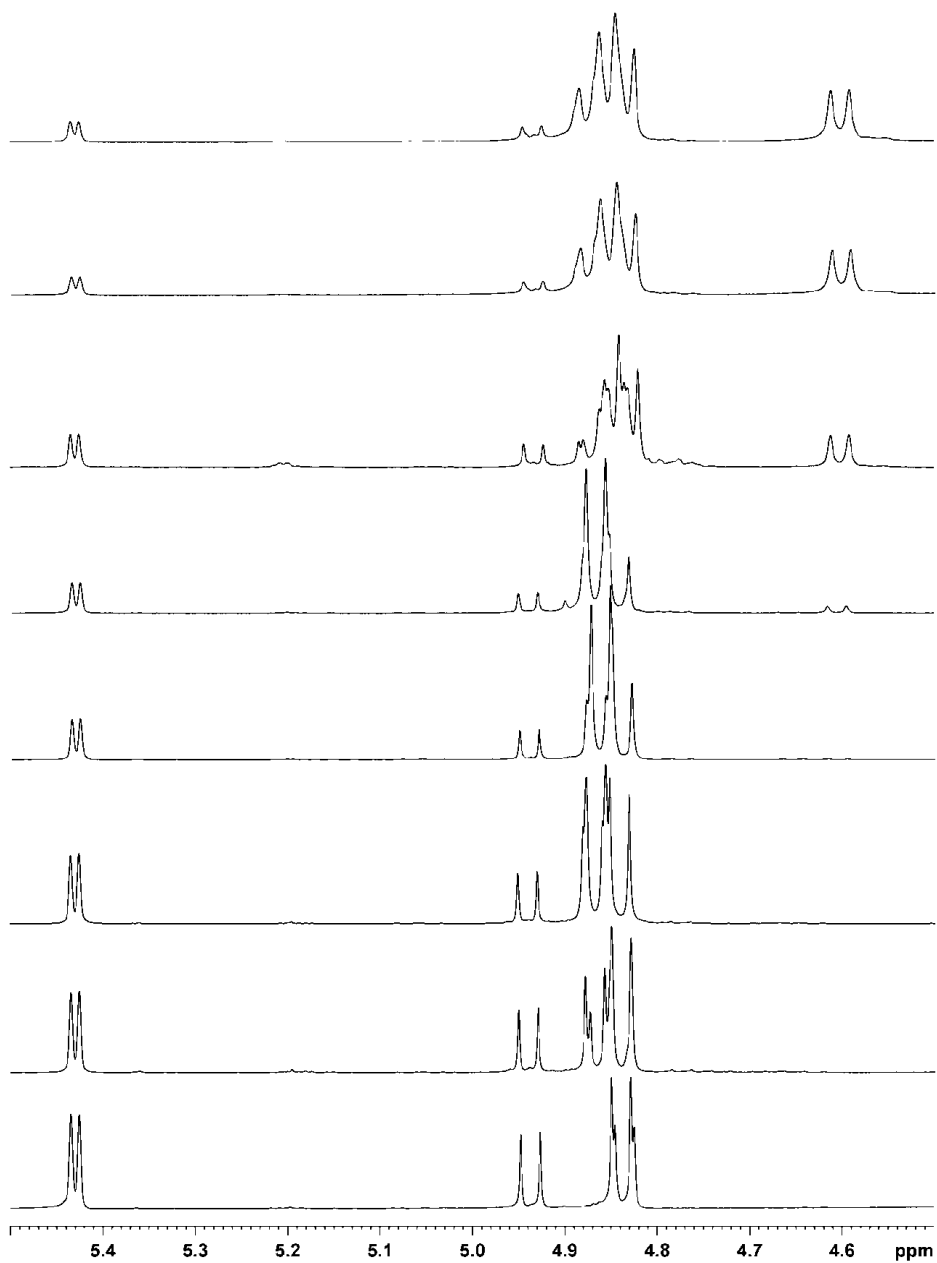
Figure 2. ^{1}H NMR of separated oligomers and fractions of MCO. Showing gradually increasing acetylation with increasing chain length. DP from bottom to top: 2, 3, 4, 5, 6, 7-9, 10-18, ≥19

Table 1. Degree of acetylation (F_A) and content in the chitosan oligomer mixture. $DP_n = 3.96$, total $F_A = 0.045$.

DP	2	3	4	5	6	7-9	10-18	$\geq$19
content	9.8 %	22.7 %	25.5 %	19.1 %	7.0 %	5.7 %	6.6 %	3.6 %
F_A	0	0	0	0	0.05	0.13	0.19	0.28

B. Experiments for the preparation of mixed gels with calculation

Mol masses [g/mol]		Determined max. conc. [mmol/L]	
Alginate-unit	199.12	MCO-unit (100%) as $(GlcN)_2$	12.5
$CaCO_3$	100.09	Ca^{2+} (100%) for leaf alg.	15
GDL	178.14	Ca^{2+} (100%) for stipe alg.	16.5
Chitosan-dimer (MCO DP_n = 3.96)	404.34		

Table 2. Amount of the crosslinkers MCO and Ca^{2+} at different ratios related to the determined max. conc.

Ratio	100	75	50	25	0	%
MCO-unit	12.5	9.4	6.3	3.1	0.0	mmol/L
Ca^{2+} (leaf alg.)	15.0	11.3	7.5	3.8	0.0	mmol/L
Ca^{2+} (stipe alg.)	16.5	12.4	8.3	4.1	0.0	mmol/L

Table 3. Complete composition of leaf alg. gels at different ratios of the combined crosslinkers MCO and Ca^{2+}

SAMPLE	1	2	3	4	5	Units
MCO ratio	0	25	50	75	100	[% of max.]
Ca^{2+} ratio	100	75	50	25	0	[% of max.]
MCO amount	0.00	3.79	7.58	11.37	15.16	mg
MCO conc.	0.00	1.26	2.53	3.79	5.05	g/L
GlcN-units	0.00	6.25	12.50	18.75	25.00	mmol/L
MCO stock sol. (100 g/L)	0.0	37.9	75.8	113.7	151.6	µl
$CaCO_3$ amount	4.50	3.38	2.25	1.13	0.00	mg
Ca^{2+} conc.	1.50	1.13	0.75	0.38	0.00	g/L
Ca^{2+} units	15.00	11.25	7.50	3.75	0.00	mmol/L
Alg. stock sol. (15 g/L)	2.00	2.00	2.00	2.00	2.00	mL
Alg. Amount	30.00	30.00	30.00	30.00	30.00	mg
Alg. conc.	10	10	10	10	10	g/L
Alg. Units	50.22	50.22	50.22	50.22	50.22	mmol/L
NaOH vol. (1 mol/L)	0.0	9.4	18.8	28.1	37. 5	µl
GDL amount	16.05	15.39	14.72	14.05	13.38	mg
H2O vol. (for GDL sol.)	1000.0	943.3	886.7	830.0	773.4	µl
Final vol.	3.00	3.00	3.00	3.00	3.00	mL

Example:

Preparation of leaf alginate gel cross-linked with 50% MCO and 50% calcium. (See Table 4 on the previous page, Sample 3)

Sample

Volume	3 ml
Alginate conc.	10 g/L
MCO ratio	50%
Ca^{2+} ratio	50%

1. Required amount of MCO

$$m(\text{MCO}) = 0.0125 \text{ mol} \cdot \text{L}^{-1} \cdot 0.5 \cdot 0.003 \text{ L} \cdot 404.34 \text{ g} \cdot \text{mol}^{-1} = \textbf{7.58 mg}$$

Added as stock solution (100 g/L) → 75.8 µL
Equalling a final conc. of **12.5 mmol/L**

2. Adjusting MCO solution to pH = 8 with NaOH (1 mol/L)

$$V(1 \text{ M (NaOH)}) = \underbrace{\frac{0.025 \text{ mol} \cdot \text{L}^{-1} \cdot 0.5 \cdot 0.003 \text{ L} \cdot 0.5}{1 \text{ mol} \cdot \text{L}^{-1}}}_{\text{neutralizing MCO}} + \underbrace{\frac{10^{-6} \text{ mol} \cdot \text{L}^{-1} \cdot 0.003 \text{ L}}{1 \text{ mol} \cdot \text{L}^{-1}}}_{\text{adjusting pH}} = \textbf{18.8 µL}$$

3. Mixing the alginate stock solution (15 g/L) with the pH adjusted MCO solution and the calcium carbonate

Required amount of $CaCO_3$

$$m(\text{CaCO}_3) = 0.015 \text{ mol} \cdot \text{L}^{-1} \cdot 0.5 \cdot 0.003 \text{ L} \cdot 100.09 \text{ g} \cdot \text{mol}^{-1} = \textbf{2.25 mg}$$

Equalling a final conc. of **7.5 mmol/L**

4. Adding a freshly prepared GDL solution through intensive stirring

Required amount of GDL (adjusted for MCO, $CaCO_3$ and pH)

$$m(\text{GDL}) = (0.025 \text{ mol} \cdot \text{L}^{-1} \cdot 0.5 \cdot 0.003 \text{ L} + 0.015 \text{ mol} \cdot \text{L}^{-1} \cdot 0.5 \cdot 0.003 \text{ L} \cdot 2 + 10^{-6} \text{ mol} \cdot \text{L}^{-1} \cdot 0.003 \text{ L}) \cdot 178.14 \text{ g} \cdot \text{mol}^{-1} = \textbf{14.72 mg}$$

Required amount of H_2O to solve the GDL

$$m(\text{H}_2\text{O}) = 3 \text{ mL} - 2 \text{ mL} - 75.8 \text{ µL} - 37.5 \text{ µL} = \textbf{886.7 µL}$$

Paper 2

Structural Characterization of Fucoidan from *Laminaria hyperborea*: Assessment of Coagulation and Inflammatory Properties and Their Structure−Function Relationship

Georg Kopplin,[†] Anne Mari Rokstad,[‡] Hugo Mélida,[§] Vincent Bulone,[§] Gudmund Skjåk-Bræk,[†] and Finn Lillelund Aachmann*,[†]

[†]Norwegian Biopolymer Laboratory (NOBIPOL), Department of Biotechnology, NTNU, Trondheim 7491, Norway

[‡]Centre of Molecular Inflammation Research (CEMIR), Department of Clinical and Molecular Medicine, NTNU, Trondheim 7030, Norway

[§]Division of Glycoscience, School of Engineering Sciences in Chemistry, Biotechnology and Health, Royal Institute of Technology (KTH), Stockholm SE-10691, Sweden

S *Supporting Information*

ABSTRACT: The structure of fucoidan isolated from *Laminaria hyperborea* was elucidated and chemically tailored in order to obtain a clear structure−function relationship on bioactive properties with a minimal amount of variations among the tested molecules. Analysis revealed a sugar composition of 97.8% fucose and 2.2% galactose. Analysis of the glycosidic linkages showed $(1{\rightarrow}3)$-α-L-fuco-pyranose (31.9%) to be the dominant residue, followed by $1{\rightarrow}2$-linked (13.2%) and $1{\rightarrow}4$-linked (7.7%) fuco-pyranose as well as a high degree of branching (22.4%). Inductively coupled plasma mass spectrometry (ICP-MS) revealed a sulfate content of 53.8% (degree of sulfation (DS) = 1.7). Raman spectroscopy determined SO_4 located axial at 4C and equatorial at 2C as well as an absence of acetylation. SEC-MALS analysis determined a high molecular weight (M_w = 469 kDa), suggesting a highly flexible main chain with short side chains. Both chemical shifts of the fucoidan, proton, and carbon were assigned by NMR and revealed a highly heterogeneous structure in terms of glycosidic linkages. Bioactivity was assessed using a lepirudin-based whole blood model. The immediate responses by coagulation and complement cascades were measured by prothrombine factor 1 and 2 (PTF1.2) and the terminal complement complex (TCC). Cytokines involved in inflammation were detected in a 27-plex cytokine assay. Fucoidan with a high M_w and DS inhibited coagulation, complement, and the cytokines PDGF-BB, RANTES, and IP-10, while activating MCP-1. These effects were obtained at the concentration of 1000 ug/mL and partly at 100 ug/mL. In low concentrations (10 ug/mL), a coagulation stimulating effect of highly sulfated fucoidans (DS = 1.7, M_w = 469 kDa or 20.3) was obtained. These data point to a multitude of effects linked to the sulfation degree that needs further mechanistic exploration.

KEYWORDS: *sulfated fucans, desulfation, NMR, Raman, SEC-MALS, inflammation*
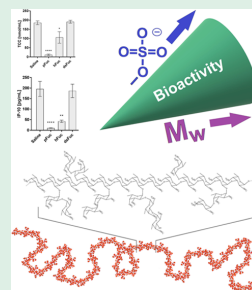
INTRODUCTION

Fucoidans are sulfated polysaccharides found in brown algae and essentially consist of L-fucose. They exhibit high and strongly diversified biological activities such as anticoagulant, antiinflammatory, antitumor, and antiviral activities.[1−5]

The term fucoidan has changed over time, covering a large array of fucose-containing sulfated polysaccharides (FCSP), including polysaccharides with a fucose backbone structure (fucans), FCSPs of heterogeneous compositions (i.e., fucogalactans, xylofucoglucuromannans) and of different origin. In order to systematize this highly diverse group, biomacromolecules, Deniaud-Bouët et al. (2017) have extensively discussed structural features of FCSPs and attributed IUPAC nomenclature recommendations accordingly.[6] Due to the high prevalence, the authors of this study continue to refer to this diverse group of polysaccharides with the well-established term of fucoidan.

Depending on the algal species, the structure of fucoidan varies in terms of sugar composition, glycosidic linkages, branching, and degree of sulfation and acetylation.[7] While some fucoidans, also known as galactofucan, contain predominantly fucose and galactose (e.g., *Saccharina longicruris*, *Saccharina latissima*, *Sargassum polycystum*, *Laminaria japonica*),[8−11] others comprise substantial amounts of additional monosaccharides such as glucose, mannose, xylose, and uronic acids.[3] The backbone of these macromolecules largely consists of $(1{\rightarrow}3)$ and $(1{\rightarrow}4)$ glycosidic linkages as dominant in most backbone structures (e.g., *Fucus vesiculosus*, *Fucus serratus*, *Ascophyllum nodosum*).[3,12−14] The structures vary in complexity

from linear 1→3-linked main chains that carry a few branched fucose residues (*Chorda filum*) to highly complex and heavily branched backbone structures (e.g., *Analipus japonicus, Undaria pinnatifida*).[15−17] The sulfate content also varies considerably from 14.5% in *Cladosiphon novae* up to 36.8% in *Laminaria saccharina*.[18,19] Mass spectrometry and Raman spectroscopy analysis revealed that sulfate groups are most commonly found at the C-2 position. However, disulfated structures also occur in some fucoidans alongside C-3 and C-4 monosulfated fucose units.[9,20,21] With the exception of fucans from invertebrates, regular, repetitive patterns in fucoidans in terms of intercepting sugar units, glycosidic linkages, branching points, sulfation, or acetylation are extremely rare.[1,22]

It has previously been shown that the degree of sulfation is related to anticoagulative effects and that angiogenesis is highly dependent on the molecular weight of the polymers.[7,23] Highly sulfated fucoidans were also shown to inhibit endothelial cell migration and vascular tube formation and to selectively stimulate the secretion of various antigens and block the infection of human cell lines with HIV, herpes, and cytomegalo viruses.[24,25] A detailed structural elucidation of fucoidans remains extremely challenging due to their high heterogeneity and lack of repetitive motifs. This further hinders the establishment of a relationship between structure and bioactivity. Most studies on the bioactive properties of fucoidans involve only loosely characterized chemical structures and assessments of biological activities that essentially rely on comparative analyses of fucoidans from different algal sources. As a result, the activities observed are typically linked to common structural features and, disregard the possible influence of finer structural differences, as well synergistic or antagonistic effects of different glycan epitopes.[3,7,25]

Here we present a detailed structural characterization of a purified fucoidan from *L. hyperborea*. The polymer was analyzed using a series of complementary approaches, i.e., NMR, ICP-MS, Raman spectroscopy, and monosaccharide linkage analysis. To establish a clear structure−function relationship, the structure of the purified fucoidan was tailored using a mild desulfation method or hydrolysis in mild acidic conditions. The bioactivity of the native and modified polymer was further evaluated, focusing on blood coagulation, complement, and cytokine responses in a lepirudin-based human whole blood model.[26] To our knowledge, this is the first study that combines a detailed structural characterization of a fucoidan polymer from *Laminaria hyperborea* with the analysis of its structure−function relationship using a controlled modification of multiple structural features.

■ EXPERIMENTAL SECTION

Materials and Methods. Fucoidan from *L. hyperborea* was manufactured by FMC BioPolymer (Sandvika, Norway) under GMP as a nonsterile bulk powder and ultrapurified and spray-dried by NovaMatrix as previously described (Halling et al., 2015) and will be referred to as purified fucoidan (pFuc).[27] All other starting materials were received from commercial sources with purities ≥99%. Hydrolyzed fucoidan (hFuc) was generated by mild acid degradation of pFuc with HCl at pH 3.0 and 70 °C for 30 min to achieve a similar degree of polymerization (DP) as for the desulfated fucoidan (dsFuc).

Sulfated alginate (SAlg) was synthesized from ultrapure alginate (F_G = 0.67, M_w = 199 kDa) provided by FMC Biopolymer using chlorosulfonic acid (99%; Sigma-Aldrich, St. Louis, MO, USA) and formamide (Merck, Whitehouse Station, NJ, USA) as previously described.[28]

The low molecular weight heparin (M_w = 12−14 kDa) from LEO Pharma (Ballerup, Denmark) was used as a control.

Desulfation. A complete desulfation was performed by a modified version of the solvolytic desulfation procedure from Inoue et al. (1976).[29] Sodium cations were exchanged with pyridinium ions by dissolving 150 mg of pFuc in water and rinsing the solution through an AG 50W cation exchange resin (Bio-Rad), which was beforehand equilibrated with pyridine (Sigma-Aldrich). The effluent was neutralized with 0.3 mL of pyridine and lyophilized. The fucoidan-pyridinium salt was dissolved in 15 mL of DMSO (Sigma-Aldrich), and 75 μL of water was added. The mixture was kept at 80 °C for 30 min and subsequently dialyzed (12K molecular weight cutoff) against 1 M NaCl and distilled water prior to lyophilization.

Mass Spectrometry. Sulfur contents were determined by dissolving 5.0 mg of dried fucoidan (70 °C for 90 min) in 15.0 mL of 1 M HNO_3. The samples were analyzed by high-resolution inductively coupled plasma mass spectrometry (HR-ICP-MS) at the NTNU Depatment of Chemistry (Trondheim, Norway). The sulfation degree was calculated by using a mass balance equation, assuming that every sulfate group is associated with a sodium counterion.

SEC-MALS. The molecular weight of fucoidan was measured by size-exclusion chromatography (SEC) using an HPLC system fitted with online multi-angle static light scattering (MALS) and with viscometry (VISC) detectors. The measurements were performed at ambient temperature using two serially connected columns of TSK G-6000PWXL and 5000 PWXL or TSK 4000 PWXL and 2500 PWXL. The column outlet was connected to a Dawn HELEOS-II multi-angle laser light scattering photometer (Wyatt, USA) (λ_0 = 663.8 nm) followed by an Optilab T-rEX differential refractometer and finally a ViscoStar II viscometer. The eluent was 0.15 M $NaNO_3$/0.01 M EDTA (pH = 6, I = 0.17 M), and the flow rate was 0.5 mL/min. Samples were filtered (pore size = 0.8 μm) before injection. The injection volume was 100−500 μL, and the sample concentration was adjusted to obtain the best possible light scattering signal without influencing the RI profile (overloading). The data were collected and processed using the Astra (v. 6.1) software (Wyatt, USA).

Refractive Index Increment (d*n*/d*c*)$_μ$. The (d*n*/d*c*)$_μ$ was determined for pFuc and dsFuc with a series of eight concentrations each measured on an Optilab rEX differential refractometer (Wyatt, USA) at λ_0 = 658.0 nm. Prior to the analysis, the samples were extensively dialyzed at pH 6 against a 0.05 M Na_2SO_4 solution, containing 0.01 M EDTA.

Intrinsic Viscosity Measurements. An Ubbelohde capillary viscometer (Schott-Geräte) equipped with an AVS 310 control unit and PC-operated titrator was used to perform the measurements and sequential dilutions. Five concentrations (10−2 g/L) were analyzed at 20.0 °C with 4 repetitions each. Automatic data acquisition and calculations were used, applying a Huggins, Mead−Fouss, Billmeyer, and Herman plot.

Raman Microspectroscopy. Raman microspectroscopy was performed at room temperature using a Renishaw InVia Reflex spectrometer equipped with a 785 nm laser. The pure fucoidan samples were scanned extendedly from 200 to 3200 cm⁻¹ (integration time = 30 s, 3 accumulations). Sample sizes of less than 0.5 mg gave sufficient resolution due to the microscope array. No further sample preparation was necessary.

Monosaccharide Analysis. Total sugar analysis was performed as described by Mélida et al. (2013).[30] The samples were hydrolyzed in the presence of 2 M trifluoroacetic acid (TFA) at 121 °C for 1.5 h. Myo inositol was used as an internal standard. For the determination of uronic acids, TFA hydrolysates were analyzed by high-performance anion-exchange chromatography (HPAEC). For neutral sugar analysis, the monosaccharides in the hydrolysates were converted to alditol acetates (Albersheim et al., 1967)[31] and separated and analyzed by GC/EI-MS as described by Mélida et al. (2013). Monosaccharide linkage analysis was performed by methylation using the CH_3I/NaOH method (Ciucanu and Kerek, 1984; Mélida et al., 2013).[32] The resulting partially methylated alditol acetates were analyzed by GC/EI-MS. Three replicates for each of the samples were analyzed using inositol as a standard.

Table 1. Linkage Analysis of the Desulfated Fucoidan, Performed in Three Technical Replicates[a]

	t-Fucp	1,2-Fucp	1,3-Fucp	1,4-Fucp	1,2,3-Fucp	1,2,4-Fucp	1,3,4-Fucp	1,6-Galp	1,4,6-Galp	1,3,6-Galp
mol %	23.2	13.2	31.9	7.7	13.1	4.5	4.8	0.8	0.5	0.4
SD	2.2	0.5	1.0	0.2	1.1	0.5	0.2	0.1	0.1	0.0

[a]Molecular percentage and the corresponding standard deviations are indicated.

NMR Spectroscopy. The purified fucoidan (10 mg) was first dissolved in 1 mL of 99.9% D_2O (Chiron) and lyophilized in order to reduce the residual water signal. Subsequently, the sample was dissolved in 595 μL of D_2O, and 5 μL of 1% 3-(trimethylsilyl)-propionic-2,2,3,3-d_4 acid sodium salt (TSP) (Sigma-Aldrich) was added for a chemical shift reference. The desulfated fucoidan (25 mg) was dissolved in 1 mL of 99.9% D_2O, and the solution was lyophilized. Residual DMSO from the desulfation procedure (see above) was used as a chemical shift reference.

All homo- and heteronuclear NMR experiments were recorded on a Bruker Avance 600 MHz or Bruker AVIIIHD 800 MHz (Bruker BioSpin AG, Fälladen, Switzerland) equipped with a 5 mm cryogenic CP-TCI z-gradient probe. All NMR recordings were performed at 25 °C.

For the chemical shift assignment of desulfated fucoidan, the following spectra were recorded: 1D proton, 2D double quantum filtered correlation spectroscopy (DQF-COSY), 2D total correlation spectroscopy (TOCSY) with a 70 ms mixing time, 2D ^{13}C heteronuclear single quantum coherence (HSQC) with multiplicity editing, 2D ^{13}C heteronuclear 2 bond correlation (H2BC), 2D ^{13}C HSQC-[^{1}H,^{1}H]TOCSY with a 70 ms mixing time on protons, and 2D heteronuclear multiple bond correlation (HMBC) with BIRD filter to suppress first-order correlations.

The spectra were recorded, processed, and analyzed using the TopSpin 3.2 or 3.5 software (Bruker BioSpin AG).

Purification for Inflammatory Property Assessment. Polysaccharide samples were purified through graphene filters (Millistak+ MCR4023CL3) for 24 h in a circular flow. Endotoxin content was measured by the LAL assay using the manufacturer's recommendations. The polysaccharide samples had final endotoxin levels of 6.9−38 EU/g and thus were considered ultrapure with respect to endotoxin (below 100 EU/g).

Viability by High-Throughput Screening (HTS). Purified fucoidan (pFuc), hydrolyzed fucoidan (hFuc), desulfated fucoidan (dsFuc), sulfated alginate (SAlg), and heparin samples were tested on various human cell lines (HOP 92, UACC-62, SF-295, A498, OVCAR-3, MDA-MB-468, COLO 205, SW-620, DU-145, HL-60 (TB), IMR-90). The viability was determined by quantification of the ATP content after 24 h of exposure to various concentrations (highest 333 mg/mL) of the samples. The ATP amount after lysis was determined through luminescence by the CellTiter-Glo luminescent cell viability assay from Promega Biotech AB (Madison, USA).

Assessment in Whole Blood. The ability to activate coagulation and inflammatory properties was investigated by a lepirudin-based human whole blood model. This model was first described by Mollnes et al. (2002)[26] and later modified for alginate materials (Rokstad, 2011[33]). The model is based on specific inhibition of thrombin by lepirudin, while maintaining the reactivity of the upstream coagulation factors and all of the complement factors as well as the leukocytes. Briefly, fresh human blood was withdrawn in polystyrene vials containing lepirudin (50 ug/mL final conc). Immediately after, for each condition, 500 μL of fresh blood was added to a 100 μL saline/polysaccharide solution and 100 μL of PBS. The final concentration of the ultrapurified polysaccharides was 10, 100, and 1000 μg/mL, and the control heparin was 20 IE/mL as previously described in Samstad (2014).[34] The samples were incubated under continuous rotative agitation, for 30 min (for complement) or 4 h (for coagulation and cytokines) at 37 °C. To stop further reactivity by complement and coagulation, EDTA was added to a final concentration of 10 mM. Subsequently, the samples were centrifuged (3000 rpm, 15 min), and plasma was aliquoted and stored at −20 °C until further analysis. Blood from six healthy donors were used running in total six experiments.

Complement Activation. The human terminal complement complex (TCC) ELISA kit (Hycult Biotech, Uden, The Netherlands) was used for quantification of human TCC in the blood plasma, according to the manufacturer's protocol.

Coagulation Activation (PTF1.2). The Enzygnost prothrombin F1+2 ELISA kit was used to detect prothrombin fragments 1 and 2, following the manufacturer's recommendations. PTF1.2 is a cleavage product formed upon the cleavage of prothrombin to thrombin and is thus reflecting the initial coagulation activation steps. Of note, PTF1.2 is not diverging between the intrinsic or extrinsic pathway of coagulation, since it is formed in the common pathway upon the second last step of thrombin formation.

Quantification of Cytokine Induction. The cytokine induction potentials were quantified using the Bio-Plex Human cytokine 27-Plex Panel (Bio-RadLaboratories, Hercules, CA). The following analytics were included: IL-1 beta (IL-1β), IL-1 receptor antagonist (IL-1ra), IL-2, IL-4, IL-5, IL-6, IL-7, IL-8 (CXCL8), IL-9, IL-10, IL-12, IL-13, IL-15, IL-17, eotaxin (CCL11), basic fibroblast growth factor (bFGF), granulocyte colony stimulating factor (GCSF), granulocyte-macrophage colony stimulating factor (GMCSF), interferon gamma (IFN-g), chemokin (C-X-C motif) ligand 10 (IP-10 or CXCL10), monocyte chemoattractant protein 1 (MCP-1 or CCL2), macrophage inflammatory protein-1-alfa (MIP-1a or CCL3), macrophage inflammatory protein-1-beta (MIP-1b or CCL4), platelet derived growth factor-BB (PDGFBB), regulated upon activation T-cell expressed and secreted (RANTES or CCL5), tumor necrosis factor alpha (TNF), and vascular endothelial growth factor (VEGF). The multiplex analyses were performed as recommended by the manufacturer using half amounts of beads.

Statistical Analysis. The GraphPad Prism Software v.7.01 was used for statistical analysis. A one-way ANOVA followed by a Dunnet's multiple comparison test was applied, including a saline control for comparison. Values at $p \leq 0.05$ were considered statistically significant.

Ethics. The use of human whole blood for basal experiments was approved by the Regional Committees for Medical and Health Research Ethics (REC) under REC Central [REK2009/2245]. The experiments were in accordance with their recommendation and followed the guidelines of the Helsinki declaration.

■ **RESULTS AND DISCUSSION**

Monosaccharide Analysis Reveals Fucose as the Almost Exclusive Sugar Unit. The GC profile of fucoidan revealed the presence of fucose (retention time = 8.1 min) and galactose (17.2 min) together with traces of glucose (18.5 min) (Figure S1). Mol % values for each of the components were calculated taking into consideration the chromatographic response factors for each of the monosaccharides, leading to a content of 97.8 ± 0.2 fucose and 2.2 ± 0.2 galactose, resulting in a fucoidan composition almost entirely made of fucose. The traces of glucose may arise from minor impurities.

Glycosidic Linkage Analysis Shows Extensive Branching. Glycosidic linkage analysis revealed 1,3-linked fucose as the most abundant (31.9%) unit in the polymer (see Table 1), followed by 1,2-linked fucose (13.2%) and 1,4-linked fucose (7.7%). The added number of branched fucose residues (22.4%) matches with the number of terminal fucose residues, proving the length of desulfated fucoidan samples as sufficient and internally verifying the data, pointing toward a dominant 1→3 backbone structure, as previously determined in *L. digitata*, intercepted with a high number of 1→2,3 branching points as

Table 2. Data Overview of Fucoidan Samples Used in This Study[a]

	DS	M_w [kDa]	M_n [kDa]	DP	R_w [nm]	R_n [nm]	dn/dc	$[\eta]$ [mL/g]	$[\eta]*$ [mL/g]	a	b
pFuc	1.70	469	218	750	37.1	27.4	0.115	98	121	0.78	0.65
dsFuc	0.12	7.3	5.8	40			0.140	6	8		
hFuc	1.70	20.3	10.6	37			0.115	5	7		

[a]Degree of sulfation (DS), weight average molar mass (M_w), number average molar mass (M_n), degree of polymerization (DP), weight average radius of gyration (R_w), number average radius of gyration (R_n), refractive index increment (dn/dc), intrinsic viscosity determined by SMV[1] ($[\eta]$), intrinsic viscosity determined by an Ubbelohde viscometer ($[\eta]*$), slope of a Mark−Houwink−Sakurada plot (a = $[\eta]$ versus M), slope of an RMS conformation plot (b = R_n versus M).

assigned in *S. latissima*, showing similarities to fucoidans of related *Laminariales* species.[3]

SEC-MALS Reveals a Large, Flexible Molecule with Short Side Chains. The (dn/dc)$_\mu$ for pFuc and dsFuc was determined to be 0.115 (±0.001) mL/g and 0.140 (±0.002) mL/g, respectively (Table 2). Through SEC-MALS analysis, a molecular weight average (M_w) of 469.2 (±1.9) kDa, a molecular number average (M_n) of 218.6 (±0.9) kDa were determined, resulting in a degree of polymerization (DP$_n$) of 720 monomer units for pFuc. (See below; a chromatogram of the full molecular weight distribution is given in Figure S2.) The radius of gyration as the weight average (R_w) was found to be 34.4 nm and 27.4 as the number average (R_n). In addition to the SMV analysis, the intrinsic viscosity ($[\eta]$) was also determined with use of an Ubbelohde viscometer (as Huggins, Mead−Fouss, and Billmeyer plots) resulting in 121 mL/g for pFuc. The process of desulfation lead to a slight depolymerization, by simultaneously hydrolyzing the glycosidic bonds. The lowest degree of sulfation, while remaining structurally representative, was achieved for desulfated fucoidan (dsFuc) with a DS = 0.12 (see below) and DP$_n$ = 37.

The overall shape of the molecule was determined through an RMS conformation plot, where R_n was plotted against M and a slope (b) of 0.65 was obtained, being closest to the random coil vector model (sphere b = 0.3; random coil b = 0.5; rigid rod b = 1).[35] A Mark−Houwink−Sakurada plot ($[\eta]$ versus M), which resulted in a slope (a) of 0.78 (Figures S2 and S3), also aligns with the theoretical value of a random coil shape (sphere a = 0; random coil a = 0.8; rigid rod a = 1.8), both indicating a large polymer with a highly flexible chain.

Combined with the results from the monosaccharide linkage analysis of a dominant glycosidic linkage and a high interception of branching points, the overall structure of a large, highly flexible molecule with short side chains can be deduced.

Mass Spectrometry Revealed a High Degree of Sulfation. The degree of sulfation of pFuc was determined from the sulfur (S) content of the polymer using HR-ICP-MS. The sulfur content of 16.92% (±0.39%) correspond to a sulfate content (SO_3^- + Na^+ − H) of 53.8%, which results in 1.70 sulfate groups per sugar unit.

$$w(SO_4) = \frac{w(S) \cdot M(SO_3 + Na - H)}{M(S)} = 1 - w(\text{fucose}) \tag{1}$$

$$DS = \frac{w(SO_4) \cdot M(\text{fucose} - H_2O)}{M(SO_3 + Na - H) \cdot w(\text{fucose})} \tag{2}$$

where w = mass fraction, M = molar mass [g mol^{-1}], and DS = degree of sulfaion.

Since a fucose unit ($C_6O_4H_{10}$) in a polysaccharide chain possesses only 2 theoretically available hydroxyl groups, a sulfation degree (DS) of 1.70 translates to 85% of all possible

hydroxyl groups being sulfated, which displays an almost fully sulfated fucoidan molecule. This represents, to our knowledge, the highest sulfation degree for a full fucoidan polymer reported to date.[1,3,20]

For the dsFuc, a sulfur content of 2.48% (±0.05%) was determined, equivalent to a sulfate content of 7.9% and a DS of 0.12, showing that 93% of the former sulfate groups could be removed through the given desulfation procedure.

Sulfation Analysis by Raman Microspectroscopy. The Raman spectra corresponding to the native and desulfated fucoidans are presented in Figure 1 and Table 3. Characteristic
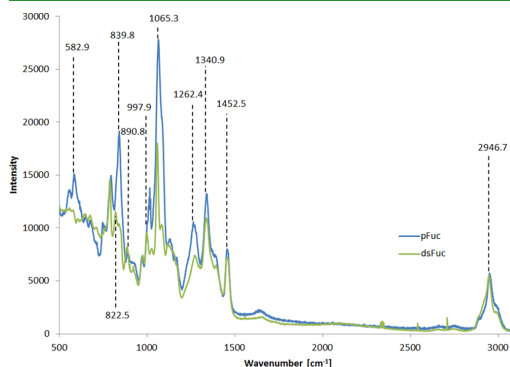
Figure 1. Raman spectra of purified fucoidan (blue) and desulfated fucoidan (green) from 500 to 3100 cm^{-1}.

Table 3. Assignment of the Chemical Groups in Raman Spectra of Fucoidan from *L. hyperborea*[a]

wavenumber [cm^{-1}]	assignment
582.9	$\delta_s(O=S=O)$
822.5	$\delta(2C—O—S)$
839.8	$\delta(4C—O—S)$
890.8	$\delta(\beta\text{-anomeric } C—H)$
997.9	$\nu_s(C—O—S)$, $\nu(\text{glycosidic } C—O)$
1065.3	$\nu_s(O=S=O)$, 2C—O—S
~970−1200	$\nu(\text{pyranoid ring } C—C, C—O)$
1262.4	$\nu_{as}(O=S=O)$
1340.9	$\delta_s(CH_2)$
1452.5	$\delta_s(CH_3)$
~1650−1800	$\nu(C=O)$
2946.7	$\nu(C—H)$

[a]δ and ν correspond to bending and stretching vibrations, respectively, and s and as correspond to symmetrical antisymmetrical modes, respectively.
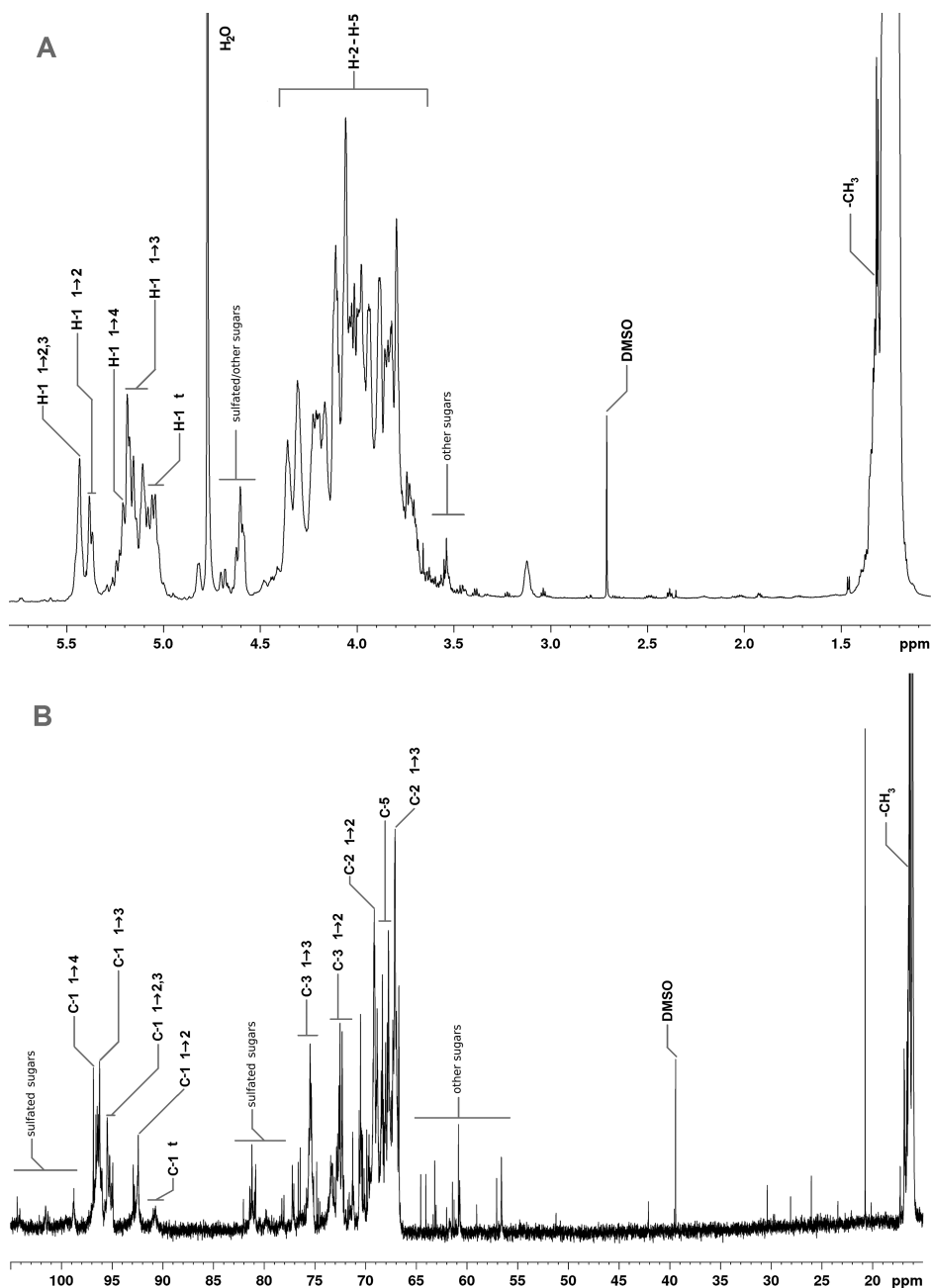
Figure 2. ^{1}H and ^{13}C NMR (A and B) analysis of desulfated fucoidan (recorded in D$_2$O at 800 MHz and 25 °C)

vibration bands for fucoidan are found at 1452.5 cm^{-1} and were assigned to symmetric CH$_3$ deformations, from the fucose 6C methyl group. An associated symmetric CH$_2$ deformation was detected at 1340.9 cm^{-1}.[21,36,37] A further characteristic peak is

the very intense Raman band at 1065.3 cm^{-1}, which originates from symmetric sulfate ester stretching vibrations.[38]

Most fucoidans exhibit strong peaks between 1650 and 1800 cm^{-1}, which are related to C=O vibrations. The absence of such

Table 4. Proton and Carbon Chemical Shifts [ppm] of Desulfated Fucoidan (Top) and Purified Fucoidan (Bottom) from *Laminaria hyperborea*[a]

glyc link.	H-1	C-1	H-2	C-2	H-3	C-3	H-4	C-4	H-5	C-5	H-6	C-6
1→2	5.38	92.6	4.06	69.2	3.99	67.8						
1→3	5.19	95.5	3.85	66.6−67.1	4.01	75.6			4.31	67.1	1.21−1.25	16.1
1→4	5.21	96.6							4.37	68.8	1.32	16.9
1→2,3	5.44	92.4	4.06	69.2	3.86	73.4						
1→t	5.11−5.05	96.3	4.31	67.2								
1→2	5.55											
1→3	5.35										1.29	
1→4											1.32	

[a]Determined in D_2O at 800 MHz and 25°C.

signals verifies the absence of acetyl groups as well as uronic acids.[37]

A small peak at 890.8 cm^{-1} originated from β-anomeric C—H deformations, which correlates to either β-glycosidic linkages or reducing end fucose residues in β-configuration. The corresponding α-anomeric C—H deformation at around 860.0 cm^{-1} is overlapped by stronger sulfate bands and can therefore not be identified clearly.[21,39]

Vibrations related to sulfate groups or sulfate esters were found in various parts of the spectra. Beside the very intense Raman band at 1065.3 cm^{-1}, strong bands occurred at 839.8 cm^{-1}, correlating to an axial 4C—O—S bending vibration with a shoulder at 822.5 cm^{-1} caused by a 2C—O—S bending.[25,40] Raman bands at 1262.4 cm^{-1} were assigned to antisymmetric O=S=O stretchings.[21,41] The envelope around 582.9 cm^{-1} reflects a variety of different symmetric and antisymmetric internal SO_4 vibrations.[42−44]

A semiquantitative evaluation of the degree of sulfation (DS) of the sulfated and desulfated fucoidan can be achieved through relating the C—H stretching vibration bands found at 2800−3000 cm^{-1}[45] as well as the (fucose) methyl group vibrations at 1452.5 and 1340.9 cm^{-1} to the various sulfate bands. These C—H and CH_3 vibration bands provide an internal standard. Changes in sulfate concentration are in agreement with the decrease in the intensity of each sulfate peak.

A comparison between the native and desulfated fucoidan shows that the sulfate group in axial 4C position (839.8 cm^{-1}) was almost entirely removed by the desulfation treatment, whereas the sulfate group in 2C remained to a greater extend, as indicated by the former shoulder peak (822.5 cm^{-1}) as well as by the less affected band at 1065.3 cm^{-1}. These data provide information about different susceptibilities toward the desulfation method used above. The O=S=O stretching band at 1065.3 cm^{-1} is commonly used to estimate the degree of polysaccharide sulfation because of its high intensity even though a general overlap with C—O and C—C vibrations between 970 and 1200 cm^{-1} coming from the pyranoid ring and O—C—O stretching vibrations originating from glycosidic linkages occurs.[44,46,47] In this study, the highest agreement between the DS measured by mass spectrometry (removal of 93% of sulfate groups) and the calculated DS from Raman band integrals was found for the bands at 582.9 cm^{-1} (80% reduction) and at 1262.4 cm^{-1} (75% reduction). These signals can therefore be recommended for a quantifie estimation of DS, in addition to the commonly used 1065.3 cm^{-1} peak, which displayed just 65% reduction due to overlaps with other vibration bands.

NMR Spectroscopy. The proton spectra of the purified (pFuc) and desulfated fucoidan (dsFuc) are given in the Figure

S4. The proton spectrum of pFuc reveals two broad and dominant signals in the anomeric region as well as strong signals in the methyl region, which correspond to the C-6 methyl protons of fucopyranose. The ratio between the integral for the anomeric signals {H-1} (5.1−5.8 ppm; integral = 1.000), internal {H-2,3,4,5} (3.6−5.1 ppm; integral = 4.186), and methyl {H3−6} (1.0−1.8 ppm; integral = 3.122) protons supports the results from the monosaccharide analysis of a polysaccharide almost exclusively consisting of fucose units. No acetyl or carboxylic acid signals could be detected in the 1D proton and carbon spectra (Figure 2). This is in good agreement with the results from the monosaccharide analysis and vibrational spectroscopy (see above) displaying no other functional groups than sulfate. The broad signals for pFuc did not allow extracting more structural relevant data for the sample.

Previously, desulfation of fucoidans has been shown to reduce the complexity for the NMR spectra, without significant depolymerization and effect on the glycosidic linkages. This pretreatment of the sample allows the use of 2D NMR spectroscopy for the assignment of the resonances.[13,48] Desulfation lead to an overall alteration of the chemical shifts for dsFuc toward higher fields as a result of the removal of deshielding effects of the sulfate groups (Figure S4). Desulfation also caused a partial depolymerization of the sample, which also contributed resolving the signals. Altogether, after desulfation, the few broad signals have split up into many individual sets of signals being more dependent on the individual sugar linkage and their inner molecular environments. Due to the complexity of the resulting spectra, only the main fucoidan components were possible to assign. Those main monosaccharide residues were assigned by starting at the anomeric signal and then following the proton−proton connectivity using TOCSY, DQF-COSY, and ^{13}C H2BC and ^{13}C HSQC-[^{1}H,^{1}H] TOCSY spectra. ^{13}C HSQC is used for assigning the carbon chemical shifts. The fucose units were identified by comparison of the chemical shift to literature values,[13−15] chemical shift calculations generated with CASPER,[49] and matching intensity to data obtained from the monosaccharide linkage analysis (Table 4). The ^{13}C HMBC spectrum was used to identify the glycosidic linkages for the main monosaccharide units of dsFuc (Table 5).

The most intense signals can be assigned to 1→3-linked α-L-fuco-pyranose units (Figure 2) with the following correlations (obtained from the DQF-COSY, H2BC, and HCCH-TOCSY) forming an anomeric H-1/C-1 signal at 5.19/95.1 ppm, followed by H-2/C-3 at 3.85/66.1 ppm and H-3/C-3 at 4.01/75.38 ppm. Except for the chemical shifts of H-4/C-4, the rest of the signals could be assigned to 1→3-linked α-L-fuco-pyranose.

The anomeric signals corresponding to 1→2 and 1→2,3 glycosidic linkages can be found separated at 5.38/92.6 and

Table 5. Crosspeak Assignment from ^{1}H/^{13}C HSQC (Figure 3) of dsFuc

crosspeak	coord H/C [ppm]	assignment
A	5.44/92.6	{H-1/C-1} 1→2
B	5.43/90.8	{H-1/C-1} 1→2
C	5.38/92.4	{H-1/C-1} 1→2,3
D	5.23/92.9	
E	5.21/96.6	{H-1/C-1} 1→4
F	5.19/95.2	{H-1/C-1} 1→3
G	5.15/95.5	{H-1/C-1} 1→3
H	5.11/96.2	{H-1/C-1} 1→3
I	5.06/96.3	{H-1/C-1} 1→t
J	5.04/96.5	{H-1/C-1} 1→t
K	4.31/67.2	{H-2/C-2} 1→t
L	4.06/69.2	{H-2/C-2} 1→2
M	3.85/66.6	{H-2/C-2} 1→3
O	3.83/68.3	{H-2/C-2} 1→3
P	1.24/16.1	{H-6/C-6} 1→3
Q	1.32/16.9	{H-6/C-6} 1→4

5.44/96.6 ppm, respectively (Figure 3 and Table 5). Furthermore, the anomeric crosspeak of 1→4-linked α-L-fuco-
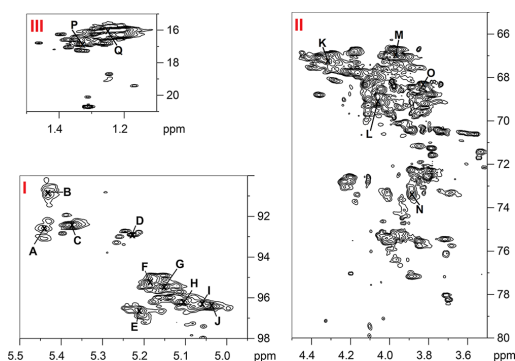
Figure 3. HSQC NMR spectrum of desulfated fucoidan recorded in D$_2$O at 800 MHz and 25 °C. Anomeric (I), inner sugar ring 2H–5H (II), methyl group (III) region. Crosspeaks (A–Q).

pyranose could be assigned from the 5.21/96.6 ppm signals. Chemical shift calculations done by CASPER[49] are supporting these assignments, predicting a H-1 shift of 5.38 ppm for 1→2, 5.24 ppm for 1→4, and 5.22 ppm for 1→3-linked α-L-fuco-pyranose.

The fucose methyl group displays a cluster of proton signals between 1.21 and 1.25 ppm with a separated signal at 1.32 ppm attributed to 1→4-linked α-L-fuco-pyranose.[9,49] The correlated 5H/5C signals were found at 4.21/67.1 ppm and 4.37/68.8, ppm respectively. The purified highly sulfated fucoidan showed fewer but broader proton signals than the desulfated fucoidan due to its higher molecular weight and degree of polymerization. However, some anomeric protons within pFuc could be assigned (see Table 4), such as 5.35 ppm for the dominant 1→3 glycosidic linkage and 5.55 ppm for the 1→2- and 1→2,3-linked fucose residues. Furthermore, methyl protons were determined at 1.29 ppm, and signals of 1→4-linked fucose residues were shifted to 1.32 ppm.

Mild acid degradations lead to sharper signals but increased the complexity drastically (Figure S5), which can be attributed to the diversification of otherwise almost fully sulfated α-L-fuco-pyranose units with a similar glycosidic linkage pattern through the formation of new reducing and nonreducing ends. The high homogeneity of the pFuc spectrum in contrast to the increased complexity of the mildly acid hydrolyzed spectra supports the argument for a 1→3-linked main chain deduced by glycosidic linkage analysis and SEC-MALS as well as NMR analysis for dsFuc.

Five possible structural fragments (equal ratio) of desulfated fucoidan are suggested in Scheme 1, and assigned in accordance with data obtained from NMR, Raman, and glycosidic linkage analysis.

Scheme 1. Suggested Structural Fragments (I−V) of Desulfated Fucoidan from *Laminaria Hyperborea*, Occurring in an Equal Ratio
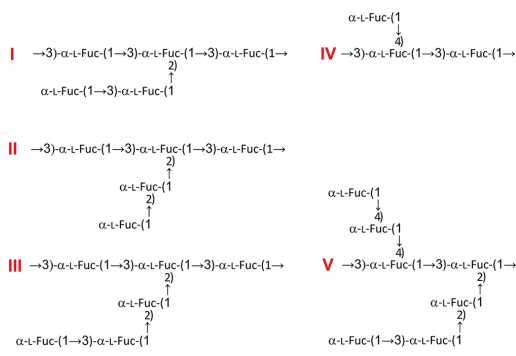
Effect on Coagulation and Inflammatory Properties.
Effect on Coagulation. The coagulation activation potential measured by the cleavage product PTF1.2 in human whole blood demonstrates the impact of molecular size, degree of sulfation, as well as the concentration of fucoidan (Figure 4). An inhibitory effect was seen by all fucoidan samples at the highest concentration (1000 μg/mL), contrasting with the data obtained for the saline control representing background stimulation (Figure 4A). This effect was maintained for a ten time lower dose of pFuc (100 μg/mL), but not for the hFuc and dsFuc (Figure 4B), demonstrating both the dependence of molecular weight and degree of sulfation for coagulation inhibition. In contrast to the inhibitory effects at 1000 and 100 μg/mL, the lowest concentration of 10 μg/mL resulted in a stimulatory effect by the sulfated pFuc and hFuc, resulting in an increased PTF1.2 concentration, but not for dsFuc (Figure 4C). The lack of stimulation after desulfation indicates the importance of sulfate groups for biological activity. This is further supported by similar outcomes in the presence of SAlg, representing a polysaccharide backbone of mannuronic and guluronic acid-containing sulfated groups.

The concentration-dependent effect on coagulation sheds light on previous contradictory findings demonstrating both pro- and anticoagulant properties of fucoidans.[50−52] The concentration effects might be explained by two different mechanisms, involving inhibition of coagulation proteins and stimulation of monocytes to express tissue factor (TF). A direct inhibitory effect has been shown by the fucan derived from
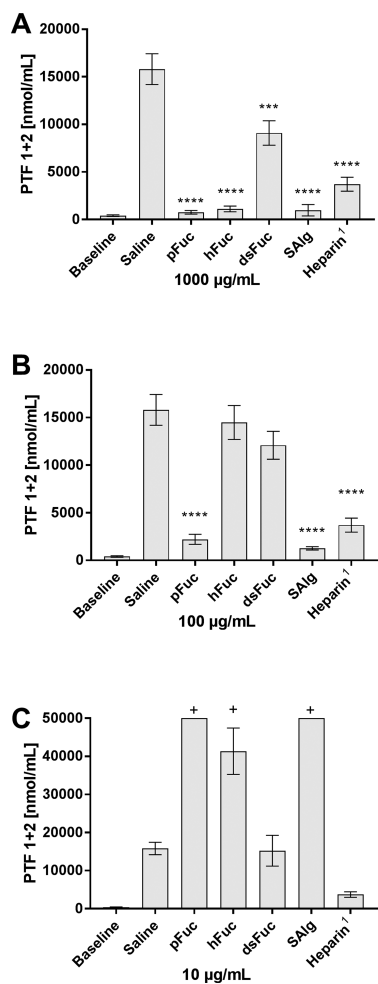
Figure 4. Coagulation activation measured as plasma PTF1.2 (nmol/mL) following exposure of pFuc, hFuc, or dsFuc in a lepirudin-based human whole blood for 4 h. Fucoidans were incubated in low-activating (polystyrene) conditions at concentrations of 10 (C), 100 (B), or 1000 (A) ug/mL. Significant values are given as $p \leq 0.05$ (*), $p \leq 0.01$ (**), $p \leq 0.001$ (***), $p \leq 0.0001$ (****) compared to the saline control. Data are expressed as the mean value of 6 donors ± SEM.

Punctaria plantaginea involving binding of thrombin and FXa, the latter in assistance with antithrombin III (ATIII).[53] The inhibitory effect at high concentrations of fucoidan in the current study could be explained by such interactions and would affect the common pathway of coagulation. Since our blood model is based on the specific inhibition of thrombin, the inhibitory effects in the current study rather involves the interaction with fXa-ATIII than thrombin. The extrinsic pathway of coagulation is initiated by monocytes expressing TF following stimulation and is activated following blood activation in polystyrene vials.[54] Activation can be mediated through complement C5a−C5aR1 and LPS−TLR4 interactions.[55] Although yet unexplored in relation to monocyte TF,

fucoidan has been described to trigger cytokines through TLR4,[56] and thus, this could be a possible activation pathway promoting coagulation.

Effect on Complement. The effects of fucoidan on complement TCC are shown in Figure 5. Among the different
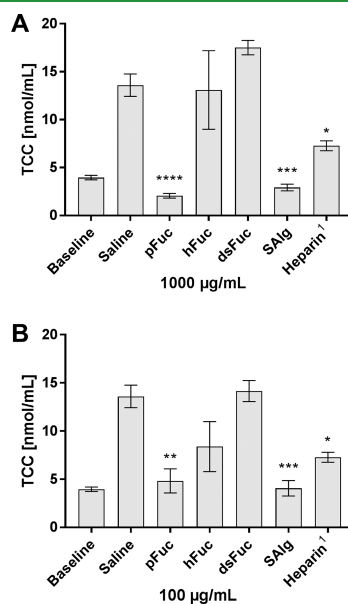
Figure 5. Complement activation following exposure of pFuc, hFuc, or dsFuc measured as the soluble terminal complement complex (TCC). Samples were incubated in lepirudin anticoagulated human whole blood for 0.5 h. Fucoidans were incubated in low-activating (polystyrene) conditions under exposure at concentrations of 100 (B) or 1000 (A) ug/mL. Significant values are given as $p \leq 0.05$ (*), $p \leq 0.01$ (**), $p \leq 0.001$ (***), $p \leq 0.0001$ (****) compared to the control saline value. Data are expressed as the mean value of 6 donors ± SEM.

fucoidan samples, pFuc most efficiently inhibited complement with a significant effect at the concentration of 1000 μg/mL (Figure 5A). This confirms the importance of both molecular size and degree of sulfation for biological activity. Reducing the concentration of pFuc 10-fold significantly maintained the inhibitory effect (Figure 5B). At a dose of 10 ug/mL, no changes on TCC formation (inhibition or activation) was found (data not shown). The strongest inhibition of complement was provided by SAlg (Figure 5A,B), which could be explained by its ability to associate with the anticomplement factor H (fH), as previously demonstrated.[57] We cannot exclude a similar mechanism of the sulfation groups in fucoidan, but this needs further exploration. The inhibitory effect of fucoidan on complement might also contribute to a reduced coagulation activation as previously demonstrated.[54] Still, a pFuc concentration of 100 μg/mL inhibited coagulation, but not complement, thus pointing to the involvement of additional independent factors.

Effect on Cytokines. Of the 27 cytokines evaluated, significant changes following the treatment with fucoidan samples were detected for only 4 cytokines (Figure 6), namely, MCP-1 (CCL2), IP-10 (CXCL10), PDGF-BB, and RANTES
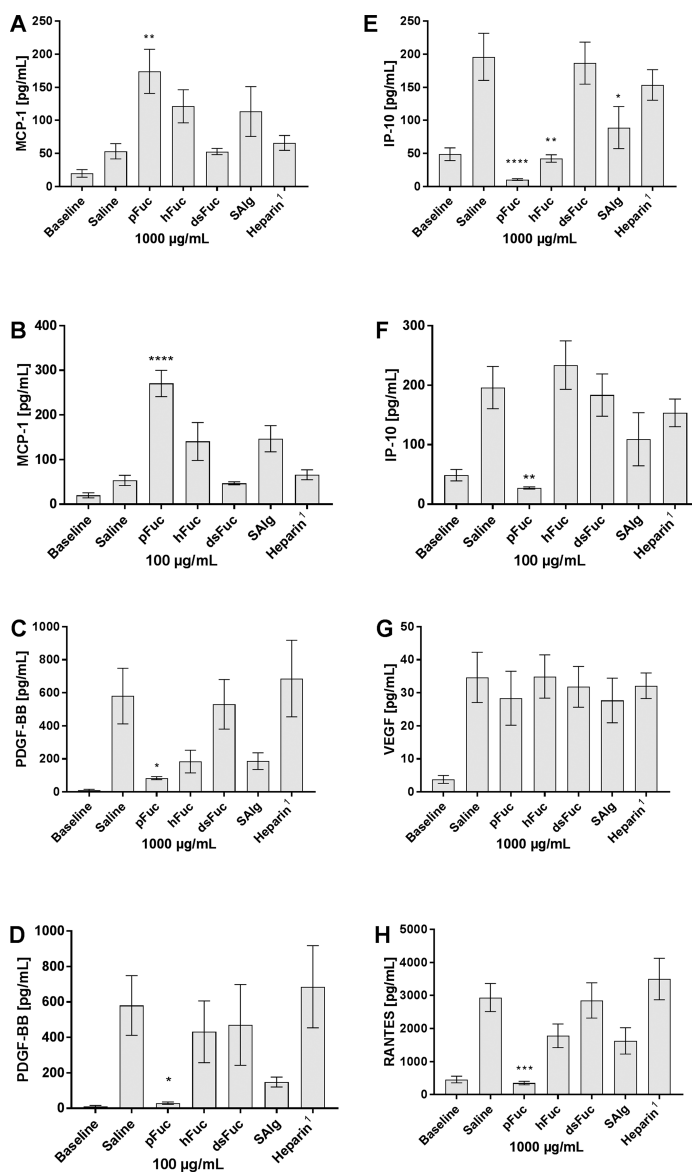
Figure 6. Effects on cytokines concentrations (pg/mL) of MCP-1 (CCL2) [A, B], PDGF-BB [C, D], IP-10 (CXCL10) [E, F], VEGF [G], and RANTES (CCL5) [H] following exposure of pFuc, hFuc, or dsFuc in a lepirudin-based human whole blood for 4 h. Significant values are given as $p \leq$ 0.05 (*), $p \leq 0.01$ (**), $p \leq 0.001$ (***), $p \leq 0.0001$ (****) compared to the saline control value. Data are expressed as the mean value of 6 donors ± SEM.

(CCL5). The monocyte attractor chemokine MCP-1 was significantly elevated upon addition of pFuc in a 1000 or 100 μg/mL dose compared to the saline control (Figure 6A,B). Interferon γ-induced protein 10 (IP-10) is reported to possess several functions among being a chemoattractor for mono- cytes.[52,58,59] A significant inhibition was found upon addition of pFuc and hFuc at a concentration of 1000 μg/mL (Figure 6E,F).

The growth factor PDGF-BB was significantly decreased by pFuc at 1000 and 100 μg/mL, and hFuc and dsFuc displayed no decrease in PDGF-BB concentration, relating the inhibition again to molecular size and degree of sulfation. Platelets produce and secrete PDGF-BB as well as RANTES;[60] thus, this inhibition could be due to reduced activation of the platelets, in consistence with previous findings of inhibition of thrombotic

Scheme 2. Possible Structural Fragment of 25 Fucose Residues Applied as Building Blocks for a Full-Scale Structural Model (DP = 750, R_w = 37 nm) of Fucoidan from *L. hyperborea*[a]
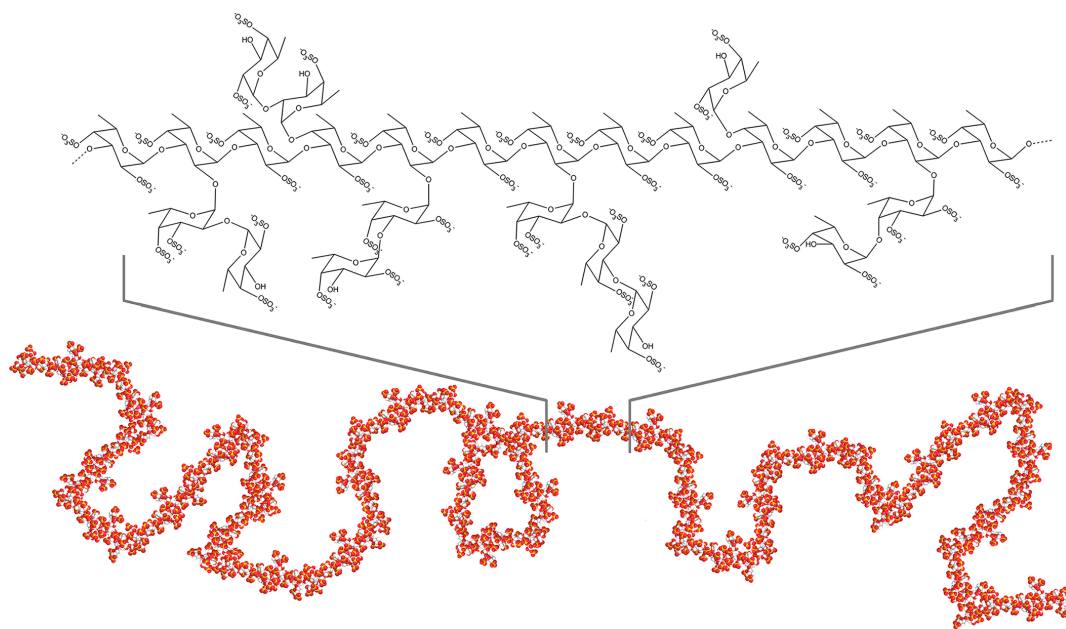
[a]Atom color: H = white, C = grey, O = red, S = yellow.

activities.[53] Other effects that might be involved are possible electrostatic interactions between the negatively charged sulfated groups with positively charged cytokines. Of note, the basal isoelectric point of MCP-1, PDGF-BB, RANTES, and IP-10 are above 9 (https://www.phosphosite.org/homeAction.action); thus, they are expected to be highly positive charged mediators under physiological conditions. Cytokines as IL-1β, IL-6, TNF, and IL-8 have previously been shown to be dependent on an initial complement activation where blocking of complement activation completely inhibits these cytokines.[61] The complement inhibition by the pFuc alginate could thus explain the lack of significant responses of the pro-inflammatory cytokines IL-1β, IL-6, TNF, and IL-8 (Figures S6 and S7). Of note, RANTES and PDGF-BB have been among the cytokines that show a partly complement dependency.[61] Also, previously reported inhibition of the growth factor VEGF[5,24] could not be confirmed for this particular fucoidan (Figures S6 and S7), which might be explained by different binding properties due to the high diversity of fucoidans.

■ CONCLUSIONS AND FUTURE PERSPECTIVES

Structure. The finding that fucose is the principal sugar unit combined with the fact that almost full sulfation is observed provides a high overall simplicity of the analyzed polysaccharide molecule isolated from *L. hyperborea*. Nevertheless, the large variety of glycosidic linkages, branching points, and their random distribution still results in a heterogeneous structure.

Due to the lack of repeating units, a fully defined primary structure cannot be determined, but through the combination of several analytical techniques, a reasonable approximation of a hypothetical structure of the fucoidan can be given. Mono-saccharide linkage analysis and NMR revealed 1→3 glycosidic bonds with the interception of 1→2 and 1→4 branching points to be the dominant glycosidic structure (suggested fragments given in Scheme 1). ICP-MS and Raman spectroscopy determined a sulfate content of 53.8% (DS = 1.70) as well as the position of certain sulfate groups and the lack of acetylation. SEC-MALS revealed a high molecular weight (M_w = 496 kDa, DP = 750) and indicated a highly flexible chain with short side chains.

In order to obtain a full concept structure, an oligomer building block of 25 fucose residues was designed in full agreement with all data from NMR, ICP-MS, Raman, and monosaccharide linkage analysis (shown in Scheme 2). Although, the branching points of this 25 sugar unit fragment could be arranged in random order, the overall chemical and physical properties would be very similar for every possible combination. The tertiary structure was calculated and optimized by GaussView 5.0 and applied to a full-scale model of 30 building blocks (DP = 750) simulated in BIOVIA Materials Studio to fit a radius of gyration of 37 nm previously determined by SEC-MALS and is in line with previous structure suggestions derived from SAXS experiments.[62]

Bioactivity. Through comparison of the well-defined samples pFuc, hFuc, dsFuc, SAlg, and heparin, it was demonstrated that the anticoagulant effects of these poly-saccharides depend predominantly on the degree of sulfation, to lesser extend on the molecular weight, whereas branching and sugar composition showed no significant influence on coagulation.

The measurement of a terminal complement complex as a parameter of initial inflammation suggested that both sulfation

and high molecular weight were necessary to induce anti-inflammatory effects. Accordingly, the strongest inhibition was displayed by pFuc and SAlg, respectively.

Among the 27 cytokines, four, namely, MCP-1, IP-10, PDGF-BB, and RANTES, showed a significant response to pFuc, the polysaccharide displaying both a high degree of sulfation and high molecular weight. The reduced secretion of PDGF-BB and RANTES is likely connected to platelet inhibition; thus, the effects on platelets warrant further explorations. Moreover, the strong stimulatory effect of pFuc on MCP-1 points to a pattern recognition stimulation that also warrants further investigations. The mechanisms behind the coagulation activation following low-concentration pFuc and dFuc are suggested to involve the interaction with PRRs and induction of monocyte TF, which also warrants further exploration in the near future.

■ ASSOCIATED CONTENT

Ⓢ Supporting Information

The Supporting Information is available free of charge on the ACS Publications website at DOI: 10.1021/acsabm.8b00436.

GC profile of pFuc; SEC-MALS chromatogram of pFuc, including refractive index, light scattering, and molar mass profile; Mark−Houwink−Sakurada plot of pFuc; ^{1}H NMR of pFuc and dsFuc at 600 MHz; ^{1}H NMR signal intensities of pFuc; ^{1}H NMR of pFuc after acidic hydrolysis (pH 3.5, 50 °C) for 5, 10, and 60 min; plasma concentrations of the cytokines IL-1b, TNF, and IL-6; plasma concentrations of the cytokines IL-10, IL-1ra, IL-8, MIP-1a, PDGF-BB, MCP-1, and IP-10 (PDF)

■ AUTHOR INFORMATION

Corresponding Author
*E-mail: finn.l.aachmann@ntnu.no.

ORCID Ⓘ
Hugo Mélida: 0000-0003-1792-0113
Finn Lillelund Aachmann: 0000-0003-1613-4663

Notes
The authors declare no competing financial interest.

■ DEDICATION

This project is in memory of Professor Kjell Morten Vårum, NTNU, who passed away during this work. We are grateful to his sincere and passionate leadership in this project.

■ REFERENCES

(1) Berteau, O.; Mulloy, B. Sulfated Fucans, Fresh Perspectives: Structures, Functions, and Biological Properties of Sulfated Fucans and an Overview of Enzymes Active toward This Class of Polysaccharide. *Glycobiology* **2003**, *13* (6), 29−40.

(2) Kusaykin, M.; Bakunina, I.; Sova, V.; Ermakova, S.; Kuznetsova, T.; Besednova, N.; Zaporozhets, T.; Zvyagintseva, T. Structure,

Biological Activity, and Enzymatic Transformation of Fucoidans from the Brown Seaweeds. *Biotechnol. J.* **2008**, *3* (7), 904−915.

(3) Cumashi, A.; Ushakova, N. A.; Preobrazhenskaya, M. E.; D'Incecco, A.; Piccoli, A.; Totani, L.; Tinari, N.; Morozevich, G. E.; Berman, A. E.; Bilan, M. I.; Usov, A.; Ustyuzhanina, N. E.; Grachev, A. A.; Sanderson, C. J.; Kelly, M.; Rabinovich, G. A.; Iacobelli, S.; Nifantiev, N. E. A Comparative Study of the Anti-Inflammatory, Anticoagulant, Antiangiogenic, and Antiadhesive Activities of Nine Different Fucoidans from Brown Seaweeds. *Glycobiology* **2007**, *17* (5), 541−552.

(4) Chen, S.; Zhao, Y.; Zhang, Y.; Zhang, D. Fucoidan Induces Cancer Cell Apoptosis by Modulating the Endoplasmic Reticulum Stress Cascades. *PLoS One* **2014**, *9* (9), e108157.

(5) Chen, H.; Cong, Q.; Du, Z.; Liao, W.; Zhang, L.; Yao, Y.; Ding, K. Sulfated Fucoidan FP08S2 Inhibits Lung Cancer Cell Growth in Vivo by Disrupting Angiogenesis via Targeting VEGFR2/VEGF and Blocking VEGFR2/Erk/VEGF Signaling. *Cancer Lett.* **2016**, *382* (1), 44−52.

(6) Deniaud-Bouët, E.; Hardouin, K.; Potin, P.; Kloareg, B.; Hervé, C. A Review about Brown Algal Cell Walls and Fucose-Containing Sulfated Polysaccharides: Cell Wall Context, Biomedical Properties and Key Research Challenges. *Carbohydr. Polym.* **2017**, *175*, 395−408.

(7) Ustyuzhanina, N. E.; Bilan, M. I.; Ushakova, N. A.; Usov, A. I.; Kiselevskiy, M. V.; Nifantiev, N. E. Fucoidans: Pro- or Antiangiogenic Agents? *Glycobiology* **2014**, *24* (12), 1265−1274.

(8) Rioux, L. E.; Turgeon, S. L.; Beaulieu, M. Structural Characterization of Laminaran and Galactofucan Extracted from the Brown Seaweed Saccharina longicruris. *Phytochemistry* **2010**, *71* (13), 1586−1595.

(9) Bilan, M. I.; Grachev, A. a.; Shashkov, A. S.; Thuy, T. T. T.; Thanh Van, T. T.; Ly, B. M.; Nifantiev, N. E.; Usov, A. I. Preliminary Investigation of a Highly Sulfated Galactofucan Fraction Isolated from the Brown Alga Sargassum polycystum. *Carbohydr. Res.* **2013**, *377*, 48−57.

(10) Zvyagintseva, T. N.; Shevchenko, N. M.; Chizhov, A. O.; Krupnova, T. N.; Sundukova, E. V.; Isakov, V. V. Water-Soluble Polysaccharides of Some Far-Eastern Brown Seaweeds. Distribution, Structure, and Their Dependence on the Developmental Conditions. *J. Exp. Mar. Biol. Ecol.* **2003**, *294* (1), 1−13.

(11) Bilan, M. I.; Grachev, A. A.; Shashkov, A. S.; Kelly, M.; Sanderson, C. J.; Nifantiev, N. E.; Usov, A. I. Further Studies on the Composition and Structure of a Fucoidan Preparation from the Brown Alga Saccharina latissima. *Carbohydr. Res.* **2010**, *345* (14), 2038−2047.

(12) Bilan, M. I.; Grachev, A. a.; Shashkov, A. S.; Nifantiev, N. E.; Usov, A. I. Structure of a Fucoidan from the Brown Seaweed Fucus serratus L. *Carbohydr. Res.* **2006**, *341* (2), 238−245.

(13) Chevolot, L.; Mulloy, B.; Ratiskol, J.; Foucault, A.; Colliec-Jouault, S. A Disaccharide Repeat Unit Is the Major Structure in Fucoidans from Two Species of Brown Algae. *Carbohydr. Res.* **2001**, *330* (4), 529−535.

(14) Daniel, R.; Berteau, O.; Chevolot, L.; Varenne, A.; Gareil, P.; Goasdoue, N. Regioselective Desulfation of Sulfated L-Fucopyranoside by a New Sulfoesterase from the Marine Mollusk Pecten maximus: Application to the Structural Study of Algal Fucoidan (Ascophyllum Nodosum). *Eur. J. Biochem.* **2001**, *268* (21), 5617−5626.

(15) Chizhov, A. O.; Dell, A.; Morris, H. R.; Haslam, S. M.; McDowell, R. a.; Shashkov, A. S.; Nifant'ev, N. E.; Khatuntseva, E. a.; Usov, A. I. A Study of Fucoidan from the Brown Seaweed Chorda Filum. *Carbohydr. Res.* **1999**, *320* (1−2), 108−119.

(16) Bilan, M. I.; Zakharova, A. N.; Grachev, A. A.; Shashkov, A. S.; Nifantiev, N. E.; Usov, A. I. Polysaccharides of Algae: 60. Fucoidan from the Pacific Brown Alga Analipus japonicus (Harv.) Winne (Ectocarpales, Scytosiphonaceae). *Russ. J. Bioorg. Chem.* **2007**, *33* (1), 38−46.

(17) Liu, F.; Wang, J.; Chang, A. K.; Liu, B.; Yang, L.; Li, Q.; Wang, P.; Zou, X. Fucoidan Extract Derived from Undaria pinnatifida Inhibits Angiogenesis by Human Umbilical Vein Endothelial Cells. *Phytomedicine* **2012**, *19* (8−9), 797−803.

(18) Ye, J.; Li, Y.; Teruya, K.; Katakura, Y.; Ichikawa, A.; Eto, H.; Hosoi, H.; Hosoi, M.; Nishimoto, S.; Shirahata, S. Enzyme-Digested Fucoidan Extracts Derived from Seaweed Mozuku of Cladosiphon novae-caledoniae kylin Inhibit Invasion and Angiogenesis of Tumor Cells. *Cytotechnology* **2005**, *47* (1−3), 117−126.

(19) Croci, D. O.; Cumashi, A.; Ushakova, N. A.; Preobrazhenskaya, M. E.; Piccoli, A.; Totani, L.; Ustyuzhanina, N. E.; Bilan, M. I.; Usov, A. I.; Grachev, A. A.; Morozevich, G. E.; Berman, A. E.; Sanderson, C. J.; Kelly, M.; Di Gregorio, P.; Rossi, C.; Tinari, N.; Iacobelli, S.; Rabinovich, S. A.; Nifantiev, N. E. Fucans, but Not Fucomannoglucuronans, Determine the Biological Activities of Sulfated Polysaccharides from Laminaria Saccharina Brown Seaweed. *PLoS One* **2011**, *6* (2), e17283.

(20) Anastyuk, S. D.; Shevchenko, N. M.; Nazarenko, E. L.; Imbs, T. I.; Gorbach, V. I.; Dmitrenok, P. S.; Zvyagintseva, T. N. Structural Analysis of a Highly Sulfated Fucan from the Brown Alga Laminaria Cichorioides by Tandem MALDI and ESI Mass Spectrometry. *Carbohydr. Res.* **2010**, *345* (15), 2206−2212.

(21) Synytsya, A.; Kim, W. J.; Kim, S. M.; Pohl, R.; Synytsya, A.; Kvasnička, F.; Čopíková, J.; Il Park, Y. Structure and Antitumour Activity of Fucoidan Isolated from Sporophyll of Korean Brown Seaweed Undaria pinnatifida. *Carbohydr. Polym.* **2010**, *81* (1), 41−48.

(22) Bilan, M. I.; Grachev, A. A.; Ustuzhanina, N. E.; Shashkov, A. S.; Nifantiev, N. E.; Usov, A. I. A Highly Regular Fraction of a Fucoidan from the Brown Seaweed Fucus distichus L. *Carbohydr. Res.* **2004**, *339* (3), 511−517.

(23) Matsubara, K.; Xue, C.; Zhao, X.; Mori, M.; Sugawara, T.; Hirata, T. Effects of Middle Molecular Weight Fucoidans on in Vitro and Ex Vivo Angiogenesis of Endothelial Cells. *Int. J. Mol. Med.* **2005**, *15* (4), 695−699.

(24) Koyanagi, S.; Tanigawa, N.; Nakagawa, H.; Soeda, S.; Shimeno, H. Oversulfation of Fucoidan Enhances Its Anti-Angiogenic and Antitumor Activities. *Biochem. Pharmacol.* **2003**, *65* (2), 173−179.

(25) Patankar, M. S.; Oehninger, S.; Barnett, T.; Williams, R. L.; Clark, G. F. A Revised Structure for Fucoidan May Explain Some of Its Biological Activities. *J. Biol. Chem.* **1993**, *268* (29), 21770−21776.

(26) Mollnes, T. E.; Brekke, O.; Fung, M.; Fure, H.; Christiansen, D.; Bergseth, G.; Videm, V.; Lappegård, K. T.; Köhl, J.; Lambris, J. D. Essential Role of the C5a Receptor in E Coli − Induced Oxidative Burst and Phagocytosis Revealed by a Novel Lepirudin-Based Human Whole Blood Model of Inflammation Essential Role of the C5a Receptor in E Coli − Induced Oxidative Burst and Phagocytosis Rev. *Blood* **2002**, *100* (5), 1869−1877.

(27) Halling, B.; Vetvicka, V.; Blakemore, W. Evaluation of The Immunomodulatory in Vivo Activity of Laminaria Hyperborea Fucoidan Relative to Commercial (1,3/1,6)-B-D-Glucans from Yeast and Mushrooms. *J. Nutr. Heal. Sci.* **2015**, *2* (2), 1−13.

(28) Arlov, Ø.; Aachmann, F. L.; Sundan, A.; Espevik, T.; Skjåk-Bræk, G. Heparin-like Properties of Sulfated Alginates with Defined Sequences and Sulfation Degrees. *Biomacromolecules* **2014**, *15* (7), 2744−2750.

(29) Inoue, Y.; Nagasawa, K. Selective N-Desulfation of Heparin with Dimethyl Sulfoxide Containing Water or Methanol. *Carbohydr. Res.* **1976**, *46* (1), 87−95.

(30) Mélida, H.; Sandoval-Sierra, J. V.; Diéguez-Uribeondo, J.; Bulone, V. Analyses of Extracellular Carbohydrates in Oomycetes Unveil the Existence of Three Different Cell Wall Types. *Eukaryotic Cell* **2013**, *12* (2), 194−203.

(31) Albersheim, P.; Nevins, D. J.; English, P. D.; Karr, A. A Method for the Analysis of Sugars in Plant Cell-Wall Polysaccharides by Gas-Liquid Chromatography. *Carbohydr. Res.* **1967**, *5*, 340−345.

(32) Ciucanu, I.; Kerek, F. A Simple and Rapid Method for the Permethylation of Carbohydrates. *Carbohydr. Res.* **1984**, *131* (2), 209−217.

(33) Rokstad, A. M.; Brekke, O. L.; Steinkjer, B.; Ryan, L.; Kolláriková, G.; Strand, B. L.; Skjåk-Bræk, G.; Lacík, I.; Espevik, T.; Mollnes, T. E. Alginate Microbeads Are Complement Compatible, in Contrast to Polycation Containing Microcapsules, as Revealed in a Human Whole Blood Model. *Acta Biomater.* **2011**, *7* (6), 2566−2578.

(34) Samstad, E. O.; Niyonzima, N.; Nymo, S.; Aune, M. H.; Ryan, L.; Bakke, S. S.; Lappegard, K. T.; Brekke, O.-L. O.-L.; Lambris, J. D.; Damas, J. K.; Latz, E.; Mollnes, T. E.; Espevik, T. Cholesterol Crystals Induce Complement-Dependent Inflammasome Activation and Cytokine Release. *J. Immunol.* **2014**, *192* (6), 2837−2845.

(35) Smidsrød, O.; Moe, S. *Biopolymer Chemistry*, 2nd ed.; Postmyr, L., Ed.; Tapir Uttrykk, 2008.

(36) Kačuráková, M.; Mathlouthi, M. FTIR and Laser-Raman Spectra of Oligosaccharides in Water: Characterization of the Glycosidic Bond. *Carbohydr. Res.* **1996**, *284* (2), 145−157.

(37) Adebajo, M. O.; Frost, R. L.; Kloprogge, J. T.; Kokot, S. Raman Spectroscopic Investigation of Acetylation of Raw Cotton. *Spectrochim. Acta, Part A* **2006**, *64* (2), 448−453.

(38) Pielesz, A.; Biniaś, W.; Paluch, J. Mild Acid Hydrolysis of Fucoidan: Characterization by Electrophoresis and FT-Raman Spectroscopy. *Carbohydr. Res.* **2011**, *346* (13), 1937−1944.

(39) Atha, D. H.; Gaigalas, A. K.; Reipa, V. Structural Analysis of Heparin by Raman Spectroscopy. *J. Pharm. Sci.* **1996**, *85* (1), 52−56.

(40) Qiu, X.; Amarasekara, A.; Doctor, V. Effect of Oversulfation on the Chemical and Biological Properties of Fucoidan. *Carbohydr. Polym.* **2006**, *63* (2), 224−228.

(41) Pereira, L.; Amado, A. M.; Critchley, A. T.; van de Velde, F.; Ribeiro-Claro, P. J. A. A. Identification of Selected Seaweed Polysaccharides (Phycocolloids) by Vibrational Spectroscopy (FTIR-ATR and FT-Raman). *Food Hydrocolloids* **2009**, *23* (7), 1903−1909.

(42) Ben Mabrouk, K.; Kauffmann, T. H.; Aroui, H.; Fontana, M. D. Raman Study of Cation Effect on Sulfate Vibration Modes in Solid State and in Aqueous Solutions. *J. Raman Spectrosc.* **2013**, *44* (11), 1603−1608.

(43) Buzgar, N.; Buzatu, A.; Sanislav, I. V. The Raman Study on Certain Sulfates. *Analele Stiintifice ale Universitatii Al. I. Cuza* **2009**, 5−23.

(44) Pielesz, A.; Biniaś, W. Cellulose Acetate Membrane Electrophoresis and FTIR Spectroscopy as Methods of Identifying a Fucoidan in Fucus Vesiculosus Linnaeus. *Carbohydr. Res.* **2010**, *345* (18), 2676−2682.

(45) Abbate, S.; Conti, G.; Naggi, A. Characterisation of the Glycosidic Linkage by Infrared and Raman Spectroscopy in the C-H Stretching Region: α,α-Trehalose and α,α-Trehalose-2,3,4,6,6-D10. *Carbohydr. Res.* **1991**, *210*, 1−12.

(46) Sekkal, M.; Legrand, P.; Huvenne, J. P.; Verdus, M. C. The Use of FTIR Microspectrometry as a New Tool for the Identification in Situ of Polygalactanes in Red Seaweeds. *J. Mol. Struct.* **1993**, *294* (C), 227−230.

(47) Kiefer, W.; Mazzolini, A. P.; Stoddart, P. R. Recent Advances in Linear and Nonlinear Raman Spectroscopy I. *J. Raman Spectrosc.* **2007**, *38* (April), 1538−1553.

(48) Chandía, N. P.; Matsuhiro, B. Characterization of a Fucoidan from Lessonia Vadosa (Phaeophyta) and Its Anticoagulant and Elicitor Properties. *Int. J. Biol. Macromol.* **2008**, *42* (3), 235−240.

(49) Lundborg, M.; Widmalm, G. Structural Analysis of Glycans by NMR Chemical Shift Prediction. *Anal. Chem.* **2011**, *83* (5), 1514−1517.

(50) Dockal, M.; Panholzer, E.; Hartmann, R.; Ehrlich, H. J.; Scheiflinger, F. A New Procoagulant Mechanism Mediated by Fucoidans. *Blood* **2010**, *116* (21), 4420−4432.

(51) Zhu, C.; Cao, R.; Zhang, S. X.; Man, Y. N.; Wu, X. Z. Fucoidan Inhibits the Growth of Hepatocellular Carcinoma Independent of Angiogenesis. *Evidence-based Complement. Altern. Med.* **2013**, *2013*, 1−7.

(52) Zhang, Z.; Till, S.; Jiang, C.; Knappe, S.; Reutterer, S.; Scheiflinger, F.; Szabo, C.; Dockal, M. Structure-Activity Relationship of Pro- and Anticoagulant Effects of Fucus vesiculosus Fucoidan. *Thromb. Haemostasis* **2014**, *111* (21), 429−437.

(53) Ustyuzhanina, N. E.; Bilan, M. I.; Gerbst, A. G.; Ushakova, N. A.; Tsvetkova, E. A.; Dmitrenok, A. S.; Usov, A. I.; Nifantiev, N. E. Anticoagulant and Antithrombotic Activities of Modified Xylofucan Sulfate from the Brown Alga Punctaria plantaginea. *Carbohydr. Polym.* **2016**, *136*, 826−833.

(54) Gravastrand, C.; Hamad, S.; Fure, H.; Steinkjer, B.; Ryan, L.; Oberholzer, J.; Lambris, J. D.; Lacík, I.; Mollnes, T. E.; Espevik, T.; Brekke, O.; Rokstad, A. M. Alginate Microbeads Are Coagulation Compatible, While Alginate Microcapsules Activate Coagulation Secondary to Complement or Directly through FXII. *Acta Biomater.* **2017**, *58*, 158−167.

(55) Chu, A. J. Tissue Factor, Blood Coagulation, and Beyond: An Overview. *Int. J. Inflammation* **2011**, *2011*, 1−30.

(56) Makarenkova, I. D.; Logunov, D. I.; Tukhvatulin, A. I.; Semenova, I. B.; Zvyagintseva, T. N.; Gorbach, V. I.; Ermakova, S. P.; Besednova, N. N. [Sulfated Polysaccharides of Brown Seaweeds–Ligands of Toll-like Receptors]. *Biomed. Khim.* **2012**, *58* (3), 318−325.

(57) Arlov, Ø.; Skjæk-Bræk, G.; Rokstad, A. M. Sulfated Alginate Microspheres Associate with Factor H and Dampen the Inflammatory Cytokine Response. *Acta Biomater.* **2016**, *42*, 180−188.

(58) Taub, D. D.; Lloyd, A. R.; Conlon, K.; Wang, J. M.; Ortaldo, J. R.; Harada, A.; Matsushima, K.; Kelvin, D. J.; Oppenheim, J. J. Recombinant Human Interferon-Inducible Protein 10 Is a Chemo-attractant for Human Monocytes and T Lymphocytes and Promotes T Cell Adhesion to Endothelial Cells. *J. Exp. Med.* **1993**, *177*, 1809−1814.

(59) Dufour, J. H.; Dziejman, M.; Liu, M. T.; Leung, J. H.; Lane, T. E.; Luster, A. D. IFN-γ-Inducible Protein 10 (IP-10; CXCL10)-Deficient Mice Reveal a Role for IP-10 in Effector T Cell Generation and Trafficking. *J. Immunol.* **2002**, *168* (7), 3195−3204.

(60) Hart, C. E.; Bailey, M.; Curtis, D. A.; Osborn, S.; Raines, E.; Ross, R.; Forstrom, J. W. Purification of PDGF-AB and PDGF-BB from Human Platelet Extracts and Identification of All Three PDGF Dimers in Human Platelets. *Biochemistry* **1990**, *29* (1), 166−172.

(61) Rokstad, A. M.; Strand, B. L.; Espevik, T.; Mollnes, T. E. Biocompatibility and Biotolerability Assessment of Microspheres Using a Whole Blood Model. *Micro Nanosyst.* **2013**, *5* (3), 177−185.

(62) Thanh, T. T. T.; Tran, V. T. T.; Yuguchi, Y.; Bui, L. M.; Nguyen, T. T. Structure of Fucoidan from Brown Seaweed Turbinaria Ornata as Studied by Electrospray Ionization Mass Spectrometry (ESIMS) and Small Angle x-Ray Scattering (SAXS) Techniques. *Mar. Drugs* **2013**, *11* (7), 2431−2443.

Supporting Information:

Structural characterization of fucoidan from *Laminaria hyperborea*: Assessment of coagulation and inflammatory properties and their structure–function relationship

Georg Kopplin[1], Anne Mari Rokstad[2], Hugo Mélida[3], Vincent Bulone[3], Gudmund Skjåk-Bræk[1], Finn Lillelund Aachmann[1*]

[1] Norwegian Biopolymer Laboratory (NOBIPOL), Department of Biotechnology,

NTNU, 7491 Trondheim, Norway;

[2] Centre of Molecular Inflammation Research (CEMIR), Department of Clinical and Molecular Medicine,

NTNU, 7030 Trondheim, Norway;

[3] Division of Glycoscience, School of Engineering Sciences in Chemistry, Biotechnology and Health, Royal

Institute of Technology (KTH), SE-10691 Stockholm, Sweden

[*] Corresponding author. E-mail: finn.l.aachmann@ntnu.no

Supporting Information
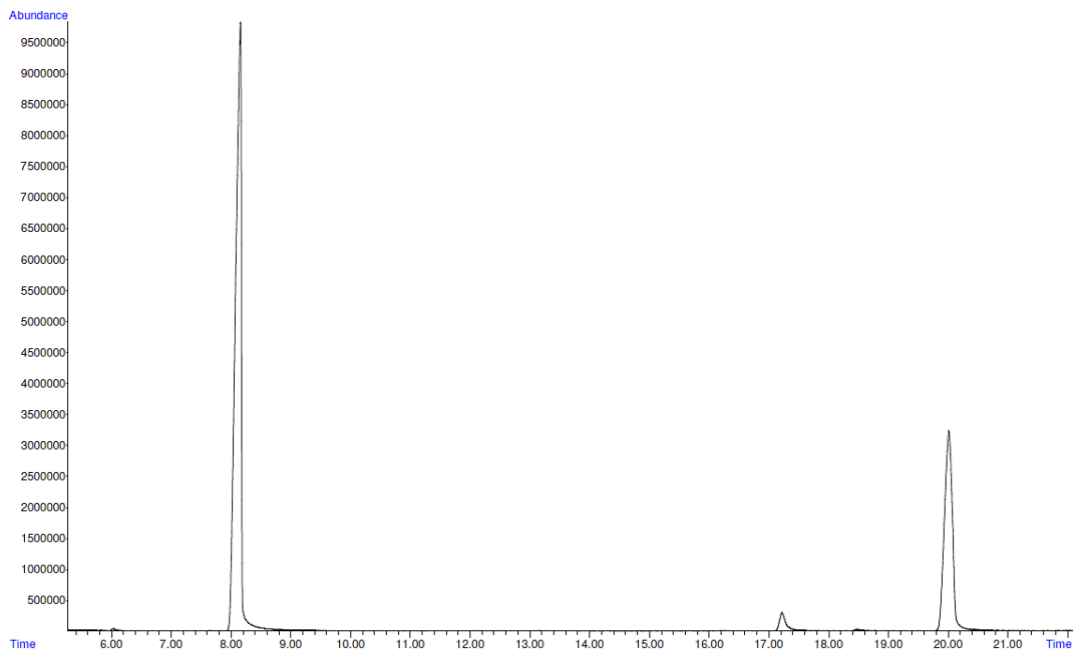
FIGURE S1: GC profile of pFuc. Fucose (8.1 min) and galactose (17.2 min) were detected. In addition, traces of glucose (18.5 min) were found. Three replicates for each of the samples were analyzed. Inositol (20.0) is used as standard.
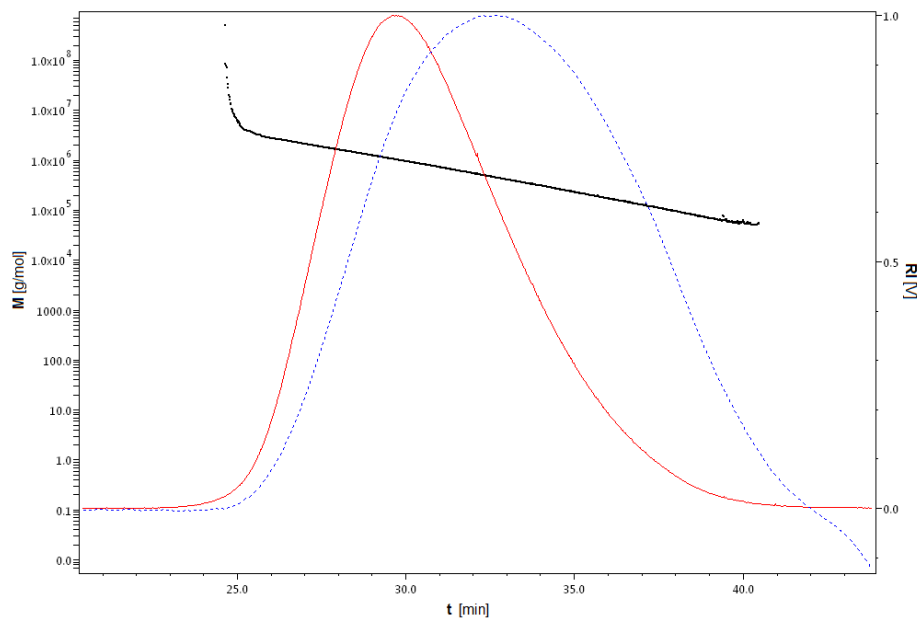
FIGURE S2: SEC-MALS chromatogram of pFuc. Light scattering (red), refractive index (blue), molar mass (black).
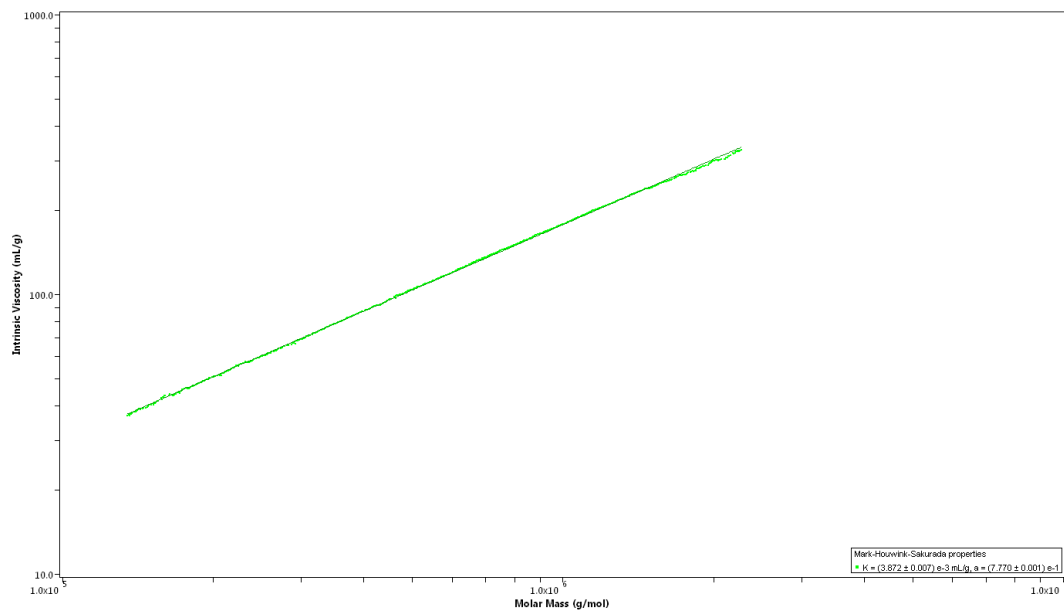
FIGURE S3: Mark-Houwink-Sakurada plot ([η] versus M) of purified Fucoidan from *L. hyperborea.*
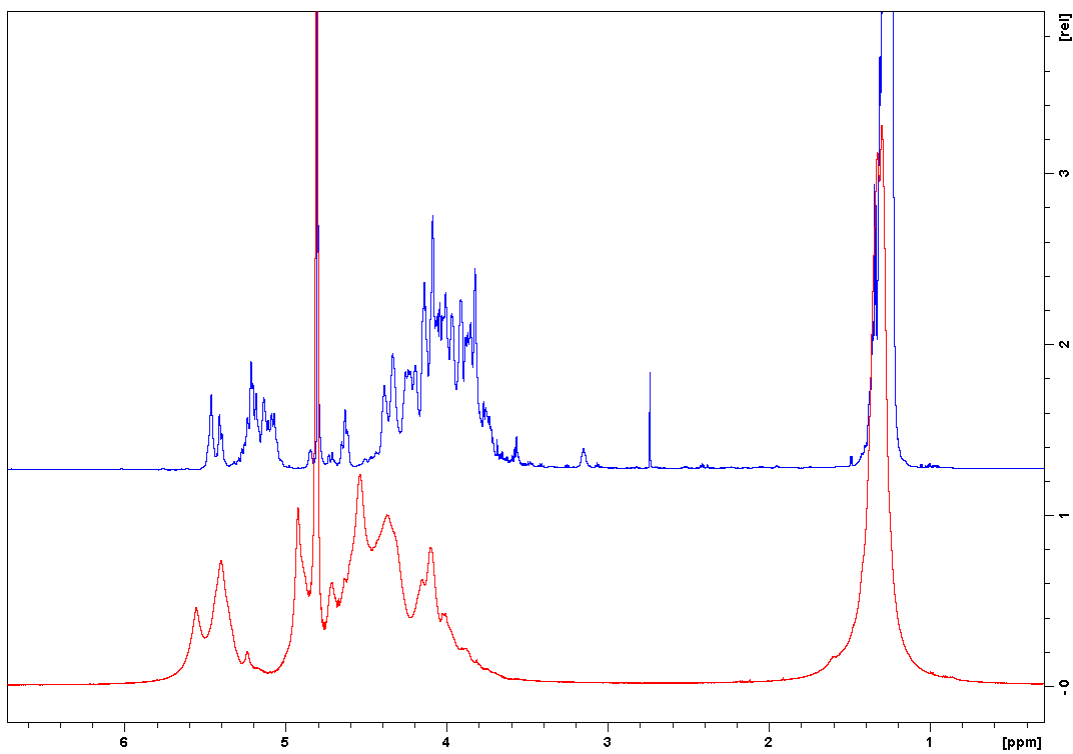
FIGURE S4: ^{1}H NMR of purified fucoidan (red) and desulfated fucoidan (blue) at 600 MHz, 298 K and in D_2O.

Table S1: ^{1}H NMR Signal intensities of purified fucoidan

Shift [ppm]	Identification	Intensity
5.1 – 5.8	H1	1.000
3.6 – 5.1	H2-H5	4.1864
1.0 – 1.8	-CH_3	3.1224
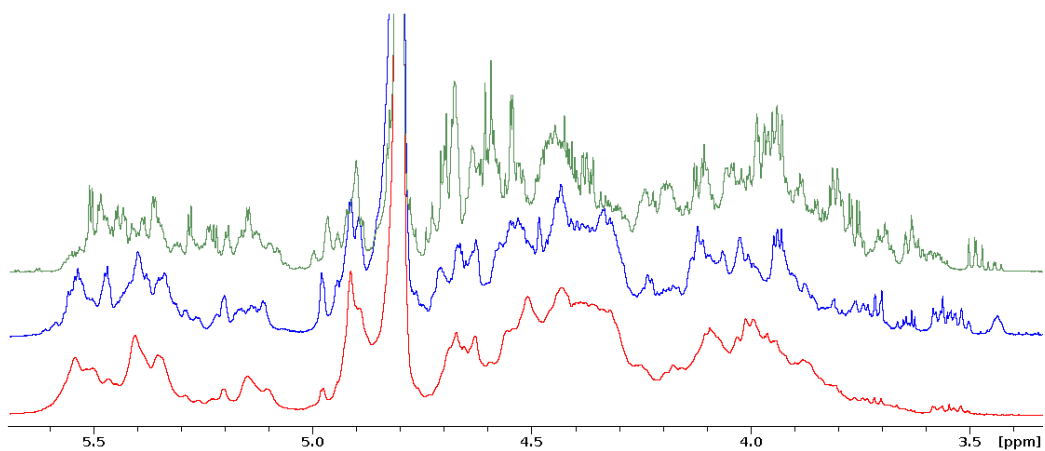
FIGURE S5: ^{1}H NMR of purified fucoidan degraded at pH 3.5 and 50°C for 5 (red) 10 (blue) and 60 (green) min. 600 MHz, 298 K and in D_2O. Complexity increases with lower molecular size.
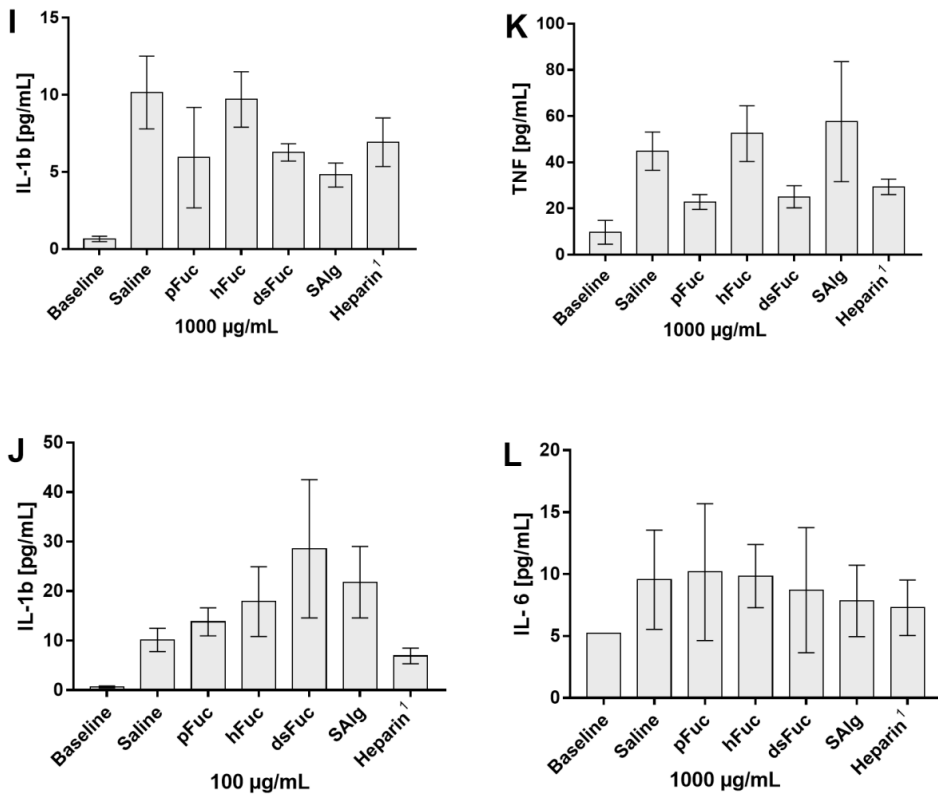
FIGURE S6: Plasma concentrations (pg/mL) of the cytokines IL-1b [I,J], TNF [K] and IL-6 [L] following an incubation of the sample with polystyrene backround and saline solution as control, under continuous rotation, for 4 h at 37°C using a using a lepirudin based human whole blood model. Significant values are given as $p \leq 0.05$ (*), ≤ 0.01 (**), ≤ 0.001 (***), ≤ 0.0001 (****) compared to the saline value and internal comparison. Data are expressed as the mean value of 6 donors ± SEM.
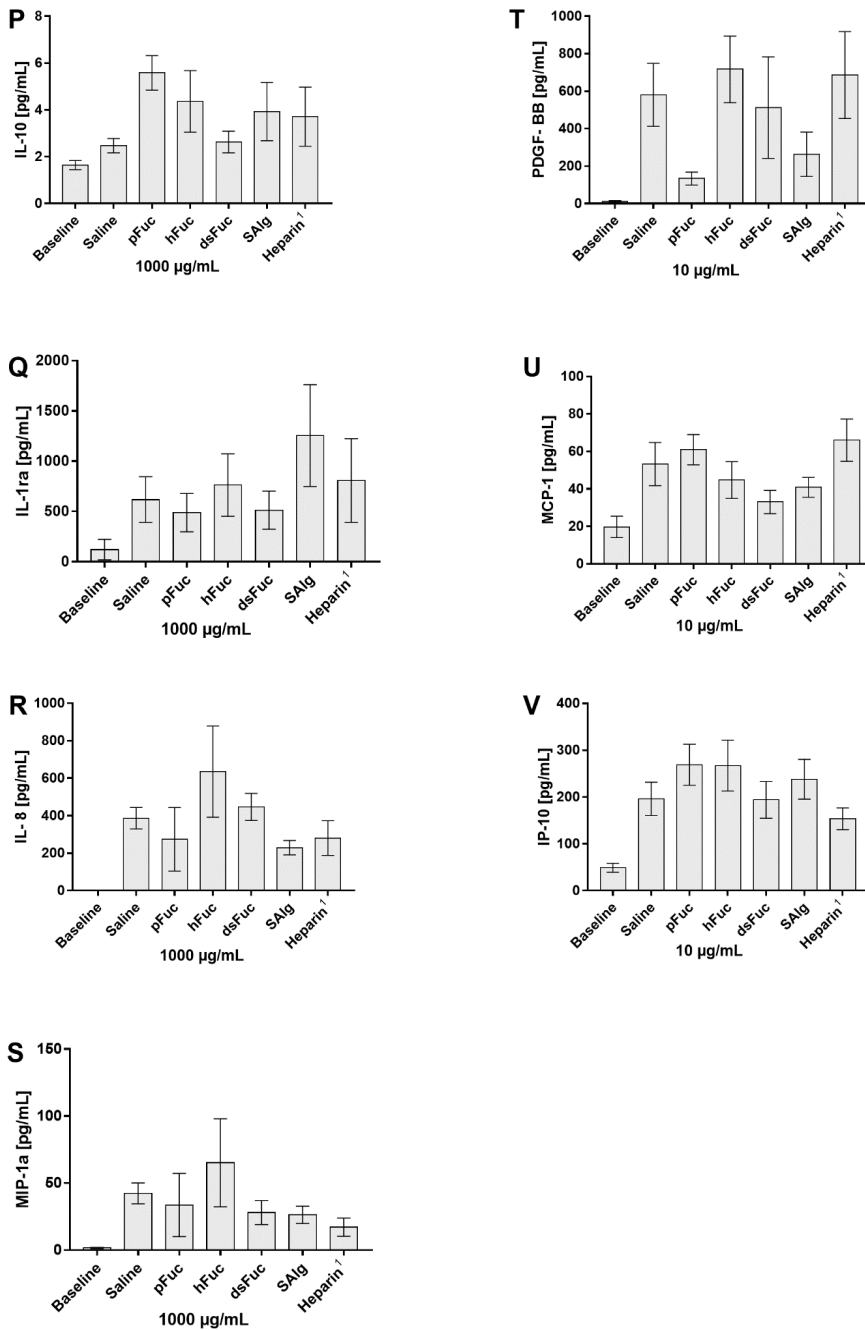
FIGURE S7: Plasma concentrations (pg/mL) of the cytokines IL-10 [P], IL-1ra [Q], IL-8 [R], MIP-1a [S], PDGF-BB [T], MCP-1 [U] and IP-10 [V] following an incubation of the sample with polystyrene backround and saline solution as control, under continuous rotation, for 4 h at 37°C using a using a lepirudin based human whole blood model. Significant values are given as $p \leq 0.05$ (*), ≤ 0.01 (**), ≤ 0.001 (***), ≤ 0.0001 (****) compared to the saline value and internal comparison. Data are expressed as the mean value of 6 donors ± SEM.

Paper 3

Effects of Sulfated Fucans from *Laminaria hyperborea* Regarding VEGF Secretion, Cell Viability, and Oxidative Stress and Correlation with Molecular Weight

Philipp Dörschmann [1,*], Georg Kopplin [2,3] , Johann Roider [1] and Alexa Klettner [1]

[1] Department of Ophthalmology, University Medical Center, University of Kiel, Arnold-Heller-Str. 3, Haus 25, 24105 Kiel, Germany; Johann.Roider@uksh.de (J.R.); Alexa.Klettner@uksh.de (A.K.)

[2] Alginor ASA, Haraldsgata 162, 5525 Haugesund, Norway; Georg@alginor.no

[3] Norwegian Biopolymer Laboratory (NOBIPOL), Department of Biotechnology and Food Science, NTNU, 7491 Trondheim, Norway; Georg.Kopplin@ntnu.no

[*] Correspondence: philipp.doerschmann@uksh.de; Tel.: +49-431-500-13712

check for updates

Abstract: Background: Sulfated fucans show interesting effects in the treatment of ocular diseases (e.g., age-related macular degeneration), depending on their chemical structure. Here, we compared three purified sulfated fucans from *Laminaria hyperborea* (LH) regarding cell viability, oxidative stress protection, and vascular endothelial growth factor (VEGF) secretion in ocular cells. Methods: High-molecular-weight sulfated fucan (M_w = 1548.6 kDa, Fuc1) was extracted with warm water and purified through ultrafiltration. Lower-molecular-weight samples (M_w = 499 kDa, Fuc2; 26.9 kDa, Fuc3) were obtained by mild acid hydrolysis of ultrapurified sulfated fucan and analyzed (SEC-MALS (Size-exclusion chromatography-Multi-Angle Light Scattering), ICP-MS, and GC). Concentrations between 1 and 100 μg/mL were tested. Cell viability was measured after 24 h (uveal melanoma cell line (OMM-1), retinal pigment epithelium (RPE) cell line ARPE-19, primary RPE cells) via MTT/MTS (3-(4,5-dimethylthiazol-2-yl)-2,5-diphenyltetrazolium bromide/3-(4,5-Dimethylthiazol-2-yl)-5-(3-carboxymethoxyphenyl)-2-(4-sulfophenyl)-2H-tetrazolium) assay. Oxidative stress protection was determined after 24 h (OMM-1, ARPE-19). VEGF secretion was analyzed via ELISA after three days (ARPE-19, RPE). Results: Fuc2 and Fuc3 were antiproliferative for OMM-1, but not for ARPE. Fuc1 protected OMM-1. VEGF secretion was lowered with all fucans except Fuc3 in ARPE-19 and RPE. The results suggest a correlation between molecular weight and biological activity, with efficiency increasing with size. Conclusion: The LH sulfated fucan Fuc1 showed promising results regarding VEGF inhibition and protection, encouraging further medical research.

Keywords: fucoidan; fucan; age-related macular degeneration; VEGF; oxidative stress; *Laminaria hyperborea*; brown seaweed extracts; proliferation; retinal pigment epithelium

1. Introduction

Laminaria hyperborea (LH), commonly known as tangle or cuvie, belongs to the large brown seaweed family of the Laminariaceae (alias kelp). It mainly grows in the northeast Atlantic Ocean, especially around Scandinavia. LH, like all brown algal species, contains fucose-containing sulfated polysaccharides (FCSP), commonly known as fucoidan, as a cell wall component. FCSP predominantly based on sulfated L-fucose residues are defined as sulfated fucans [1]. FCSP are a very heterogeneous group of polysaccharides with strong variations in sugar composition, degree of branching and

sulfation, and molecular weight. Their structure depends on different aspects, like species, harvest time, place, and extraction method [2]. This heterogeneity in structures also leads to a variety of different biological activities. Sulfated fucans have been described as being able to reduce oxidative stress and inflammation, as well as being capable of interfering with vascular endothelial growth factor (VEGF) and blood lipids [3]. These properties render sulfated fucans very interesting for medical purposes, especially for the treatment of age-related macular degeneration (AMD) [4]. AMD is the main cause of blindness in the industrialized world and may cause an irreversible loss in central vision in the elderly due to the degeneration of photoreceptors within the macula lutea. This may happen in two ways: starting in the early phase with the deposition of drusen and an accumulation of lipid peroxidation products (lipofuscin), it may progress to dry AMD, where retinal pigment epithelium (RPE) degeneration is followed by a death of photoreceptors, leading to geographical atrophy of the retina as a late stage [5,6]. In wet AMD, the major growth factor of blood vessels, VEGF, is abnormally increased, leading to the growth of blood vessels under and into the retina. Followed by edema and sometimes bleeding, it leads to a disruption of the retina [5]. The pathology of AMD is based on four molecular mechanisms that increase the risk of this illness: inflammation, complement activation, oxidative burden, and disturbed VEGF generation [5,7–9]. The only therapy possibility is repeated anti-VEGF injections into the eyes of the patient [10], which slows down the pathology of wet AMD.

Because of their biological activities, FCSP are very interesting as possible new therapeutics for the treatment of AMD [3]. We showed previously that commercial sulfated fucan from *Fucus vesiculosus* reduces VEGF and the angiogenesis of RPE cells [4]. We also described the protective effects of *Saccharina latissima* (SL) sulfated fucan for ARPE-19 cells against oxidative stress insult; this fucan also lowered VEGF in ARPE-19 and RPE cells [11]. Other extracts from *Fucus serratus*, *Fucus distichus* subsp. *evanescens*, and *Laminaria digitata* also inhibited VEGF secretion in ARPE-19 cells [11]. The chemical structure and composition of sulfated fucan from LH has been previously described [12]. It was shown that the biological activity of LH sulfated fucan is dependent on the molecular weight and the degree of sulfation [12]. LH sulfated fucans with higher molecular weight and degree of sulfation were capable to reduce coagulation and had anti-inflammatory effects [12]. Stefaniak-Vidarsson et al. (2017) described the anti-proliferative effects of *Laminaria* sulfated fucans in activated human macrophages and showed that these sulfated fucans triggered tumor necrosis factor-α and interleukins 6 and 10 [13]. However, only few reports about the activity of LH sulfated fucans can be found in the literature. Because of the described connected effects to molecular weight and to the high degree of sulfation, as well as the different species-dependent structures and activities, we tested LH sulfated fucans additionally to the other mentioned species to find the best sulfated fucans for further AMD-relevant research.

With this study we wanted to investigate whether these LH sulfated fucans display toxic effects and whether they are capable of interfering with VEGF secretion and the oxidative burden in ocular cells, with a view to making an important step further to new AMD treatment possibilities. For this purpose, three pure sulfated fucans from LH were tested; these fucans differed only in their molecular weight and were harvested at the same time, at the same place, with the same extraction method to achieve high comparability.

2. Results

2.1. Structural Characterization of the Sulfated Fucans

Monosaccharide anion-exchange chromatography of Fuc1 revealed a sugar composition of 97.0% ± 0.1% fucose (retention time 3.134 min) and 3.0% ± 0.1% galactose (retention time 7.910 min). Neither uronic acid residues nor glucose were detected.

Mass spectrometry of Fuc1 revealed a sulfite content (-SO$_3$) of 29.44%, which converts into a sulfation degree (DS) of approximately 1.7 sulfate groups per sugar residue (Table 1). Both (sugar composition and DS) are in full agreement with the previously elucidated molecular structure [12]. An overlay of the Raman spectra from samples Fuc1, Fuc2, and Fuc3 showed no change in the relative

intensities of the sulfate group vibrations (822.5 cm^{-1}, 839.8 cm^{-1}, 1065.3 cm^{-1}, 1262.4 cm^{-1}) and methyl group vibrations (1340.9 cm^{-1}, 1452.5 cm^{-1}), indicating an equal ratio between the two groups and thereby showing that no desulfation occurred during the mild acid hydrolysis.

SEC-MALS (Size-exclusion chromatography-Multi-Angle Light Scattering) analysis of Fuc1 revealed a very high molecular weight average of M_w = 1548 (± 4.1) kDa [14], resulting in an average degree of polymerization (DP$_n$) of 3512, with an approximated average monosaccharide unit weight of 290 g/mol [12]. The molar mass was broadly distributed between 300 kDa and 7 MDa, displaying coherent results throughout different injected volumes (50 µL and 100 µL, c = 1 g/L, see Figure 1). The radius of gyration as the Z-average (R_z) was found to be 83.0 nm. The overall shape of the molecule was determined through an rms conformation plot (rms radius [nm] versus M [g/mol], see Figure 2), displaying a slope (b) of 0.66 and thus indicating an overall random coil shape of the molecule (sphere b = 0.3; random coil b = 0.5; rigid rod b = 1) [15]. Considering the previously reported high degree of branching of the molecule, while having obtained the same sugar composition and degree of sulfation as shown in Kopplin et al. (2018) [12], the obtained shape of a random coil for an LH sulfated fucan molecule 3 times bigger supports the previously suggested overall structure of a large, highly flexible main chain with short side chains. Fuc2 and Fuc3 showed almost identical structural features, only differing in their degree of polymerization.
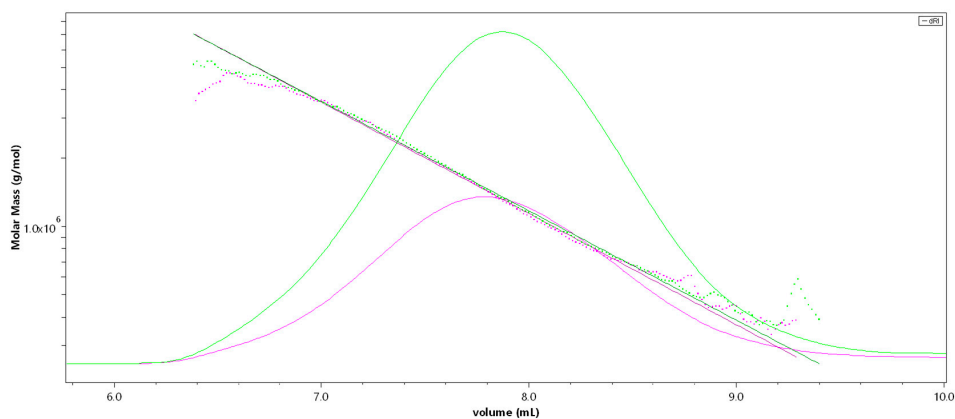
Figure 1. SEC-MALS (Size-exclusion chromatography-Multi-Angle Light Scattering) chromatogram of the high-molecular-weight sulfated fucan (Fuc1) giving M [g/mol] versus V [mL]; 50 µL injection (pink), 100 µL injection (green). The molar mass is plotted as a dotted line, the refractive index is displayed as an overlay.

Table 1. Data overview of the sulfated fucan samples used in this study. Degree of sulfation (DS), weight average molar mass (M_w), number average molar mass (M_n), degree of polymerization (DP), Z-average radius of gyration (R_z), refractive index increment (dn/dc), and slope of the RMS conformation plot (b = rms versus M).

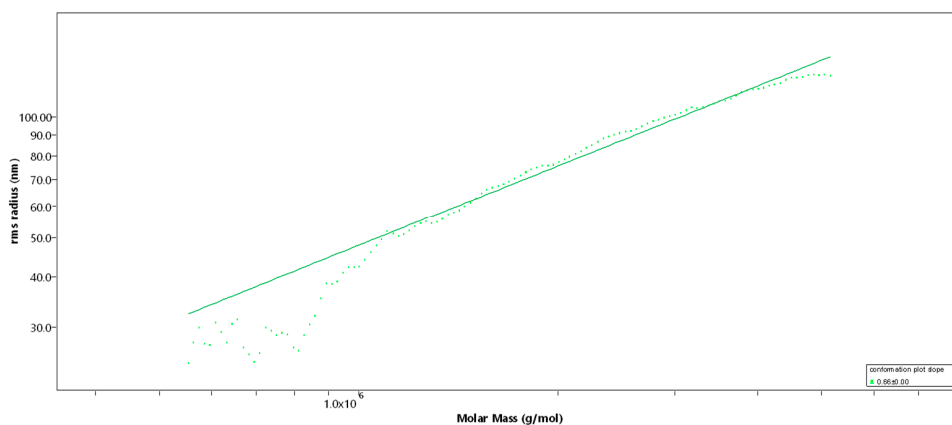|	DS	M_w [kDa]	M_n [kDa]	DP$_n$	R_z [nm]	dn/dc	b
Fuc1	1.7	1548	1021	3512	83.0	0.115	0.66
Fuc2	1.7	499	241	829	47.1	0.115	0.66
Fuc3	1.7	26.9	13.9	48	-	0.115	-

Figure 2. Rms conformation plot of the high-molecular-weight sulfated fucan (Fuc1) giving the rms radius [nm] versus M [g/mol], 100 μL injection. The slope (b) = 0.66 indicates a random coil.

2.2. Effects on Cell Viability

The uveal melanoma cell line OMM-1 was treated with the three LH sulfated fucans for 24 h; after that, an MTS (3-(4,5-Dimethylthiazol-2-yl)-5-(3-carboxymethoxyphenyl)-2-(4-sulfophenyl)-2H-tetrazolium) assay was conducted. In all three cases a dose-dependent decrease in cell viability starting with 1 μg/mL could be seen (Figure 3), but only Fuc2 and Fuc3 showed significant effects: 50 and 100 μg/mL Fuc2 lowered cell viability to 83% ± 5% ($p < 0.01$) and 76% ± 6% ($p < 0.001$), respectively. Quantities of 10, 50, and 100 μg/mL Fuc3 reduced cell viability even further to 87% ± 6%, 76% ± 5%, and 70% ± 9%, respectively. Fuc1, the sulfated fucan with the highest molecular weight, showed no significant effects on cell viability but showed a tendency at 100 μg/mL, which is not significant because of the higher variability.
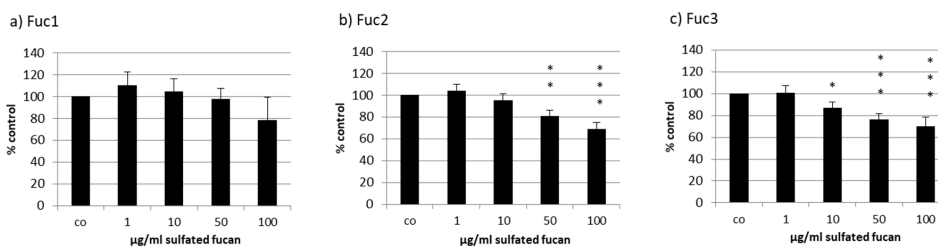
Figure 3. Cell viability was tested in uveal melanoma cell line OMM-1 after treatment with *Laminaria hyperborea* (LH) sulfated fucans Fuc1 (**a**), Fuc2 (**b**), and Fuc3 (**c**) for 24 h. Cell viability was determined via MTS (3-(4,5-Dimethylthiazol-2-yl)-5-(3-carboxymethoxyphenyl)-2-(4-sulfophenyl)-2H-tetrazolium) assay and is shown as the mean and standard deviation in relation to a 100% control. Significance was evaluated with ANOVA; * $p < 0.05$, ** $p < 0.01$, *** $p < 0.001$ compared to control ($n = 4$).

The human RPE cell line ARPE-19 was treated with the three LH sulfated fucans for 24 h and tested with a consecutive MTS assay. Only 50 μg/mL Fuc1 increased cell viability slightly (Figure 4).
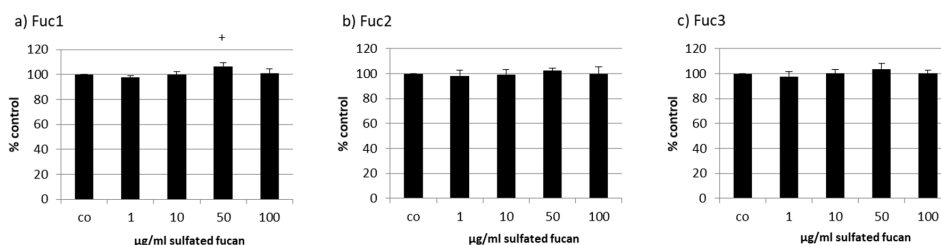
Figure 4. Cell viability was tested in retinal pigment epithelium (RPE) cell line ARPE-19 after treatment with LH sulfated fucans Fuc1 (**a**), Fuc2 (**b**), and Fuc3 (**c**) for 24 h. Cell viability was determined via MTS assay and is shown as the mean and standard deviation in relation to a 100% control. Significance was evaluated with ANOVA compared to the control (*n* = 4); [+] *p* < 0.05.

Primary porcine RPE cells were treated with the three LH sulfated fucans for 24 h and tested with an MTT (3-(4,5-dimethylthiazol-2-yl)-2,5-diphenyltetrazolium bromide) assay. The 10 µg/mL Fuc1 lowered viability slightly, but not to a biologically relevant degree (Figure 5). This paved the way for extended incubation times to measure VEGF secretion after 72 h (see below).
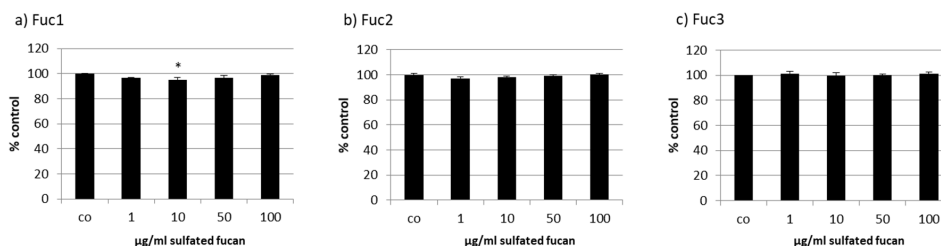
Figure 5. Cell viability was tested in RPE cells after treatment with LH sulfated fucans Fuc1 (**a**), Fuc2 (**b**), and Fuc3 (**c**) for 24 h. Cell viability was determined via MTT (3-(4,5-dimethylthiazol-2-yl)-2,5-diphenyltetrazolium bromide) assay and is shown as the mean and standard deviation in relation to an untreated control (100%). Significance was evaluated with ANOVA compared to the control (*n* = 3); * *p* < 0.05.

2.3. Oxidative Stress Protection

Oxidative stress protection by sulfated fucans from brown seaweed was already shown before for OMM-1 with *Fucus vesiculosus* sulfated fucan from Sigma-Aldrich [16] and with sulfated fucans from other seaweed, especially from SL, which was also protective for ARPE-19 [11]. So, these two cellular model systems are suitable for testing LH sulfated fucans.

Starting with the melanoma cell line OMM-1, stress induction with 1 mM H_2O_2 led to decreased cell viability of between 49% and 57% (Figure 6). The addition of 1–100 µg/mL Fuc2 showed no protection. The same outcome was achieved via treatment with Fuc3, which significantly reduced viability at 100 µg/mL (44% ± 9%, *p* < 0.05). Also, 50 µg/mL Fuc3 showed a slightly antiproliferative effect which was not significant. Only the sulfated fucan with the highest molecular weight, Fuc1, had significant protective effects at 10 µg/mL (65% ± 7%, *p* < 0.05).

RPE cells have the important role of protecting the cells of the retina against oxidative burden [7]. The RPE cell line ARPE19 was described to be rather resistant against hydrogen peroxide [17]. However, treatment with 0.5 mM *tert*-butyl hydroperoxide (TBHP) has a significant, consistent effect on the cell viability of ARPE-19 after 24 h, as previously shown [11].
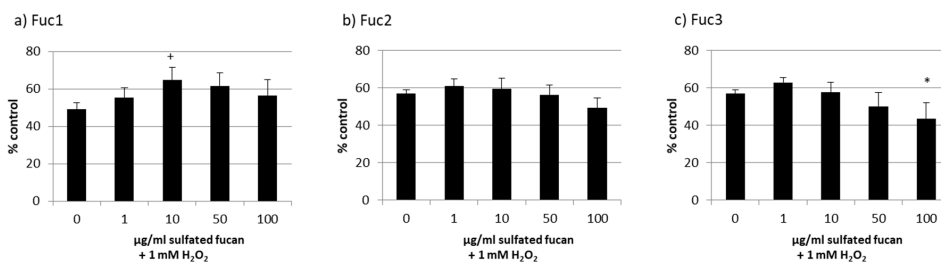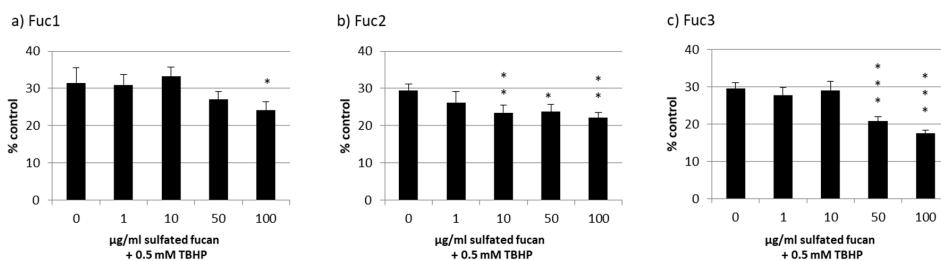
Figure 6. OMM-1 cell viability after treatment with Fuc1 (**a**), Fuc2 (**b**), and Fuc3 (**c**) and stress insult after 30 min incubation with the sulfated fucans. The oxidative agent was 1 mM H_2O_2, which reduced cell viability to under 60% in all cases. Viability was tested via MTS assay and is shown as the mean and standard deviation in relation to an untreated control (100%). The 10 µg/mL Fuc1 showed significant protective effects for the cell line. Significance was evaluated via ANOVA; */+ $p < 0.05$, versus 0 µg/mL sulfated fucan + 1 mM H_2O_2 ($n = 4$).

Cell viability was effectively lowered to nearly 30% through oxidative stress with TBHP, but all LH sulfated fucans lowered the viability additionally to a lesser extent (Figure 7); the strongest effect was from 100 µg/mL of the Fuc3 sulfated fucan, which lowered the viability even further down to 18% ± 1% ($p < 0.05$).

Figure 7. ARPE-19 cell viability after treatment with Fuc1 (**a**), Fuc2 (**b**), and Fuc3 (**c**) and stress insult after 30 min incubation with the sulfated fucans. The oxidative agent was 0.5 mM *tert*-butyl hydroperoxide (TBHP), which reduced cell viability to nearly 30% in all cases. Viability was tested via MTS assay and is shown as the mean and standard deviation in relation to an untreated control (100%). No sulfated fucan showed a significant protective effect for the RPE cell line. Significance was evaluated with ANOVA; * $p < 0.05$, ** $p < 0.01$, *** $p < 0.001$, versus 0 µg/mL sulfated fucan + 0.5 mM TBHP ($n = 4$).

2.4. VEGF Secretion

The effect of the three LH sulfated fucans on the secretion of VEGF was determined in the primary, porcine RPE cells and the human RPE cell line ARPE-19. ARPE-19 secreted nearly 4 times less VEGF compared to the primary RPE cells (ARPE-19: 66 pg/h and RPE: 243 pg/h). The VEGF content secreted into the supernatant of the cells was collected for ARPE-19 over 24 h and for RPE over 4 h because of the higher VEGF outcome. At this time point a medium exchange with added sulfated fucans was performed. The VEGF content [pg/mL] was normalized to the cell viability (after 72 h sulfated fucan treatment), giving the ratio of VEGF/cell viability (in arbitrary units [arb. unit]). The cell viability of both cell types with all sulfated fucans and all test concentrations was essentially unaffected (data not shown).

The secreted VEGF was lowered by all tested sulfated fucans in ARPE-19 (Figure 8). Fuc3 reduced VEGF to 0.84 ± 0.05 [arb. unit], $p < 0.001$, and Fuc2 lowered it to 0.66 ± 0.01 [arb. unit], $p < 0.001$, at 100 µg/mL. The effect of Fuc2 and Fuc3 on VEGF was concentration dependent. This did not apply

for Fuc1, the sulfated fucan with the highest molecular weight, which reduced VEGF to 0.48 ± 0.04 [arb. unit], $p < 0.01$, at 50 µg/mL and had the strongest effect of all sulfated fucans at this concentration.
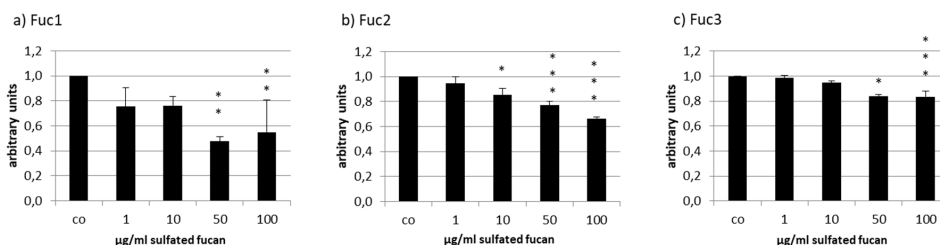

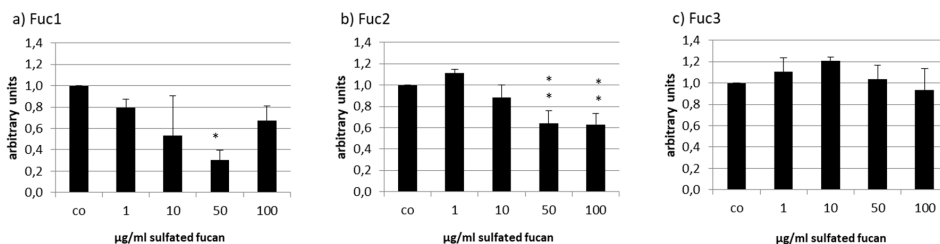**Figure 8.** Vascular endothelial growth factor (VEGF) secretion of ARPE19 cells after incubation with Fuc1 (**a**), Fuc2 (**b**), and Fuc3 (**c**). VEGF content was analyzed with ELISA and normalized to cell viability. All LH extracts reduced VEGF content with 50 µg/mL Fuc1 as the most efficient. Significance was evaluated with ANOVA; * $p < 0.05$, ** $p < 0.01$, *** $p < 0.001$ compared to the control ($n = 4$).

Due to the high amount of VEGF production in RPE cells, weaker effects could be expected, but again VEGF was reduced by Fuc2 and Fuc1 (Figure 9). Fuc3, the smallest LH sulfated fucan, seemed to increased VEGF secretion at 10 µg/mL (1.21 ± 0.04 [arb. unit]); however, this change was not significant. Fuc2 reduced VEGF at 50 µg/mL to 0.64 ± 0.12 and at 100 µg/mL to 0.63 ± 0.10 [arb. unit], $p < 0.01$, and Fuc1 reduced VEGF at 50 µg/mL to 0.30 ± 0.09 [arb. unit], $p < 0.001$. Once more, Fuc1 had the highest efficiency and, similar to what was seen in ARPE-19, again showed the strongest effect at 50 µg/mL.

Figure 9. VEGF secretion of RPE cells after incubation with Fuc1 (**a**), Fuc2 (**b**), and Fuc3 (**c**). VEGF content was analyzed via ELISA and normalized to the cell viability. Fuc2 and Fuc1 reduced the VEGF content. Significance was evaluated via ANOVA; * $p < 0.05$, ** $p < 0.01$, compared to the control ($n = 3$).

3. Discussion

The different biological effects of sulfated fucans make them very interesting for medical research, but each sulfated fucan should be exactly characterized because of the high heterogeneity concerning these biological effects. Effects that are beneficial for the treatment of AMD were already described [2]. In this study we compared three purified sulfated fucans extracted from LH by Alginor ASA. The chemical structure was previously characterized and differs among the three samples only by the molecular weight average, which makes comparison in relation to the molecular weight possible. The aim was to prescreen these extracts as to whether they are suitable for further AMD-related research. To our knowledge, LH sulfated fucans had not been tested for this purpose before. Oxidative burden and VEGF secretion are two important factors in the risk of developing AMD and were therefore the main focus of this study. Because RPE cells are the target of the pathological mechanisms, they were chosen as the cellular models. The melanoma cell line OMM-1 acted as a model for oxidative stress protection as it is more susceptible to oxidative stress than the RPE cells.

First, the LH sulfated fucans were tested for their effects on the viability of primary RPE cells and the RPE cell line ARPE-19. In both cases there were no significant effects, which is in line with earlier studies like that by Bittkau et al. 2019, which reported that sulfated fucans in general are not antiproliferative for adherent cell lines [18]. However, this is dependent on the specific fucoidan and model system. For example Banafa et al. described antiproliferative effects of *Fucus vesiculosus* sulfated fucan in human breast cancer cells [19]. It was demonstrated that it arrests the cell cycle at G_1, has pro-apoptotic properties, and enhances ROS formation [19]. Fuc2 and Fuc3 showed cell viability lowering effects in the melanoma cell line OMM-1, which could be desirable for possible use in anticancer treatments. They both have a size below 500 kDa, so the effects could be connected to the molecular weight and structure. Possibly, these sulfated fucans interfere with fibronectin, disturbing the adherence of the tumor cell line [20]. Of note, the attachment of OMM-1 to well plates is rather weak and the cells have no tight junctions, in contrast to the RPE and ARPE-19 cell lines. In addition, OMM-1 cells were treated at subconfluence and the sulfated fucans could slow down the proliferation of this cell line, whereas the RPE cells were already confluent.

Because oxidative burden is considered one of the main causes of the development of AMD [7], the capability of the sulfated fucans to lower oxidative stress induced by TBHP or H_2O_2 was investigated. In ARPE-19, no protective effects could be detected, and 100 µg/mL Fuc3 had a cumulative toxic effect (also for OMM-1), which means that the smallest LH sulfated fucan enhanced the toxic effect of TBHP and H_2O_2. The same outcome was achieved for the OMM-1 cell line, except for the biggest sulfated fucan Fuc1, which was protective. These results are in contrast to those for the sulfated fucans of *Sargassum angustifolium*, in which the antioxidant activity through the scavenging of radicals and reducing power increased with decreasing size of the sulfated fucan (size range from 421 to 64 kDa) [21]. Because Fuc2 and Fuc3, which were also in that range, had no effect at all, and due to the absence of polyphenols by virtue of the high purity, it could be assumed that Fuc1 had no scavenging effect but rather interacted with the antioxidant defense system of the OMM-1 cell line. The RPE cells have an already improved antioxidant defense system, controlled via Nrf-2 (transcription factor nuclear factor erythroid 2-like 2), because of the high accumulation of oxygen radicals in the photoreceptors [7]. We already showed before that several sulfated fucans have protective effects in the OMM-1 cell line, but rarely do they in the ARPE-19 cell line [11,16]. OMM-1 cells have decreased superoxide dismutase activity [22], which could mean that the protective effects of ARPE-19 are concealed by already existing antioxidant enzyme activity. That sulfated fucans can activate superoxide dismutase and Nrf-2 was shown previously [23–26].

A further important factor, mainly for the development of wet AMD, is the secretion of VEGF, which supports the angiogenesis of blood vessels in the eye. ARPE-19 cell lines and the primary RPE cells tested for their VEGF output after sulfated fucan treatment for three days. The secreted VEGF was normalized to the cell viability. As shown before, primary RPE cells produce significantly more VEGF compared to the cell line [11] (nearly 4 times more than ARPE-19); therefore, any significant reduction of the growth factor in primary RPE cells is even more remarkable. All three LH sulfated fucans decreased VEGF significantly at 50 and 100 µg/mL, with efficiency decreasing with smaller size in the RPE and ARPE-19 cells. This reducing effect could be due to the direct binding of VEGF, which inhibits the activation of the VEGF receptor. The negatively charged side chains of sulfated fucans can interact with the positively charged residues of the VEGF molecule, which could explain the interference in the binding between VEGF and its receptor [27]. This corresponds to findings in the literature [28,29]. It could be assumed that bigger size of the sulfated fucan is more efficient in VEGF inhibition. Also, direct interaction with the VEGF receptor (VEGF-R) [28] or the suppression of the VEGF and VEGF receptor genes could be possible, as VEGF has been shown to be involved in its own regulation [3,30–33]. Additional VEGF binding assays should be performed to determine the affinity of the fucoidan to the growth factor, which should be considered for further studies with LH sulfated fucans. Even more striking is the effect in the RPE cells, in which Fuc1 and Fuc2 also decreased VEGF despite the higher secretion. For both cell types, 50 µg/mL Fuc1 had the strongest effect. Fuc3 showed a

tendency to stimulate VEGF secretion in RPE cells; however, this was not significant and its biological relevance is therefore uncertain. Nevertheless, it is of interest, as this small sulfated fucan may interact with VEGF differently to its high-molecular-weight counterpart, possibly by binding to VEGF in a VEGF-R-activating manner [34] The DS is also an important factor for the angiogenesis influencing effect [29], but the DS for all three sulfated fucans was the same.

The monosaccharide analysis by anion-exchange chromatography revealed a polysaccharide almost exclusively composed of fucose (97.0% fucose, 3.0% galactose). In addition, the sulfite content ($-SO_3$) of 29.44% (DS = 1.7) determined by ICP-MS is in strong agreement with data from the previously elucidated LH sulfated fucan structure [12]. The obtained rms conformation plot slope (b) of 0.66 through SEC-MALS revealed a random coil shape for both Fuc1 and Fuc2, further supporting the previously suggested long backbone structure (1→3 glycosidic linkages) with short side chains at 1→2 and 1→4 branching points. Therefore, the main difference between Fuc1, Fuc2, and Fuc3 was the degree of polymerization, directly associating the effects on proliferation, oxidative stress protection, and VEGF secretion with one structural property.

It has been shown that fucoidan, due to its high degree of sulfation, is able to bind to FGF (fibroblast growth factor) receptors, similar to heparin, heparan sulfate, and sulfated alginate [35–37]. Further has it been shown that the binding and inhibition of chemo- and cytokines, such as transforming growth factor-β1 (TGF-β1), by sulfated fucans is size dependent. Even though the underlying mechanism is not yet resolved, a similar binding preference could play a role [38].

Koyanagi et al. demonstrated that highly sulfated fucans are able to bind VEGF [29].

In addition, it has been found that polymers with conjugated inhibitors have a higher inhibitory effect on tumor necrosis factor-α (TNF-α) if the inhibitors are attached to higher-molecular-weight polymers; this is due to an increased diffusion time [39]. Since the binding of VEGF to highly sulfated fucans has been proven, a similar effect of increased diffusion time could play a role.

FCSP are a diverse group of macromolecules with heterogeneous molecular structures. Still, due to its almost exclusive fucose sugar composition and the full sulfation of almost every sugar unit, LH sulfated fucan is rather homogeneous in nature, even when hydrolyzed to different molecular weight averages. Hence, it can be speculated that biological effects on cells and the metabolism are less likely caused by chemical reaction or direct receptor interactions only expressed by Fuc1 and not Fuc2 and Fuc3, but rather by physical and steric interactions such as stronger cell surface adhesion or stronger entanglement with proteins (cadherins or cytokines) due to the higher average molecular weight.

For further clarification, other FCSP with similar M_w but lower DS [14] should be included in future studies, as well as high-molecular-weight hyaluronic acids, alginates, and sulfated alginates [40,41] to better elucidate and distinguish the effects caused by molecular size, charge density, and degree of sulfation and to determine if branching points and sugar composition play an additional role. Potential FCSP–cytokine binding needs to be investigated to exclude potential masking of the determined VEGF secretion. Finally, a chromatographic fractionation of high-molecular-weight LH sulfated fucan should be applied to narrow down the molecular weight range and the polydispersity and to get access to LH sulfated fucan fractions of even higher molecular weight, potentially amplifying the previously expressed effects and directly relating them to specific molecular weight ranges.

From the results taken together, the sulfated fucan Fuc1 from LH with a molecular weight average of 1548 kDa seems to be best candidate for further research concerning AMD-relevant mechanisms. It did not lower the cell viability of primary RPE cells, and 50 µg/mL inhibited VEGF most efficiently. High molecular weight appears to be desirable for VEGF inhibition. We tested several sulfated fucans from different algal species previously; sulfated fucans from SL were also effective in oxidative stress protection in the OMM-1 and ARPE-19 cell lines, and 10 µg/mL SL sulfated fucan inhibited VEGF in ARPE-19 and RPE cells [11]. The molecular weight for this sulfated fucan was 1407 kDa (unpublished data), so it is comparable to Fuc1, which also lowered VEGF significantly at 10 µg/mL in RPE and ARPE-19. This renders SL and LH sulfated fucans as promising candidates for further AMD-related

studies. Of note, the pure LH sulfated fucan in this study can be sustainably reproduced in high amounts for further experiments in perfusion cultures or in vivo studies. Furthermore, because of its protective effect in the sensitive OMM-1 cell line, it could be considered for future studies with neuronal model systems concerning oxidative stress protection. For further research, tests concerning inflammation, lipid metabolism, and complement systems would be of additional interest.

4. Material and Methods

4.1. Cell Culture

The uveal melanoma cell line OMM-1 [42] was provided by Dr. Sarah Coupland. RPMI 1640 (Merck, Darmstadt, Germany) was used for cultivation (with 10% fetal calf serum (Linaris GmbH, Wertheim-Bettingen, Germany) and 1% penicillin/streptomycin (Merck, Darmstadt, Germany)).

The human RPE cell line ARPE-19 [43] was purchased from ATCC. The cultivation medium was HyClone DMEM (GE Healthcare, München, Germany) with 1% penicillin/streptomycin, 1.2% HEPES, 1% non-essential amino acids (all from Merck, Darmstadt, Germany), and 10% fetal calf serum, as previously described [11].

Primary porcine RPE cells were prepared as described before [30,44]. RPE cells were detached from porcine eyes by trypsin incubation and cultivated in HyClone DMEM (GE Healthcare, München, Germany) supplemented with penicillin/streptomycin (1%), HEPES (2.5%), non-essential amino acids (1%) (all Merck, Darmstadt, Germany), and 10% fetal calf serum.

ARPE-19 and RPE were treated at confluence, and OMM-1 cells were treated at subconfluence.

4.2. Sulfated Fucan

Extraction: Freshly frozen LH was thawed, blended into small particles ($\leq$ 3 mm), and kept in 90 °C H_2O for 6 h. The solution was filtered (20–25 µm particle retention) using a vacuum pump; $CaCl_2$ was added to the filtrate and it was filtrated again (5 µm particle retention). The newly obtained filtrate was purified through ultrafiltration (300 kDa MWCO) and lyophilized.

Hydrolyzation: Lower-molecular-weight samples were obtained by mild acid hydrolysis of the ultrapurified sulfated fucan at pH = 3.0, 70 °C, and 5 min for Fuc2 and 35 min for Fuc3. The hydrolysates were cooled in ice water, dialyzed again with distilled water for 3 h (12 kDa MWCO), and lyophilized.

The purified and dried LH sulfated fucans Fuc1, Fuc2, and Fuc3 were dissolved in 5 mg/mL Ampuwa bidest (Fresenius, Schweinfurt, Germany). Before testing, the extracts were filtered with 0.2 µm Sarstedt filters (Nümbrecht, Germany) and further diluted in adequate medium to the concentrations mentioned in 4.6, 4.7, 4.8 and 4.9.

4.3. Monosaccharide Analysis

The sulfated fucan samples were hydrolyzed using 3 mol/L trifluoroacetic acid (TFA) at 95 °C for 12 h. The hydrolyzed monosaccharides were fractionated and analyzed through ion-exchange chromatography equipped with a CarboPac PA20 (Thermo Fisher Scientific Inc., Waltham, MA, USA) column.

4.4. Sulfate Content

The sulfate content of the ultrapurified sulfated fucan Fuc1 was externally analyzed using an Agilent 7500 Series quadrupole ICP-MS. The sulfate content of the hydrolyzed sulfated fucans was analyzed by Raman spectroscopy as previously described [12]. Raman spectra were recorded at room temperature using a Horiba Jobin–Yvon LabRAM HR system equipped with a Raman microscope (HORIBA Ltd., Kyoto, Japan).

4.5. Molecular Weight Determination

The molecular weight of the sulfated fucan was determined by size-exclusion chromatography (SEC) in the form of HPLC equipped with online multiangle static light scattering (MALS). The measurements were performed at ambient temperature using a Shodex LB-806 and a 2500 PWXL column as a separator. The measurement was executed with a Dawn HELEOS-8+ multiangle laser light scattering photometer (Wyatt, Santa Barbara, CA, USA) (λ_0 = 660 nm) and a subsequent Optilab T-rEX differential refractometer. The mobile phase was 0.10 mol/L Na_2HPO_4 (pH = 7), and the flow rate was 0.2 mL/min. The injection volumes were 50 μL and 100 μL, with 1 g/mL. The data were obtained and processed using Astra (v. 7) software (Wyatt, Santa Barbara, CA, USA).

4.6. Oxidative Stress

To induce oxidative-stress-related cell death, OMM-1 cells were treated with 1 mM H_2O_2 and ARPE-19 cells were treated with 500 μM TBHP as previously established [11,16] to reduce cell viability to nearly 50% (tested via MTS assay, see below). Before insult with the oxidative agents, cells were incubated with 1, 10, 50, and 100 μg/mL LH extracts.

4.7. Methyl Thiazolyl Tetrazolium (MTT) Assay

The widely used MTT assay [45] was conducted as previously described [4,11] and was used after taking supernatants for the VEGF ELISA (see below) and after 24 h sulfated fucan (1–100 μg/mL) stimulation. The cells were incubated with 0.5 mg/mL MTT for 2 h and dissolved in DMSO. Measurement was taken at 550 nm with an Elx800 (BioTek Instruments Inc., Bad Friedrichshall, Germany).

4.8. MTS Assay

The CellTiter 96® AQueous One Solution Cell Proliferation Assay from Promega Corporation (Mannheim, Germany) was used to measure the cell viability after 24 h treatment with 1–100 μg/mL LH extracts and in parallel to determine any protective effects after insult with oxidative stress. The abovementioned media and supplements were used without phenol red. To each well, 20 μl MTS was added, and the plates were incubated for 1 h.

4.9. VEGF ELISA

ARPE-19 and RPE supernatants were collected after treatment with LH extracts (1, 10, 50, and 100 μg/mL) on Day 3 after stimulation [11]. Medium with sulfated fucan was exchanged 24 h (ARPE-19) or 4 h (RPE) before collecting supernatants. Human VEGF DuoSet® ELISA was used for ARPE-19, whereas the Human VEGF Quantikine® ELISA was used for RPE supernatants (both R&D Systems, Wiesbaden, Germany). ELISAs were performed according to the manufacturer's instructions. Untreated cells and medium samples were tested as controls. To set the VEGF secretion in relation to the cell viability, MTT assay was conducted after collection of the supernatants on Day 3.

4.10. Statistics

Experiments were independently repeated at least three times. Statistics were calculated in Microsoft Excel (Excel 2010, Microsoft) and GraphPad PRISM 7 (GraphPad Software, Inc. 2017). *p* values of <0.05, calculated via ANOVA, were considered significant. The diagram bars and lines represent the mean and standard deviation, respectively.

5. Conclusions

The aim of this study was to investigate the effects of three pure sulfated fucans from *Laminaria hyperborea*, which differed in their molecular size. The sulfated fucan origin and extraction method were the same, and they differed only in the molecular weight average (Fuc1 > Fuc2 > Fuc3), paving the way for comparable data. To test whether they are suitable for further testing for potential

treatment of, e.g., AMD, different tests regarding oxidative stress protection (MTS), cell viability (MTT/MTS), and VEGF interference (VEGF ELISA) in ocular cells (OMM-1, ARPE-19, and RPE) were performed. The cell viability of ARPE-19 and RPE was not influenced by up to three days of treatment; this is important for further studies because it excludes toxic effects. Fuc2 and Fuc3 lowered the cell viability of the melanoma cell line OMM-1 and should therefore be tested in further tumor cell lines as to whether this is cell line specific or in general for tumor cells, which could pave the way for anticancer studies. Fuc1, the biggest sulfated fucan, was the only one which showed protective effects against oxidative stress (in OMM-1). Fuc3 reduced VEGF secretion in ARPE19 but stimulated VEGF secretion in primary RPE cells. Conversely, Fuc2 and Fuc1 inhibited VEGF in ARPE-19 as well as in RPE, with the strongest effect seen for 50 μg/mL Fuc1. Altogether, the results showed that the biological activity of sulfated fucans is dependent on the molecular weight, and the desired effect for the treatment of ocular diseases increases with the size of the sulfated fucan.

References

1. Deniaud-Bouët, E.; Hardouin, K.; Potin, P.; Kloareg, B.; Hervé, C. A review about brown algal cell walls and fucose-containing sulfated polysaccharides: Cell wall context, biomedical properties and key research challenges. *Carbohydr. Polym.* **2017**, *175*, 395–408. [CrossRef]
2. Li, B.; Lu, F.; Wei, X.; Zhao, R. Fucoidan: Structure and bioactivity. *Molecules* **2008**, *13*, 1671–1695. [CrossRef] [PubMed]
3. Klettner, A. Fucoidan as a Potential Therapeutic for Major Blinding Diseases—A Hypothesis. *Mar. Drugs* **2016**, *14*, 31. [CrossRef] [PubMed]
4. Dithmer, M.; Fuchs, S.; Shi, Y.; Schmidt, H.; Richert, E.; Roider, J.; Klettner, A. Fucoidan reduces secretion and expression of vascular endothelial growth factor in the retinal pigment epithelium and reduces angiogenesis in vitro. *PLoS ONE* **2014**, *9*, e89150. [CrossRef] [PubMed]
5. Miller, J.W. Age-related macular degeneration revisited—piecing the puzzle: The LXIX Edward Jackson memorial lecture. *Am. J. Ophthalmol.* **2013**, *155*, 1–35.e13. [CrossRef] [PubMed]
6. Ding, X.; Patel, M.; Chan, C.-C. Molecular pathology of age-related macular degeneration. *Prog. Retin. Eye Res.* **2009**, *28*, 1–18. [CrossRef] [PubMed]
7. Klettner, A. Oxidative stress induced cellular signaling in RPE cells. *Front. Biosci.* **2012**, *4*, 392–411. [CrossRef]
8. Hageman, G.S.; Anderson, D.H.; Johnson, L.V.; Hancox, L.S.; Taiber, A.J.; Hardisty, L.I.; Hageman, J.L.; Stockman, H.A.; Borchardt, J.D.; Gehrs, K.M.; et al. A common haplotype in the complement regulatory gene factor H (HF1/CFH) predisposes individuals to age-related macular degeneration. *Proc. Natl. Acad. Sci. USA* **2005**, *102*, 7227–7232. [CrossRef] [PubMed]
9. McHarg, S.; Clark, S.J.; Day, A.J.; Bishop, P.N. Age-related macular degeneration and the role of the complement system. *Mol. Immunol.* **2015**, *67*, 43–50. [CrossRef] [PubMed]
10. Schmidt-Erfurth, U.; Chong, V.; Loewenstein, A.; Larsen, M.; Souied, E.; Schlingemann, R.; Eldem, B.; Monés, J.; Richard, G.; Bandello, F. Guidelines for the management of neovascular age-related macular degeneration by the European Society of Retina Specialists (EURETINA). *Br. J. Ophthalmol.* **2014**, *98*, 1144–1167. [CrossRef] [PubMed]
11. Dörschmann, P.; Bittkau, K.S.; Neupane, S.; Roider, J.; Alban, S.; Klettner, A. Effects of fucoidans from five different brown algae on oxidative stress and VEGF interference in ocular cells. *Mar. Drugs* **2019**, *17*, 258. [CrossRef] [PubMed]

12. Kopplin, G.; Rokstad, A.M.; Mélida, H.; Bulone, V.; Skjåk-Bræk, G.; Aachmann, F.L. Structural Characterization of Fucoidan from Laminaria hyperborea: Assessment of Coagulation and Inflammatory Properties and Their Structure–Function Relationship. *ACS Appl. Bio Mater.* **2018**, *1*, 1880–1892. [CrossRef]

13. Stefaniak–Vidarsson, M.M.; Gudjónsdóttir, M.; Marteinsdottir, G.; Sigurjonsson, O.E.; Kristbergsson, K. Evaluation of bioactivity of fucoidan from laminaria with in vitro human cell cultures (THP-1). *Funct. Foods Health Dis.* **2017**, *7*, 688. [CrossRef]

14. Fitton, J.H.; Stringer, D.N.; Karpiniec, S.S. Therapies from Fucoidan: An Update. *Mar. Drugs* **2015**, *13*, 5920–5946. [CrossRef] [PubMed]

15. Smidsrød, O.; Moe, S. *Biopolymer Chemistry*, 2nd ed.; Tapir Academic Press: Trondheim, Norway, 2008.

16. Dithmer, M.; Kirsch, A.-M.; Richert, E.; Fuchs, S.; Wang, F.; Schmidt, H.; Coupland, S.E.; Roider, J.; Klettner, A. Fucoidan Does Not Exert Anti-Tumorigenic Effects on Uveal Melanoma Cell Lines. *Mar. Drugs* **2017**, *15*, 193. [CrossRef] [PubMed]

17. Karlsson, M.; Kurz, T. Attenuation of iron-binding proteins in ARPE-19 cells reduces their resistance to oxidative stress. *Acta Ophthalmol.* **2016**, *94*, 556–564. [CrossRef] [PubMed]

18. Bittkau, K.S.; Dörschmann, P.; Blümel, M.; Tasdemir, D.; Roider, J.; Klettner, A.; Alban, S. Comparison of the Effects of Fucoidans on the Cell Viability of Tumor and Non-Tumor Cell Lines. *Mar. Drugs* **2019**, *17*, 441. [CrossRef]

19. Banafa, A.M.; Roshan, S.; Liu, Y.-Y.; Chen, H.-J.; Chen, M.-J.; Yang, G.-X.; He, G.-Y. Fucoidan induces G1 phase arrest and apoptosis through caspases-dependent pathway and ROS induction in human breast cancer MCF-7 cells. *J. Huazhong Univ. Sci. Technol.* **2013**, *33*, 717–724. [CrossRef]

20. Liu, J.M.; Bignon, J.; Haroun-Bouhedia, F.; Bittoun, P.; Vassy, J.; Fermandjian, S.; Wdzieczak-Bakala, J.; Boisson-Vidal, C. Inhibitory Effect of Fucoidan on the Adhesion of Adenocarcinoma Cells to Fibronectin. *Anticancer Res.* **2005**, *25*, 2129–2134.

21. Borazjani, N.J.; Tabarsa, M.; You, S.; Rezaei, M. Improved immunomodulatory and antioxidant properties of unrefined fucoidans from Sargassum angustifolium by hydrolysis. *J. Food Sci. Technol.* **2017**, *54*, 4016–4025. [CrossRef]

22. Blasi, M.A.; Maresca, V.; Roccella, M.; Roccella, F.; Sansolini, T.; Grammatico, P.; Balestrazzi, E.; Picardo, M. Antioxidant pattern in uveal melanocytes and melanoma cell cultures. *Investig. Ophthalmol. Vis. Sci.* **1999**, *40*, 3012–3016.

23. Foresti, R.; Bucolo, C.; Platania, C.M.B.; Drago, F.; Dubois-Randé, J.-L.; Motterlini, R. Nrf2 activators modulate oxidative stress responses and bioenergetic profiles of human retinal epithelial cells cultured in normal or high glucose conditions. *Pharmacol. Res.* **2015**, *99*, 296–307. [CrossRef] [PubMed]

24. Ryu, M.J.; Chung, H.S. Fucoidan reduces oxidative stress by regulating the gene expression of HO-1 and SOD-1 through the Nrf2/ERK signaling pathway in HaCaT cells. *Mol. Med. Rep.* **2016**, *14*, 3255–3260. [CrossRef] [PubMed]

25. Vomund, S.; Schäfer, A.; Parnham, M.J.; Brüne, B.; von Knethen, A. Nrf2, the Master Regulator of Anti-Oxidative Responses. *Int. J. Mol. Sci.* **2017**, *18*, 2772. [CrossRef] [PubMed]

26. Wang, Y.-Q.; Wei, J.-G.; Tu, M.-J.; Gu, J.-G.; Zhang, W. Fucoidan Alleviates Acetaminophen-Induced Hepatotoxicity via Oxidative Stress Inhibition and Nrf2 Translocation. *Int. J. Mol. Sci.* **2018**, *19*, 4050. [CrossRef] [PubMed]

27. Marinval, N.; Saboural, P.; Haddad, O.; Maire, M.; Bassand, K.; Geinguenaud, F.; Djaker, N.; Ben Akrout, K.; La Lamy de Chapelle, M.; Robert, R.; et al. Identification of a Pro-Angiogenic Potential and Cellular Uptake Mechanism of a LMW Highly Sulfated Fraction of Fucoidan from Ascophyllum nodosum. *Mar. Drugs* **2016**, *14*, 185. [CrossRef] [PubMed]

28. Chen, H.; Cong, Q.; Du, Z.; Liao, W.; Zhang, L.; Yao, Y.; Ding, K. Sulfated fucoidan FP08S2 inhibits lung cancer cell growth in vivo by disrupting angiogenesis via targeting VEGFR2/VEGF and blocking VEGFR2/Erk/VEGF signaling. *Cancer Lett.* **2016**, *382*, 44–52. [CrossRef] [PubMed]

29. Koyanagi, S.; Tanigawa, N.; Nakagawa, H.; Soeda, S.; Shimeno, H. Oversulfation of fucoidan enhances its anti-angiogenic and antitumor activities. *Biochem. Pharmacol.* **2003**, *65*, 173–179. [CrossRef]

30. Klettner, A.; Roider, J. Comparison of bevacizumab, ranibizumab, and pegaptanib in vitro: Efficiency and possible additional pathways. *Investig. Ophthalmol. Vis. Sci.* **2008**, *49*, 4523–4527. [CrossRef]

31. Klettner, A.; Westhues, D.; Lassen, J.; Bartsch, S.; Roider, J. Regulation of constitutive vascular endothelial growth factor secretion in retinal pigment epithelium/choroid organ cultures, P38, nuclear factor κB, and the vascular endothelial growth factor receptor-2/phosphatidylinositol 3 kinase pathway. *Mol. Vis.* **2013**, *19*, 281–291.

32. Liu, F.; Wang, J.; Chang, A.K.; Liu, B.; Yang, L.; Li, Q.; Wang, P.; Zou, X. Fucoidan extract derived from Undaria pinnatifida inhibits angiogenesis by human umbilical vein endothelial cells. *Phytomedicine* **2012**, *19*, 797–803. [CrossRef] [PubMed]

33. Narazaki, M.; Segarra, M.; Tosato, G. Sulfated polysaccharides identified as inducers of neuropilin-1 internalization and functional inhibition of VEGF165 and semaphorin3A. *Blood* **2008**, *111*, 4126–4136. [CrossRef] [PubMed]

34. Lake, A.C.; Vassy, R.; Di Benedetto, M.; Lavigne, D.; Le Visage, C.; Perret, G.Y.; Letourneur, D. Low molecular weight fucoidan increases VEGF165-induced endothelial cell migration by enhancing VEGF165 binding to VEGFR-2 and NRP1. *J. Biol. Chem.* **2006**, *281*, 37844–37852. [CrossRef] [PubMed]

35. Foxall, C.; Wei, Z.; Schaefer, M.E.; Casabonne, M.; Fugedi, P.; Peto, C.; Castellot, J.J.; Brandley, B.K. Sulfated malto-oligosaccharides bind to basic FGF, inhibit endothelial cell proliferation, and disrupt endothelial cell tube formation. *J. Cell. Physiol.* **1996**, *168*, 657–667. [CrossRef]

36. Kwak, J.-Y. Fucoidan as a marine anticancer agent in preclinical development. *Mar. Drugs* **2014**, *12*, 851–870. [CrossRef] [PubMed]

37. Arlov, Ø.; Aachmann, F.L.; Feyzi, E.; Sundan, A.; Skjåk-Bræk, G. The Impact of Chain Length and Flexibility in the Interaction between Sulfated Alginates and HGF and FGF-2. *Biomacromolecules* **2015**, *16*, 3417–3424. [CrossRef] [PubMed]

38. Kim, T.H.; Lee, E.K.; Lee, M.J.; Kim, J.H.; Yang, W.S. Fucoidan inhibits activation and receptor binding of transforming growth factor-β1. *Biochem. Biophys. Res. Commun.* **2013**, *432*, 163–168. [CrossRef] [PubMed]

39. Washburn, N.R.; Prata, J.E.; Friedrich, E.E.; Ramadan, M.H.; Elder, A.N.; Sun, L.T. Polymer-conjugated inhibitors of tumor necrosis factor-α for local control of inflammation. *Biomatter* **2013**, *3*, e25597. [CrossRef] [PubMed]

40. Rayahin, J.E.; Buhrman, J.S.; Zhang, Y.; Koh, T.J.; Gemeinhart, R.A. High and low molecular weight hyaluronic acid differentially influence macrophage activation. *ACS Biomater. Sci. Eng.* **2015**, *1*, 481–493. [CrossRef]

41. Arlov, Ø.; Skjåk-Bræk, G.; Rokstad, A.M. Sulfated alginate microspheres associate with factor H and dampen the inflammatory cytokine response. *Acta Biomater.* **2016**, *42*, 180–188. [CrossRef]

42. Luyten, G.P.; Naus, N.C.; Mooy, C.M.; Hagemeijer, A.; Kan-Mitchell, J.; van Drunen, E.; Vuzevski, V.; de Jong, P.T.; Luider, T.M. Establishment and characterization of primary and metastatic uveal melanoma cell lines. *Int. J. Cancer* **1996**, *66*, 380–387. [CrossRef]

43. Dunn, K.C.; Aotaki-Keen, A.E.; Putkey, F.R.; Hjelmeland, L.M. ARPE-19, a human retinal pigment epithelial cell line with differentiated properties. *Exp. Eye Res.* **1996**, *62*, 155–169. [CrossRef] [PubMed]

44. Wiencke, A.K.; Kiilgaard, J.F.; Nicolini, J.; Bundgaard, M.; Röpke, C.; La Cour, M. Growth of cultured porcine retinal pigment epithelial cells. *Acta Ophthalmol. Scand.* **2003**, *81*, 170–176. [CrossRef] [PubMed]

45. Riss, T.L.; Moravec, R.A.; Niles, A.L.; Duellman, S.; Benink, H.A.; Worzella, T.J.; Minor, L. Cell Viability Assays. In *Assay Guidance Manual [Internet]*; Sittampalam, G.S., Coussens, N.P., Brimacombe, K., Grossman, A., Arkin, M., Auld, D., Austin, C., Baell, J., Bejcek, B., Caaveiro, J.M.M., et al., Eds.; Eli Lilly & Company and the National Center for Advancing Translational Sciences: Indianapolis, IN, USA, 2016.

Paper 4

Check for updates

Alginate gels crosslinked with chitosan oligomers – a systematic investigation into alginate block structure and chitosan oligomer interaction†

Georg Kopplin, [ID]^a Anders Lervik,^b Kurt I. Draget^a and Finn L. Aachmann [ID] *^a

Three alginates with fundamentally different block structures, poly-M, poly-G, and poly-MG, have been investigated upon ionic crosslinking with chitosan oligosaccharides (CHOS), using circular dichroism (CD), rheology, and computer simulations, supporting the previously proposed gelling principle of poly-M forming zipper-like junction zones with chitosan (match in charge distance along the two polyelectrolytes) and revealing a unique high gel strength poly-MG chitosan gelling system. CD spectroscopy revealed an increased chiroptical activity exclusively for the poly-M chitosan gelling system, indicative of induced conformational changes and higher ordered structures. Rheological measurement revealed gel strengths (G' < 900 Pa) for poly-MG (1%) CHOS (0.3%) hydrogels, magnitudes of order greater than displayed by its poly-M analogue. Furthermore, the ionically crosslinked poly-MG chitosan hydrogel increased in gel strength upon the addition of salt (G' < 1600 at 50 mM NaCl), suggesting a stabilization of the junction zones through hydrophobic interactions and/or a phase separation. Molecular dynamics simulations have been used to further investigate these findings, comparing interaction energies, charge distances and chain alignments. These alginates are displaying high gel strengths, are known to be fully biocompatible and have revealed a broad range of tolerance to salt concentrations present in biological systems, proving high relevance for biomedical applications.

1 Introduction

Alginate is a linear polysaccharide predominantly occurring in nature in the class of brown seaweed *Phaeophyta*,[1] although various bacteria such as *Pseudomonas* and *Azotobacter vinelandii* incorporate alginate as exocellular polymeric material.[2,3] Alginates form a polysaccharide family composed of $(1 \rightarrow 4)$-linked β-D-mannuronic acid (M-unit) in $^4C_1$ conformation and its C5-epimer, α-L-guluronic acid (G-unit) in the $^1C_4$ conformation with a pK_a-value of circa 3.5. These unbranched polyanionic block copolymers are composed of homopolymeric regions of M-units (M-blocks), G-units (G-blocks), and regions of alternating epimers (MG-blocks) of various lengths.[4,5]

Chitosans form a family of linear polysaccharides consisting of $(1 \rightarrow 4)$-β-linked 2-acetamido-2-deoxy-D-glucopyranose (GlcNAc) and its de-*N*-acetylated analogue (GlcN). These polycationic derivatives of chitin can be prepared with varying degrees of acetylation (F_A) and polymerization (DP).[6] The amine-

group of the D-unit (GlcN) has a pK_a-value of circa 6.5,[7–9] and therefore their water-solubility correlates with their F_A and the surrounding pH.[10]

Oligomer fragments of these polysaccharides, referred to as CHito-OligoSaccharides (CHOS), can be prepared using chemical or enzymatic methods. CHOS have attracted increasing attention in recent years as they have been associated with numerous biological effects.[11–14] Chitosan is known for its high biocompatibility, biodegradability[15,16] and low toxicity.[17,18]

Moreover, antimicrobial effects have been shown,[19–22] which are relevant for applications such as drug delivery, wound healing and implants.[23–25] For the development of novel applications, chitosans with a tailored DP, polydispersity, F_A and acetyl distribution are providing another tool for influencing the functions, physical properties and biological effects of biomaterials.

Hydrogels are networks of cross-linked hydrophilic polymer chains able to retain large amounts of water. They are defined by specific physical properties regarding their dynamic moduli, describing elastic and viscous response to mechanical force.[26] Cross-links within hydrogels can be established through hydrogen bonds[27] and hydrophobic interactions.[28,29] Ionically crosslinked hydrogels are stronger affected by changes in pH and exhibit a higher sensitivity towards swelling than their covalently crosslinked counterparts. These different properties

^a*Norwegian Biopolymer Laboratory (NOBIPOL), Department of Biotechnology, Norwegian University of Science and Technology, 7491 Trondheim, Norway. E-mail: finn.l.aachmann@ntnu.no*

^b*Department of Chemistry, Norwegian University of Science and Technology, 7491 Trondheim, Norway*

† Electronic supplementary information (ESI) available. See DOI: 10.1039/d1ra01003d

broaden their spectrum of applications since further adjustments to their specific environment are possible.[30]

The most common ionically crosslinked alginate gels are established by the addition or release of multivalent cations (e.g. Ca^{2+}, Sr^{2+} and Ba^{2+}). Calcium–alginate hydrogels are intensively studied and exhibit a broad utilization for cell immobilization and the protection of cells from the host's immune system.[31–34] These ionically cross-linked gels can be prepared through a diffusion method or internal gelation.[4] The internal gelation method is carried out by mixing insoluble calcium carbonate into the alginate solution, followed by a controlled decrease of the pH through a slow proton-donor such as the D-glucono-δ-lactone (GDL), which results in the homogeneous release of calcium ions and a subsequent gel formation. The calcium ions show specific interactions with the G-units and create junction zones between G-blocks (egg-box formation) and partially MG-blocks.[35]

As an alternative to the formation of junction zones between the G-blocks with divalent cations, cross-linking consecutive M-units of polymannuronic acid with fully deacetylated chitosan oligomers has been previously investigated and the gelling concept, gel strength, kinetics and swelling properties have been characterized.[36,37] These junction zones are stabilized by a match in charge distance between chitosan and poly-M ($^4C_1$ conformation, diequatorial glycosidic linkage) which are both at 10.4 Å (ref. 38 and [39]) whereas the G-blocks ($^1C_4$ conformation, diaxial glycosidic linkage) exhibit a shorter charge distance of only 8.7 Å (ref. 40) and do not form (strong) gels with chitosan.

To gain further insight into this new gelling concept, we isolated fully de-N-acetylated chitosan oligomers of different DP and systematically applied these CHOS as crosslinker to highly purified and characterized poly-M, poly-G and strictly alternating poly-MG ($F_G = 0.47$, $F_{GG} = 0$) alginate.[41]

Through rheological methods detailed information about gel strength and gelling kinetics have been obtained. During this characterization, it has been discovered that while poly-G does not form gels at all, poly-MG is able to form up to 10-fold stronger gels than its poly-M analogue.

This counterintuitive phenomenon that the strongest hydrogel is formed by an alginate deviating in charge distance from its crosslinker chitosan, has been further investigated through circular dichroism in order to determine potential structures of higher order or conformational changes within the alginate molecule,[42] as well as through molecular dynamics simulations to calculate differences in interaction strengths, ionic bond lengths and alignments, ruling out different explanations for this peculiar phenomenon and refining the previously presented gelling concept.

2 Experimental

2.1 Materials

Alginates. High molecular weight mannuronan (poly-M) was isolated from a C-5 epimerase negative mutant of *Pseudomonas fluorescens* according to Holtan (2006).[43] Poly-MG was synthesized by epimerizing a poly-M alginate using AlgE4 epimerase as

previously described.[44] The enzyme processively epimerizes every second mannuronic acid residue into guluronic acid, converting the substrate almost entirely into a strictly poly-alternating MG-sequence ($F_G = 0.47$, $F_{GG} = 0$).[41] A guluronic acid enriched alginate (poly-G) was prepared by in vitro epimerization with recombinantly produced C-5 epimerase AlgE6 as previously described.[45] The intrinsic viscosity of all 3 alginates was determined using an Ubbelohde capillary viscometer (Schott-Geräte) equipped with an AVS 310 control unit and PC-operated titrator. Nine concentrations (10 to 0.5 g L^{-1}, solvent 0.1 M NaCl) were analysed at 20.0 °C with 4 repetitions each. Automatic data acquisition and calculations was used, applying a Mead–Fouss, Huggins, Billmeyer, and Herman plot.

The molecular weight average was measured by Size-Exclusion Chromatography (SEC) using an HPLC system fitted with online Multi-Angle static Light Scattering (MALS) Dawn HELEOS-II multi-angle laser light scattering photometer (Wyatt, U.S.A.) ($\lambda_0 = 663.8$ nm) followed by an Optilab T-rEX differential refractometer. The eluent was 0.15 M NaNO$_3$/0.01 M EDTA (pH = 6, I = 0.17 M) and the flow rate was 0.5 mL min^{-1}. The data were collected and processed using the Astra (v. 6.1) software (Wyatt, U.S.A.).

Chitosan oligomers. Fully de-N-acetylated chitosan ($F_A = 0.001$) was prepared by a further heterogeneous de-N-acetylation of a commercially available chitosan (Kimica, Japan). Fully de-N-acetylated chitosan oligomers were prepared by enzymatic hydrolysis of the fully de-N-acetylated chitosan using a commercial chitosanase from *Streptomyces griseus* (Sigma C9830) and a subsequent separation using size exclusion chromatography.[39]

In addition a chitosan oligomer mixture ($DP_n = 3.96$, $F_A = 0.045$) provided by Koyo Ltd Co (Japan), lot number 121017WG was used in comparison.[37] D-Glucono δ-lactone (GDL) was purchased from Sigma-Aldrich (U.S.A.). All other chemicals were of analytical grade and used without any further purification.

2.2 Gel preparation

The different alginates were dissolved in distilled water at a concentration of 3% (30 g L^{-1}). The selected chitosan oligomers were dissolved in distilled water at a concentration of 10% and the pH was adjusted to 8.0, using 1 M NaOH. 1.0 mL of 3% alginate solution was weighted into a glass vial and a maximum of 182 μL of the selected chitosan oligomer solution (equaling 0.6% final concentration, see ESI†) was added together with distilled water to obtain a total volume of 2 mL. The mixture was stirred for 10 minutes. 15.95 mg of GDL were solved in 1 mL distilled water right before adding to mixture (final alginate concentration of 1%) followed by intensive stirring for 30 s and immediate casting on the rheometer bottom plate.

2.3 Rheological measurements

Rheological measurements were performed with a Kinexus rheometer (Malvern Instruments, United Kingdom), using a 40 mm serrated plate probe and a serrated bottom plate with a 1 mm gap.

Table 1 Characterization of alginates through their monad and diad fraction, their molecular weight and number average and their intrinsic viscosity

Alginate	F_G	F_M	F_{GG}	F_{GM}	F_{MM}	M_w [kDa]	M_n [kDa]	$[\eta]$ [mL g^{-1}]
Poly-M	0.00	1.00	0.00	0.00	1.00	232	104	740
Poly-MG	0.47	0.53	0.00	0.47	0.07	158	65	534
Poly-G	0.88	0.12	0.83	0.05	0.07	225	105	727

The test methods employed were oscillatory time and stress sweep at a constant temperature of 20 °C. For the time sweep, the experiments were performed at a low oscillation frequency (1 Hz) and a shear strain (0.001) to ensure that the measuring conditions did not disrupt the gelation process. The strain sweep (0.0005 to 0.1), at a constant frequency of 1 Hz, was used to ensure the strain lays in the linear viscoelastic region (LVR) of the hydrogels. Frequency sweep experiments were performed in the linear viscoelastic region (0.01 to 10 Hz) with a constant strain of 0.001 and a delay time of 2 seconds between the measurements to characterize the viscoelastic properties as a function of frequency. Three parallels were performed for each experiment.

2.4 Circular dichroism

Circular dichroism spectra were recorded using a Chirascan™ V100 equipped with a Chirascan™ monochromator using two synthetic, single-crystal quartz prisms. All samples were

recorded in distilled water at 25 °C. A quartz cuvette with 5 mm optical pathlength was used and an array from 180 to 260 nm was scanned with a bandwidth of 1 nm, a time constant of 3 s (scan rate 20 nm min^{-1}). The stock solutions of the different alginates and chitosan oligomers were prepared short before the experiments and adjusted to pH 4.5 to ensure strong interaction between the chitosan oligomers and the alginate.[37] The final concentration of alginate was kept constant at 0.4 g L^{-1}, the chitosan oligomer concentration was systematically increased from 0.1 to 0.8 g L^{-1}.

2.5 Molecular dynamics simulations

Molecular dynamics (MD) simulations were carried out using GROMACS (version 5.1.4).[46] Initial configurations, consisting of the different types of alginates and chitosan tetramers or octamers, were created using the 3D builder tool in Maestro.[47] These initial geometries were optimized at the B3LYP-D3/6-31** level of theory using Jaguar,[48] and the different configurations we considered are detailed in Section 3.6. After the geometry optimization, the configurations were converted to GROMACS, and the OPLS-AA force field was used to model the interactions.[49] Coulombic forces were obtained using the smooth particle mesh Ewald (PME) method,[50] van der Waals interactions were truncated at 1.4 nm, and dispersion corrections were applied to the energy and pressure terms. Further, periodic boundary conditions were applied in all directions, and all bonds were constrained using the LINCS algorithm.[51] Following a geometry optimization using a steepest descent algorithm as implemented in GROMACS, the alginate-chitosan molecules
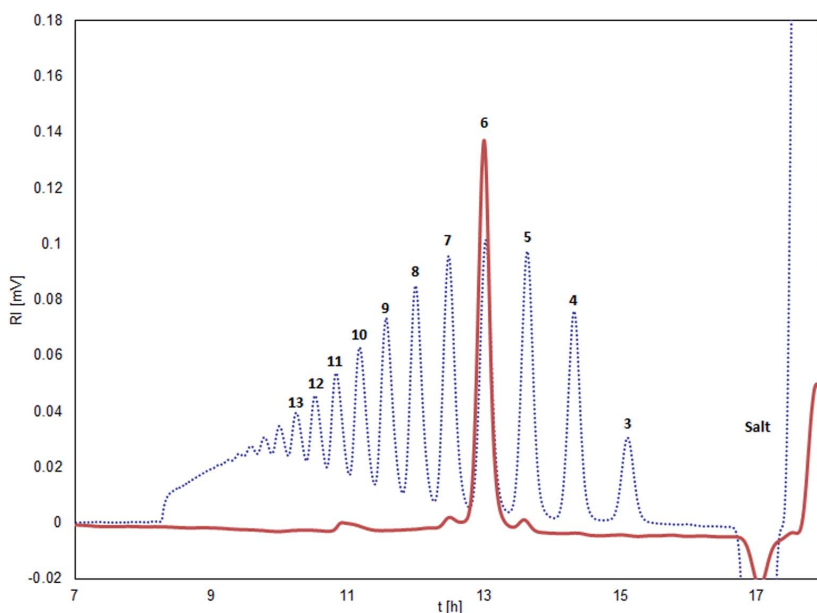

Fig. 1 Size exclusion chromatogram of chitosan ($F_A = 0.001$) degraded by chitinase from *Streptomyces griseus* (blue dotted line). Isolated chitosan hexamer (red line). The number of glucosamine units in the oligomer peak is given in bold numbers.

were solvated by adding ions (Na^+ and Cl^-) and water molecules using the TIP4P model of water,[52] in agreement with experimental concentrations and electroneutrality. To equilibrate the solvated system, a short (100 ps) MD simulation was carried out using the thermostat of Bussi et al. (2007) (with a target temperature of 300 K and a coupling parameter of 0.1 ps) and an isotropic Berendsen barostat (with a target pressure of 1 bar, coupling parameter of 2 ps and isothermal compressibility of 4.5×10^5 bar^{-1}).[53,54] Production MD simulations were then carried out in the isothermal–isobaric ensemble where the temperature was controlled using the same thermostat as detailed above, and the pressure was controlled with an isotropic Parrinello–Rahman barostat (same settings as given

above).[55] The equations of motion were integrated using a Leap–Frog integrator with a time step of 2 fs and the production simulations were carried out for 100–350 ns in which we monitored the interactions and the configurations.

3 Results

3.1 Characterization of alginates

The three different types of alginate of poly-M, poly-G and poly-MG used in this study, were selected based on their guluronic acid (G) and mannuronic acid (M) composition as well as their diad fraction F_{GG}, F_{MG} and F_{MM} (see Table 1). Monad and diad composition were determined using NMR spectroscopy
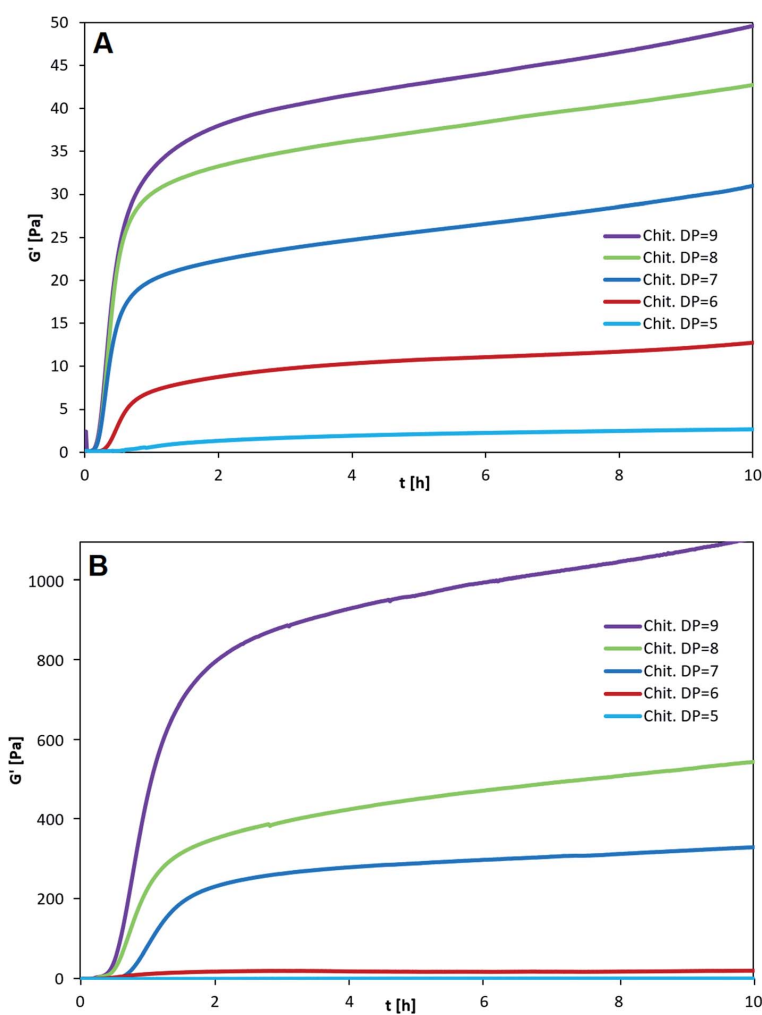
Fig. 2 Influence of NaCl concentration on the kinetics of gelation for (A) poly-M and (B) poly-MG. Alginate concentration at 10 g L^{-1} (1%), chitosan octamer concentration at 3 g L^{-1} (0.3%), GDL at 2 g L^{-1}, NaCl concentration added at 0 mM (red), 50 mM (blue), 150 mM (green), 500 mM (purple). G' was determined as a function of time. G'' and delta are not shown in the figure for reasons of clarity.

according to Grasdalen *et al.* (1981, 1983), revealing three alginates with different almost exclusively homopolymeric block-structures.[56,57] Additionally, the three samples were selected based on their molecular weight average (M_w) and intrinsic viscosity ($[\eta]$), to mitigate the influence of their molecular size on the conducted gelling experiments.[58,59]

3.2 Characterization of chitosan oligomers

The isolated chitosan oligomers through SEC-fractionation, showed a purity of ≥95% with only minor impurities from the sequentially neighboring oligomers $DP_{n\pm1}$ (see Fig. 1).

3.3 Gel strength and kinetics of gelation as function of chitosan oligomer length

The three types of homogeneous block-polymers poly-M, poly-MG and poly-G were tested against a set of purified chitosan oligosaccharides (CHOS), consecutively increasing in degree of polymerization from DP = 5 to 9 (see Fig. 2). The kinetics of gelation were followed by measuring the storage modulus (G') and the loss modulus (G'') as a function of time (t). The CHOS concentration (w/v%) was identical for each setup and the pH was monitored, resulting in a final pH of 4.35 ± 0.05 (measured after 5 h). This pH has previously been found to give the strongest CHOS-alginate gels while simultaneously showing small pH related deviations in gel strength.[37]

In agreement with previously reported data, poly-G displayed no signs of gel formation for any chitosan oligomer independent of DP and concentration.[36] Through rheological measurements of poly-G chitosan oligomer gelling systems high phase angles (δ) close to 90° were obtained, representative of a viscous solution (see ESI†). An increase in chitosan oligomer concentration to half of the poly-G concentration (or higher), lead to a precipitation of the alginate, likely caused by non-specific electrostatic interactions.

When comparing poly-M with poly-MG the mannuronic acid homopolymer showed faster gelling kinetics, reaching an apparent equilibrium after about 20–30 min for all different chitosan DPs (Fig. 2A), while the poly-MG gelling system reached the apparent equilibrium after approximately 60–90 min (Fig. 2B).

For all CHOS-poly-M gelling systems, the phase transition from predominant viscous ($G' < G''$) to predominant elastic ($G' > G''$) properties, where the phase angle drops below 45°, occurred within the first minute, which indicates a fast gelling system (G'' and δ are not depicted here). For poly-MG the phase transition occurred after about 5 minutes for DP = 6–9 and after 30 min for DP = 5.

The smallest CHOS capable of forming poly-M gelling systems is the fully de-*N*-acetylated chitosan tetramer.[37] However, poly-MG was not capable of forming a gel with chitosan at DP = 4, neither with a pure tetramer nor with a commercial chitosan oligomer mixture (DP_n = 3.96) (see ESI†). For DP = 4 the viscoelastic properties of poly-MG are mimicking the ones of poly-G, resulting in a precipitation of the alginate instead of a gel formation. CHOS at DP = 5 are the shortest fully de-*N*-acetylated chitosan oligomers capable of establishing a poly-MG hydrogel. Those poly-MG chitosan gels at DP = 5 expressing a lower G' than their poly-M counterpart. While the chitosan hexamer displays in a similar G' value in poly-M and poly-MG systems. For CHOS with a DP ≥ 7 poly-MG expresses a sharp increase in gel strength, displaying a storage modulus orders of magnitude greater than for poly-M. Furthermore, a different trend for both types of alginate can be observed. While an increase in chitosan oligomer DP leads to an increase in gel strength in both types of alginate, the relative increase between consecutive oligomers becomes smaller in poly-M systems (see Fig. 3). In poly-MG systems on the other hand, the formed gels exhibit a strong increase in the storage modulus towards DP = 9, both in absolute and relative amounts.
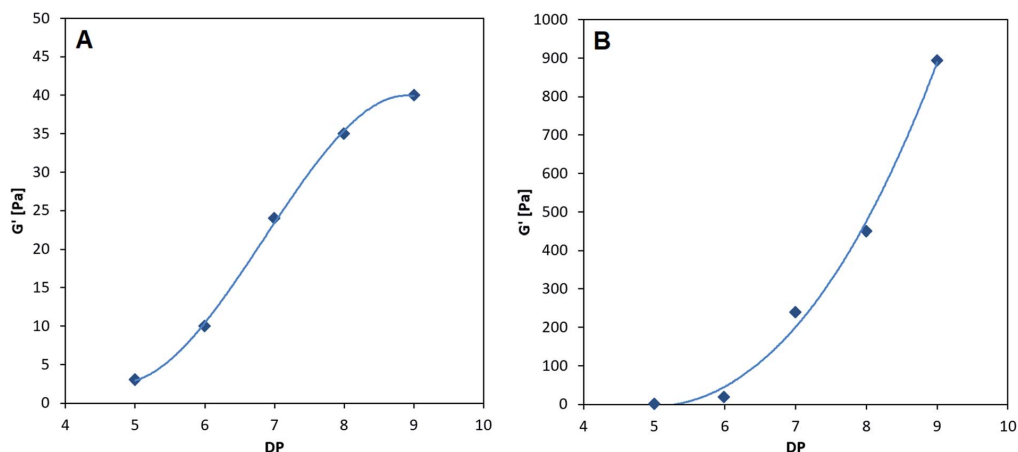

Fig. 3 Final gel strength as a function of degree of polymerization of chitosan. (A) Poly-M; (B) poly-MG. Alginate concentration at 10 g L⁻¹ (1%). Chitosan concentration at 3 g L⁻¹ (0.3%). GDL at 2 g L⁻¹. G' value determined after 5 h.

Alginate-CHOS gelling systems with chitosan oligomer DPs ≥ 10 have been prepared, but the formed hydrogels were inconsistent in texture due to a decreasing solubility at pH 8 of the higher chain length CHOS and measurements showed strong deviations.[10,36]

A frequency sweep control experiment of the poly-MG CHOS nonamer system was performed, without adding the proton donor D-glucono-δ-lactone (GDL), showing liquid like properties at pH 7.5 (phase angle close to 90°) along a broad frequency range from 0.01 to 10 Hz (see ESI†). Those findings are in agreement with previously measured poly-M and poly-G systems.[36,37] To control for temperature related effects on the gel formation potentially caused by an increased or decreased molecular mobility, both poly-M and poly-MG were gelled at 4 °C, 20 °C and 40 °C, using the CHOS octamer. After 5 h the temperature was adjusted to 20 °C where no significant difference in final gel strength between the 3 samples gelled at different temperatures could be observed (data not shown).

3.4 Gel strength and kinetics of gelation as function of salt concentration

Chitosan (DP = 8) crosslinked alginates hydrogels made from either poly-M or poly-MG were tested against a set of different salt (NaCl) concentration. The kinetics of gelation were followed by measuring the storage modulus (G') and the loss modulus (G'') as a function of time (t). Since both, alginate as well as chitosan oligomers are introduced in their salt form, the formation of each ionic bond between the carboxyl and amino
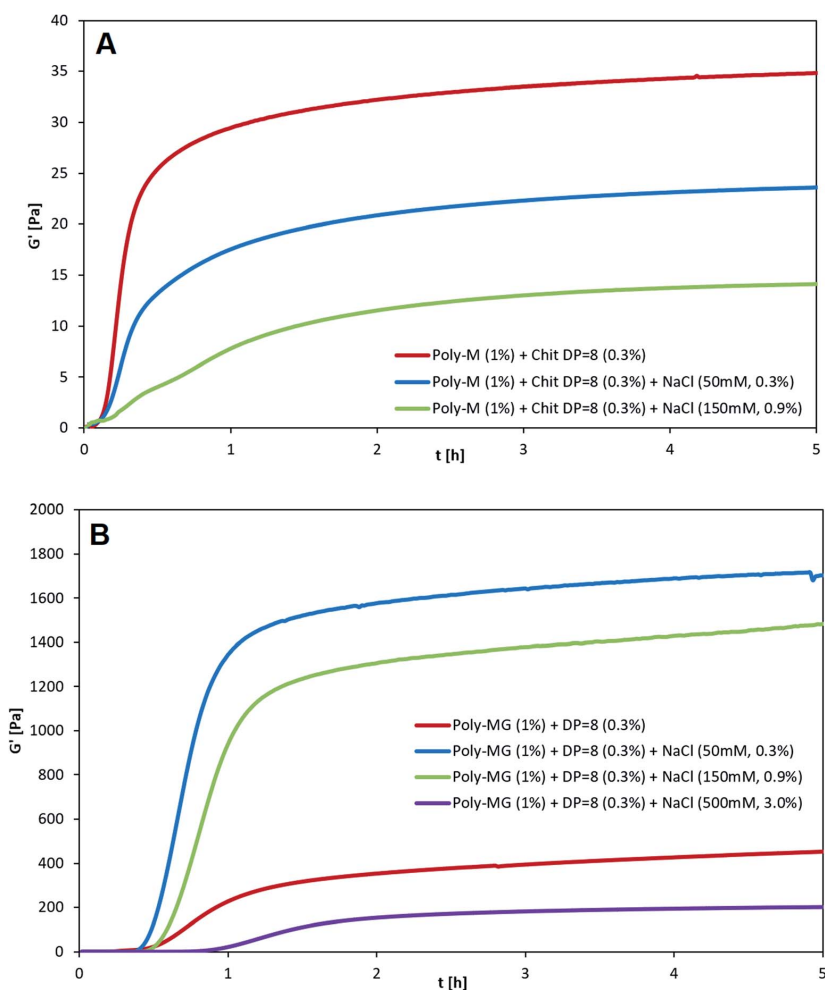
Fig. 4 Influence of NaCl concentration on the kinetics of gelation for (A) poly-M and (B) poly-MG. Alginate concentration at 10 g L^{-1} (1%), chitosan octamer concentration at 3 g L^{-1} (0.3%), GDL at 2 g L^{-1}, NaCl concentration added at 0 mM (red), 50 mM (blue), 150 mM (green), 500 mM (purple). G' was determined as a function of time. G'' and delta are not shown in the figure for reasons of clarity.
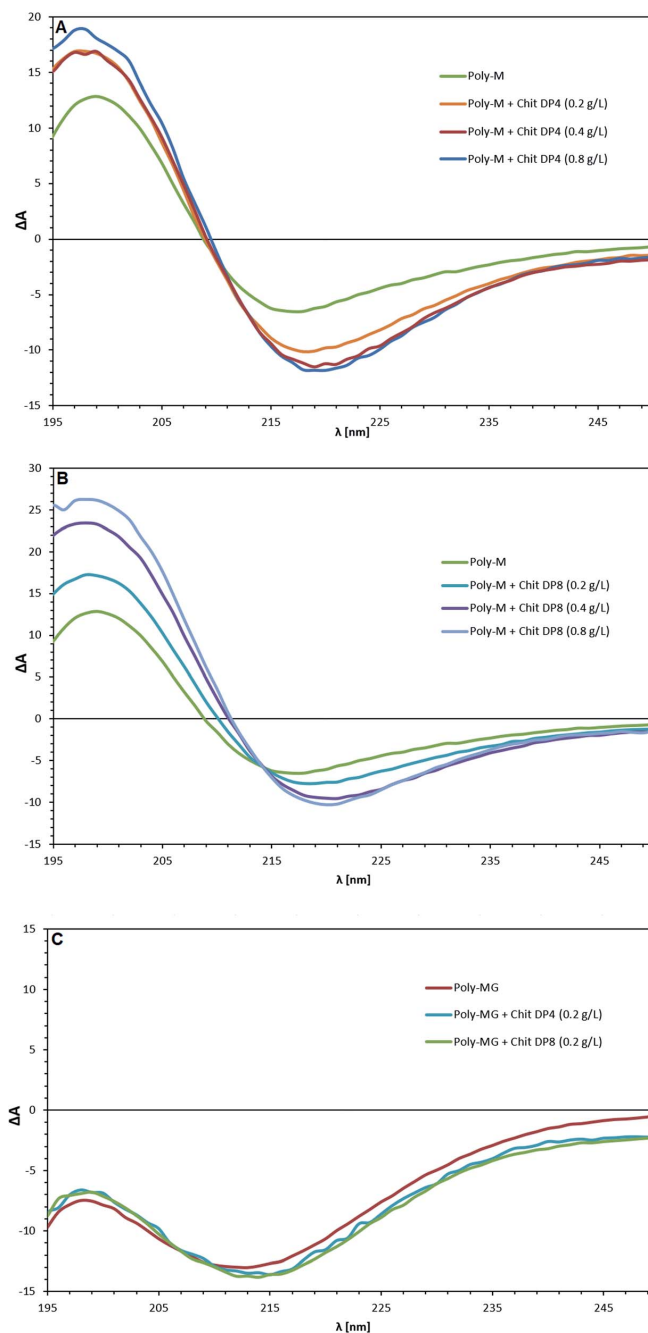
Fig. 5 Circular dichroism spectra of (A) poly-M with chitosan DP = 4; (B) poly-M with chitosan DP = 8; and (C) poly-MG with chitosan DP = 4 and DP = 8. The alginate concentration was consistently at 0.4 g L^{-1}. The chitosan concentration ranged from 0.2 to 0.8 g L^{-1}. All measurements performed at pH = 4.5 and T = 25 °C.

groups will release one NaCl equivalent. At a chitosan oligomer concentration of 3 g L^{-1} this leads to an initial NaCl concentration of maximum 15 mM.

After adding 50 mM NaCl to the chitosan poly-M gelling system, a decrease to two thirds of the original gel strength was observed (see Fig. 4). An addition of 150 mM NaCl decreased the gel strength to one third of the original gel strength. When 500 mM NaCl were added, no stable gel formation was observed any longer. Beside the decrease in gel strength, the gelling kinetics slowed down as well. The apparent equilibrium for the plain mannuronate chitosan sample occurred after 20 minutes, followed by 40 min for the 50 mM NaCl sample and 100 min for the 150 mM NaCl sample. A decrease in both gel strength and gelling kinetics is well described for alginates and other ionically crosslinked hydrogels.[60–63]

For poly-MG crosslinked with the chitosan octamer an almost opposite effect upon the addition of salt was observed. Instead of a decrease, the gel strength quadrupled when 50 mM NaCl was added to the gelling system. Upon an addition of 150 mM NaCl, the storage modulus G' was about three times higher than for the equivalent mixture without added salt. In contrast to the poly-M counterpart, the poly-MG chitosan system could form a stable gel upon the addition of 500 mM NaCl. The obtained gel strength for this high salinity mixture was reduced to about half of the original poly-MG chitosan octamer gelling system. The gelling kinetics for the poly-MG CHOS gelling systems showed to be almost not effected upon an increase in salt concentration, except for the highest salt concentration at 500 mM which displayed a decrease in gelling kinetics. The apparent equilibria occurred after 50, 60, 70 and 130 min for 0, 50, 150 and 500 mM of added NaCl, respectively.

3.5 Circular dichroism

The pure poly-M, poly-MG and poly-G alginate samples were analyzed through circular dichroism and spectral changes upon the addition of chitosan oligomers were investigated. The CD spectra of the three pure types of alginate are in agreement with previously reported data.[64] The poly-G lies completely in the area of negative ellipticity, while poly-M shows an intense positive band between 190–210 nm, originating from n→π* transitions (with minor contributions of π→π* transitions below 200 nm).[65] The CD spectrum of alternating MG-sequences, lies in between although is not identical to an equimolar mixture of poly-M and poly-G (see ESI†).[64,66] By

addition of chitosan oligomers with a degree of polymerization of 4 to poly-M alginate (Fig. 5A), the positive band between 190–210 nm shows a strong increase while the trough at 210–240 nm is deepened, suggesting an alignment of chitosan oligomers and poly-M alginate into a higher ordered conformation.[67] An increase in chitosan tetramer concentration from 0.5 to 1.0 to 2.0 times the alginate concentration (based on monosaccharide unit concentration, see ESI†) does not increase this effect. The bands only increase for the amount that chitosan itself adds to the cumulative measurement value (see ESI†). By addition of chitosan octamer, the effect at half-concentration towards the alginate was almost identical to the effect observed when using the DP = 4 oligomer but increased further at equal concentration of chitosan and alginate. Double-concentration of DP = 8 showed an even further increase of this effect, which was higher than the cumulative contribution to the CD band by the chitosan itself. The peak maxima for all poly-M-DP = 8 setups can be found at 199 nm. The trough minima are located at 220 nm (and 217 nm for pure poly-M, respectively). A cross section for all parallels was found at 214 nm.

The CD spectrum of poly-MG displayed no change upon addition of both chitosan DP = 4 and DP = 8 at half-concentration of the alginate. Equal concentration lead to a precipitation and concealed the alginate bands. Poly-G (see ESI†) followed the same trend as poly-MG, exhibiting no CD change induced through chitosan oligomers at half-concentration. An equal concentration of chitosan and poly-MG lead to precipitation of the aggregate.

3.6 Molecular dynamics simulation

Different sets of alginate dodecamers consisting of only M-, G- or strictly alternating MG-units were simulated interacting with chitosan tetra- or octamers. The chitosan and alginate oligomers, their concentration and ratio to each other were varied, as well as the present salt concentration. Water molecules were added to the system to make the concentration of alginate equal to 0.05 M. For the salt concentration, two different cases were considered: a low concentration system where ions (Na$^+$ and Cl$^-$) were added to make the whole system electroneutral and a high concentration system where ions were added to match the experimental concentrations.

When simulating one M-oligomer, one G-oligomer, or one MG-oligomer (all with DP = 12) interacting with chitosan of DP = 4, no significant difference in molecular distance or
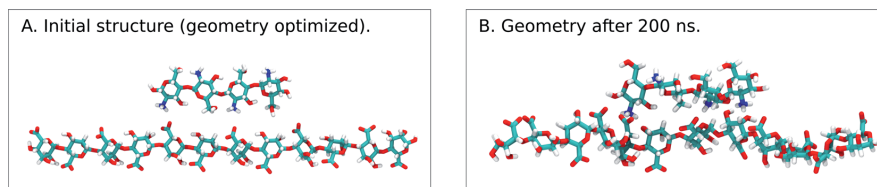

Fig. 6 Snapshots from a MD simulation of the MG-oligomer (DP = 12) and the chitosan oligomer (DP = 4) (Na$^+$ and Cl$^-$ ions are not shown). (Left) The initial geometry optimized configuration. (Right) The configuration after a MD simulation lasting 200 ns, showing some distortions compared to the initial structure.

alignment emerged. Histograms showing the interaction potential energies between the alginate and chitosan are shown in Fig. 7 and snapshots from the simulation of the MG-oligomer are shown in Fig. 6. In all these simulations, the alginate oligomer and the chitosan oligomer remain bounded.

When applying a chitosan octamer to a M-, G-, or alternating MG-dodecamer in 1 : 1 ratio, only small differences were revealed. However, within the margin of error, the interaction of chitosan with the G-oligomer appears to be slightly stronger.

The interactions between the alginate and the chitosan as well as simulation snapshots are shown in the ESI.†

The simulations of alginate and chitosan oligomers on a 2 : 1 ratio, closer to the conditions in the macroscopic gelling system, where junction zones are formed between two alginate segments ionically crosslinking through chitosan, revealed that the strongest interaction between chitosan and alginate occurred for the MG-oligomers with a high salt concentration. This was closely followed by the G-alginate (with a low salt concentration), which in macroscopic systems precipitates
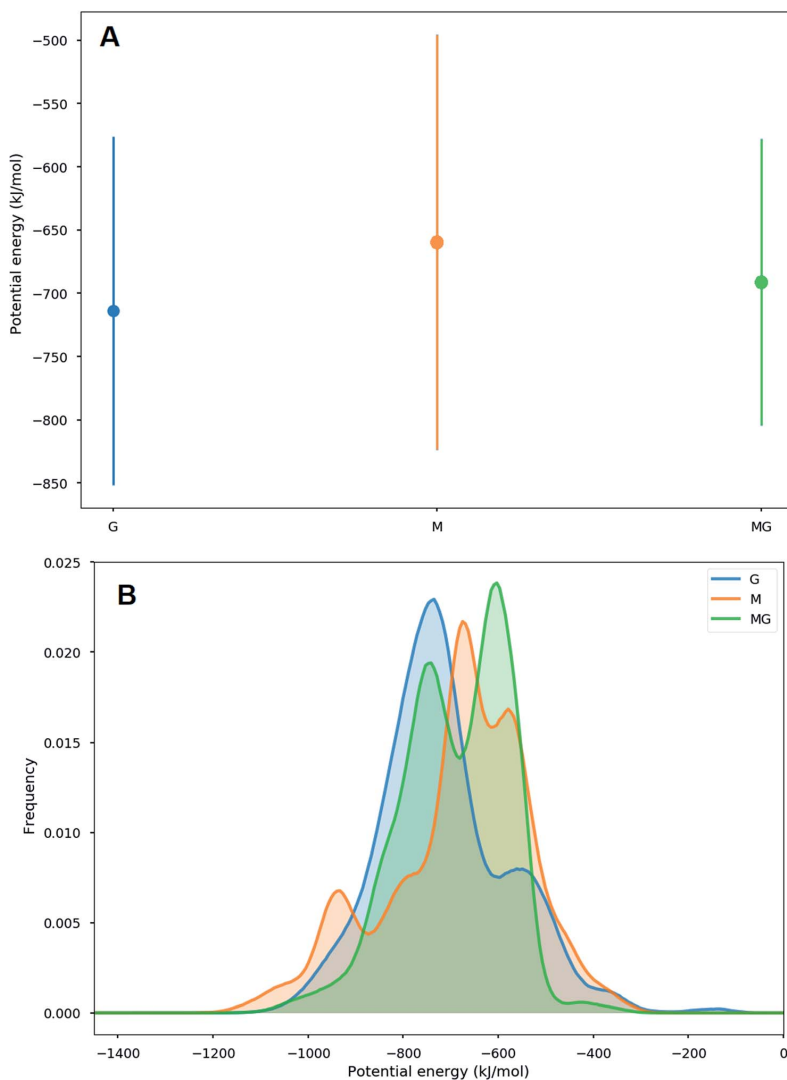
Fig. 7 Average (A) and histograms (B) of the interaction energies between alginate oligomers (DP = 12) and a chitosan oligomer (DP = 4). The average interaction energy is lowest for the G-oligomer and largest for the M oligomer, however there are significant overlaps between the distributions of the interaction energies in this case. These simulations were carried out for 200 ns for systems with a low concentration of salt. A more negative potential energy corresponds to a stronger interaction.
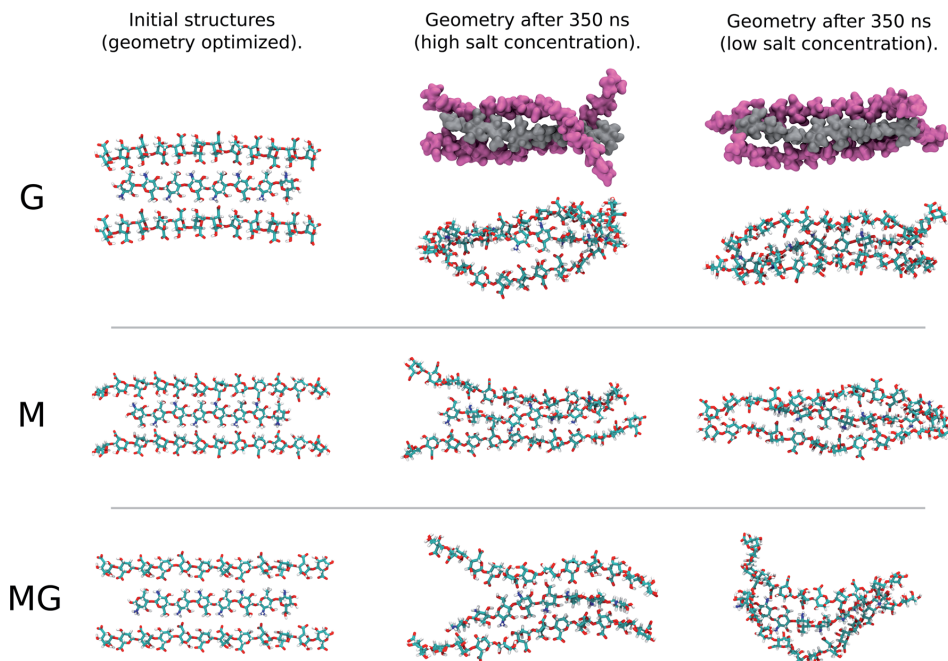
Fig. 8 Snapshots of structures from MD simulations of the 2 : 1 alginate : chitosan systems. For the G-oligomer, space filling structures are also depicted to exemplify how the alginate oligomers (color pink) can wrap around the chitosan oligomer (color gray).

upon the addition of chitosan oligomers.[36] Fig. 9 shows the interaction energies in those cases, and shows Fig. 8 snapshots of different configurations from the MD simulations. These snapshots show that the alginate oligomer can distort its structure and wrap around the chitosan oligomer in order to better align charged groups. This effect is more pronounced in low salt concentration systems and for the G-oligomer. To further compare these distortions, Fig. 10 shows the root mean squared displacement (RMSD) for the alginate–chitosan system, compared to the geometry optimized vacuum structures. This figure shows that the largest deviation from the vacuum structure occurs for the G form of the alginate, while the values are comparable for the two other forms.

Interestingly, within the scope of the simulated salt concentrations, MG-oligomers were the only ones showing an increase in interaction (lower interaction energy) with an increase in salt concentration, while M- and G-homooligomers showed a decrease. This hints towards an additional stabilization of the chitosan-MG-junction zones through hydrophobic interactions.[68,69]

Due to the distortion of the molecular structures (as shown in Fig. 8 and 10), the charge distances given in Scheme 1 may change. These charge distances were monitored in the MD simulations by calculating the 3D charge distances for every second carboxyl group or amino group along the polysaccharide chains (see Fig. 11 which show these distances for the sandwiched 2 : 1 alginate : chitosan system). An overlap in charge

distance between poly-M alginate and chitosan was previously hypothesized to establish a zipper-like junction zone between two polymer chains along the opposing sides of a chitosan oligomer (see Scheme 1 and ESI†).[36] The calculated charge distances, anticipating freely moving molecules in vacuum, were compared with previous measurements obtained from X-ray crystallography.[38–40]

The simulated oligomers showed a varying degree of good agreement for the calculated charge distances *versus* distances obtained from crystal diffraction (see Table 2). For chitosan and poly-M the measured values and calculated values are almost identical. However, we note that the values for chitosan span a small range (10.6–11.1 Å) when solvated in water. In general, the simulated structures have a larger range of possible stable conformations when solvated in water, and this is reflected in the calculated distances. In particular, the carboxyl groups at the ends of the alginate oligomers exhibit some more freedom in the simulations with water compared to the vacuum structure. For poly-G the simulation delivered a charge distance 6.9% longer than the one obtained from the crystal structures (8.7 *versus* 9.3 Å). However, it should be considered that polysaccharide crystal structures are often stabilized by intermolecular hydrogen bonds, which can lead to slight distortions of atomic bond angles and dihedral angles. Those distortions will not occur for isolated molecules in vacuum or may average out in solution.
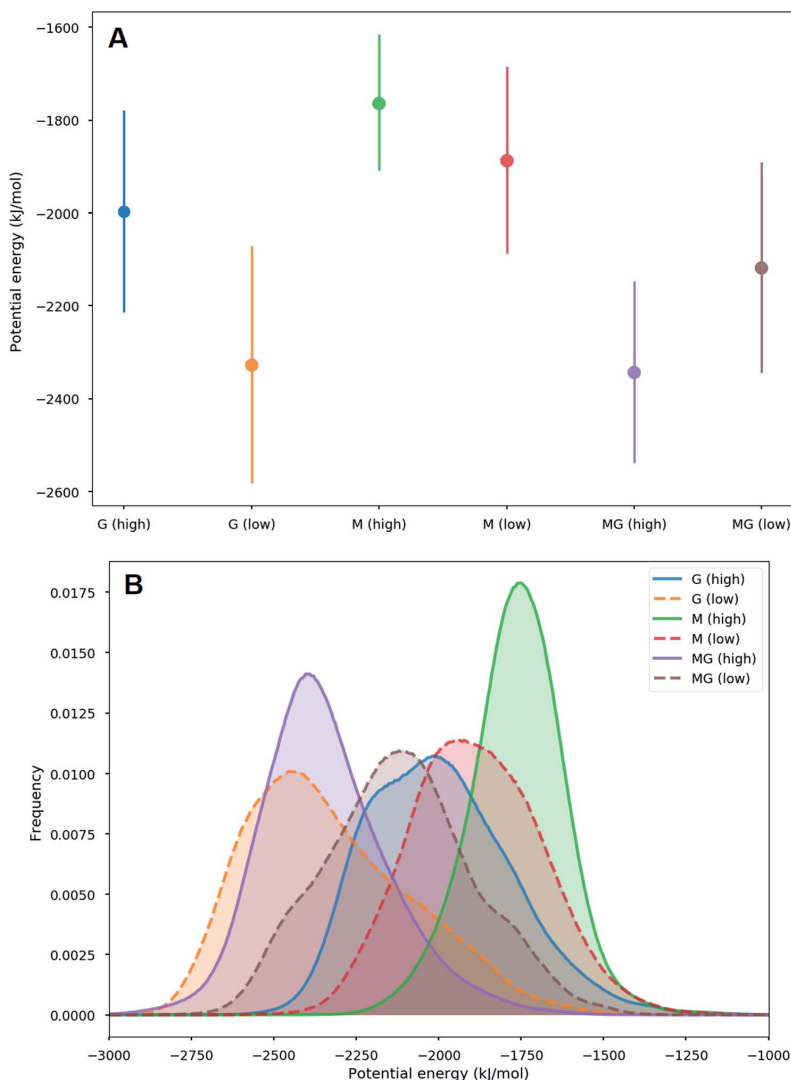
Fig. 9 Averages (A) and histograms (B) of interaction energies for the 2 : 1 alginate : chitosan systems considered, obtained in MD simulations lasting 350 ns. The average interaction energy is lowest for the MG-alginate system with a high salt concentration, while it is largest for the M-alginate system with a high salt concentration.

The calculated intramolecular charge distance for poly-MG (9.8 Å) is intermediate of the values determined for poly-M (10.6 Å) and poly-G (9.3 Å) and still relatively close to the value for chitosan (10.6–11.1 Å). This relative overlap in interval distances of poly-MG and chitosan might explain why longer chitosan oligomers are able to form stable hydrogel scaffolds, like poly-M, while CHOS applied to poly-guluronate just leads to a precipitation. Interestingly, we see that the strongest interactions are not obtained for systems where the calculated charge distances in alginate and chitosan are "best" matched. This can be explained by the observed distortions in the

structures (see Fig. 8) which may lead to alignment of charged groups.

To further characterize the chitosan alginate junction zone, the number of contacts between carboxyl and amino groups for various compositions of chitosan and alginate oligomers has been determined. Hereby, contact refers to a distance criterion of ≤ 3 Å in between any NH_3^+ with any COO^- group. For the chitosan octamer interacting with a single dodecamer of each type of alginate (see Fig. 12), the average number of contacts for the M-, and G-alginate was slightly above 4, while being slightly below 4 for the MG-alginate. The average number of contacts
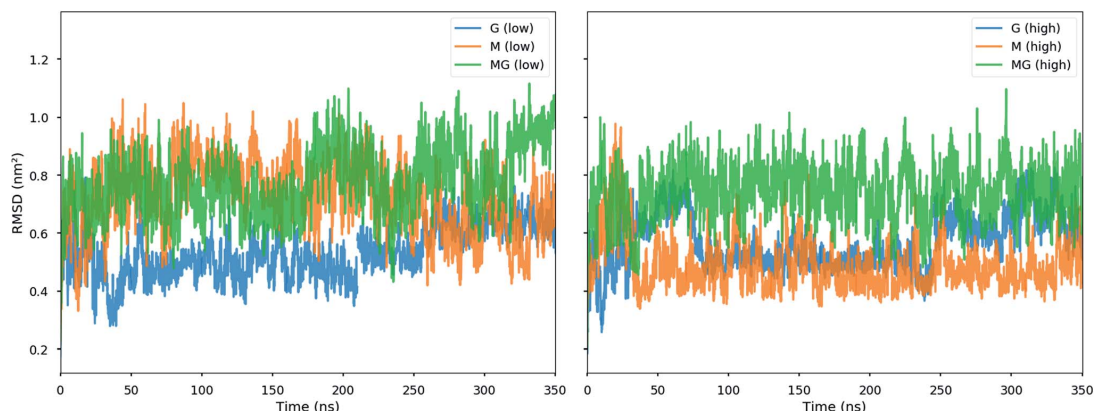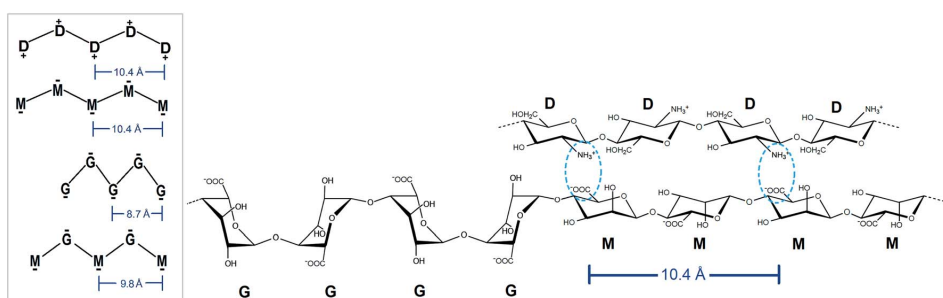
Fig. 10 Root mean square deviation (RMSD) from MD simulations of the 2 : 1 alginate : chitosan systems. The RMSD is calculated with respect to the original geometry optimized structures in vacuum and shown for the low salt concentration (left) and the high salt concentration (right).

Scheme 1 Schematic illustration of the intramolecular charge distances along each side of the used poly- and oligosaccharide chains. Ionic interactions of potentially aligned charged de-N-acetylated chitosan and a charged alginate M-block indicated (light blue), allowing for a zipper-like chain alignment. Monosaccharide units: glucosamine (D), mannuronate (M), guluronate (G).

was reduced at high salt concentration for all three types of alginate.

The calculation of contact points for alginate and chitosan oligomers on a 2 : 1 ratio revealed an average slightly below 8 (see Fig. 13), for G- and MG-segments ionically crosslinked with the chitosan octamer (low salt concentration), while showing an average of 7 contacts for the M-alginate complex. When the salt concentration was increased, the number of contacts decreased for M- and G-alginate, while it increased for the MG-segments to an average above 8. A further noteworthy observation, M-alginate showed a maximum of 8 contacts chelating the chitosan octamer, while G- and especially MG-alginate showed a major distribution towards 9 and 10 contact points. A calculation on the type of interactions, comparing the force field contributions for charge-based interactions (Coulomb) with hydrophobic interactions (Lennard-Jones), revealed that the interaction between the chitosan and alginate is dominated by coulombic interactions in all cases (see ESI†).

4 Discussion

Poly-MG alginate gel crosslinked with chitosan oligomers showed the ability to form hydrogels which are orders of magnitude stronger than their poly-M counterparts. Further, an increase in chitosan oligomer DP led to a higher relative increase in gel strength for poly-MG compared to poly-M, suggesting a different underlaying crosslinking mechanism for the two different types of alginate block structures.

To investigate the association and binding of chitosan oligomers to the different alginate block structures, a set of circular dichroism experiments was performed, comparing the three alginate types upon the addition of CHOS at various DPs and concentrations.

Circular dichroism has been used in the past as a sensitive and reliable method to investigate the diadic composition of alginates, as well as characterizing the interaction of calcium ions with the three different types of block structure.[42,64] It was previously demonstrated that the chiroptical properties of carboxyl chromophores, including guluronic and mannuronic
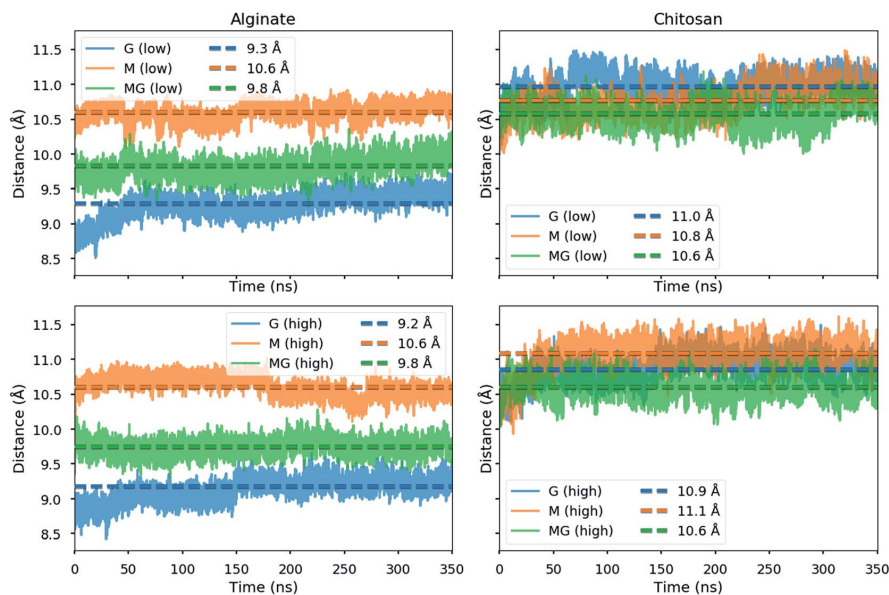
Fig. 11 Intramolecular distances between alternating carboxyl groups (left) or amino groups (right) in alginate and chitosan oligomers from the MD simulations of the sandwiched 2 : 1 alginate : chitosan systems.

Table 2 Polymer charge distance for every second carboxyl or amino group along the polysaccharide chain. Comparison of previously determined charge distances through crystal structure analysis *versus* calculated distances for the MD simulations.[38–40]

Polymer	Crystal (Å)	MD simulations in water (Å)
Chitosan	10.4	10.6–11.1
Poly-M	10.4	10.6
Poly-MG	—	9.8
Poly-G	8.7	9.2–9.3

acid, strongly depend on the local ring geometry, $^4C_1$ *versus* $^1C_4$ conformation and neighbouring units.[65,66]

Alginate exhibits strong CD bands between 190–230 nm, originating from n → π* transitions of the carboxylic acid group (with some contributions from π → π* transitions below 200 nm).[65,70]

The chain–chain association expressed when G-sequences are ionically connecting through calcium in a chelate type binding, have been previously described using circular dichroism. The interpretation of CD spectral intensity changes as a consequence of G-block dimerization through calcium ("egg-box" formation) are widely accepted.[67] Morris *et al.* (1975) demonstrated a linear change in band intensity when the concentration of calcium ions was increased at constant poly-guluronate concentration, whereas no change was observed when applied for poly-mannuronate. This clearly indicated a conformational effect on the poly-G chain (secondary structure) induced by Ca^{2+}. No similar effect was observed for the poly-M analog. Donati *et al.* (2005) extended this investigation using enzymatically produced strictly alternating poly-MG alginate.[42] Variations in molar ellipticity, showed an induced conformational effect through Ca^{2+} on MG-blocks similar to poly-G (albeit with smaller intensity differences).

In this study, a similar approach was conducted, comparing chiroptical properties of three different alginate block types upon the addition of stoichiometric amounts of CHOS. Since the CD bands of carboxylic acid groups are influenced by their protonation, the pH of all CD sample solutions was adjusted to 4.5 in advance (strong interaction of alginate and CHOS previously determined).[65,70] The molar ellipticities of the three different pure alginates and two chitosans were in excellent agreement with earlier reported data.[64,71]

The addition of chitosan tetramers to poly-M at half the alginate concentration, lead to an elevated positive peak at 199 nm and a deepened negative ellipticity with a minimum at 220 nm. The observed CD change aligns with the concept of "zipper like" junction zones between chitosan and mannuronan, proposed by Khong *et al.* (2013) due to their match in charge distance. The structural effect induced by the chitosan tetramer at half the poly-M concentration, does not further increase at equal and double concentration of tetramer to alginate, suggesting a sandwich like conjugation of chitosan in between two poly-M chains. When the chitosan octamer is applied, the effect at half the alginate concentration overlaps with the effect induced by CHOS DP = 4. However, unlike for the tetramer, the gain in molar ellipticity doubles when the CHOS DP = 8 concentration is increased to equal concentration of alginate.
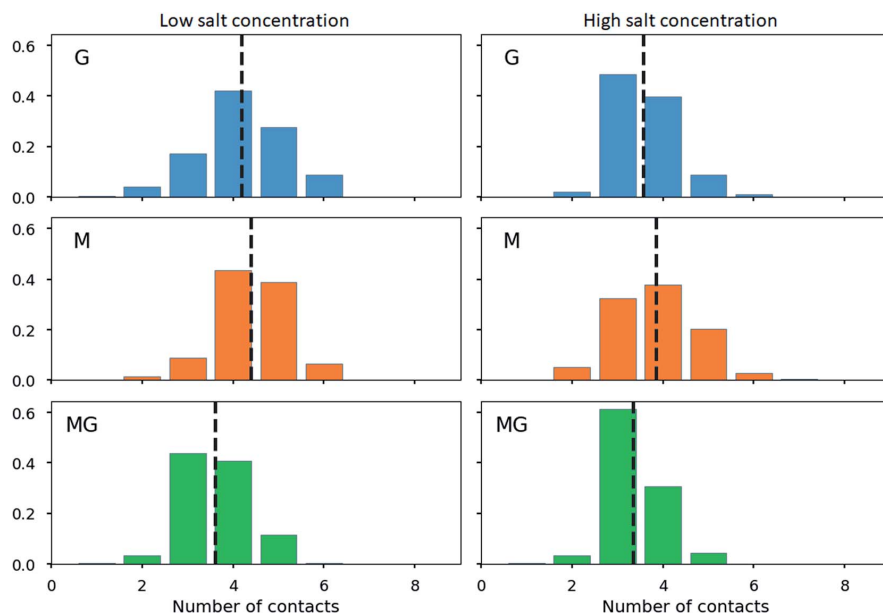
Fig. 12 Distribution of number of contacts between COO^- groups in an alginate oligomer (DP = 12) and NH_3^+ groups in a chitosan oligomer (DP = 8). A contact is defined as a COO^- group in alginate being within 3 Å of any NH_3^+ group in chitosan. The dashed vertical lines show the average number of contacts in each case. The figure show results for a low (left) and a high (right) concentration of ions (Na^+/Cl^-).
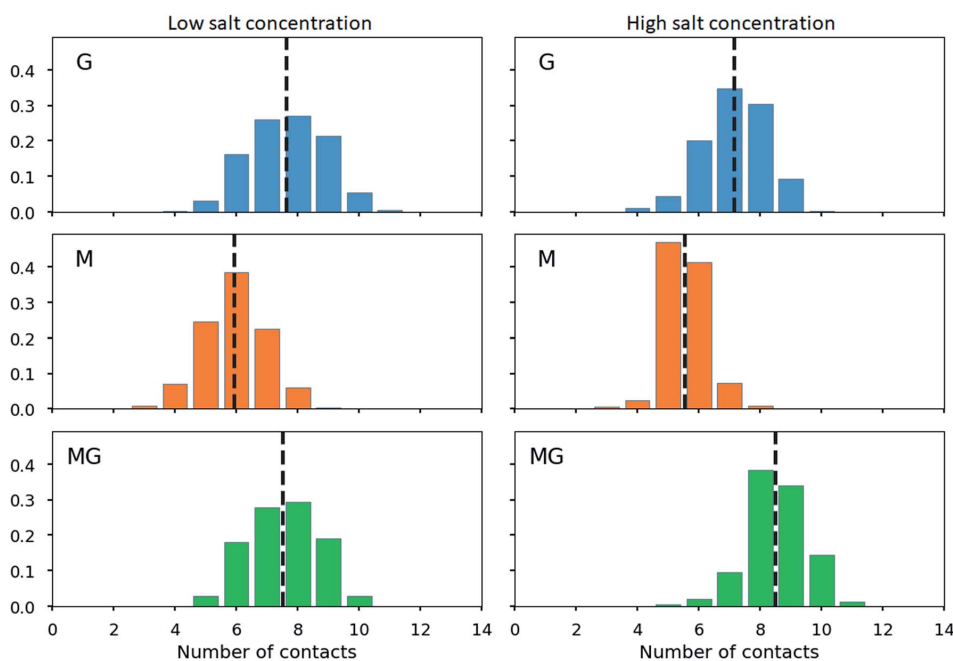

Fig. 13 Distribution of number of contacts between COO^- groups in alginate oligomers (DP = 12) and NH_3^+ groups in a chitosan oligomer (DP = 8) for 2 : 1 alginate : chitosan mixtures. A contact is defined as a COO^- group in alginate being within 3 Å of any NH_3^+ group in chitosan. The dashed vertical lines show the average number of contacts in each case. The figure show results for a low (left) and a high (right) concentration of ions (Na^+/Cl^-).

A possible interpretation could be a more rigid conformational change by the chitosan octamer due to less flexibility along the 2/1 helical alginate chain. More likely however, is that the chitosan octamer is able to form more stable associations with isolated alginate segments, due to its four charges per side, ionically stabilizing the association instead of two charges per side for the tetramer.

The fact that the induced conformational effect further increases when the octamer concentration is increased to double the alginate concentration, gives more validity to this hypothesis. When the chitosan DP = 8 concentration is twice the alginate concentration, a further stabilization of the alginate chain might occur by CHOS associating from both sides of the alginate chain.

None of these induced structural effects, detected by CD spectroscopy, was observed for poly-G or poly-MG. Additionally, an equal concentration of CHOS lead to precipitation of the polysaccharide aggregates for both poly-G and poly-MG. The CD results for poly-M provide further evidence for the "zipper like" gelling concept, where probably a match in charge distance between chitosan and mannuronan, leads to a conformational change in the polymer chain and to the formation of a higher ordered structures.[36,72] While none of these induced structural effects was observed for MG-blocks, the poly-MG-CHOS gelling systems still displays high gel strengths during rheological experiments, orders of magnitude above their poly-M analogue (when chitosan DP > 6). This suggest a fundamentally different gelling mechanism, underlaying the formation of chitosan-poly-MG junction zones.

A clue to the different underlaying gelling mechanism might be taken from the visual appearance of the hydrogels. While poly-M-CHOS gels are clear and almost fully transparent, poly-MG-CHOS gels were visually observed to be highly turbid, indicative of a possible phase separation.[68]

According to gel theory, ionically crosslinked hydrogels are weakened upon the addition of salt. The salt ions are shielding off attractive electrostatic forces of the ionic crosslinker and reduce the entropic driving force for electrostatic interaction, leading to a decrease in gel strength and gelling kinetics, potentially even to the collapse of gel network or precipitation.[73] If the junction zone, however, is stabilised through a phase separation, the addition of salt increases the difference in polarity between the solvent and junction zone and is further stabilising the association.

Nowak et al. (2003) demonstrated for amphiphilic polypeptide hydrogels, containing hydrophilic charged segments of poly-L-lysine and poly-L-glutamic acid as well as hydrophobic segments of poly-L-leucine, that the hydrogels (at 3.0 wt%) are increasing in gel strength when 50 mM NaCl is added to the system, up until 250 mM NaCl. Simultaneously an increasing turbidity was observed. For amphiphilic polypeptide hydrogels at 1.0 wt% (or lower), a weakening of the gels and subsequent precipitation upon the addition of salt was detected. The combination of hydrophobic and hydrophilic segments for the hydrogels showed a unique tolerance towards different pH and salt conditions, attributed to self-assembly of hydrophobic R-helical domains.[68,74] A similar approach was conducted by Boisseson et al. (2004), who modified alginates covalently linking long hydrophobic alkanes (octadecyl and dodecyl chains) to the polysaccharide backbone. The hydrogels beads were formed through ionotropic gelation using the alginate dropping method into calcium solution. The addition NaCl in the CaCl₂ solution increased the stability of the calcium alginate hydrogels due to increasing hydrophobic interactions of the alkyl side chains and reduced swelling of the beads.[69]

To investigate a stabilization through a phase separation and potentially the involvement of hydrophobic interactions stabilizing the poly-MG-CHOS junction zones, rheological experiments have been conducted analyzing poly-M and poly-MG crosslinked with a pure chitosan octamer upon the addition of 0, 50, 150, 500 mM NaCl. The transparent poly-M-chitosan gel followed the trend of a typical ionic tropic gelation, displaying reduced overall gel strength and slower gelling kinetics with an increasing salt concentration. Further supporting the zipper-like gelling concept of the two biopolymers. The turbid poly-MG chitosan octamer gelling system on the other hand, showed a sharp increase in gel strength (approx. doubling of G') when 50 mM NaCl was introduced. Furthermore, no deceleration of the kinetics was observed. Unlike poly-M, the alternating MG-blocks were able to form a hydrogel at the highest applied salt concentration of 500 mM. Those results suggest the stabilization of junction zones either through hydrophobic interactions between chitosan and alginates MG-blocks or through a phase separation based on a more efficient compensation of charges in the chelate like complex, creating a localized segment with low polarity. This, to our knowledge, not been reported before.

The rheological results upon the addition of NaCl, as well as the appearance are aligning with previously reported studies on phase separations within hydrogels.[68,75,76]

To gain further inside into the formation of junction zones, chain alignments and binding energies, computer simulations of alginate block oligomers (DP = 12 and 24) and chitosan oligomers (DP = 4, 8) were performed. The interactions of alginate and chitosan at different concentration, ratio, DP, and salt concentration have been calculated. Within the scope of the simulations, no particular conformation of CHOS and alginate strongly differed from the other alginate block types and associations, nor did the binding energies reveal large differences between binding energies and junction zones. Nevertheless, the strongest interaction for a sandwich type chelation (junction zone) was observed for the chitosan octamer chelated in between two MG-blocks at high salt concentration. Further was the chitosan-MG-complex, the only simulated chain association where the binding energy increased upon the addition of salt instead of decreased suggesting an additional stabilization of the junction zone by hydrophobic interactions, not present in poly-M-chitosan-hydrogels. Calculations on the coulomb and Lennard-Jones potential revealed only small contributions of hydrophobic interactions.

When calculating the number of contacts between the chitosan octamer and the different alginates, the contact number for M-alginate was close to but never exceeded 8 (the number of available amino groups), giving further evidence to the

previously hypothesised zipper-like chain alignment of these to poly- and oligosaccharides. For the chitosan octamer chelated by MG-alginate the number of contacts was close to 8 but with a significant distribution towards 9 contacts. Upon the addition of salt, those values further increased, showing an average number of contacts above 8 with even a significant distribution at 10 contacts.

The high number of contacts indicates a very compact junction zone formation for CHOS-poly-MG. While the data for poly-M chitosan junction zones clearly indicates a gel formation based on poly-ionic interactions, for MG-alginate we suggest (at least) two different interaction mechanism working simultaneously: electrostatic and hydrophobic.

The calculated distance of consecutive charges along MG-blocks (9.8 Å) will be close enough to chitosan (10.5 Å) to initiate a Manning condensation between the two block counterions and electrostatic interactions will be the predominant factor for the formation of chitosan poly-MG junction zones.[77] However, it was demonstrated through molecular dynamics that hydrophobic interactions (Lennard-Jones) still contribute to some extent. At various ionic strengths, the different processes would contribute to the formation of junction zones to a different extent, which is observed both at the increase in G' as well as the delay in gelling kinetics upon the addition of NaCl to the CHOS-poly-MG gelling system.

The CHOS poly-MG hydrogel might be further stabilized through a precipitation or local phase separation effect along the junction zone. Although this effect remains speculative, the increasing turbidity during the poly-MG chitosan hydrogel formation as well as the gel strength with magnitudes of order greater than for the equivalent poly-M gel supports this hypothesis.

Alternatively, the increasing turbidity with increasing gelling time could be attributed to a formations of higher order (random) structures as seen with (e.g.) alginic acid gels described through SAXS experiments.[78] Also an additional formation of hydrogen bonds within the poly-MG chitosan junction zone has to be considered.[38,79]

5 Conclusion

Strong evidences have been obtained, supporting the previously proposed gelling principle of poly-M alginate crosslinked with chitosan oligomers due to a match in charge distance between the two polyelectrolytes.[36] CD spectroscopy revealed an increased chiroptical activity for poly-M chitosan gelling systems, indictive of induced conformational changes and formation of higher ordered structures.[42,80]

A unique chitosan oligomer poly-MG gelling system was described using circular dichroism beside rheology and computer simulations. Rheological measurement revealed gel strengths magnitudes of order higher than displayed for its poly-M analogue. Furthermore, a strong increase in gel strength upon the addition of 50 and even 150 mM NaCl for the chitosan and poly-MG gelling system was detected, suggesting a stabilization of the junction zones through hydrophobic interactions and/or a phase separation, which to our knowledge has not

been reported before. Those findings were supported by molecular dynamics simulations, showing an increase in interaction energies between chitosan and alginate upon the addition of NaCl for poly-MG, while for poly-M and poly-G the addition of NaCl decreased the interaction energies with chitosan. CD measurements showed no systematic alignment or induced conformational change within the poly-MG chitosan system, which further implies a fundamentally different effect supporting the chitosan poly-MG junction zones. The high gel strengths, especially upon the addition of salt, as well as the turbidity of the poly-MG chitosan gelling system are indictive of a more complex formation of junction zones within these hydrogels, than seen within comparable ionically crosslinked alginate gelling systems.[68]

The described CHOS poly-MG gelling systems are displaying high gel strengths, are known to be fully biocompatible and have revealed a high tolerance to a broad range of salt concentrations present in various biological systems, which might prove poly-MG chitosan gels highly relevant for biomedical applications.

Conflicts of interest

There are no conflicts to declare.

Acknowledgements

References

1 T. J. Painter, in *The Polysaccharides*, ed. G. O. Aspinall, 1983, pp. 195–285.

2 A. Linker and R. S. Jones, A new polysaccharide resembling alginic acid isolated from pseudomonads, *J. Biol. Chem.*, 1966, **241**, 3845–3851.

3 P. A. J. Gorin and J. F. T. Spencer, Exocellular aginic acid from Azotobacter vinelandii, *Can. J. Chem.*, 1966, **44**, 993–998.

4 K. I. Draget, S. Moe, G. Skjåk-Bræk and O. Smidsrød, *Food Polysaccharides and Their Applications*, 2nd edn, CRC Press, Taylor & Francis Group, 2006, pp. 290–328, ISBN: 0-8247-5922-2.

5 M. Fukushima, K. Tatsumi and S. Wada, Evaluation of the Intrinsic Acid-Dissociation Constant of Alginic Acid by Considering the Electrostatic Effect, *Anal. Sci.*, 1999, **15**, 1153–1155.

6 K. M. Vårum and O. Smidsrød, in *Polysaccharides - Structural Diversity and Functional Versatility*, ed. S. Dumitriu, CRC Press, Boca Raton, 2nd edn, 2005, pp. 625–642.

7 M. W. Anthonsen and O. Smidsrød, Hydrogen ion titration of chitosans with varying degrees of N-acetylation by

monitoring induced 1H-NMR chemical shifts, *Carbohydr. Polym.*, 1995, **26**, 303–305.

8 S. P. Strand, K. Tømmeraas, K. M. Vårum and K. Østgaard, Electrophoretic Light Scattering Studies of Chitosans with Different Degrees of N-acetylation, *Biomacromolecules*, 2001, **2**, 1310–1314.

9 S. Tsukada and Y. Inoue, Conformational properties of chito-oligosaccharides: titration, optical rotation, and carbon-[13]NMR. studies of chito-oligosaccharides, *Carbohydr. Res.*, 1981, **88**, 19–38.

10 K. M. Vårum, M. H. Ottøy and O. Smidsrød, Water-solubility of partially N-acetylated chitosans as a function of pH: effect of chemical composition and depolymerisation, *Carbohydr. Polym.*, 1994, **25**, 65–70.

11 B. B. Aam, E. B. Heggset, A. L. Norberg, M. Sørlie, K. M. Vårum and V. G. H. Eijsink, Production of chitooligosaccharides and their potential applications in medicine, *Mar. Drugs*, 2010, **8**, 1482–1517.

12 J. Nilsen-Nygaard, S. Strand, K. Vårum, K. Draget and C. Nordgård, Chitosan: Gels and Interfacial Properties, *Polymers*, 2015, **7**, 552–579.

13 P. Sacco, F. Furlani, G. de Marzo, E. Marsich, S. Paoletti and I. Donati, Concepts for Developing Physical Gels of Chitosan and of Chitosan Derivatives, *Gels*, 2018, **4**, 67.

14 F. Furlani, P. Sacco, F. Scognamiglio, F. Asaro, A. Travan, M. Borgogna, E. Marsich, M. Cok, S. Paoletti and I. Donati, Nucleation, reorganization and disassembly of an active network from lactose-modified chitosan mimicking biological matrices, *Carbohydr. Polym.*, 2019, **208**, 451–456.

15 R. J. Nordtveit, K. M. Vårum and O. Smidsrød, Degradation of partially N-acetylated chitosans with hen egg white and human lysozyme, *Carbohydr. Polym.*, 1996, **29**, 163–167.

16 K. M. Vårum, M. M. Myhr, R. J. N. Hjerde and O. Smidsrød, *In vitro* degradation rates of partially N-acetylated chitosans in human serum, *Carbohydr. Res.*, 1997, **299**, 99–101.

17 M. Köping-Höggård, I. Tubulekas, H. Guan, K. Edwards, M. Nilsson, K. M. Vårum and P. Artursson, Chitosan as a nonviral gene delivery system. Structure-property relationships and characteristics compared with polyethylenimine *in vitro* and after lung administration in vivo, *Gene Ther.*, 2001, **8**, 1108–1121.

18 S. Strand, S. Danielsen, B. E. Christensen and K. M. Vårum, Influence of Chitosan Structure on the Formation and Stability of DNA-Chitosan Polyelectrolyte Complexes, *Biomacromolecules*, 2005, **6**, 3357–3366.

19 P. K. Dutta, S. Tripathi, G. K. Mehrotra and J. Dutta, Perspectives for chitosan based antimicrobial films in food applications, *Food Chem.*, 2009, **114**, 1173–1182.

20 O. Felt, A. Carrel, P. Baehni, P. Buri and R. Gurny, Chitosan as tear substitute: a wetting agent endowed with antimicrobial efficacy, *J. Ocul. Pharmacol. Ther.*, 2000, **16**, 261–270.

21 X. F. Liu, Y. L. Guan, D. Z. Yang, Z. Li and K. D. Yao, Antibacterial Action of Chitosan and Carboxymethlyated Chitosan, *J. Appl. Polym. Sci.*, 2000, **79**, 1324–1335.

22 H. Mellegård, S. P. Strand, B. E. Christensen, P. E. Granum and S. P. Hardy, Antibacterial activity of chemically defined chitosans: Influence of molecular weight, degree of acetylation and test organism, *Int. J. Food Microbiol.*, 2011, **148**, 48–54.

23 W. Xia, P. Liu, J. Zhang and J. Chen, Biological activities of chitosan and chitooligosaccharides, *Food Hydrocolloids*, 2011, **25**, 170–179.

24 S. Y. Ong, J. Wu, S. M. Moochhala, M. H. Tan and J. Lu, Development of a chitosan-based wound dressing with improved hemostatic and antimicrobial properties, *Biomaterials*, 2008, **29**, 4323–4332.

25 H. Ueno, T. Mori and T. Fujinaga, Topical formulations and wound healing applications of chitosan, *Adv. Drug Delivery Rev.*, 2001, **52**, 105–115.

26 S. B. Ross-Murphy, in *Biophysical Methods in Food Research*, ed. H. W. S. Chan, Blackwell Scientific Publications, 1984, pp. 137–199.

27 F. L. Mi, S. S. Shyu, T. B. Wong, S. F. Jang, S. T. Lee and K. T. Lu, Chitosan-polyelectrolyte complexation for the preparation of gel beads and controlled release of anticancer drug. II. Effect of pH-dependent ionic crosslinking or interpolymer complex using tripolyphosphate or polyphosphate as reagent, *J. Appl. Polym. Sci.*, 1999, **74**, 1093–1107.

28 R. M. Desai, S. T. Koshy, S. a. Hilderbrand, D. J. Mooney and N. S. Joshi, Versatile click alginate hydrogels crosslinked via tetrazine-norbornene chemistry, *Biomaterials*, 2015, **50**, 30–37.

29 H. Li, Preparation and Characterization of Homogeneous Hydroxyapatite/Chitosan Composite Scaffolds via In-Situ Hydration, *J. Biomater. Nanobiotechnol.*, 2010, **01**, 42–49.

30 Y. L. Guan, L. E. I. Shao and K. De Yao, A Study on Correlation Between Water State and Swelling Kinetics of Chitosan-Based Hydrogels, *J. Appl. Polym. Sci.*, 1996, **61**, 2325–2335.

31 K. I. Draget and G. Skjåk-Bræk, *Renewable Resources for Functional Polymers and Biomaterials: Polysaccharides, Proteins and Polyesters*, 2011, pp. 186–209, ISBN: 978-1-84973-245-1.

32 J.-Y. Leong, W.-H. Lam, K.-W. Ho, W.-P. Voo, M. F.-X. Lee, H.-P. Lim, S.-L. Lim, B.-T. Tey, D. Poncelet and E.-S. Chan, Advances in fabricating spherical alginate hydrogels with controlled particle designs by ionotropic gelation as encapsulation systems, *Particuology*, 2015, **24**, 44–60.

33 O. Smidsrød and G. Skjåk-Bræk, Alginate as immobilization matrix for cells, *Minerva Biotecnol.*, 1990, **8**, 71–78.

34 Ý. Mørch, I. Donati and B. Strand, Effect of Ca^{2+}, Ba^{2+}, and Sr^{2+} on Alginate Microbeads, *Biomacromolecules*, 2006, **7**, 1471–1480.

35 P. Sikorski, F. Mo, G. Skjåk-Bræk and B. T. Stokke, Evidence for egg-box-compatible interactions in calcium-Alginate gels from fiber x-ray diffraction, *Biomacromolecules*, 2007, **8**, 2098–2103.

36 T. T. Khong, O. A. Aarstad, G. Skjåk-Bræk, K. I. Draget and K. M. Vårum, Gelling concept combining chitosan and alginate - Proof of principle, *Biomacromolecules*, 2013, **14**, 2765–2771.

37 Y. Feng, G. Kopplin, K. Sato, K. I. Draget and K. M. Vårum, Alginate gels with a combination of calcium and chitosan oligomer mixtures as crosslinkers, *Carbohydr. Polym.*, 2017, **156**, 490–497.

38 R. Minke and J. Blackwell, The structure of α-chitin, *J. Mol. Biol.*, 1978, **120**, 167–181.

39 A. Sørbotten, S. J. Horn, V. G. H. Eijsink and K. M. Vårum, Degradation of chitosans with chitinase B from Serratia marcescens, *FEBS J.*, 2005, **272**, 538–549.

40 E. D. Atkins, W. Mackie and E. E. Smolko, Crystalline structures of alginic acids, *Nature*, 1970, **225**, 626–628.

41 H. K. Høidal, H. Ertesvåg, G. Skjåk-Bræk, B. T. Stokke and S. Valla, The recombinant Azotobacter vinelandii mannuronan C-5-epimerase AlgE4 epimerizes alginate by a nonrandom attack mechanism, *J. Biol. Chem.*, 1999, **274**, 12316–12322.

42 I. Donati, S. Holtan, Y. A. Mørch, M. Borgogna, M. Dentini and G. Skjåk-Bræk, New hypothesis on the role of alternating sequences in calcium-alginate gels, *Biomacromolecules*, 2005, **6**, 1031–1040.

43 S. Holtan, Q. Zhang, W. I. Strand and G. Skjåk-Bræk, Characterization of the Hydrolysis Mechanism of Polyalternating Alginate in Weak Acid and Assignment of the Resulting MG-Oligosaccharides by NMR Spectroscopy and ESI−Mass Spectrometry, *Biomacromolecules*, 2006, **7**, 2108–2121.

44 Ø. Arlov, F. L. Aachmann, A. Sundan, T. Espevik and G. Skjåk-Bræk, Heparin-like properties of sulfated alginates with defined sequences and sulfation degrees, *Biomacromolecules*, 2014, **15**, 2744–2750.

45 O. A. Aarstad, A. Tøndervik, H. Sletta and G. Skjåk-Bræk, Alginate sequencing: An analysis of block distribution in alginates using specific alginate degrading enzymes, *Biomacromolecules*, 2012, **13**, 106–116.

46 S. Páll, R. Schulz, B. Hess, J. C. Smith, T. Murtola, M. J. Abraham and E. Lindahl, GROMACS: High performance molecular simulations through multi-level parallelism from laptops to supercomputers, *SoftwareX*, 2015, **1–2**, 19–25.

47 L. Schrödinger, *Schrödinger Release 2018-1: Maestro*, Schrödinger, LLC, New York, NY, 2018.

48 A. D. Bochevarov, E. Harder, T. F. Hughes, J. R. Greenwood, D. A. Braden, D. M. Philipp, D. Rinaldo, M. D. Halls, J. Zhang and R. A. Friesner, Jaguar: A high-performance quantum chemistry software program with strengths in life and materials sciences, *Int. J. Quantum Chem.*, 2013, **113**, 2110–2142.

49 D. Shivakumar, J. Williams, Y. Wu, W. Damm, J. Shelley and W. Sherman, Prediction of absolute solvation free energies using molecular dynamics free energy perturbation and the opls force field, *J. Chem. Theory Comput.*, 2010, **6**, 1509–1519.

50 U. Essmann, L. Perera, M. L. Berkowitz, T. Darden, H. Lee and L. G. Pedersen, A smooth particle mesh Ewald method, *J. Chem. Phys.*, 1995, **103**, 8577–8593.

51 B. Hess, H. Bekker, H. J. C. Berendsen and J. G. E. M. Fraaije, LINCS: A linear constraint solver for molecular simulations, *J. Comput. Chem.*, 1997, **18**, 1463–1472.

52 M. W. Mahoney and W. L. Jorgensen, A five-site model for liquid water and the reproduction of the density anomaly by rigid, nonpolarizable potential functions, *J. Chem. Phys.*, 2000, **112**, 8910–8922.

53 G. Bussi, D. Donadio and M. Parrinello, Canonical sampling through velocity rescaling, *J. Chem. Phys.*, 2007, **126**, 014101.

54 H. J. C. Berendsen, J. P. M. Postma, W. F. Van Gunsteren, A. Dinola and J. R. Haak, Molecular dynamics with coupling to an external bath, *J. Chem. Phys.*, 1984, **81**, 3684–3690.

55 M. Parrinello and A. Rahman, Polymorphic transitions in single crystals: A new molecular dynamics method, *J. Appl. Phys.*, 1981, **52**, 7182–7190.

56 H. Grasdalen, B. Larsen and O. Smidsrød, ^{13}C NMR Studies of Monomeric Coposition and Sequence in Alginate, *Carbohydr. Res.*, 1981, **89**, 179–191.

57 H. Grasdalen, High-field, ^{1}H-NMR spectroscopy of alginate: sequential structure and linkage conformations, *Carbohydr. Res.*, 1983, **118**, 255–260.

58 K. I. Draget, G. Skjakbrak, O. Smidsrod, G. S. Bræk and O. Smidsrød, Alginic acid gels: the effect of alginate chemical composition and molecular weight, *Carbohydr. Polym.*, 1994, **25**, 31–38.

59 K. I. Draget, M. K. Simensen, E. Onsøyen and O. Smidsrød, *Fourteenth International Seaweed Symposium*, Springer, Netherlands, 1993, pp. 563–569.

60 X. Wang and H. G. Spencer, Calcium alginate gels: Formation and stability in the presence of an inert electrolyte, *Polymer*, 1998, **39**, 2759–2764.

61 O. Smidsrod and A. Haug, Dependence upon the gel-sol state of the ion-exchange properties of alginates, *Acta Chem. Scand.*, 1972, **26**, 2063–2074.

62 T. Tanaka, Gels, *Sci. Am.*, 1981, **244**, 124–138.

63 O. Gåserød, A. Sannes and G. Skjåk-Bræk, Microcapsules of alginate-chitosan. II. A study of capsule stability and permeability, *Biomaterials*, 1999, **20**, 773–783.

64 I. Donati, A. Gamini, G. Skjåk-Bræk, A. Vetere, C. Campa, A. Coslovi and S. Paoletti, Determination of the diadic composition of alginate by means of circular dichroism: A fast and accurate improved method, *Carbohydr. Res.*, 2003, **338**, 1139–1142.

65 E. R. Morris, D. A. Rees, G. R. Sanderson and D. Thom, Conformation and circular dichroism of uronic acid residues in glycosides and polysaccharides, *J. Chem. Soc., Perkin Trans. 2*, 1975, 1418–1425.

66 E. R. Morris, D. A. Rees and D. Thom, Characterisation of alginate composition and block-structure by circular dichroism, *Carbohydr. Res.*, 1980, **81**, 305–314.

67 E. R. Morris, D. A. Rees, D. Thom and J. Boyd, Chiroptical and stoichiometric evidence of a specific, primary dimerisation process in alginate gelation, *Carbohydr. Res.*, 1978, **66**, 145–154.

68 A. P. Nowak, V. Breedveld, D. J. Pine and T. J. Deming, Unusual Salt Stability in Highly Charged Diblock Co-

polypeptide Hydrogels, *J. Am. Chem. Soc.*, 2003, **125**, 15666–15670.

69 M. R. De Boisseson, M. Leonard, P. Hubert, P. Marchal, A. Stequert, C. Castel, E. Favre and E. Dellacherie, Physical alginate hydrogels based on hydrophobic or dual hydrophobic/ionic interactions: Bead formation, structure, and stability, *J. Colloid Interface Sci.*, 2004, **273**, 131–139.

70 I. Listowsky, G. Avigad and S. Englard, Conformational Equilibria and Stereochemical Relationships among Carboxylic Acids, *J. Org. Chem.*, 1970, **35**, 1080–1085.

71 A. Domard, Determination of N-acetyl content in chitosan samples by c.d. measurements, *Int. J. Biol. Macromol.*, 1987, **9**(6), 333–336.

72 S. J. Khouri, R. Knierim and V. Buss, Induced circular dichroism of the interaction between pinacyanol and algal alginates, *Carbohydr. Res.*, 2009, **344**, 1729–1733.

73 Y. Tang, X. Wang, Y. Li, M. Lei, Y. Du, J. F. Kennedy and C. J. Knill, Production and characterisation of novel injectable chitosan/methylcellulose/salt blend hydrogels with potential application as tissue engineering scaffolds, *Carbohydr. Polym.*, 2010, **82**, 833–841.

74 A. P. Nowak, J. Sato, V. Breedveld and T. J. Deming, Hydrogel Formation in Amphiphilic Triblock Copolypeptides, *Supramol. Chem.*, 2006, **18**, 423–427.

75 Q. Liu, E. L. Hedberg, Z. Liu, R. Bahulekar, R. K. Meszlenyi and A. G. Mikos, Preparation of macroporous poly(2-hydroxyethyl methacrylate) hydrogels by enhanced phase separation, *Biomaterials*, 2000, **21**, 2163–2169.

76 F. J. Hua, J. Do Nam and D. S. Lee, Preparation of a Macroporous Poly(L-lactide) Scaffold by Liquid-Liquid Phase Separation of a PLLA/1,4-Dioxane/Water Ternary System in the Presence of NaCl, *Macromol. Rapid Commun.*, 2001, **22**, 1053–1057.

77 G. S. Manning, Limiting laws and counterion condensation in polyelectrolyte solutions I. Colligative properties, *J. Chem. Phys.*, 1969, **51**, 924–933.

78 K. I. Draget, B. T. Stokke, Y. Yuguchi, H. Urakawa and K. Kajiwara, Small-angle X-ray scattering and rheological characterization of alginate gels. 3. Alginic acid gels, *Biomacromolecules*, 2003, **4**, 1661–1668.

79 V. I. Kovalenko, Crystalline cellulose: structure and hydrogen bonds, *Russ. Chem. Rev.*, 2010, **79**, 231–241.

80 Y. Matsuda, Y. Biyajima and T. Sato, Thermal denaturation, renaturation, and aggregation of a double-helical polysaccharide xanthan in aqueous solution, *Polym. J.*, 2009, **41**, 526–532.

Supporting Informattion:

Alginate gels crosslinked with chitosan oligomers — A systematic investigation into alginate block structure and chitosan oligomer interaction

Georg Kopplin[a], Anders Lervik[b], Kurt I. Draget[a] and Finn L. Aachmann*[a]

a Norwegian Biopolymer Laboratory (NOBIPOL), Department of Biotechnology, Norwegian University of Science and Technology, 7491 Trondheim, Norway
b Department of Chemistry, Norwegian University of Science and Technology, 7491 Trondheim, Norway

*Corresponding author. E-mail finn.l.aachmann@ntnu.no

Supporting Informattion
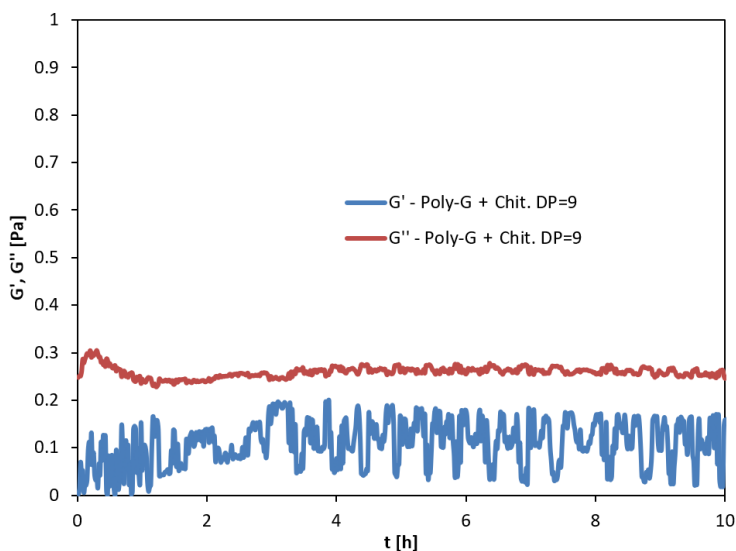
Figure S1: Kinetics of gelation of poly-G alginate concentration at 10 g/L (1%) with chitosan oligomers DP = 9 and concentration at 3 g/L (0.3%). GDL concentration 2 g/L. G' (blue line) and G'' (red line), was determined as a function of time.
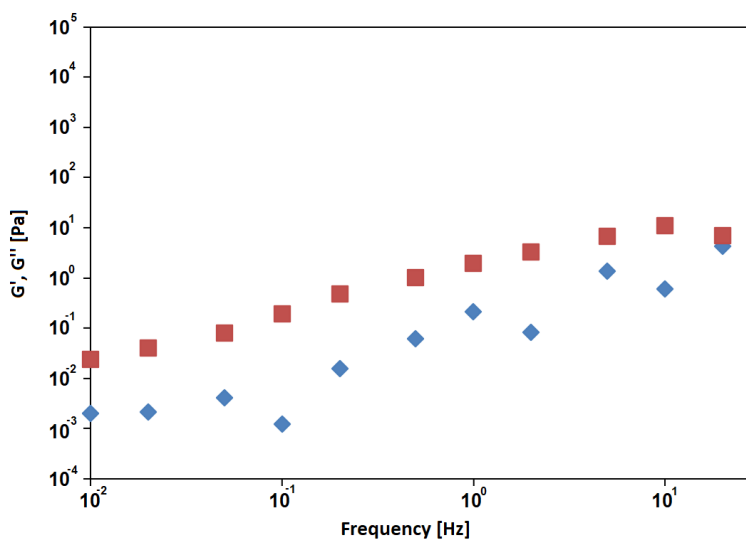
Figure S2: Frequency sweep of poly-MG (1.0%) and CHOS DP = 9 (0.3%), without GDL. G' (blue diamonds), G'' (red squares). All measurements performed at 20°C.

Table S1: Complete composition of alginate hydrogels, used for rheological experiments. Alginate was ionically crosslinked with chitosan oligosaccharides (CHOS) at various CHOS/Alginate monosaccharide unit ratios. The amounts of NaOH was adjusted to reach pH to 8 when mixing CHOS and Alginate. The amount of Glucono δ-lactone (GDL) was adjusted to reach a final pH of 4.35 ± 0.05. For calculations based on the monosaccharide ratio, the molar masses 199.12 g/mol and 197.62 g/mol were assigned to the sodium alginate unit and to the glucosamine chloride unit respectively.

| SAMPLE	1	2	3	4	5	Unit
Monosacch. unit ratio: CHOS/Alginate	0.2	0.3	0.4	0.5	0.6	
Alginate solution (30 g/L) added	1.00	1.00	1.00	1.00	1.00	g
Alginate amount	30.00	30.00	30.00	30.00	30.00	mg
Alginate concentration (final)	10.00	10.00	10.00	10.00	10.00	g/L
CHOS amount	6.08	9.12	12.16	15.20	18.24	mg
CHOS solution (100 g/L) added	60.8	91.2	121.6	152.0	182.4	µl
CHOS concentration (final)	2.03	3.04	4.05	5.07	6.08	g/L
NaOH (1 M) added	14.9	22.4	29.8	37.3	44.7	µl
GDL amount	5.32	7.98	10.63	13.29	15.95	mg
GDL concentration (final)	1.77	2.66	3.54	4.43	5.32	g/L
H_2O added (final Vol. 3 mL)	1924	1886	1849	1811	1773	µl
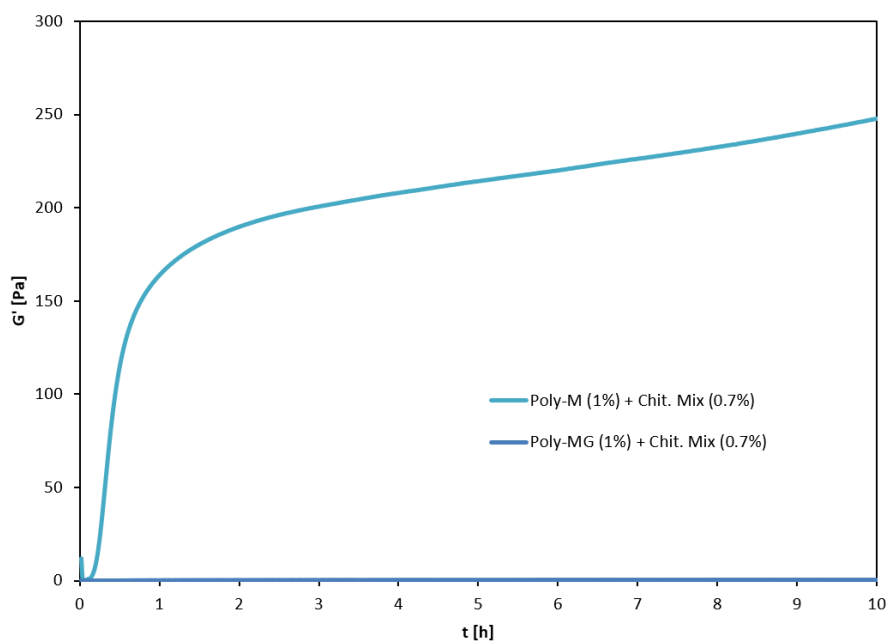
Figure S3: Kinetics of gelation as a function of time. Alginate concentration (poly-M: light blue, poly-MG: dark blue) at 10 g/L (1%). Chitosan oligomer mix (DP_n = 3.96, FA = 0.045) concentration at 7 g/L (0.7%). GDL at 2 g/L. G' was determined as a function of time. G" and delta are not shown in the Figure for reasons of clarity.
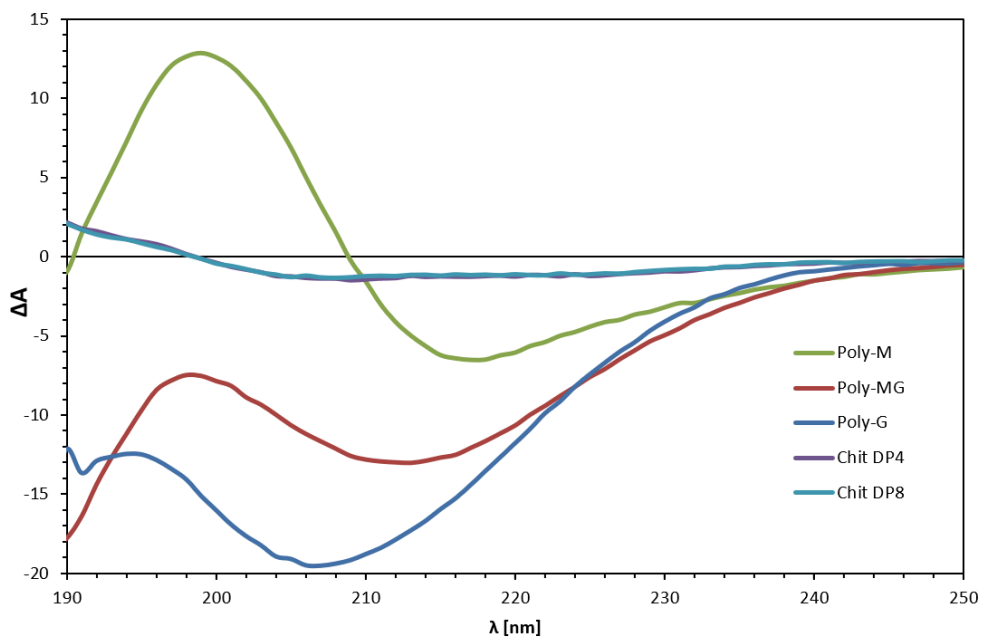
Figure S4: Circular dichroism spectra of poly-M (green), poly-MG (red), poly-G (blue) and chitosan DP = 4 (purple) and DP = 8 (light blue). All measurements were performed at pH = 4.5 and T = 25°C with a sample concentration of 0.4 g/L.
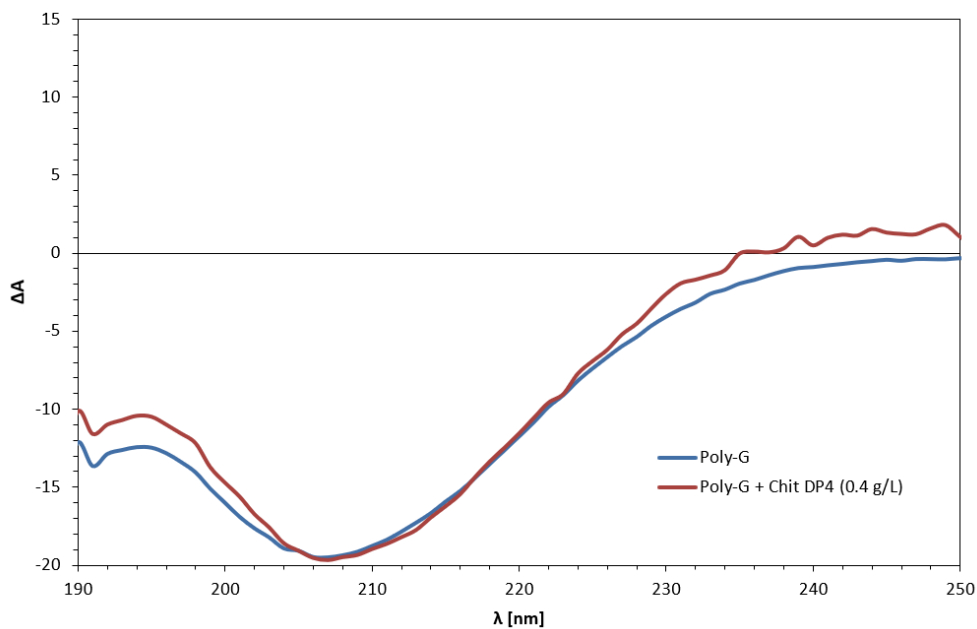

Figure S5: Circular dichroism spectra of poly-G (blue line) and poly-G upon addition of chitosan DP = 4 (red). The alginate and chitosan concentration was at 0.4 g/L. All measurements were performed at pH = 4.5 and T = 25°C.
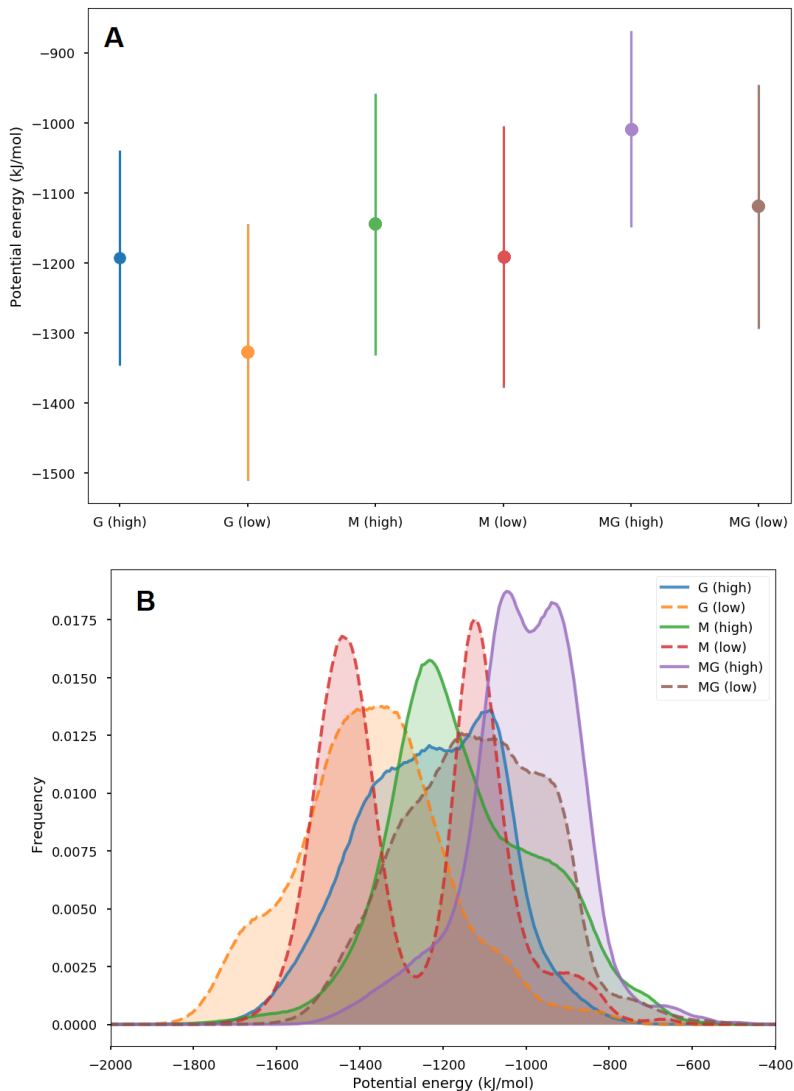
Figure S6: Average (A) and histograms (B) of the interaction energies between alginate oligomers (DP = 12) and a chitosan oligomer (DP = 8), obtained in MD simulations lasting 100 ns. The average interaction energy is lowest for the G oligomer with a low concentration of salt and largest for the MG-oligomer with a high concentration of salt.
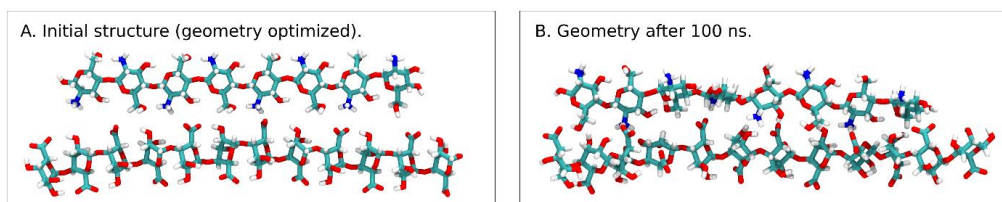

Figure S7: Simulation snapshots of the alginate G-oligomer and a chitosan oligomer (DP = 8) for a low concentration of salt (salt ions are not shown). (Left) The initial geometry optimized structure. (Right) The structure after a MD simulation lasting 100 ns. In this case, distortions of the molecular structures allow for a closer approach of charged groups in the molecules.
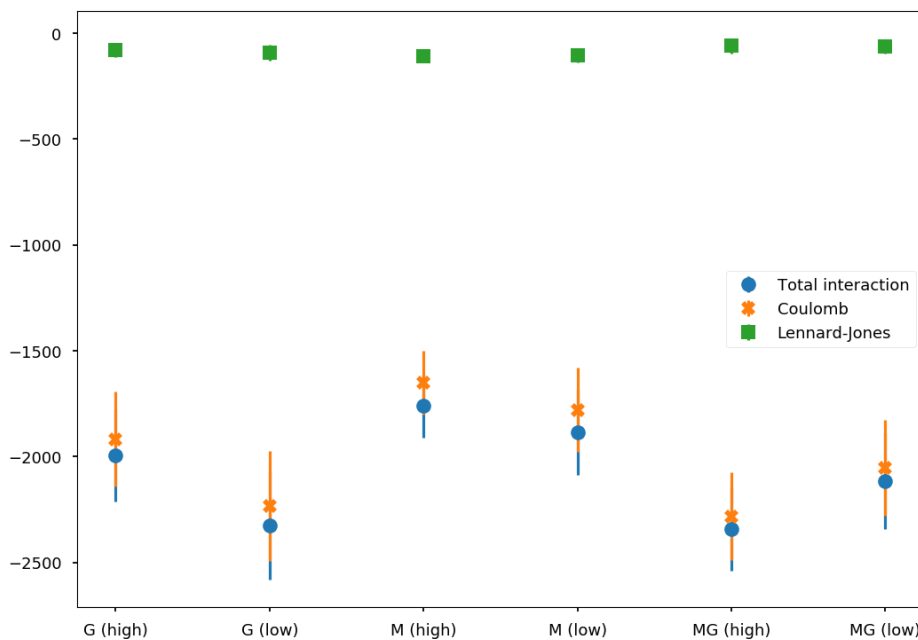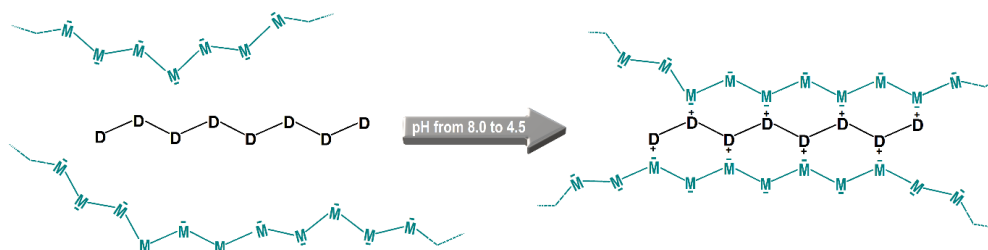
Figure S8: Average interaction energy between alginate (DP = 12) and chitosan (DP = 8) oligomers for 2:1 alginate:chitosan mixtures and high and low ion (Na$^+$/Cl$^-$) concentrations.

Scheme S1: Schematic illustration of the interaction between a chitosan oligomer (black) and poly-M alginate (green) at different pHs. Monosaccharide units: glucosamine (D), mannuronate (M). At pH ≤ 8 the amino groups of chitosan are mostly uncharged, while the carboxyl groups of alginate are mostly charged. At pH 4.0–5.0 both chitosan and alginate are predominantly charged, leading to ionic crosslinking of the two components and a zipper-like chain alignment due to the similar charge distance in both compounds.

NTNU

Norwegian University of
Science and Technology